(2) LEVEL II

AFML-TR-78-40

DEVELOPMENT OF STANDARD METHODS OF TESTING AND ANALYZING FATIGUE CRACK GROWTH RATE DATA

S.J. HUDAK, Jr.
A. SAXENA
R.J. BUCCI
R.C. MALCOLM

WESTINGHOUSE ELECTRIC CORPORATION
WESTINGHOUSE R&D CENTER
PITTSBURGH, PENNSYLVANIA 15235

May 1978

TECHNICAL REPORT AFML-TR-78-40
Final Report for Period June 1975–December 1977

AIR FORCE MATERIALS LABORATORY
AIR FORCE SYSTEMS COMMAND
WRIGHT-PATTERSON AIR FORCE BASE, OHIO 45433

NOTICE

When Government drawings, specifications, or other data are used for any purpose other than in connection with a definitely related Government procurement operation, the United States Government thereby incurs no responsibility nor any obligation whatsoever; and the fact that the government may have formulated, furnished, or in any way supplied the said drawings, specifications, or other data, is not to be regarded by implication or otherwise as in any manner licensing the holder or any other person or corporation, or conveying any rights or permission to manufacture, use, or sell any patented invention that may in any way be related thereto.

This report has been reviewed by the Information Office (OI) and is releasable to the National Technical Information Service (NTIS). At NTIS, it will be available to the general public, including foreign nations.

This technical report has been reviewed and is approved for publication.

Allan W. Gunderson

ALLAN W. GUNDERSON
Engineering and Design Data
Materials Integrity Branch

C. L. Harmsworth

C. L. HARMSWORTH
Technical Manager
Engineering and Design Data
Materials Integrity Branch

FOR THE COMMANDER

Thomas D. Cooper

THOMAS D. COOPER
Chief, Materials Integrity Branch
Systems Support Division

"If your address has changed, if you wish to be removed from our mailing list or if the addressee is no longer employed by your organization please notify AFML-MXA,W-PAFB,OH 45433 to help us maintain a current mailing list.

Copies of this report should not be returned unless return is required by security considerations, contractual obligations, or notice on a specific document.

AIR FORCE/56780/14 August 1978 — 525

UNCLASSIFIED

SECURITY CLASSIFICATION OF THIS PAGE (When Data Entered)

REPORT DOCUMENTATION PAGE

READ INSTRUCTIONS BEFORE COMPLETING FORM

1. REPORT NUMBER: (18) AFML (19) TR-78-40
2. GOVT ACCESSION NO.
3. RECIPIENT'S CATALOG NUMBER (9)
4. TITLE (and Subtitle): (6) DEVELOPMENT OF STANDARD METHODS OF TESTING AND ANALYZING FATIGUE CRACK GROWTH RATE DATA.
5. TYPE OF REPORT & PERIOD COVERED: Final rept. (20) Jun 75-Dec 77
6. PERFORMING ORG. REPORT NUMBER: (14) 77-9D3-AFCGR-R1
7. AUTHOR(s): (10) S. J. Hudak, Jr., A. Saxena, R. J. Bucci, R. C. Malcolm
8. CONTRACT OR GRANT NUMBER(s): (15) F33615-75-C-5064
9. PERFORMING ORGANIZATION NAME AND ADDRESS: Westinghouse Electric Corporation, Westinghouse R&D Center, Pittsburgh, Pennsylvania 15235
10. PROGRAM ELEMENT, PROJECT, TASK AREA & WORK UNIT NUMBERS: (16) ~~PE-1457-75-02110~~ 7381
11. CONTROLLING OFFICE NAME AND ADDRESS: Air Force Materials Laboratory, Air Force Systems Command, Wright-Patterson Air Force Base, OH 45433
12. REPORT DATE: (11) May 78
13. NUMBER OF PAGES: 95 (12) 268 p.
14. MONITORING AGENCY NAME & ADDRESS (if different from Controlling Office)
15. SECURITY CLASS. (of this report): Unclassified
15a. DECLASSIFICATION/DOWNGRADING SCHEDULE

16. DISTRIBUTION STATEMENT (of this Report)

Approved for public release; distribution unlimited.

17. DISTRIBUTION STATEMENT (of the abstract entered in Block 20, if different from Report)

18. SUPPLEMENTARY NOTES

Two of the co-authors (Bucci and Malcolm) are affiliated with the Aluminum Company of America, Alcoa Laboratories, Alcoa Center, Pennsylvania 15069.

19. KEY WORDS (Continue on reverse side if necessary and identify by block number)

fatigue, cracks, growth, fracture, design, testing, ASTM, standard, modeling

20. ABSTRACT (Continue on reverse side if necessary and identify by block number)

Results are presented which provide the basis for the development of an ASTM standard for generating, analyzing and presenting fatigue crack growth rate data. Comprehensive data were also obtained on the individual and combined effects of load ratio, cyclic frequency, test temperature and environment on fatigue crack growth rates in a 10Ni steel and a 2219-T851 aluminum alloy. These data are used to demonstrate the utility of the proposed test methods. A new mathematical representation of wide-range fatigue crack growth rate data is also proposed which has advantages over existing representations.

DD FORM 1 JAN 73 1473 EDITION OF 1 NOV 65 IS OBSOLETE

UNCLASSIFIED

SECURITY CLASSIFICATION OF THIS PAGE (When Data Entered)

376625

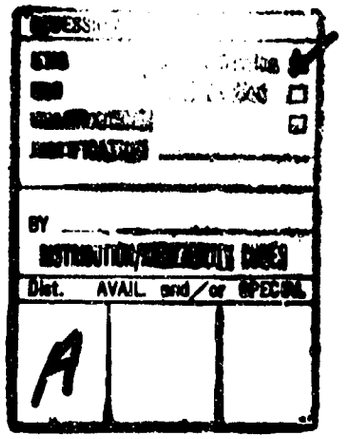

FOREWORD

This report was prepared under Air Force Contract F33615-75-C-5064, Project FY-1457-75-02110/7381, and was sponsored and administered by the Air Force Materials Laboratory, Air Force Systems Command, Wright-Patterson Air Force Base, Ohio, under the direction of Mr. Allan W. Gunderson (AFML/MXA).

This final report summarizes work conducted from June 20, 1975 to December 17, 1977 and was originally submitted on March 3, 1978.

The prime contractor for the program was the Westinghouse Electric Corporation, R&D Center, Pittsburgh, Pennsylvania 15235; portions of the programs were conducted by The Aluminum Company of America and Lehigh University on subcontractor bases. The Westinghouse program managers were E. T. Wessel and W. G. Clark, Jr. The principle investigator for Westinghouse was S. J. Hudak, Jr., the principle investigator for Alcoa was R. J. Bucci and the principle investigator for Lehigh was R. P. Wei.

The authors wish to express their appreciation to those individuals (Table 3-1) who contributed their time and effort to respond to the test method questionnaire. The helpful comments on the developing test methods by members of ASTM Task Groups E24.04.01 and E24.04.03 are also greatly appreciated. Special acknowledgments are due to the following members of the Task Group Steering Committees for their constructive suggestions during the course of several reviews of the test methods:

J. K. Donald - Del Research
N. E. Dowling - Westinghouse R&D Center
A. W. Gunderson - Air Force Materials Laboratory
B. M. Kapadia - U.S. Steel Research Laboratory
C. A. Miller - Bethlehem Steel Research Laboratory
R. P. Wei - Lehigh University

A special acknowledgment is also due to W. G. Clark, Jr. of Westinghouse who initiated and led the initial efforts in ASTM to standardize fatigue crack growth rate testing.

L. A. James of Westinghouse's Hanford Engineering Development Laboratory contributed data to the specimen size requirement evaluation. The fatigue crack growth rate tests in dry argon were conducted at Lehigh University under the direction of Prof. R. P. Wei.

Contributions to the experimental work by R. B. Hewlett, J. H. Taylor, W. H. Halligan and R. C. Brown and to report preparation by R. R. Hovan and Donna E. Gongaware of Westinghouse's Structural Behavior of Materials Department are greatly appreciated. G. M. Jouris of Westinghouse's Mathematics Department assisted the regression analysis and mathematical modeling.

The financial support of the Air Force Materials Laboratory, Air Force Systems Command, Wright-Patterson Air Force Base, Ohio and the cooperation of Mr.Allan W. Gunderson, the Air Force Project Engineer, is most gratefully acknowledged. We would also like to thank the Westinghouse Electric Corporation and the Alcoa Corporation for supporting the authors' ASTM committee activities.

TABLE OF CONTENTS

TABLE OF CONTENTS (concluded)

LIST OF ILLUSTRATIONS

LIST OF ILLUSTRATIONS (continued)

LIST OF ILLUSTRATIONS (continued)

LIST OF ILLUSTRATIONS (continued)

LIST OF ILLUSTRATIONS (continued)

LIST OF ILLUSTRATIONS (concluded)

LIST OF TABLES

1. SUMMARY

Optimum test methods for determining fatigue crack growth rates have been developed using an extensive state-of-the-art survey, experimental and analytical results of this study, and experience from a previous ASTM interlaboratory test program. These methods define procedures for generating, analyzing, and presenting data. The data generation procedures are specific to the magnitude of the growth rates being measured. A document describing test methods for use above 10^{-8} m/cycle has been formulated and established as an ASTM Tentative Test Method (ASTM E647-787). In addition, a document applicable to both high and low growth rates, was more recently formulated and is currently in the early stages of ASTM review. This consolidated test method is provided herein and is proposed as a modification to the aforementioned standard.

The different time tables followed by the two methods resulted from the additional development effort that was necessary for low growth rate testing. Here the optimum procedures require a specialized decreasing stress intensity technique consisting of either continuous or step decreases in applied cyclic loads. Experimentation was used to define acceptable rates of load shedding during the fatigue crack growth test which ensure that resulting data are independent of the loading history and efficiently generated. High growth rate testing consists of the more conventional increasing stress intensity technique for which constant-amplitude-cyclic loading is employed.

Information which is common to both high and low growth rate testing is provided on specimen preparation, loading fixtures, crack length measurement, analysis of results, data presentation, and reporting. Results from this study were used to establish requirements

which ensure that data can be properly analyzed using linear elastic fracture mechanics. These validity requirements consist of limits on minimum specimen sizes, out-of-plane cracking and nonstraight, through-thickness cracking. Definitions of terms related to testing were also formulated including an operational definition of the threshold stress intensity for fatigue crack growth.

The experimental effort of this program also provided an assessment of the individual and combined effects of load ratio, cyclic frequency, test temperature and environment on fatigue crack growth rates in a 10Ni steel and a 2219-T851 aluminum alloy.

Load ratio-effects were measured over a wide range of growth rates and are shown to be specific to material and growth rate regime. These effects can be non-linear, even in a given growth rate regime, thereby complicating interpolative procedures. The overall dependence of fatigue crack growth rates on load ratio suggests that these effects are controlled by several different underlying processes. It is demonstrated that a complete physical understanding of fatigue crack growth requires consideration of various crack tip plasticity phenomena, including stress relaxation ahead of the growing crack.

Data obtained at high growth rates show that interactions of temperature (from -100°F to 250°F), frequency (from 0.10 Hz to 200 Hz) and environment (dry argon versus laboratory air) can result in an order of magnitude change in growth rates in 2219-T851 aluminum. When results are represented in the form of an Arrhenius equation, this interaction is characterized by an apparent activation energy for crack growth in air which decreases with decreasing test frequency. Comparison data in dry argon show the temperature-frequency interaction to be caused by a sensitivity of the growth rates to water vapor in the air. Results on 10Ni steel were qualitatively similar; however, the observed changes in growth rates were never more than a factor of two.

A wide-range mathematical representation of fatigue crack growth rates is proposed. This new mathematical model has the following advantages over existing wide-range representations:

1) it consists of separate components which correspond to the three crack growth rate regions often observed, thereby facilitating modeling of load ratio effects which depend on growth rate regime.
2) it has no asympototic features, thus eliminating the prediction of "false" thresholds for fatigue crack growth and significant underestimates of cyclic lives at low growth rates.

2. INTRODUCTION

The fracture mechanics approach to the evaluation of fatigue crack growth behavior provides a valuable tool for establishing rational material selection and design criteria which are essential to assessing structural integrity and preventing failure. This technology provides a systems approach to structural integrity problems by integrating information on defect characterization, stress analysis, and materials properties consisting of fatigue crack growth rate data and fracture toughness data. A primary limitation to the use of this technology has been the absence of a standardized methodology for the generation and characterization of fatigue crack growth rate data. This limitation complicates the collection, comparison, and inter-laboratory exchange of data, thereby inhibiting evaluation of the effects of pertinent variables (e.g., mean stress, temperature, environment, test frequency, and alloy composition and microstructure) on crack growth rate performance.

The Air Force, recognizing the need to overcome this limitation, sponsored the current program through the Air Force Materials Laboratory, Wright-Patterson Air Force Base, Ohio. The program objective was to develop a standard fracture mechanics methodology for the generation, analysis and presentation of fatigue crack growth rate data. The intended use of this standard method will be as an Air Force specification as well as an industry-wide standard. Every effort was made to coordinate this program with the activities of ASTM in this same area. A similar coordinated effort between NASA and ASTM was responsible for the development of the ASTM Standard Method of Test for Plane Strain-Fracture Toughness of Metallic Materials (Designation E399) which is currently widely used by the Air Force and industry.

The scope of the program is limited to steady-state fatigue crack growth rates from fatigue threshold behavior to crack growth just prior to the onset of rapid, unstable fracture. The program has evaluated current test methods as well as developed new methods, where appropriate, using both analysis and experimentation. The experimental work has also provided extensive information on the individual and combined effect of temperature, loading frequency, environment and stress ratio on the fatigue crack growth rate behavior of two materials — a 10Ni steel and a 2219-T851 aluminum alloy.

The program is organized into five phases as follows:

- Phase I - State-of-the-art survey of fatigue crack growth testing and preparation of preliminary test method drafts. (Section 3)
- Phase II - Experimental program to provide a basis for the test methods, provide a data source for subsequent analyses and characterize test variables. (Section 4 and 5)
- Phase III - Review, analysis, and selection of adequate data processing techniques. (Section 6)
- Phase IV - Evaluation and development of methods for data presentation. (Section 7)
- Phase V - Synthesis of above four phases into a recommended standard methodology for generating, processing, and presenting fatigue crack growth rate data. (Section 3, Appendix I)

Interaction of these phases in the current program is illustrated in Fig. 1-1.

PROGRAM FLOW CHART

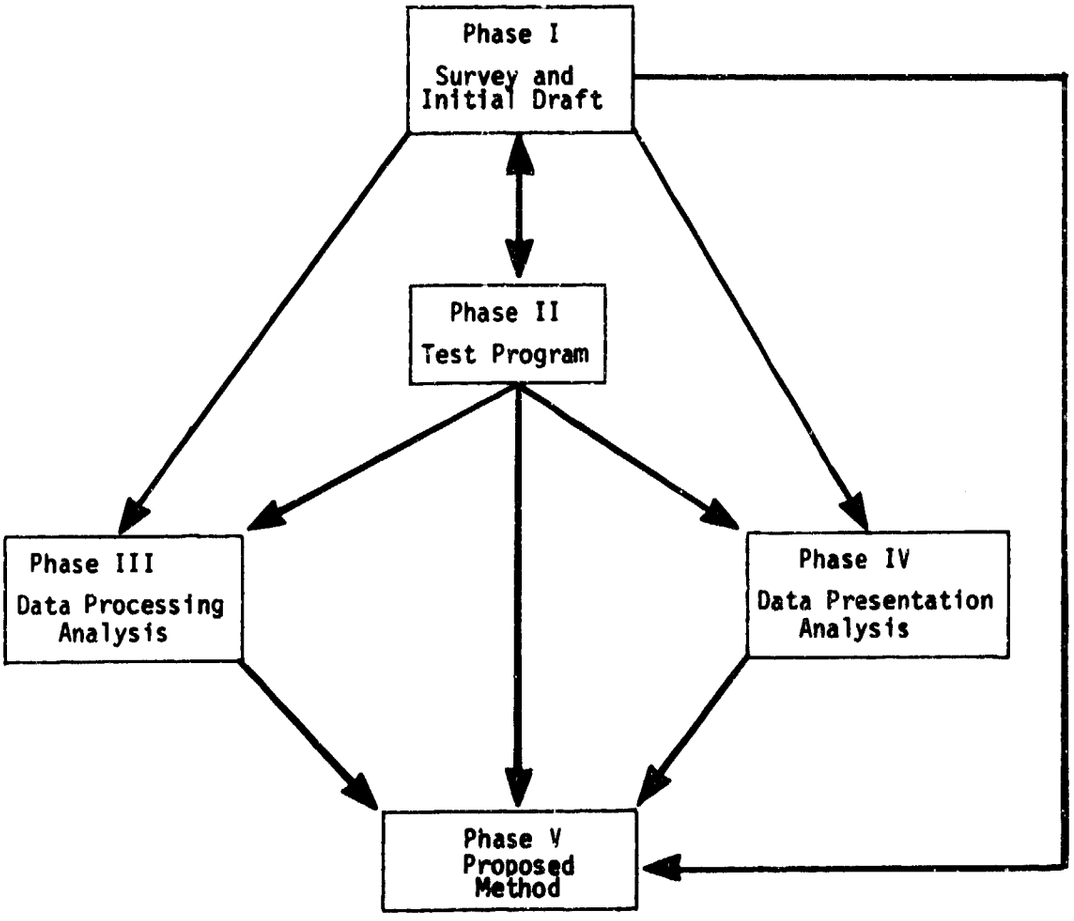

Fig.1-1 Flow chart illustrating interactions among the five phases of the program.

3. DEVELOPMENT OF STANDARD TEST METHODS

3.1 Background and Approach

An essential first step toward developing a standard test method was to assess the current state-of-the-art for generating, analyzing and reporting fatigue crack growth rate information. This task was accomplished by conducting a test method survey which consisted of two questionnaires — one on high growth rate testing ($da/dN > 10^{-7}$ in./cycle), the other on low growth rate testing ($da/dN < 10^{-7}$ in./cycle). Concurrently, a brief digest of a test method was formulated based largely on experience acquired from an ASTM cooperative, interlaboratory test program.[1] The intent of this digest was to define a clear starting point for the test method development, as well as to serve as a catalyst for comments and suggestions from the technical community.

The survey and digest was distributed to 57 individuals representing 49 laboratories throughout the United States, Canada and England. Those surveyed consisted primarily of U.S. Air Force contractors and members of ASTM Committee's E24 on Fracture Testing and E09 on Fatigue. Additional participants were also obtained by publicizing the survey at ASTM meetings. Table 3-1 provides a list of individuals and laboratories who responded to the survey. In some cases individuals from the same laboratory provided consolidated responses. Overall, 69% of the laboratories surveyed responded to the high growth rate questionnaire and 45% responded to the low growth rate questionnaire.

The questionnaire consisted of detailed questions which were organized into the following categories: 1) General Information, 2) Test Specimen Type and Preparation, 3) Testing Procedures, 4) Evaluation of Results, 5) Determination of Growth Rates, 6) Reporting Data and 7) Comments.

TABLE 3-1

LABORATORIES RESPONDING TO CRACK GROWTH QUESTIONNAIRES

J. M. Barsom	U.S. Steel Corp., Research Laboratory
R. J. Bucci/A. B. Thakker	Alcoa Laboratories
O. Buck/F. D. Frandsen	Rockwell International Corp., Science Center
P. J. Cain	MTS Systems Corp.
J. T. Cammett	Metcut Research Associates, Inc.
W. T. Chandler	Rockwell International Corp., Rocketdyne Div.
T. Crooker/G. Yoder/V. Sullivan	Naval Research Laboratory
E. J. Czyryca/H. P. Chu	U.S. Naval Ship R&D Center
D. B. Dawson	Sandia Laboratories
D. H. Dill/L. F. Impellizzeri/ J. J. Slavick	McDonnell Douglas Corp.
C. E. Feddersen	Battelle's Columbus Laboratories
J. P. Gallagher/H. D. Stalnaker	Wright-Patterson AFB, AFFDL
A. Gunderson	Wright-Patterson AFB, AFML
D. Hale	General Electric Co., San Jose
L. Hall	Boeing Aerospace Co., Research & Eng. Div.
W. D. Hanna	The Aerospace Corp.
D. W. Hoeppner	University of Missouri
J. P. Horsley	The Boeing Co., Wichita
S. J. Hudak, Jr. /J. D. Landes	Westinghouse R&D Center
F. A. Iannuzzi	Southern Research Inst.
L. H. James	Westinghouse Hanford Co.
G. A. Miller/H. S. Reemsynder	Bethlehem Steel Corp., Research Laboratories
B. Mukherjee	Ontario Hydro, Ontario, Canada
J. C. Newman, Jr.	NASA Langley Research Center
J. O'Donnell	Materials Research Laboratory
G. J. Petrak	University of Dayton Research Inst.
D. E. Pettit/J. T. Ryder/ W. E. Krupp/J. P. Sandifer	Lockheed-California Co.
L. P. Pook	National Engrg. Laboratory, Glasgow, Scotland
R. R. Seeley	Babcock & Wilcox Company
J. F. Throop	Watervliet Arsenal, Benet Weapons Laboratory
T. H. Topper	University of Waterloo, Ontario, Canada
F. M. Tovey	Garrett-Airesearch Co.
R. P. Wei	Lehigh University
R. E. Zinkham	Reynolds Metals Co.

An analysis of the survey responses showed a clear difference in the state-of-the-art of testing in the high and low growth rate regimes. It was concluded that for high growth rates there was sufficient testing experience and consistency of testing techniques to proceed with a detailed draft of a test method. However, the questionnaires indicated a relative lack of testing experience below growth rates of 10^{-7} in./cycle — especially for rates approaching a fatigue threshold at about 10^{-9} in./cycle. Furthermore, test methods in the low growth rate regime varied greatly and no consistent definition of a fatigue crack growth threshold existed. The survey results also identified specific areas, even at high growth rates, which were in need of development — most of these areas were related to the evaluation of data validity and included considerations such as specimen size requirements, limitations on out-of-plane cracking and uneven through-thickness cracking, and procedures to deal with through-thickness crack tunneling.

A complete summary and analysis of the survey response is contained in a report previously prepared under this program, Ref. (2).

3.2 Establishment of an ASTM Standard

Although the precise goal of this program was to develop fatigue crack growth rate test methods which could be used as a U.S. Air Force specification, the developing methods have been concurrently pursued as an ASTM Standard in order to promote the utility of the methods as an industry-wide concensus standard. This approach has led to a more rigorous document which has been scrutinized by a large number of technical experts.

Because of the difference in the state-of-the-art of testing in the high and low growth rate regimes, the test method development was specific to growth rate regime — thus, the pursuit of these methods as ASTM Standards followed different time schedules.

A detailed method for determining high growth rates was prepared and has undergone reviews within ASTM. This document

was subsequently transmitted to ASTM for balloting as a Tentative Method of Test.* Concurrent balloting of ASTM Committee E24 on Fracture Testing, Subcommittee E24.04 on Subcritical Crack Growth, Subcommittee E09.04 on Apparatus and Test Methods and Subcommittee E09.90, the executive subcommittee of Committee E09 on Fatigue, was completed by June 30, 1977. A vote tally is provided in Table 3-2.

TABLE 3-2

VOTE TALLY ON ASTM BALLOT E24.03 (77-3)

Committee E24			Subcommittee E24.04		
Affirmative:	124	(64%)	Affirmative:	69	(77%)
Negative:	14	(7%)	Negative:	8	(9%)
Abstaining:	57	(29%)	Abstaining:	13	(14%)
65.6% Return			66.2% Return		

Subcommittee E09.04/E09.90		
Affirmative:	29	(53%)
Negative:	6*	(11%)
Abstaining:	20	(36%)
61.8% Return		

*Note: Five of these votes are included in the E24 negative because of joint membership.

As indicated, balloting from each of the above groups satisfies the ASTM minimum return requirement of 60% of all voting members. Final action on this ballot, including resolution of negative votes, was completed in March, 1978. This high growth rate method, entitled "Tentative Test Method for Constant-Load-Amplitude Fatigue Crack Growth Rates above 10^{-8} m/Cycle" and designated ASTM E647-78T, is scheduled for publication in the 1978 Annual Book of ASTM Standards, Volume 10.

*A draft of this document as it was submitted for balloting was contained in a previous report under this program, Ref. (3).

After preparing an initial draft of a low growth rate test method, see Ref. (3), it became apparent that the high and low growth rate methods should eventually be consolidated since many features were common to both methods. A consolidated method has been formulated and is provided in Appendix I of this report. This proposed method is in the initial stages of review within ASTM and will subsequently be pursued as a modification to the aforementioned high growth rate standard.

Detailed discussions of the proposed method of Appendix I, including the basis for various specifications contained in the method, are given in subsequent sections of this report.

3.3 Recommendations on Future Standardization Efforts

It is not surprising that input from the test method survey indicated that the most important test variable is the environment in which the fatigue crack growth rate test is conducted. Since these effects are specific to the material-environment system and since no theory with quantitative predictive capability exists for environment enhanced fatigue crack growth, current efforts in this area largely consist of phenomenological characterizations. Conducting fatigue crack growth tests in aggressive environments, which must be contained around the specimen and chemically controlled, creates additional testing difficulties which were beyond the scope of the current program.

One of the most difficult testing problems is that of acquiring accurate crack length measurements on specimens which are generally obscured from view. Defining test procedures which eliminate the occurrance of significant periods of non-steady-state growth rates is also a problem which requires attention.[4-6] In addition, guidelines for acceptable environmental control — including tolerances on the control of temperature, pressure and chemical species, and avoidance of unwanted galvanic effects — need to be formulated.

These tasks are formidable and will require the efforts of several groups having different areas of expertise.

3.4 Elastic Compliance Expressions for Monitoring Crack Growth

A review and extension of information on elastic compliance for compact type (CT), center-cracked tension (CCT) and wedge-opening load (WOL) specimens has been made. Mathematical expressions have been formulated which 1) enable specimen compliance (or inversely, crack length) to be conveniently computed over a wide range of relative crack length and 2) have sufficient accuracy for use in monitoring crack length during crack growth tests. An algorithm has also been developed which enables these results to be utilized for convenient displacement measurement locations on the specimens, thus accommodating a variety of extensometer designs. The compliance technique for monitoring crack length provides an alternative to visual crack length measurements and therefore is of great utility for testing in aggressive environments where visual crack length measurements may be impossible. This information is intended to supplement the proposed test method.

These results have been given in detail in a previous report prepared under this program.[3] For completeness, results for several convenient measurement locations are provided in Table 3-3 and 3-4.* Table 3-3 lists the coefficients of the equations which represent the normalized elastic compliance, BEV_X/P, as a function of the relative crack length, $\alpha = a/W$. The term E is Young's modulus and B is the specimen thickness; measurement locations are defined in Figs. 3-1 and 3-2. Table 3-4 provides the inverse of the relationships given in Table 3-3 and is convenient for directly calculating crack length from measurements of applied load and specimen deflection obtained during a crack growth test.

*The equation representing the elastic compliance for CCT specimens is given in Section 4.3.3.

TABLE 3-3

WIDE-RANGE ELASTIC COMPLIANCE EXPRESSIONS FOR CT AND WCL SPECIMENS

Meas. Location	X/W	b_o	b_1	b_2	b_3	b_4	b_5	b_6	b_8
					CT Specimen				
V_{X1}	-0.345	1.6396	11.020	-6.4495	-31.114	47.251	-18.343	--	--
V_0	-0.25	1.6137	12.678	-14.231	-16.610	35.050	-14.494	--	--
V_1	-0.1576	2.5376	3.9043	22.443	-91.534	107.40	-40.792	--	--
V_{LL}	0	2.1630	12.219	-20.065	-0.9925	20.609	-9.9314	--	--
					WOL Specimen				
V_{X1}	-0.3294	4.1765	-37.948	367.21	-1351.0	2574.4	-2654.4	1242.5	-141.16
V_0	-0.2549	4.3838	-37.588	359.68	-1319.5	2506.8	-2577.0	1203.5	-136.40
V_1	-0.1576	5.0339	-40.072	361.64	-1306.8	2459.19	-2508.6	1164.5	-130.98
V_{LL}	0	0.63670	41.438	-181.26	527.8	-992.19	1029.5	-468.52	46.596

$$\frac{BEV_X}{P} = \left[1 - \frac{X/W}{\alpha}\right]\left[\frac{1+\alpha}{1-\alpha}\right]^2 [b_o + b_1\alpha + b_2\alpha^2 + b_3\alpha^3 + b_4\alpha^4 + b_5\alpha^5 + b_6\alpha^6 + b_8\alpha^8]$$

$\alpha = a/W$

TABLE 3-4

NORMALIZED CRACK LENGTH AS A FUNCTION OF ELASTIC COMPLIANCE FOR CT AND WOL SPECIMENS

Meas. Location	X/W	C_o	C_1	C_2	C_3	C_4	C_5
				CT Specimen			
V_{X1}	-0.345	1.0012	-4.9165	23.057	-323.91	1798.3	-3513.2
V_0	-0.250	1.0010	-4.6695	18.460	-236.82	1214.9	-2143.6
V_1	-0.1576	1.0008	-4.4473	15.400	-180.55	870.92	-1411.3
V_{LL}	0	1.0002	-4.0632	11.242	-106.04	464.33	-650.68
				WOL Specimen			
V_{X1}	-0.3294	1.0020	-5.1122	39.431	-751.19	4928.6	-10465.0
V_0	-0.2549	1.0021	-4.9472	35.749	-649.85	4110.9	-8410.8
V_1	-0.1576	1.0015	-4.664	29.660	-514.71	3126.7	-6115.6
V_{LL}	0	1.0004	-4.1200	15.202	-228.94	1253.2	-2118.8

$$\alpha = a/W = C_o + C_1 u_X + C_2 u_X^2 + C_3 u_X^3 + C_4 u_X^4 + C_5 u_X^5$$

$$u_X = \left\{ \left[\frac{BEV_X}{P} \right]^{1/2} + 1 \right\}^{-1}$$

Dwg. 6390A96

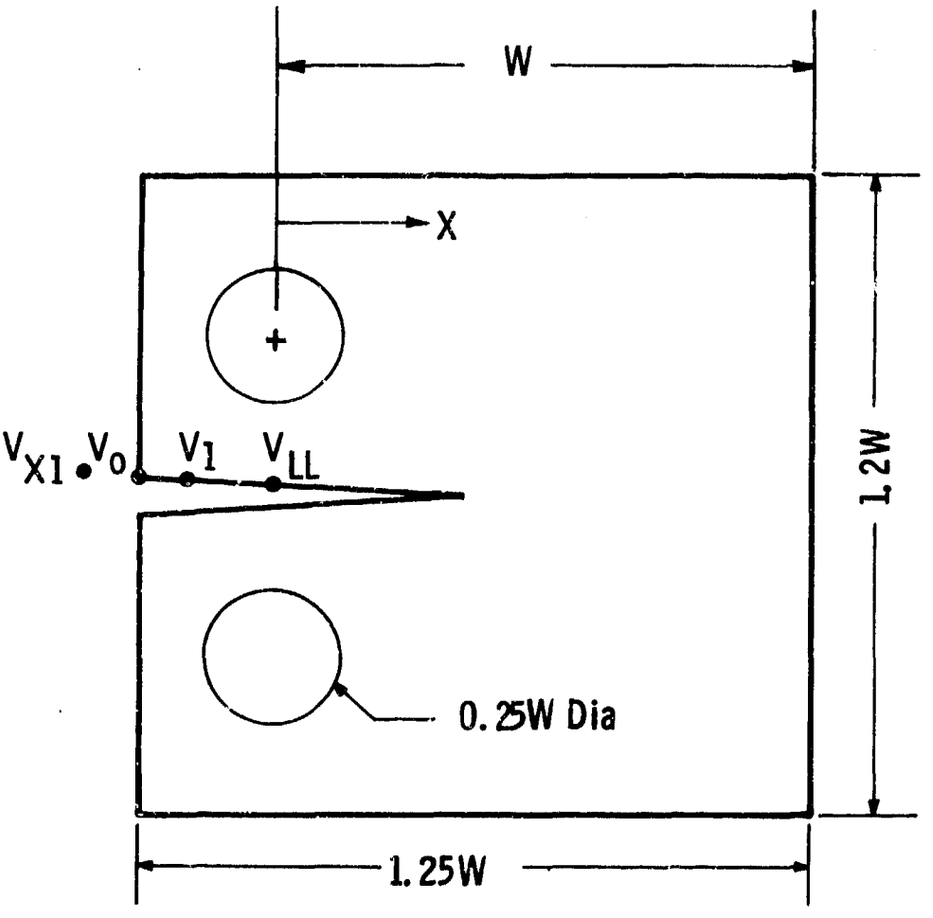

Fig. 3-1— Planar geometry of a compact type (CT) specimen showing the various deflection measurement locations

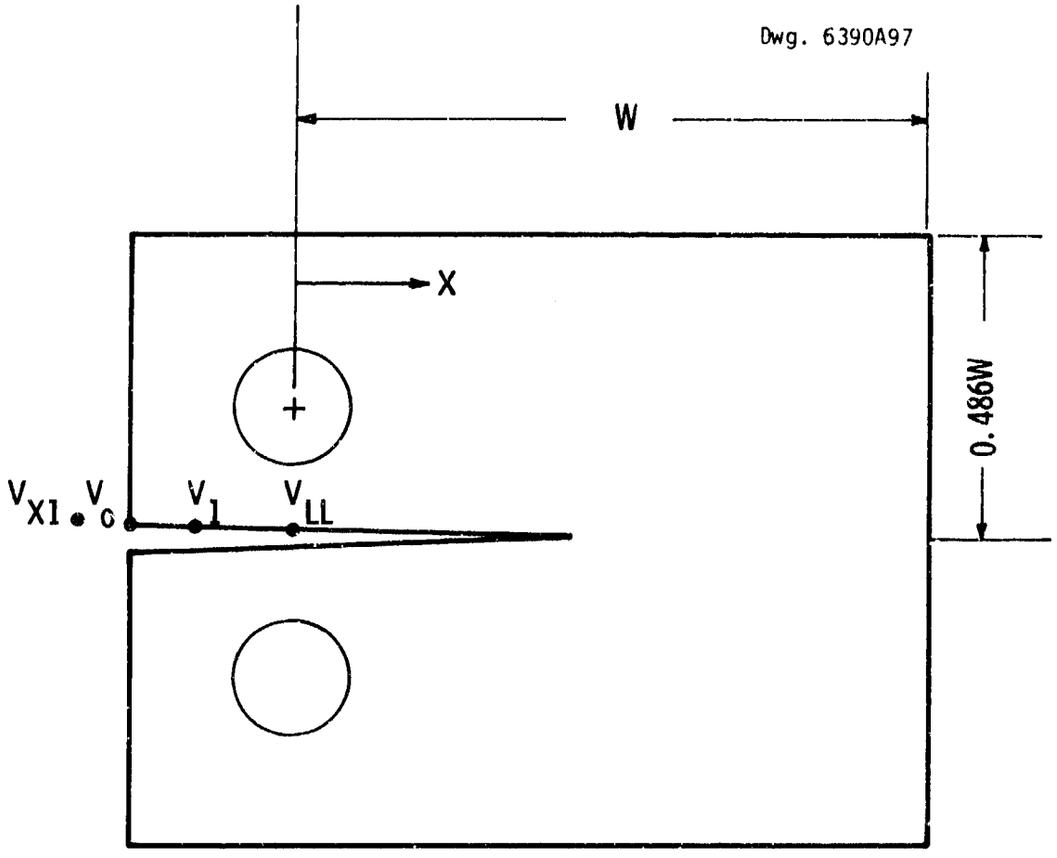

Fig. 3-2— Planar geometry of WOL specimen showing the various deflection measurement locations

4. FATIGUE CRACK GROWTH RATE TEST RESULTS

Wide-range fatigue crack growth rate data were generated on a 190 ksi yield strength 10Ni-8Co-1Mo steel and a 50 ksi yield strength 2219-T851 aluminum alloy. The objectives of the experiments were to: 1) provide support for the general utility of the proposed fatigue crack growth rate test method of Appendix I, 2) establish a reliable wide-range data base for use in fatigue crack growth rate modeling and 3) assess the individual and combined effects of load ratio, test temperature and cyclic frequency on fatigue crack growth rates.

Results on the effect of specimen planar geometry, gage length, thickness, and crack tunneling are also contained in this section. Where appropriate, results are discussed in relation to the proposed test method of Appendix I. Information, both generated in this study and extracted from the literature, related to the establishment of specimen size requirements is provided in Section 4.4.

Additional fatigue crack growth rate data are summarized in Section 5 — these data were obtained while developing specialized test techniques necessary for measuring low growth rates.

4.1 Materials

Two materials were tested in this program: a 190 ksi yield strength 10Ni-8Co-1Mo steel and a 50 ksi yield strength 2219-T851 aluminum alloy. The 10Ni steel is the same material which was previously examined as part of an ASTM cooperative, interlaboratory program on fatigue crack growth rate testing.[1] Thus, further testing of this material in the current program provides a natural extension of the previous work.

Two widely different structural alloys were selected for study, rather than a single material, since the influence of variables such as load ratio were expected to be material dependent. Thus, subsequent analyses of the data, including fatigue crack growth modeling, would provide more general results.

The 10Ni steel was supplied as an 87- by 59- by 1 in.-thick plate. The 2219-T851 aluminum was supplied as a 59- by 43- by 3-3/16-in.-thick plate. The chemical composition and mechanical properties for the two plates are summarized in Table 4-1. The chemical composition and mechanical properties of the 2219-T851 aluminum alloy are typical of commerically produced 3-in.-thick plate. In addition, note that both plate materials have uniform mechanical properties in the longitudinal and transverse direction.

All fatigue crack growth rate measurements on these plate materials were obtained with cracks propagating in the L-T orientation.

4.2 Experimental Procedures

Except where noted, all testing was conducted according to the proposed test procedures of Appendix I. Both 2-in.-wide compact (CT) specimens, Fig. 4-1, and 3-in.-wide center-cracked-tension (CCT) specimens, Fig. 4-2, were employed for tests conducted in laboratory air (40-60% RH). Dry argon tests were conducted using 2.5-in.-wide WOL specimens. Test specimens were nominally ¼-in.-thick, except for several tests on 1-in.-thick specimens designed to examine the influence of thickness on fatigue crack growth rates. All specimens were fatigue precracked at least 0.10 in. from the machined starter notch to ensure that subsequent data were unaffected by the notch geometry and notch preparation procedure. Precracking was performed such that the final K_{max} during precracking was less than or equal to the initial K_{max} for testing. In addition, low growth rate tests were precracked at the same load ratio as that used in subsequent testing.

TABLE 4-1

CHEMICAL COMPOSITION AND MECHANICAL PROPERTIES OF TEST MATERIAL

Chemical Composition, Wt %

Material	C	Si	Mn	Mg	S	P	Cr	Zn	Ti	Cu	Ni	Mo	Al	Fe
10Ni Steel	0.12	0.07	0.28	--	0.006	0.008	2.03	--	--	8.07	10.29	1.03	--	Bal.
2219-T851 Aluminum	--	0.088	0.25	0.003	--	--	<.0001	0.025	0.051	6.28	--	--	Bal.	0.25

Room Temperature Mechanical Properties*

Material	Orientation	0.2% σ_{ys} (ksi)	σ_{ult} (ksi)	% Elong. (in 2 in.)	% Red. in Area
10Ni Steel	long.	190 (188-192)	197 (195-200)	17 --	69 (68-69)
	trans.	190 (188-192)	196 (195-200)	17 --	69 (68-69)
2219-T851 Aluminum	long.	52 (51-53)	66 (64-68)	8.5 (7.3 - 9.3)	19 (15-20)
	trans.	51 (50-53)	66 (61-68)	8.2 (7.3 - 8.9)	19 (18-20)

*Steel results: average of 8 tests from 4 locations
Aluminum results: average of 6 tests from 2 locations } range of results given in brackets

Dwg. 6425A13

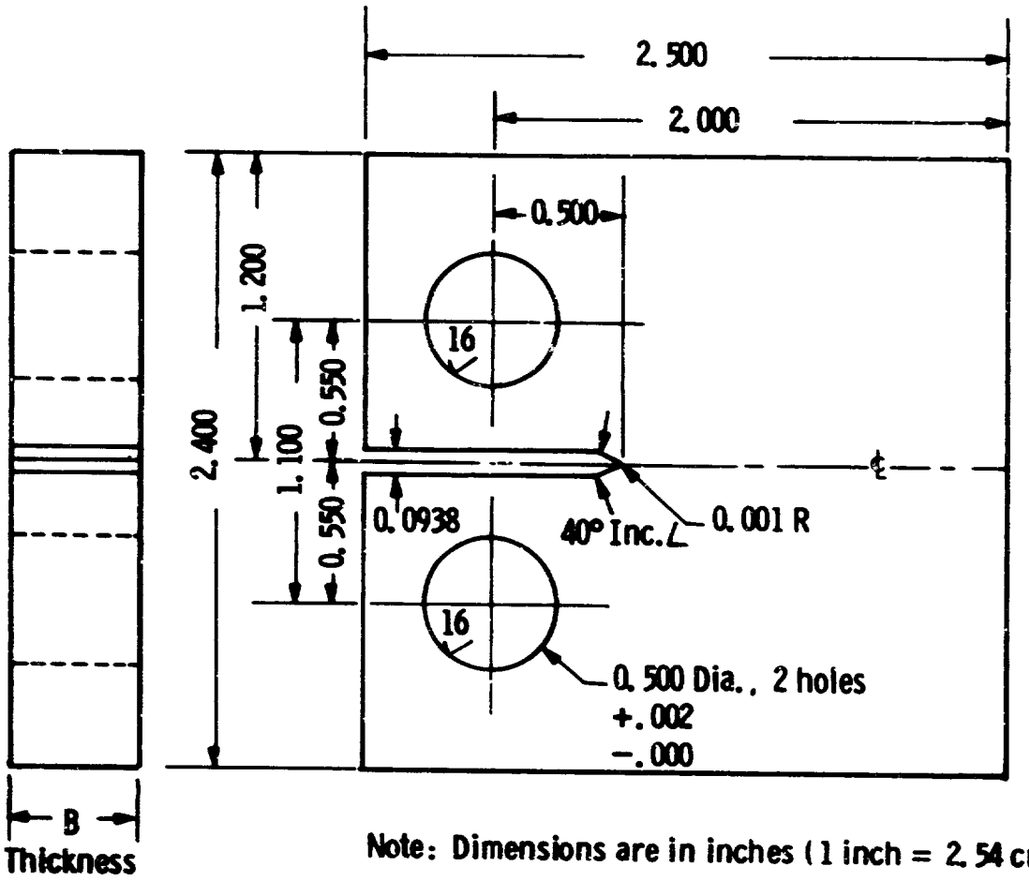

Note: Dimensions are in inches (1 inch = 2.54 cm)

Fig. 4-1— Compact type (CT) fatigue crack growth specimen

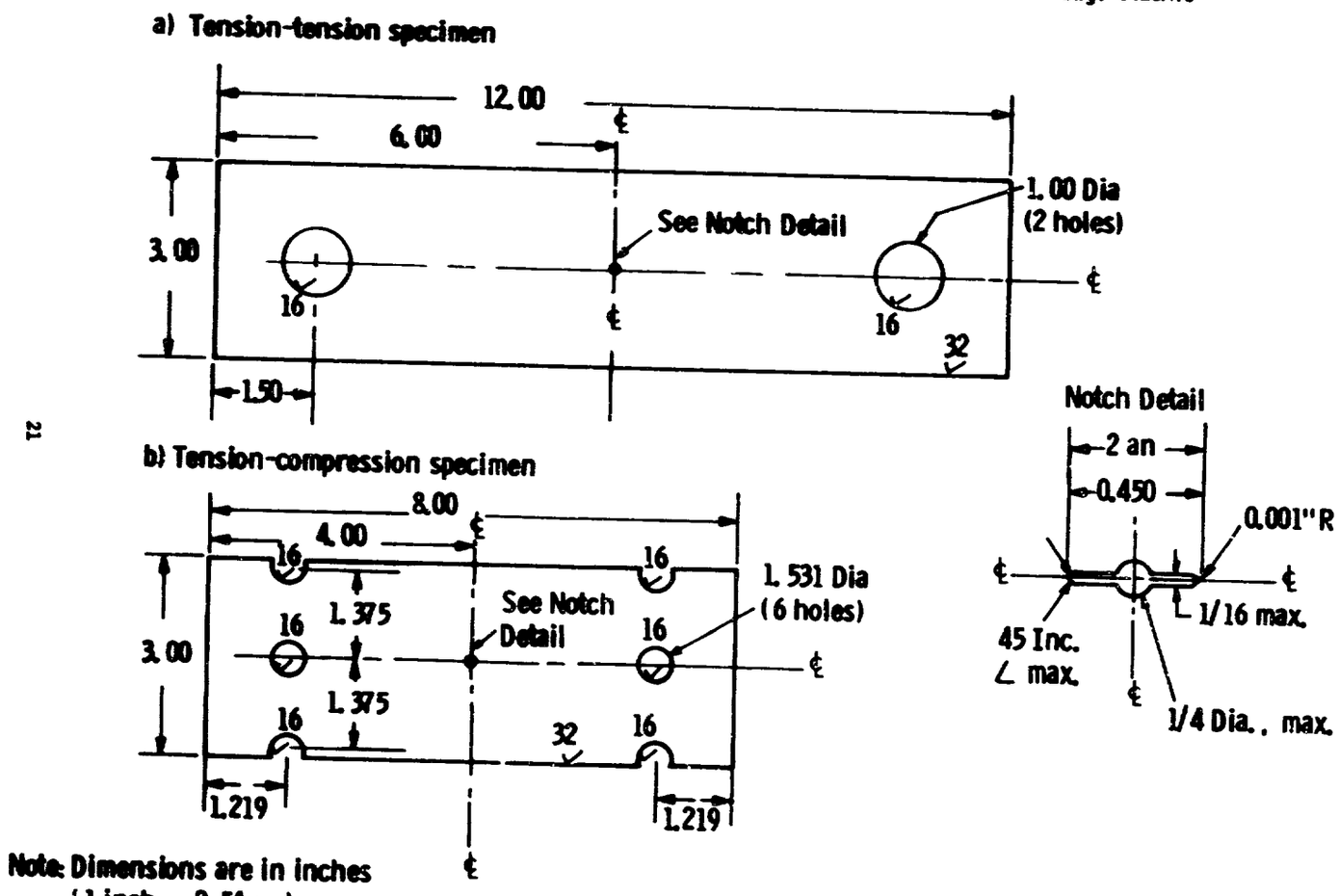

Fig. 4-2— Center cracked tension (CCT) specimens for fatigue crack growth rate testing under a) tension-tension loading and b) tension-compression loading

Tests were conducted using servohydraulic equipment operated in either load or deflection control. A sinusoidal waveform with test frequencies ranging from 0.10 Hz to 200 Hz was employed. Load accuracy over these frequencies was better than $\pm$ 2%.

Certain test details differed slightly for measurements at high growth rates, low growth rates, and in dry argon. Most of these differences served to optimize testing in each area — specific details are provided below.

4.2.1 High Growth Rate Test Details

All high crack growth tests were conducted on a 20 kip capacity servohydraulic machine. A calibrated load range of 2 kips was used when testing CT specimens. Load precision was periodically monitored using an oscilloscope. The amplitude measurement system had peak reading capability and an amplitude controller which could automatically overprogram the servohydraulic system to maintain load accuracy as the crack grew in high frequency tests.

Crack length was monitoed using visual measurements aided by scribe lines on the specimen and a 30X traveling telescope. With this system it is estimated that the crack length could be measured within $\pm$ 0.002 in. Crack length versus elapsed cycles data were converted to crack growth rates using a seven point, incremental polynomial technique which is described in Appendix I.

Low temperature tests were conducted using a liquid nitrogen cooled cryostat; high temperature tests were conducted using resistance heating tapes. An automatic controller maintained test temperatures within $\pm$ 5°C. Insulating chambers for both high and low temperature tests were equipped with windows for visual observation of crack growth.

4.2.2 Low Growth Rate Test Details

All low crack growth rate tests using CT specimens were conducted on a 5 kip capacity servohydraulic system and tests using CCT specimens were conducted on a 10 kip capacity system. Fully

calibrated load ranges of 500 and 1000 lb were used for all tests using CT specimens. Load precision was monitored by oscilloscope and digital voltmeter readings taken at about 10 to 15 minute intervals. Minor modifications to test machine controls were made as necessary by the test technicians to ensure load precision within $\pm$ 2% on P_{max} and ΔP. To shorten the test time, most data was established at the maximum machine frequency at which the required load accuracy could be maintained. The optimum operating frequency varied with test conditions and crack length. However, this procedure was justified by showing that frequency effects were minimal over the range of frequencies and low growth rates considered in this phase of the investigation (see Section 5.4). Further guidelines for the optimization of non resonant servohydraulic test machine operation at high frequency are given in Ref. 6a. Proper alignment of the load train and specimen were found to be essential for determining reproducible crack growth rate data. Therefore, in this study careful attention was given to achieving as fine as possible alignment of the test components involved.

Crack length measurement consisted of magnified visual observation of the crack as it passed through a series of precision grid lines, 0.02 in. (0.5 mm) spacing, photographically printed to the specimen surfaces. The optical system was capable of resolving crack extension to within $\pm$ 0.002 in. Conversion of crack length vs. elapsed cycles to crack growth rate, da/dN, was accomplished by the secant method described in Appendix I.

Some tests were conducted using conventional techniques in which K increased as the crack extended, namely, constant-amplitude load control. Other tests employed techniques in which K decreased as the crack extended, specifically, programmed load shedding and constant amplitude deflection control. Programmed load shedding was conducted as a series of discrete load steps as illustrated by Fig. 7 of Appendix I. A comparison of these methods is provided in Section 5.

4.2.3 Dry Argon Test Details

Tests were conducted in ultra high purity argon that was further dihumidified by using cold traps of -220°F. Additional purification was accomplished using a titanium sublimation pump. Oxygen and water vapor in this environmental system are estimated to be less than 1 ppm.

Crack length measurements in the argon environment were made using a d.c. electrical potential system. The resolution of this system for the working current and specimen geometry used is estimated to be better than $\pm$ 0.002 in. This method has been shown to agree well with other crack measurements techniques for various materials.[7] Additional information on this procedure, including the experimental calibration for the WOL specimen are given in Ref. (8).

4.3 Results and Discussion

4.3.1 Effects of Specimen Planar Geomtry/Selection of Standard Specimens

Comparison data on the effect of specimen planar geometry were obtained on 2219-T851 using 2-in.-wide CT specimens and 3-in.-wide CCT specimens. As shown in Fig. 4-3 and 4-4 data from these two specimen types are in excellent agreement over a wide range of growth rates and loading conditions. Similar results showing the independence of da/dN vs. ΔK behavior on specimen planar geometry are illustrated by the 10Ni steel data given in Fig. 4-5. Results from CT specimen are shown to agree with previous data from an ASTM cooperative inter-laboratory test program in which data were obtained on 3-in.-wide CCT specimens and 2.55-in.-wide wedge-opening-loaded (WOL) specimens.[1]

The planar geometry independence of fatigue crack growth rate data, when properly analyzed in terms of linear-elastic fracture mechanics, has been demonstrated for a wide variety of other geometries and materials (for example, see Refs. (1,9-11)). Thus, data from different specimen configurations and loading conditions can be exchanged and compared. More importantly this feature enables da/dN-ΔK information to be used quantatively in design.

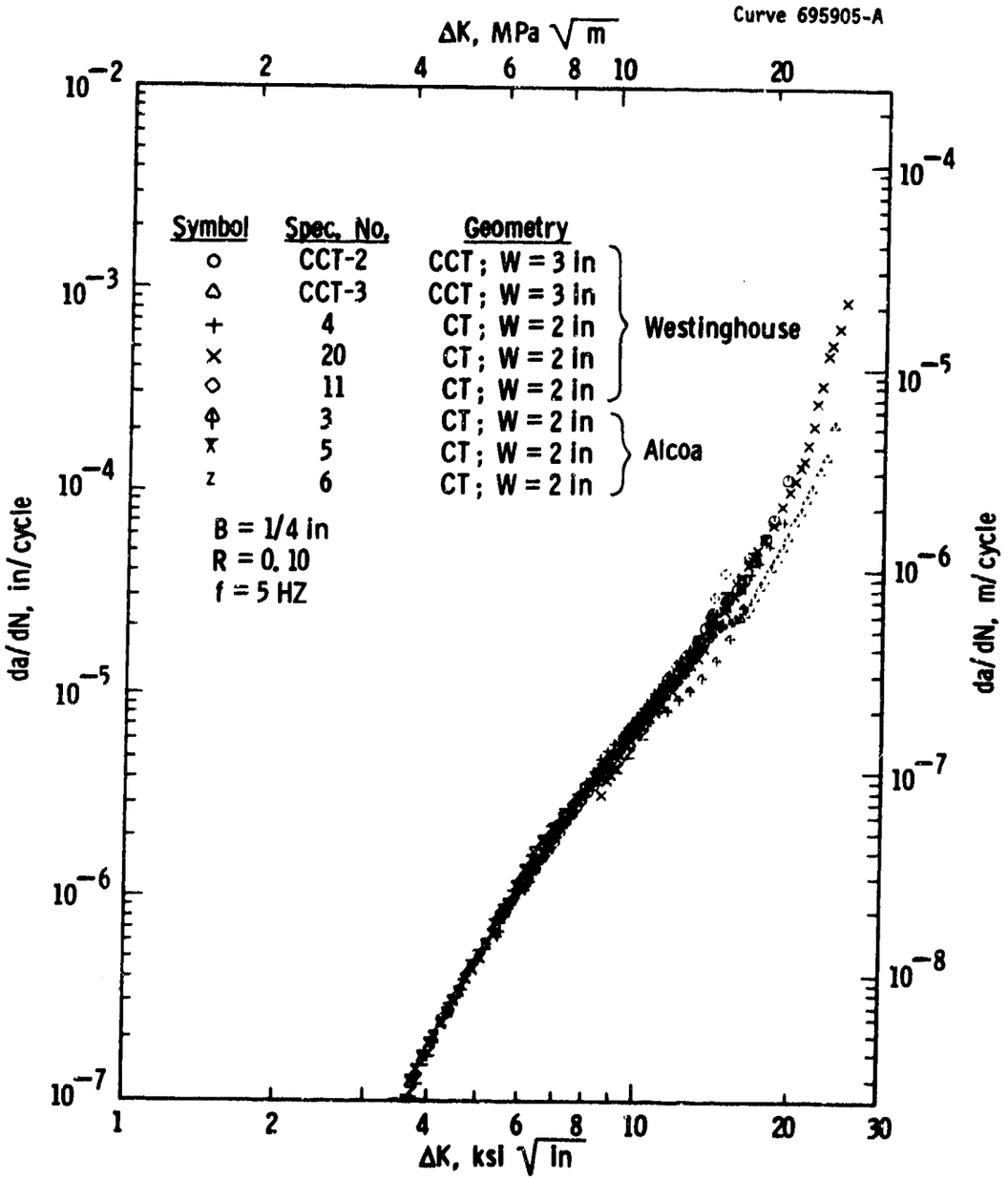

Fig. 4-3—Comparison of fatigue crack growth rates in 2219-T851 aluminum obtained using compact type (CT) and center-cracked-tension (CCT) specimens

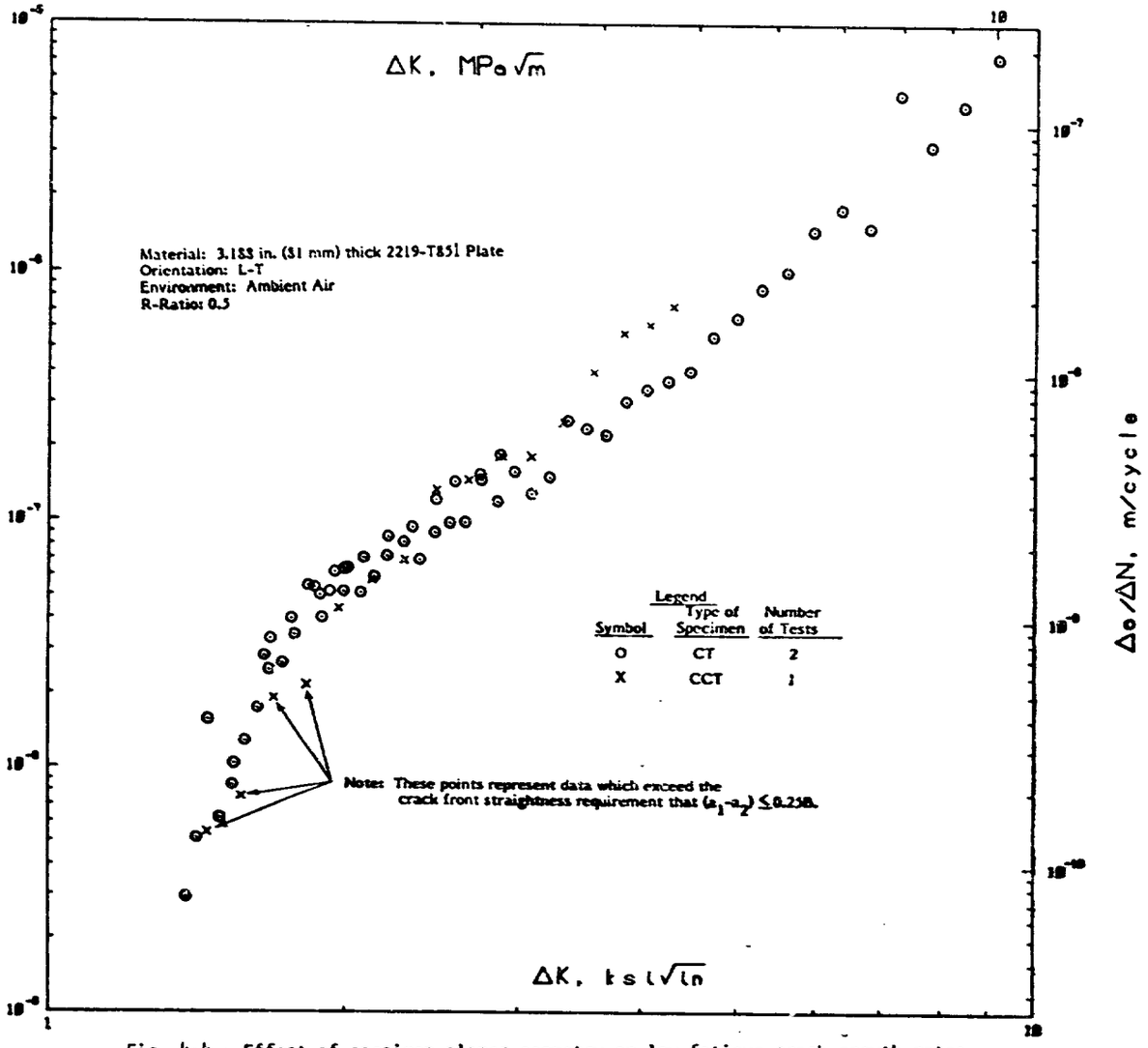

Fig. 4-4 - Effect of specimen planer geometry on low fatigue crack growth rates

Curve 695904-A

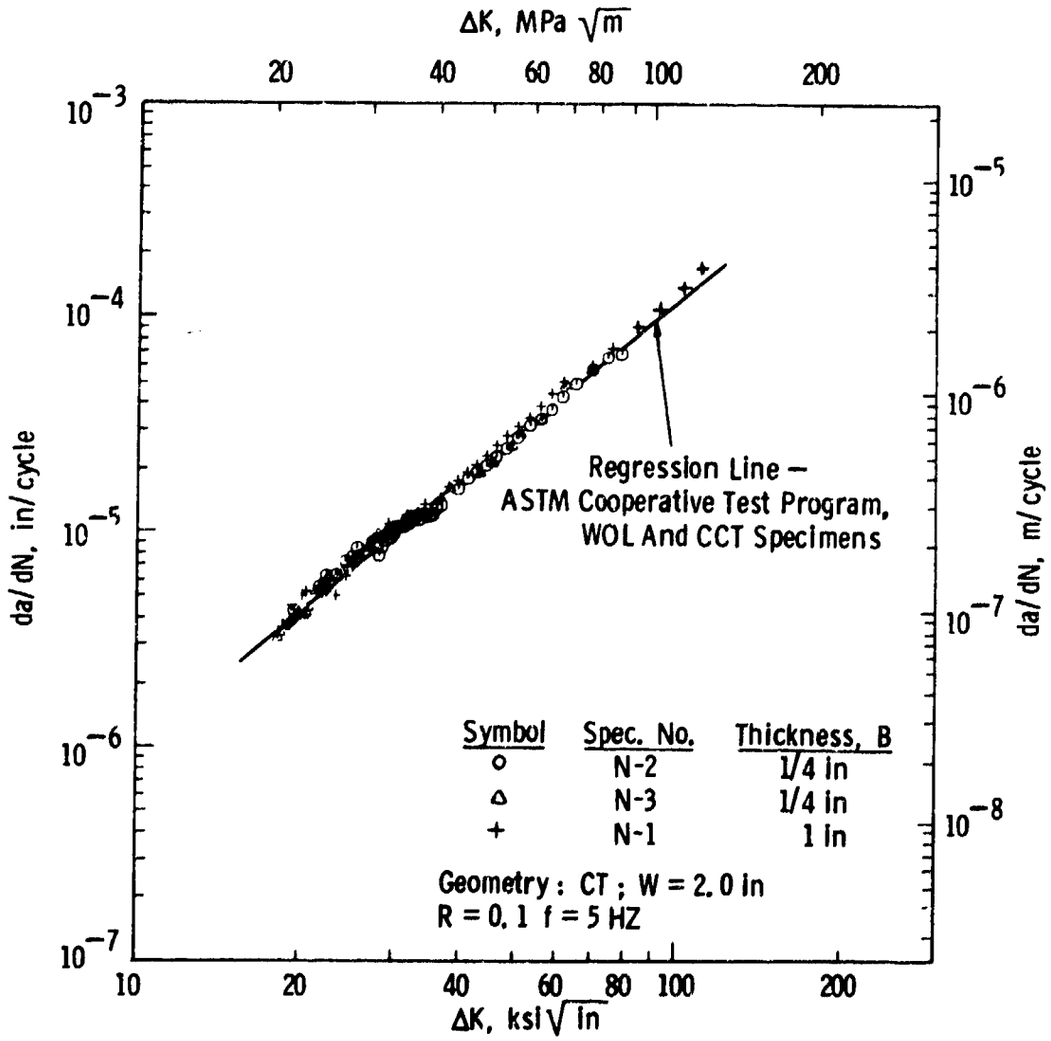

Fig. 4-5—Fatigue crack growth rates in 10 Ni steel obtained from various specimen geometries

Ideally, these results show that specimens of any configuration may be employed to generate fatigue crack growth rate data. Realistically, however, a limited number of specimen types are preferred. The proposed test method provides detailed information on compact specimens and center-cracked-tension (CCT) specimens — these are the most widely used specimen geometries based on the test method survey conducted as part of this program.[2] Alternative specimen geometries are allowed in the proposed test method provided well-established stress intensity calibrations are available. However, since the uncracked ligament size requirement is specific to specimen type, a verification that linear elastic conditions are being met in the alternative specimen is necessary. Because of this complication, especially when testing at high ΔK and R values, it is simpler to avoid alternative specimens.

Of the various compact-type specimens (that is the CT with $H/W = 0.60$, and the WOL with $H/W = 0.486$), the CT specimen was selected for inclusion in the proposed test method. The primary reason for selecting this specimen is the fact that for constant-amplitude loading its K gradient, dK/da, is steeper than that of the WOL specimen at small a/W values, thus reducing the time required to generate the same amount of da/dN-ΔK data. This difference in dK/da is illustrated in Fig. 4-6 where non-dimensional K values are shown for the two specimens types as functions of a/W, the nondimensional crack length. The shallowness of the initial segment of the curve for the WOL specimen results in an overabundance of (a,N) points during the early stage of the test which corresponds to a very narrow range of ΔK. This undesirable situation is improved when testing the CT specimen. Additional factors which favor the CT specimen are: 1) its use in ASTM E399, thus unnecessary test specimen proliferation is reduced, 2) its planar dimensions scale proportionally with increasing size, thus one non-dimensional drawing can be used to specify any size specimen (unlike the currently used WOL specimens) and 3) its larger H/W provides increased resistance to out-of-plane cracking and arm break-off — this is particulary helpful at high loads and when testing in aggressive environments where this problem is accentuated.

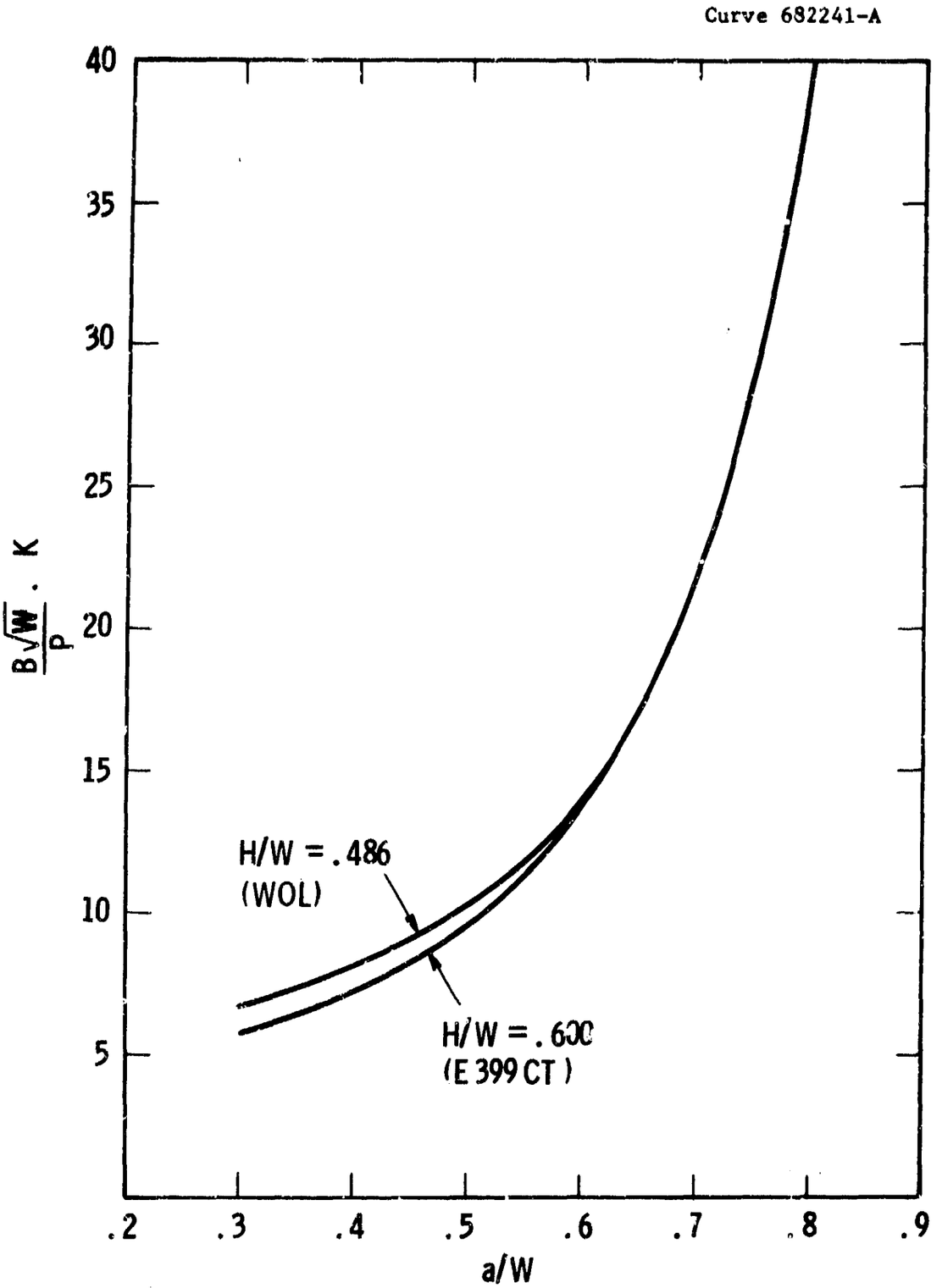

Fig. 4-6-- Comparisons of K - expressions for WOL and CT specimens as a function of relative crack length

4.3.2 Effect of Crack Tunneling/Specimen Thickness

Post-fracture analyses of fatigue crack growth specimens showed that through-thickness crack curvature — that is, crack "tunneling" — occurred in both the 2219-T851 aluminum and the 10Ni steel. The extent of crack tunneling was found to be strongly dependent on the ratio of specimen thickness-to-width, B/W, as shown in Fig. 4-7. Here δa is defined as the difference between the average surface crack length and the 5-point, through-thickness average crack length. For B/W values of 1/8 to 1/12, the extent of tunneling (normalized with respect to W) was observed to be nearly independent of crack length. These results represent a wide range of ΔK and R values, and include data from K-increasing and K-decreasing tests. Thus, when B/W is sufficiently small, the extent of crack tunneling is minimal and remains nearly constant throughout the test.

On the other hand, CT specimens with B/W = ½ exhibited significantly more tunneling than specimens with B/W ≤ 1/8. Furthermore, the extent of tunneling at B/W = ½ increased markedly as the tests proceeded. No measurable difference was observed in the extent of tunneling between the 2219-T851 aluminum and the 10Ni steel. This observation is probably due to the fact that all data collected on specimens with B/W = ½ covered the same range of growth rates. Thus, the correlation between the extent of tunneling and crack length is not expected to be a general feature of this phenomenon. However, when significant tunneling occurs (as for the case of B/W = ½) over a range of loading conditions, it is expected that a general correlation would exist between the extent of tunneling and K_{max} — or K_{max}/E when different materials are involved, where E is the materials elastic modulus.

The occurrence of significant crack tunneling was also detectable from measurements of elastic compliance on specimens with B/W = ½. These measurements were made along with surface crack length measurements during a fatigue crack growth rate test. As shown in Fig. 4-8 the experimental and analytical compliance results are in good

Curve 692930-A

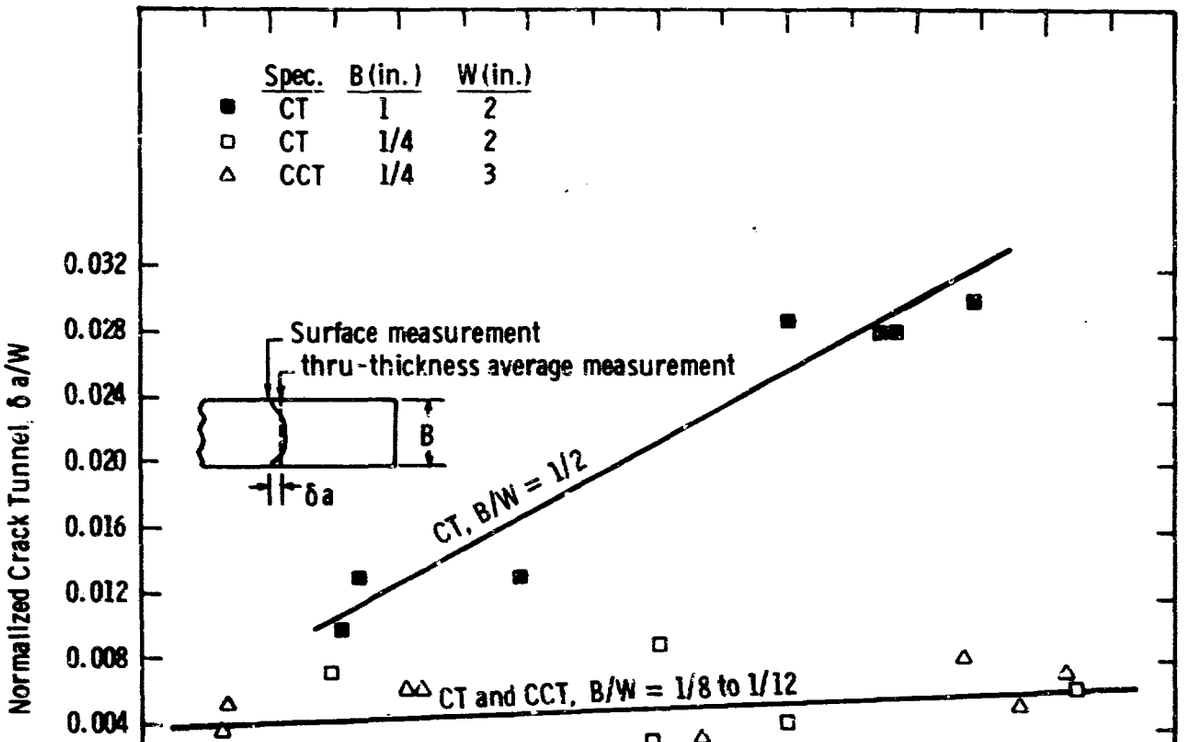

Fig. 4-7 – Extent of crack tunneling as a function of crack length for specimens of various thicknesses

Curve 692926-A

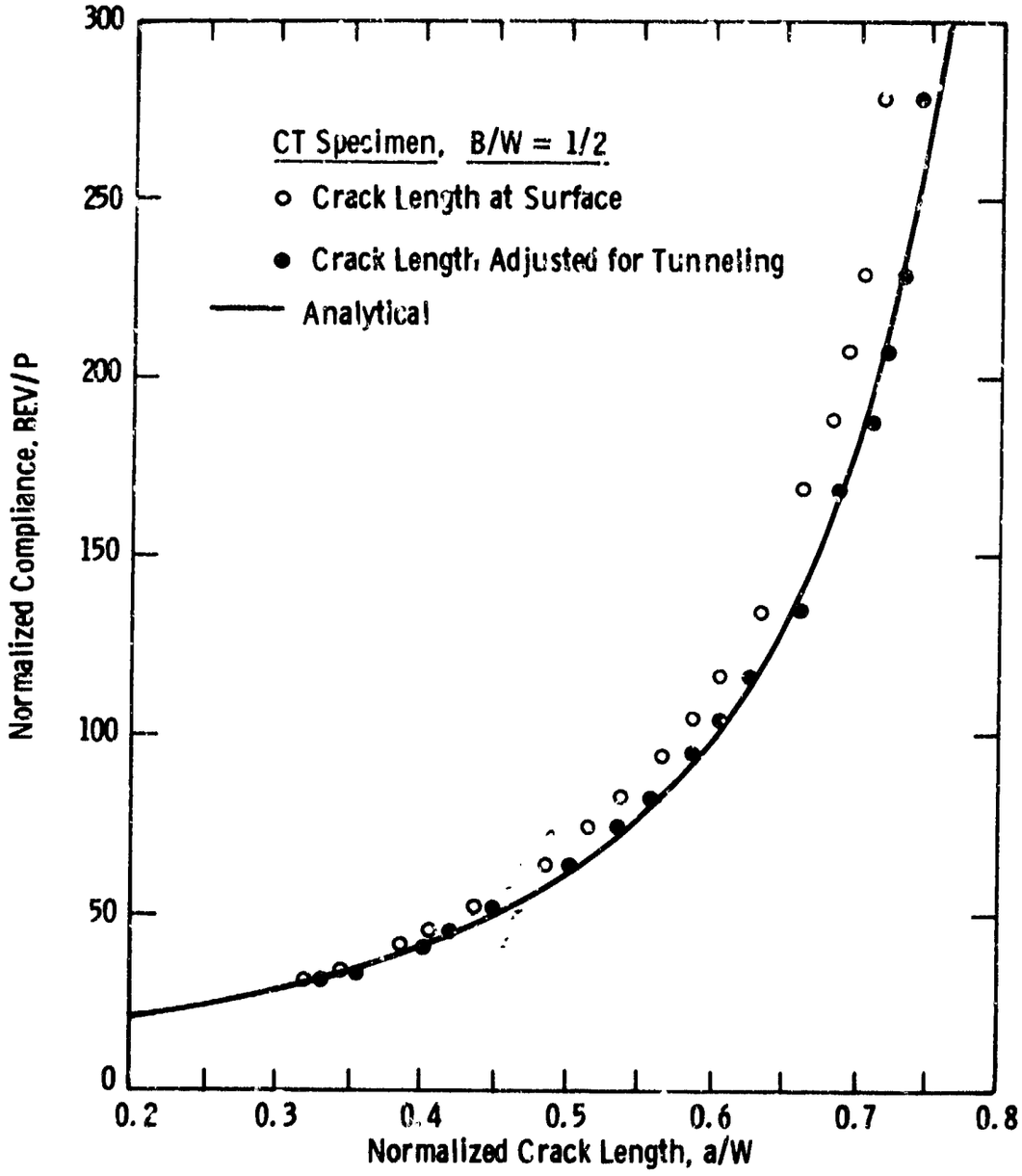

Fig. 4-8— Effect of crack tunneling on experimental versus analytical compliance in CT specimens

agreement provided an adjustment for crack tunneling is applied to the surface crack length measurements.

In some cases, the use of a surface crack length instead of a through-thickness, average crack length can result in significantly different computed K values. The difference between these two computational procedures is illustrated in Fig. 4-9 where the K for the "tunneled crack" is computed using the δa/w values of Fig. 4-7. Since the stress intensity factor based on a through-thickness, average crack is more representative of the crack tip "driving force", the ratio, K (tunneled crack)/K (surface crack), can be viewed as an error in computed K during a crack growth rate test. As shown in Fig. 4-9, these errors become significant for B/W = ½ and for large crack lengths.

If uncorrected, the errors in computed stress intensity factor cause an apparent increase in the fatigue crack growth rates.* The calculations in Table 4-2 demonstrate the factor by which da/dN is increased due to the tunneling errors of Fig. 4-7. As shown, the magnitude of the effect is also related to n, the exponent in the power law $da/dN = C_o(\Delta K)^n$. The n values of Table 4-2 are typical of aluminum alloys in the very high growth rate regime. The large influence on da/dN which can occur when B/W = ½ demonstrates the need to properly account for crack tunneling.

The above crack tunneling information is reflected in two Sections of the proposed test method in Appendix I. Section 7.1.3, Appendix I, provides a recommended range of B/W values which is designed to eliminate crack tunneling problems. However, B/W values as large as one-half are allowed in CT specimens, primarily to enable valid fatigue crack growth rate data to be obtained prior to fracture toughness testing (see ASTM E399). Although, a caution is provided for

*The increase in crack tunneling which occurs during a test is gradual enough so as not to directly affect da/dN.

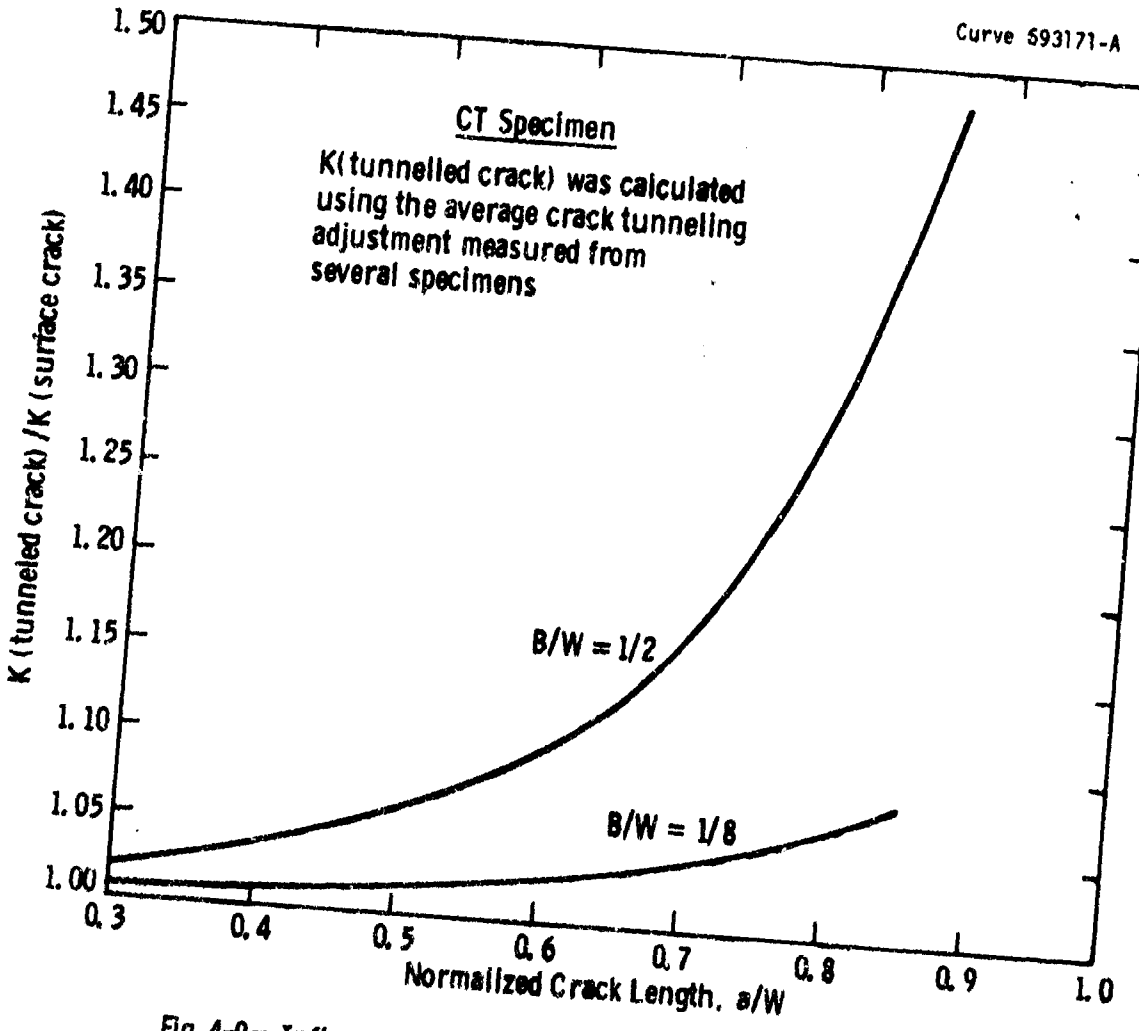

Fig. 4-9-- Influence of recommended crack tunneling adjustment on calculated stress intensity factor, K

TABLE 4-2

INFLUENCE OF CRACK TUNNELING IN CT SPECIMENS ON APPARENT FATIGUE CRACK GROWTH RATE

a/W	Factor by which da/dN appears increased			
	n=6	n=8	n=10	n=12
		B/W = ½		
0.6	1.77	2.14	2.59	3.14
0.7	2.63	3.63	5.02	6.93
0.8	5.53	9.79	17.3	30.6
		B/W = 1/8		
0.6	1.19	1.27	1.34	1.43
0.7	1.26	1.37	1.48	1.60
0.8	1.42	1.59	1.79	2.09

n = slope of log da/dN-log ΔK in a given growth rate regime.

those finding it necessary to use these large-B/W specimens. For cases where tunneling occurs, Section 9.1, Appendix I, specifies the procedure to be employed to: 1) measure the extent of through-thickness crack curvature, 2) decide when corrections are necessary and 3) apply the measured corrections to the data analysis.

It is appropriate to note that, based on the experiences of this study, crack tunneling measurements from the crack contours on the fracture surface can be difficult to resolve. In addition, the application of these corrections to the data is a time consuming process. Thus, it is expedient to design specimens to avoid this problem by using the recommended B/W values provided in Section 7.1.3 of Appendix I.

Since errors caused by crack tunneling will increase with specimen thickness (for a constant specimen width), they can influence data comparisons on the influence of thickness on da/dN. Figures 4-10 and 4-11 contain fatigue crack growth rate data on various thicknesses of 10Ni steel and 2219-T851 aluminum, respectively. As indicated by the translated data points, the apparent thickness effects at high da/dN values are eliminated when crack tunneling is accounted for using the correction factors given in Figs. 4-7 and 4-9.

Thus, for the factor of four change in thickness examined herein, thickness had no significant effect on the growth rates in either material. Although, it should be noted that since tunneling is a manifestation of the influence of stress state on fatigue crack growth, it is possible that more extreme changes in thickness (or stress state) could influence da/dN.

Data in the literature on the influence of thickness on da/dN for various materials is mixed. Fatigue crack growth rates over a wide range of ΔK have been reported to either increase[12-14], decrease[15,16] or remain uneffected[14,17-19] as specimen thickness is increased. Thickness can also interact with other variables such as environment[13] and residual stress from heat treating.[19] In addition, materials may exhibit thickness effects over the terminal range of da/dN vs. ΔK

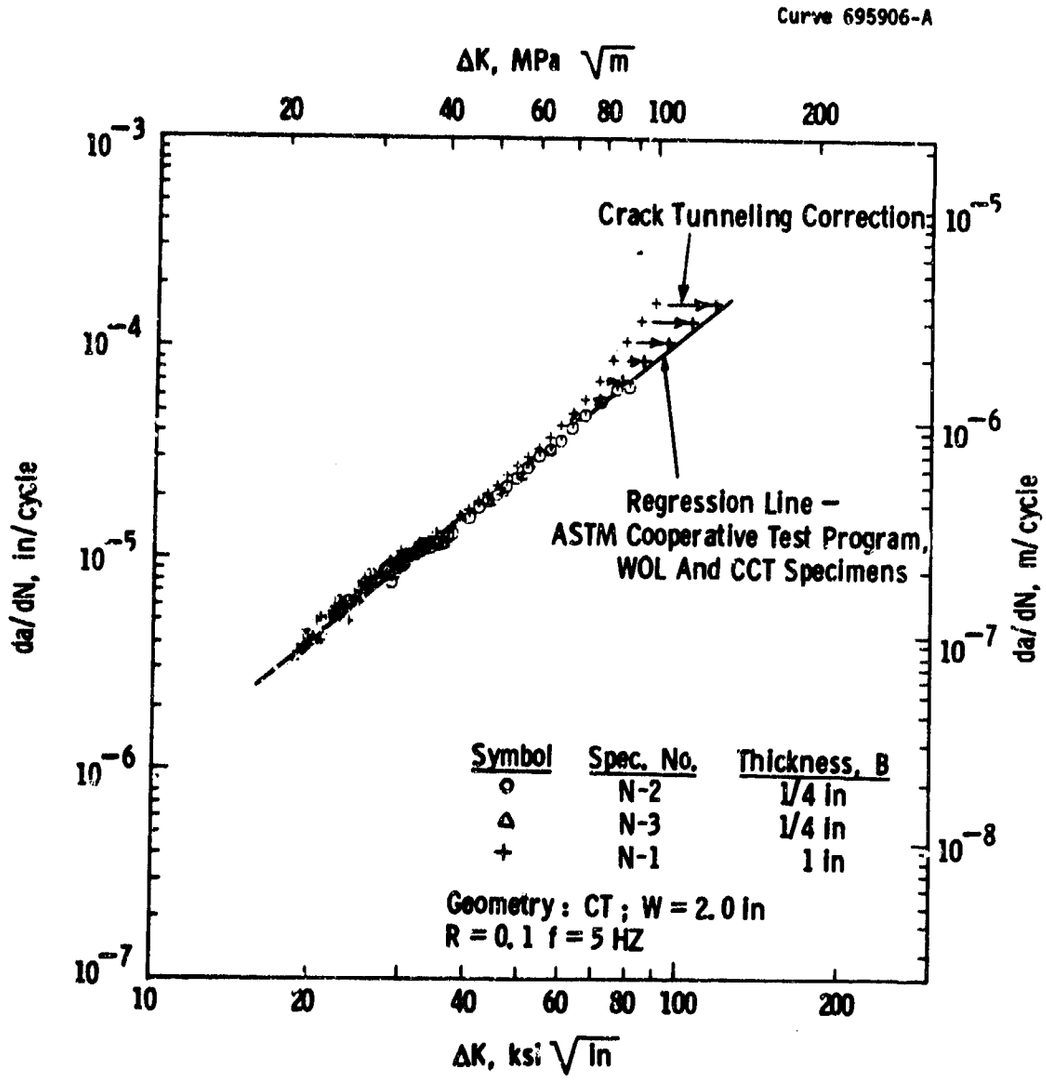

Fig. 4-10—Fatigue crack growth rates in 10 Ni steel showing effect of crack tunnelling correction

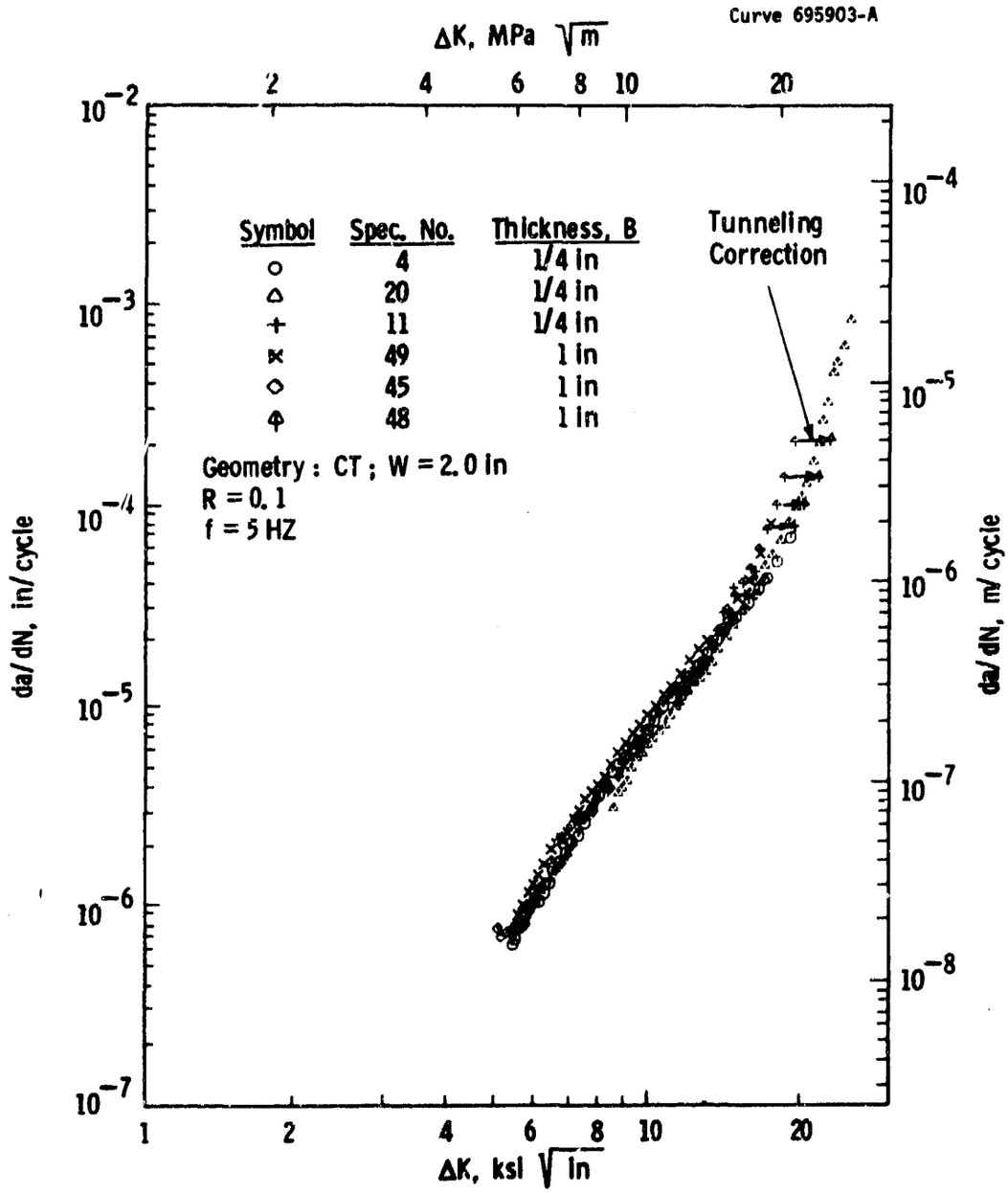

Fig. 4-11—Fatigue crack growth rates in several thicknesses of alloy 2219-T851 showing crack tunneling correction

which are associated with either nominal yielding[18] or a K_{max}-controlled instability.[20] The occurrence of crack tunneling may also have biased some data obtained on the effect of thickness on fatigue crack growth rates.

4.3.3 Effect of Gage Length in CCT Specimens

The possible influence of gage length in the CCT specimen was examined in order to develop a specimen configuration suitable for testing under compressive loading. The CCT specimen was selected for testing at $R < 0$ since the K-calibration for the CT specimen is sensitive to the "back-lash-free" gripping which is necessary for compressive loading. Furthermore, bending in the arms of the CT specimen during compressive loading may introduce extraneous crack opening modes which would further complicate the K-calibration.

Since tests at $R < 0$ were to be done on 1/4-in.-thick material, it was considered feasible to design a specimen with a short gage length to provide adequate buckling constraint instead of using anti-buckling guides.

A gage length, L, equal to 1.33W was considered suitable for this purpose in the 1/4-in.-thick specimen. The overall specimen design is shown in Fig. 4-2 and the bolt and keyway gripping assembly is shown in Fig. 4-12. This loading configuration results in the application of a nearly constant displacement across the specimen width at locations 2 in. above and below the central crack.

The K-calibration for the above specimen and loading configuration was compared to the K-calibration given in Section 9.3.2, Appendix I, by means of the following methods: 1) experimental compliance measurements, 2) numerical analysis and 3) comparison fatigue crack growth rate data.

The experimental compliance data are given in Fig. 4-13 for the conventional pin-loaded CCT specimen with $L = 3W$ and for the short, clamped CCT specimen with $L = 1.33W$. (Both compliance and crack length are given in dimensionless form; V is the displacement along the center

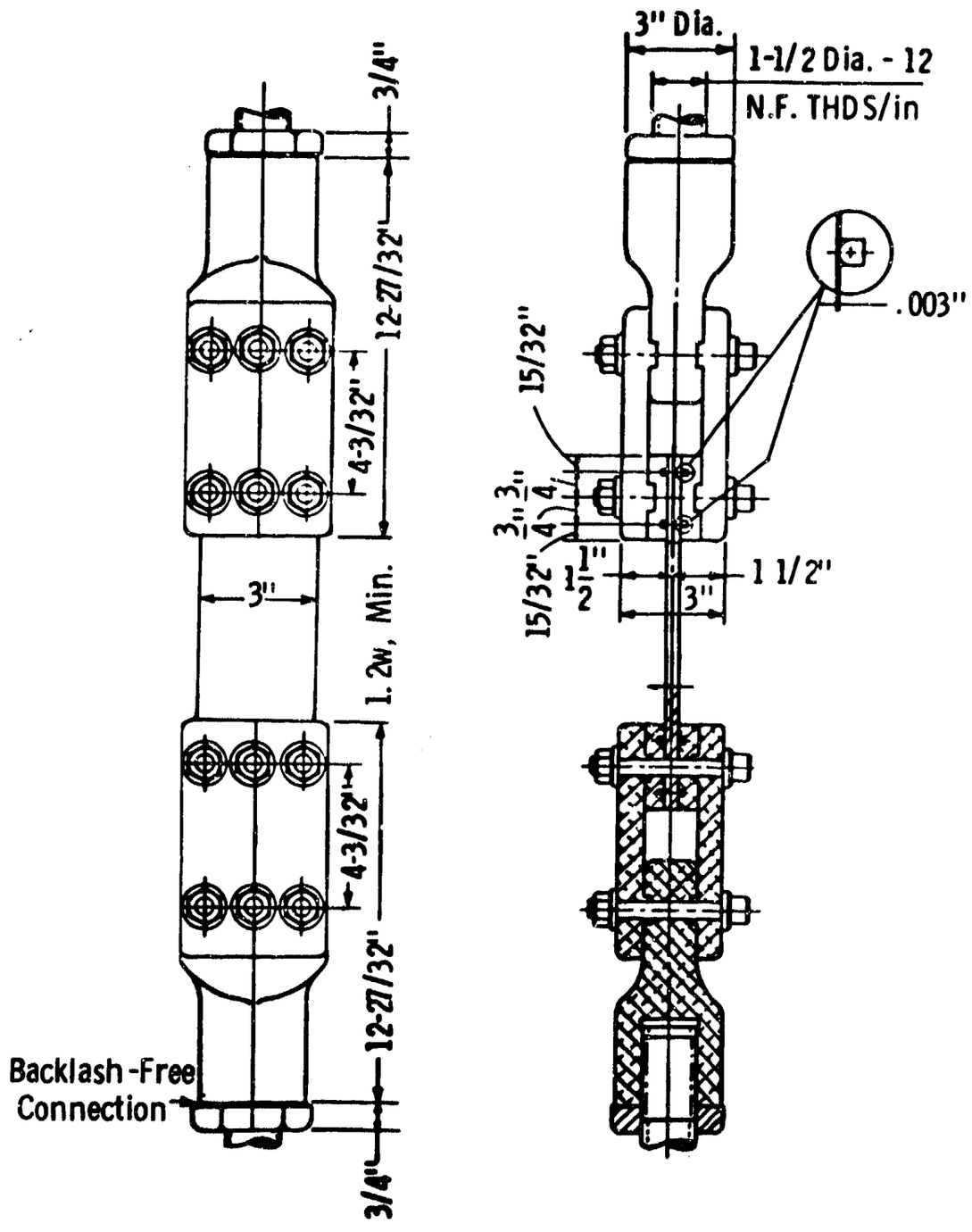

Fig. 4-12— Bolt and keyway assembly for gripping short CCT specimen

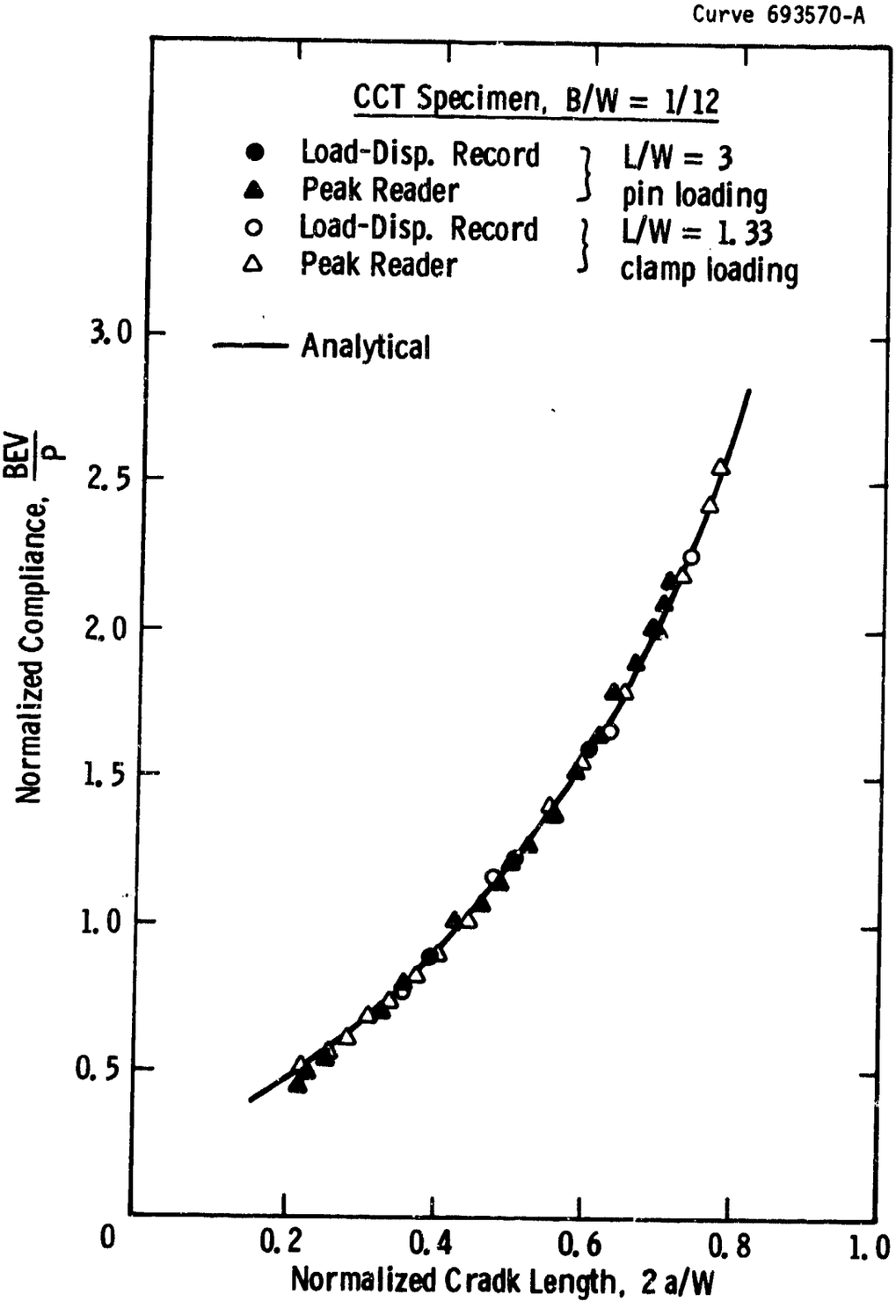

Fig. 4-13—Elastic compliance of CCT specimens with various gage lengths (L) and gripping methods

of the specimen measured between points which are .25 in. above and below the crack and E is the elastic modulus which was assumed to be 10.6×10^6 psi for the aluminum alloy.) For comparison, the solid line shows the CCT compliance predicted from analytical results according to the following equation.[21]

$$\frac{BEV}{P} = 2\left\{\frac{2}{\pi(Y/W)} \cosh^{-1}\left(\frac{\cosh\pi(Y/W)}{\cos\pi(a/W)}\right) - \frac{1+\nu}{\left[1+\left(\frac{\sin\pi(a/W)}{\sinh\pi(Y/W)}\right)^2\right]^{\frac{1}{2}}} + \nu\right\} \left(\frac{Y}{W}\right)$$

$$\left(\frac{\pi a}{W} \operatorname{cosec} \frac{\pi a}{W}\right)^{\frac{1}{2}}$$

Where Y = half of the distance between the points of displacement measurement and ν = Poisson's ratio.

The experimental results from both CCT configurations are in good agreement with the analytical results. These results are also in agreement with the numerical analysis of Isida on CCT specimens of various gage lengths and loading conditions.[22] Isida's analysis indicates that the K-expressions for the above two CCT configurations and gripping methods should differ by less than 4%.

Further verification of the K-calibration for the short, clamped CCT specimen is given by the data shown in Fig. 4-14. Good agreement was obtained for da/dN vs. ΔK data generated on short, clamped CCT specimens and long, pin-loaded CCT specimens when results were analyzed using the equation provided in the proposed test method.

Strain gage data was also obtained to assess the extent of out-of-plane bending which would be encountered during subsequent testing of the short, clamped CCT specimen in compression. Several strain gages were mounted at various locations of a test specimen as shown in Fig. 4-15. The first number identifies the strain gage on the front face, while the second number identifies the strain gage on the back face at the same location. This specimen was tested at a

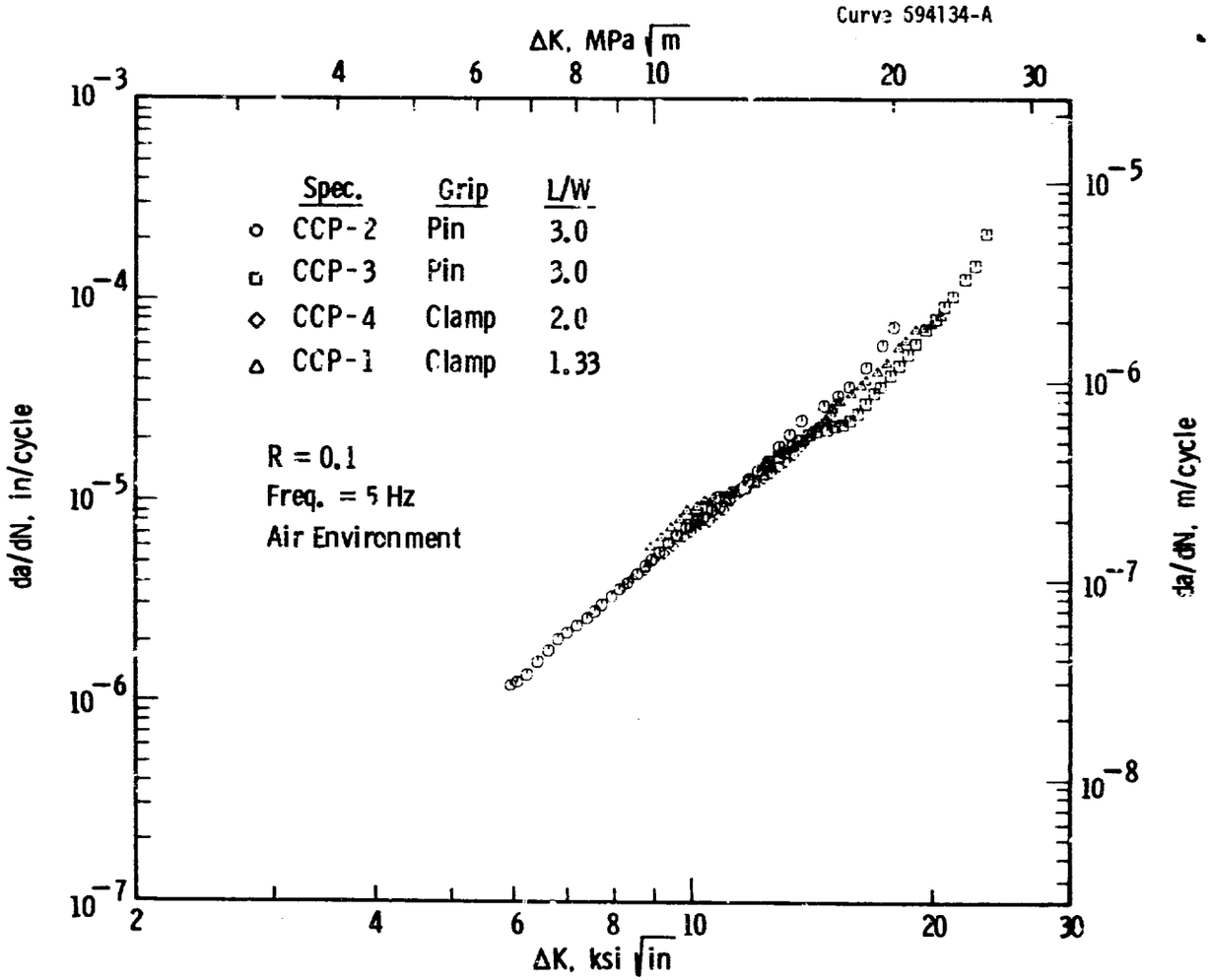

Fig. 4-14— Fatigue crack growth rate data from center-cracked-tension specimens with various gage lengths (L) and gripping methods

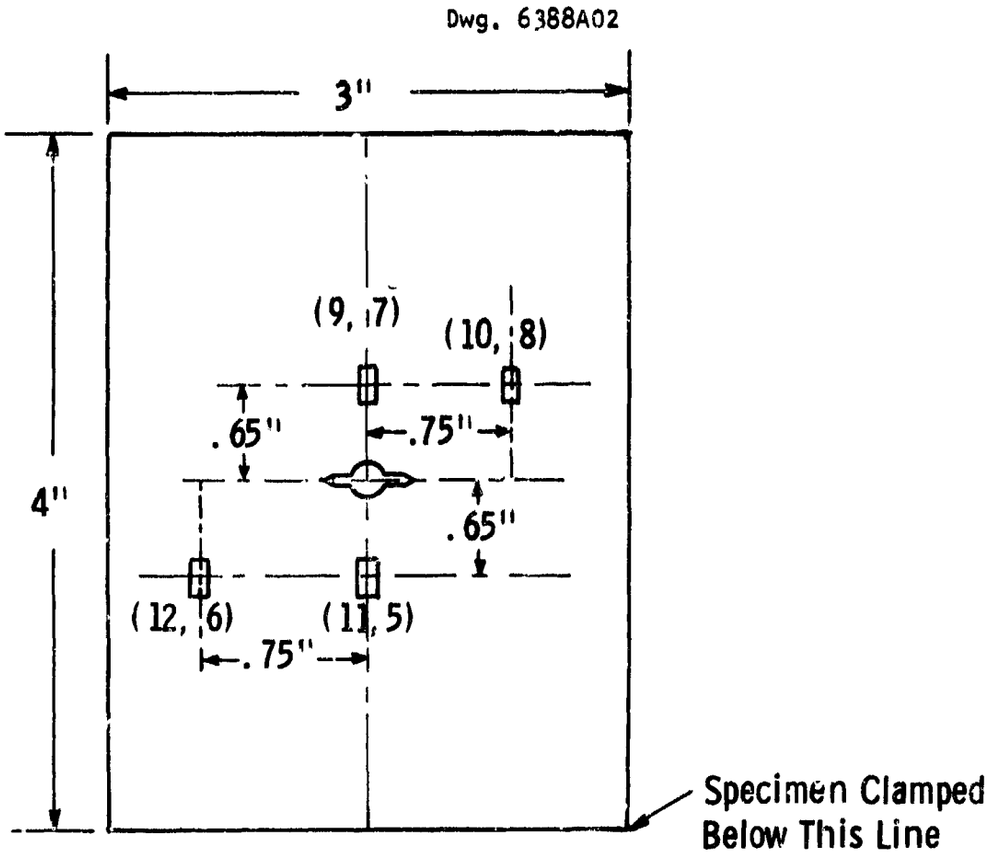

Fig. 4-15— Location of strain gages used to measure the extent of bending during compressive loading of a 4 in. — gage — length CCT specimen

TABLE 4-3

STRAINS MEASURED AT VARIOUS LOCATIONS ON A CCT SPECIMEN AS A RESULT OF: (a) TENSILE AND (b) COMPRESSIVE LOADS

No. of Cycles	Crack Length (in.)	Strain Per 1000 lbs (Strain x 10^6) at Location 5	11	6	12	9	7	8	10
		(a) Tensile Loads							
0	.3265	65.0	60.0	100.0	96.7	55.8	66.7	107.1	100
48,300	.5265	35.0	32.5	109.0	105.8	32.1	38.3	117.8	114.3
69,000	.7195	20.0	19.1	107.1	109.0	18.3	21.6	117.8	117.8
75,700	.8215	12.5	12.5	100.0	100.0	10.7	16.7	110.7	109.0
80,300	.933	--*	--	89.3	87.5	10.0	12.5	98.8	98.8
83,200	1.023	--	--	75.0	75.0	—	—	85.7	85.7
85,500	1.1405	--	--	57.1	55.4	—	—	67.8	67.8
		(b) Compressive Loads							
0	.3265	74.1	70.0	96.7	91.1	67.5	75.0	98.3	91.7
48,300	.5265	71.7	65.0	98.2	89.2	62.5	76.8	105.0	95.0
69,000	.7195	71.4	64.2	98.3	88.3	62.5	72.8	105.0	98.3
75,700	.8215	73.2	64.3	98.2	88.3	62.5	75.0	103.5	94.1
80,300	.933	71.4	62.5	98.2	86.7	60.7	73.2	105.0	96.0
83,200	1.023	71.4	64.3	96.4	85.1	64.3	73.2	105.0	96.0
85,500	1.1405	71.4	62.5	96.4	85.1	64.2	67.8	105.0	93.6

*Implies negligible strain.

constant load range of $\pm$ 7,500 lbs (R = -1). The test was interrupted briefly several times to record the load displacement and the load vs. the output of the various strain gages. Also, crack length measurements were made as a function of elapsed cycles. The strain gage data is presented in Table 4-3 for tensile and compressive loads.

During the tensile portion of the cycle the strains recorded on the opposite faces of the same location exhibit some differences which are attributed to minor variations in the position of the gages and also to differences in crack lengths on the two sides of the specimen. It was observed that the side with strain gages 11 and 12 exhibits strains that are consistently lower than those measured on the side with strain gages 5 and 6. The same observation was made for the other strain gages as well and is consistent with measured crack lengths being larger on the side with strain gages 11 and 12. As crack growth progressed, the differences in crack lengths on the two sides decreased which is also the general nature of the strain data for tensile loads.

During the compressive portion of the cycle, in general discrepancies larger than recorded in the tensile portion of the cycle were observed in the outputs from corresponding strain gages on the two sides of the specimen. This increased strain gradient is attributed to bending of the specimen. However, this small amount of bending, $\sim$5% of the nominal strain, is not large enough to influence the crack growth rate results.

4.3.4 Effect of Load Ratio

The influence of load ratio (R) was examined over a wide range of fatigue crack growth rates. Tests were conducted on the 2219-T851 aluminum at R values of -1, 0.1, 0.3, 0.5 and 0.8. Less extensive testing was conducted on the 10Ni steel after initial results indicated that it was generally less sensitive to load ratio than was the 2219-T851 aluminum — high growth rates were measured at R = -1, 0.1 and 0.8; low growth rates were measured at R = 0.1, 0.5 and 0.8. All of the above testing was conducted in laboratory air (40-60% RH) at a temperature of 75°F $\pm$ 2°F.

Data which summarize the effect of load ratio on wide-range fatigue crack growth rates are given in Figure 4-16 and 4-17. Fatigue crack growth rates in the 2219-T851 aluminum, Fig. 4-16, exhibit three distinct regions of growth which are often observed in high strength structural alloys. Low da/dN values are strongly sensitive to the applied stress intensity factor, ΔK, and da/dN becomes dimenishingly small as a threshold stress intensity, ΔK_{th}, is approached. In this growth rate regime, termed Region I, both da/dN and ΔK_{th} are strongly R-dependent. At intermediate growth rates, Region II, da/dN is much less dependent on both ΔK and R. At high growth rates, Region III, da/dN is again strongly dependent on both ΔK and R.

The occurrence of Region III in the 2219-T851 aluminum is attributed to the onset of a static component of crack growth. Quantitative electron fractography on this material[23] has shown that in Region II, where striations are the predominate fractographic feature, the microscopic growth rates obtained from striation spacing measurements are in good agreement with the macroscopic growth rates of Fig. 4-16. However, in Region III the microscopic measurements of crack growth rates are less than the macroscopic measurements and this difference is associated with the presence of additional fractographic features which are characteristics of a stable mode of static crack growth. Similar observations have also been reported for other aluminums and for steels.[24-26]

The terminal values of K_{max} corresponding to the positive load ratio data in Fig. 4-16 were found to be relatively constant ($33\ ksi\sqrt{in.} \leq K_{max} \leq 35\ ksi\sqrt{in.}$). These K_{max} values are in good agreement with K_{Ic} measurements (per ASTM E399) which have been reported for 2219-T851 aluminum.[27] Combining these results with the previously discussed fractographic observations indicates that the Region III load ratio dependence is influenced by static load subcritical crack growth associated with the approach of instability.

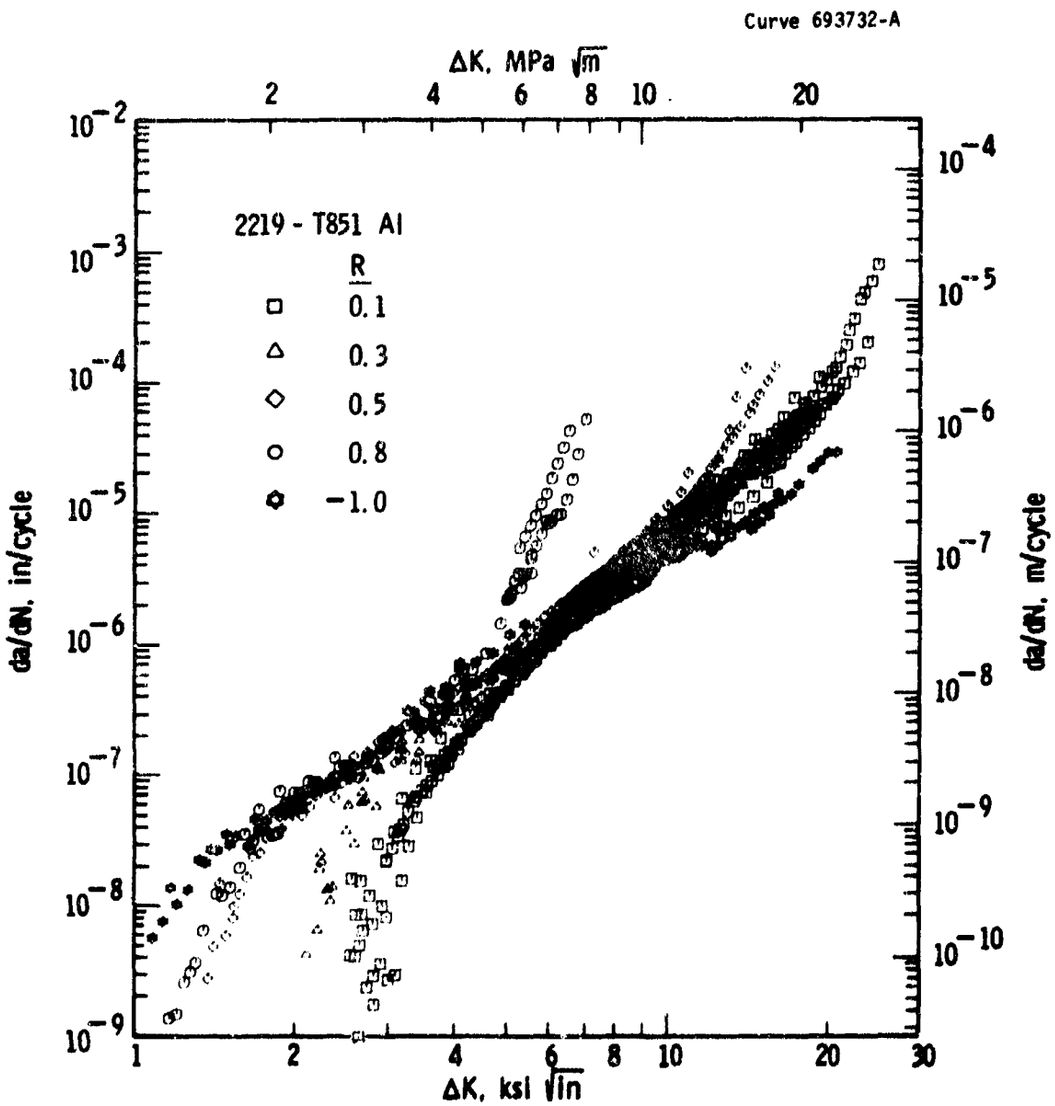

Fig. 4-16— Influence of load ratio on wide range fatigue crack growth rate for 2219 - T851 aluminum alloy

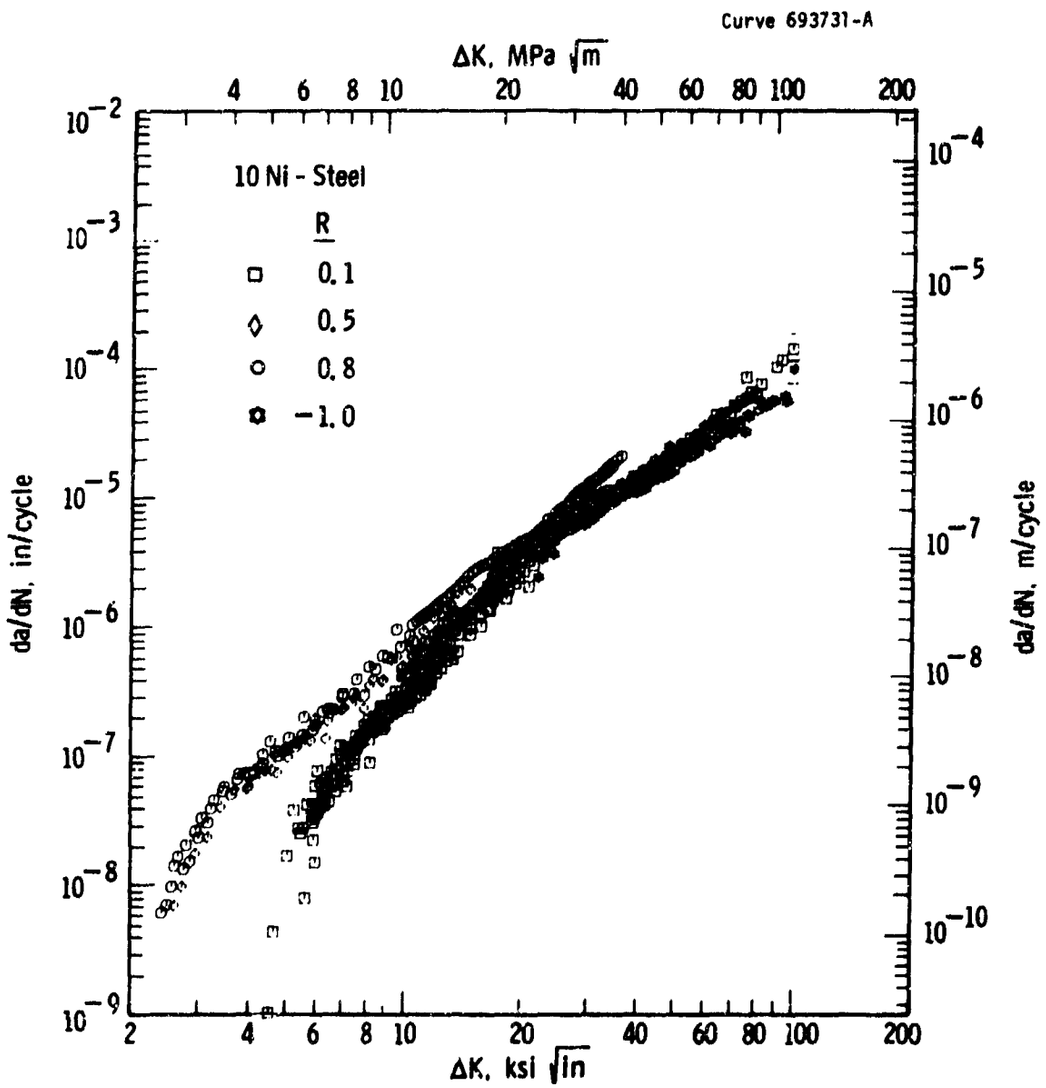

Fig. 4-17— Influence of load ratio on wide range fatigue crack growth rate for 10 Ni-steel

Data on the 10Ni steel, Fig. 4-17 exhibit similar characteristics to those observed in the 2219-T851 aluminum in Regions I and II. The primary difference in the fatigue crack growth rate behavior of these two materials is the absence of a strong R-dependence at high growth rates in the 10Ni steel, even though both materials were tested over a comparable range of growth rates. The insensitivity of high growth rates to R corresponds to the absence of Region III type behavior and is presumed to be due to the lack of a static, subcritical cracking component to the overall growth rate. This interpretation is consistent with the high fracture toughness of this alloy — a valid K_{Ic} measurement (per ASTM-E399) has never been achieved, however, the toughness is estimated to exceed 200 ksi$\sqrt{in}$.[28]. The measurement of growth rates higher than those shown in Fig. 4-17 for R = 0.8 were limited by the measurement capacity of the specimens employed (CT specimen with W = 2 in.). As discussed in Section 4.4.1 the measurement capacity is in this case limited by exceeding the fully plastic limit load of the specimen rather than by a K_{max} controlled instability. A similar behavior has been observed by Dowling in a high toughness A533B steel[29] On the other hand, high strength, low toughness steels exhibit Region III behavior.[20,24,25]

From the above discussion, it follows that the material dependence of load ratio in Region III, which were observed herein and which have been reported elsewhere[30-33], is primarily due to differences of inherent toughness of these materials.

As indicated the R-dependence of fatigue crack growth rates is specific to the growth rate regime, with R-effect predominating in Region I and III. In addition, the exact functional dependence of growth rate on R is complex for a given region. For example, in Region I the R-effects appear to saturate above R = 0.5 as evidence by the fact that data at R = 0.5 and R = 0.8 nearly coincide and are both significantly different from data at R = 0.1 (Figs. 4-16 and 4-17). On the other hand, in Region III data at R = 0.5 and 0.1 nearly coincide and are both significantly different from data at R = 0.8.

Consequently, the overall R-dependence of da/dN is rather complex and cannot be described by a simple translation along either the da/dN or ΔK axes.

Figures 4-16 and 4-17 also include data at R = -1. These data were analyzed in accord with Section 9.3.2 in Appendix I, thus the compression portion of the loading cycle was not used in computing ΔK. The center-cracked tension specimens employed to generate these data are described in Section 4.3.3.

Data on R = -1 are both interesting and controversial. At high growth rates in 2219-T851 and 10Ni steel, fatigue crack growth rates at R = -1 are less than those at R = 0.1. These results consist of overlapping data from several tests and are therefore judged to be reliable. In addition, microscopic growth rates from electron fractographic measurements of striation spacings were found to be in good agreement with the macroscopic data.[23] These same results also confirmed that at a given ΔK in this regime the growth rates at R = -1 were less than those at R = 0.1. The slower growth rates at R = -1 appear to be caused by a suppression the static-load component of subcritical crack growth which is associated with Region III type behavior. We currently have no complete explanation for the mechanism by which this phenomenon occurs. It is postulated that due to the additional reversed plasticity during compressive loading the material ahead of the crack tip experiences additional cyclic softening which is in turn responsible for an elevation in the material's inherent fracture toughness. This postulate is consistent with the fact that: 1) both materials exhibit cyclic softening and 2) a larger growth rate difference is observed at high growth rates between data at R = -1 and R = 0.1 in 2219-T851 aluminum which exhibits Region III rates which are more strongly dependent on toughness. Additional work is required to critically evaluate this hypothesis.

Low growth rate data at R = -1 were obtained for the 2219-T851 aluminum and are included in Fig. 4-16. However, much of the data generated at R = -1 below 10^{-7} in./cycle are not shown in Fig. 4-16 since they violated the requirements of Section 8.7.4 in Appendix I on crack straightness, and as a result exhibited relatively large scatter. Thus, data below 10^{-7} in./cycle were primarily obtained from one K-decreasing test on a single specimen.

Figure 4-16 shows that as fatigue crack growth rates decrease in the 2219-T851 aluminum, the slope of the log ΔK-log da/dN plot remains constant down to about 2×10^{-8} in./cycle. Consequently, at low growth rates the data at R = -1 becomes faster than those at other R values, including R = 0.8. It is tempting to rationalize the above results in terms of a simple crack closure argument [34] since it has previously been suggested that this phenomenon can explain load ratio effects at low growth rates.[34-37] Cyclic loading at R < 0 would be expected to compress the wake of plasticity deformed material along the fracture surfaces which contributes to crack closure — this compression would increase the effective ΔK, thereby increasing the fatigue crack growth rate. However, it is difficult to conceive of this phenomenon producing growth rates which are faster than those at R = 0.8.

An additional factor which may be contributing to the Region I growth rates at R = -1 is environmentally enhanced growth since these data were generated at cyclic frequencies of 20-25 Hz compared to data at other R values which were generated at 50 to 150 Hz.* No environment-related frequency effect were observed for Region I data obtained over the frequency range of 50 to 150 Hz. Nevertheless it is possible that these effects might arise upon lowering the frequency to 20 Hz. Results in the literature on frequency effects in Region I have not included

*The slower frequencies employed at R = -1 were necessary to maintain good load control with the clamping grip arrangement used on the CCT specimens for tension-compression loading.

frequencies as low as 20 Hz, thus the possibility of environment enhanced growth occurring in Region I has not been resolved. As demonstrated in Section 4.3.5, Region III rates in the 2219-T851 aluminum exhibit environmentally related frequency effects in 40-60% RH laboratory air.

Fatigue crack growth rate results in the literature for $R < 0$ are mixed.[30,37-40] A comparison of these data is complicated by the fact that the procedure used to compute ΔK for $R < 0$ is not always specified — that is, whether or not the compression portion of the loading cycle was included in the computation of ΔK. Further, complications arise due to the wide variety of test techniques which have been employed and associated problems such as specimen buckling, and extraneous loadings during compression of bend specimens. Using a consistent test technique, Kikukawa, et al.[37] have obtained extensive data indicating that compressive loading at $R = -1$ can either increase, decrease, or have no effect on fatigue crack growth rates compared to data at $R = 0$ — the specific effect appears to be material dependent. This same study also reported data on a carbon steel which showed the same trend as the 2219-T851 aluminum, that is compressive loading ($R = -1/2$ and -1) decreased da/dN at high growth rates and increased da/dN as low growth rates, compared to data at $R = 0$. Similar low growth rate data have been reported by Frost, et al.,[41] namely; ΔK_{th} at $R = -1$ was decreased by 50% compared to that measured at $R = 0$.

The need for reliable fatigue crack growth rate data at $R < 0$ is apparent — especially for structures and equipment experiencing stress induced vibrations which often include compressive loading and low da/dN values. As indicated from the above discussion, material selection can have a strong influence on the performance of such structures.

In conclusion, the results of this section, in their entirety, illustrate the complex role of load ratio in determining the fatigue crack growth rate. The fact that the functional dependence of da/dN on R varies greatly with growth rate regime indicates that several

underlying phenomena control the observed R-effects. Crack closure is known to occur during fatigue crack growth and undoubtably influences the R-dependence, particularly at low growth rates. This fact has to some degree been demonstrated.[34-37] However, additional studies have clearly identified the limitations of this concept as it is currently formulated. Crack-tip plasticity has other important manifestations which have heretofore not been studied. The work described in Appendix II examines the role of crack-tip cyclic plasticity in determining the magnitude of mean stress ahead of a growing fatigue crack. The material's ability to relax these mean, crack-tip stresses is shown to be related to measured load ratio effects in fatigue crack growth. These results illustrate that the contribution of crack-tip plasticity to events ahead of a growing crack are at least as important as the contribution to events behind the growing crack.

4.3.5 Interacting Environmental, Frequency and Temperature Effects

Fatigue crack growth rates above 10^{-7} in./cycle, were examined in both the 2219-T851 aluminum and the 10Ni steel exposed to laboratory air over a temperature range of -100°F to 250°F, and a frequency range of 0.10 Hz to 200 Hz. Reference data were also established for both materials in an inert environment of dry argon for temperatures ranging from -30°F to 250°F*. The interaction of environmental, frequency and temperature effects on fatigue crack growth rates are discussed separately for each material.

4.3.5.1 2219-T851 Aluminum

The influence of a 75°F, laboratory air environment (40-60% RH) on fatigue crack growth rates in 2219-T851 aluminum is illustrated in Fig. 4-18. Results obtained in air at R = 0.1 and R = 0.8 are shown as scatterbands which represent the data reported in

*For dry argon tests, -30°F was found to be the lowest temperature at which the test chamber could be adequately sealed to maintain less than 1 ppm of impurities in the environment.

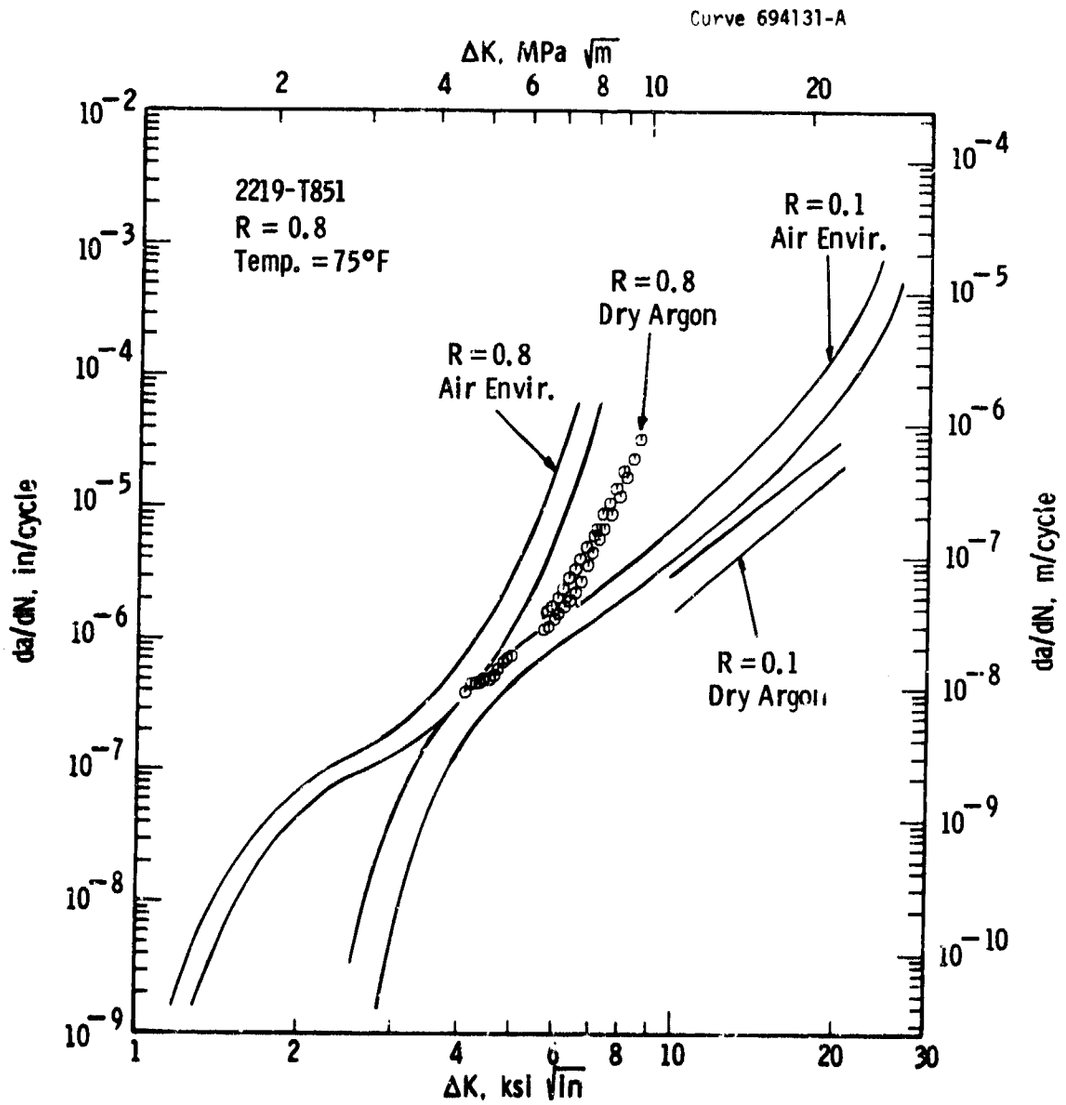

Fig. 4-18 – Influence of a laboratory air environment (40-60% RH) on fatigue crack growth rates in 2219-T851 aluminum

Section 4.3.4. The dry argon data at R = 0.8 were generated in this study; the data band for dry argon at R = 0.1 is from a previous study which employed the same quality of dry argon.[8] As shown in Fig. 4-18, the Region II growth rates at R = 0.1 are enhanced by the air environment by about a factor of 2.5 over the dry argon rates. At R = 0.8, the Region III growth rates are more sensitive to the air environment and are enhanced by as much as an order of magnitude.

A more detailed illustration of the influence of the laboratory air environment on fatigue crack growth rates at R = 0.8 is provided in Fig. 4-19. These data also show the air rates to be markedly sensitive to test frequency. Air data at 5 Hz are as much as six times faster than data at 200 Hz. In addition, the effect of frequency on growth rates in air appears to saturate at low frequencies as evidenced by the fact that data at 5 Hz and 0.10 Hz are within a factor of two. A similar saturation of the influence of frequency on da/dN occurs in other material-environment systems,[42-43] and appears to be a general phenomenon, although the specific saturation frequency is likely to depend on the kinetics of the particular material-environment systems.

All air data at 0.10 Hz were consistently slower than data at 5 Hz by about a factor of two. This observation appears to be associated with the periodic test interruption which were necessary in these long duration tests. Test interruptions are known to cause a period of transient growth rates which are slower than the eventual steady-state growth rates.[4]

The dry argon data in Fig. 4-19 also indicate that rates in this inert environment are insensitive to changes in test frequency. These results are consistent with data from the literature which show the absence of frequency effects in aluminum alloys tested in inert environments.[44-45]

The enhancement of fatigue crack growth rates in 2219-T851 aluminum exposed to air, and the associated frequency effects, are attributed to the presence of water vapor in the laboratory air. Previous studies have demonstrated that aluminum alloys are sensitive to small amounts of water vapor.[45-47]

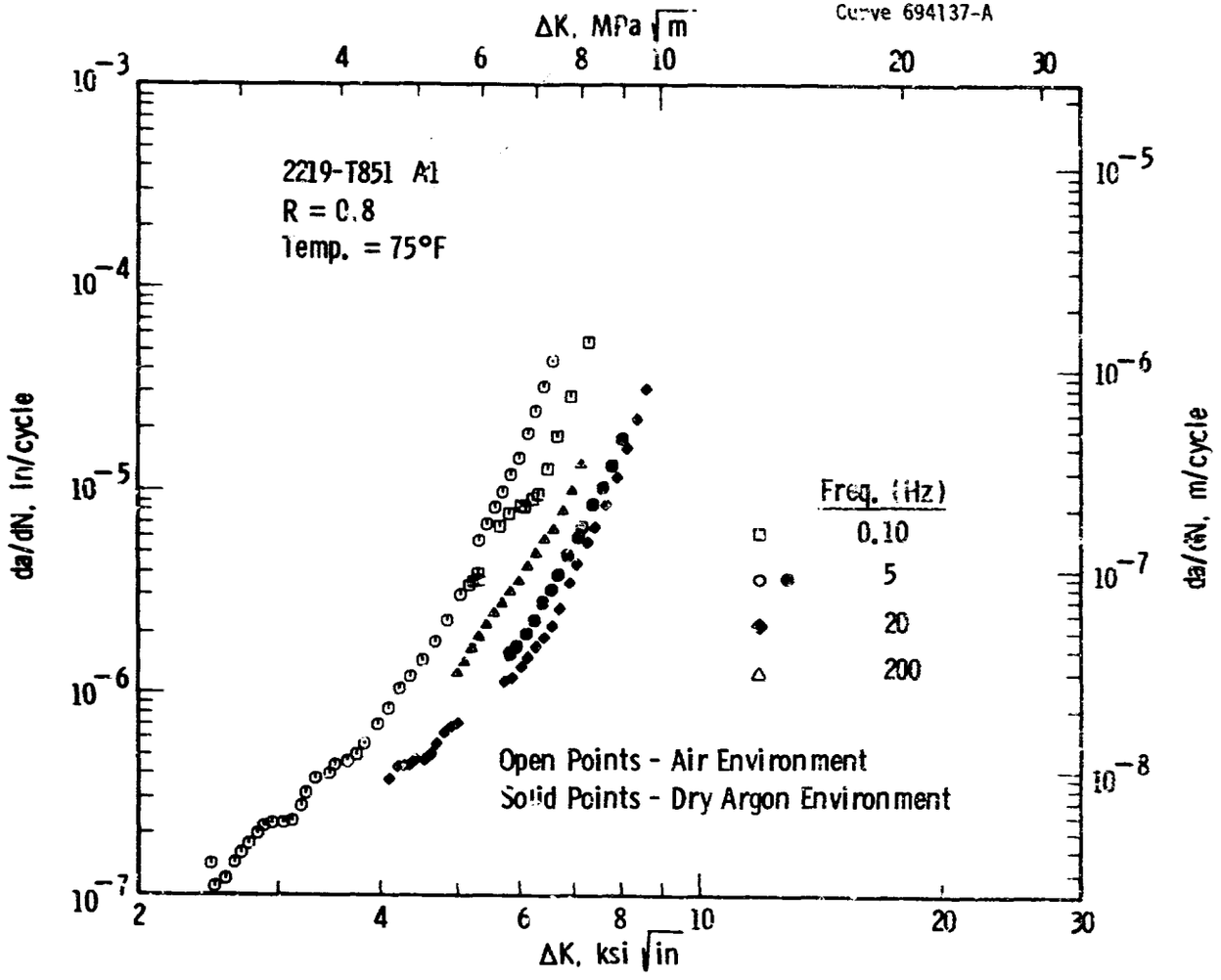

Fig. 4-19— Effect of test frequency and environment on fatigue crack growth rates in 2219-T851 Aluminum at R = 0.8

The effect of test temperature on growth rates at R = 0.8 was established in dry argon and in air at several frequencies — these results are given in Figs. 4-20 to 4-22. The dry argon data are generally slower than data in air, although the temperature dependence is strongest in dry argon. Air data exhibits a temperature dependence at 200 Hz; however, data at 0.10 Hz is essentially independent of temperature. This frequency-temperature interaction is more clearly illustrated in Fig. 4-23 where results are presented in the form of an Arrhenius plot which is commonly used to represent thermally activated, kinetic processes. Each of the linear relationships corresponds to a mechanical "driving force" of $\Delta K = 6$ ksi$\sqrt{\text{in.}}$ and R = 0.8; the general equation which represents these results is as follows:

$$da/dN = A \exp(-U/RT) \qquad (4\text{-}1)$$

where A = constant which is derivable from the da/dN intercept of Fig. 4-23.

U = apparent activation energy in units of cal/mole

R = universal gas constant in units of cal/°K-mole

T = absolute temperature in °K.

The apparent activation energy for dry argon, 2440 cal/mole, defines the temperature dependence of the purely mechanical component of fatigue crack growth. At low temperatures the air environment markedly increases the growth rates over those in dry argon. However, the apparent activation energy for the enhanced growth rates in air significantly decreases with decreasing test frequency. Furthermore, at 250°F, the growth rates in air at both frequencies and the growth rates in dry argon are essentially equal. This equivalency of growth rates is attributed to the fact that at 250°F the moisture, that was present in the laboratory air at lower temperatures, is driven off, thereby rendering the air environment inoculous. Thus, the frequency dependence of the apparent activation energy is caused by a changing environmental condition, that is, by a changing moisture level.

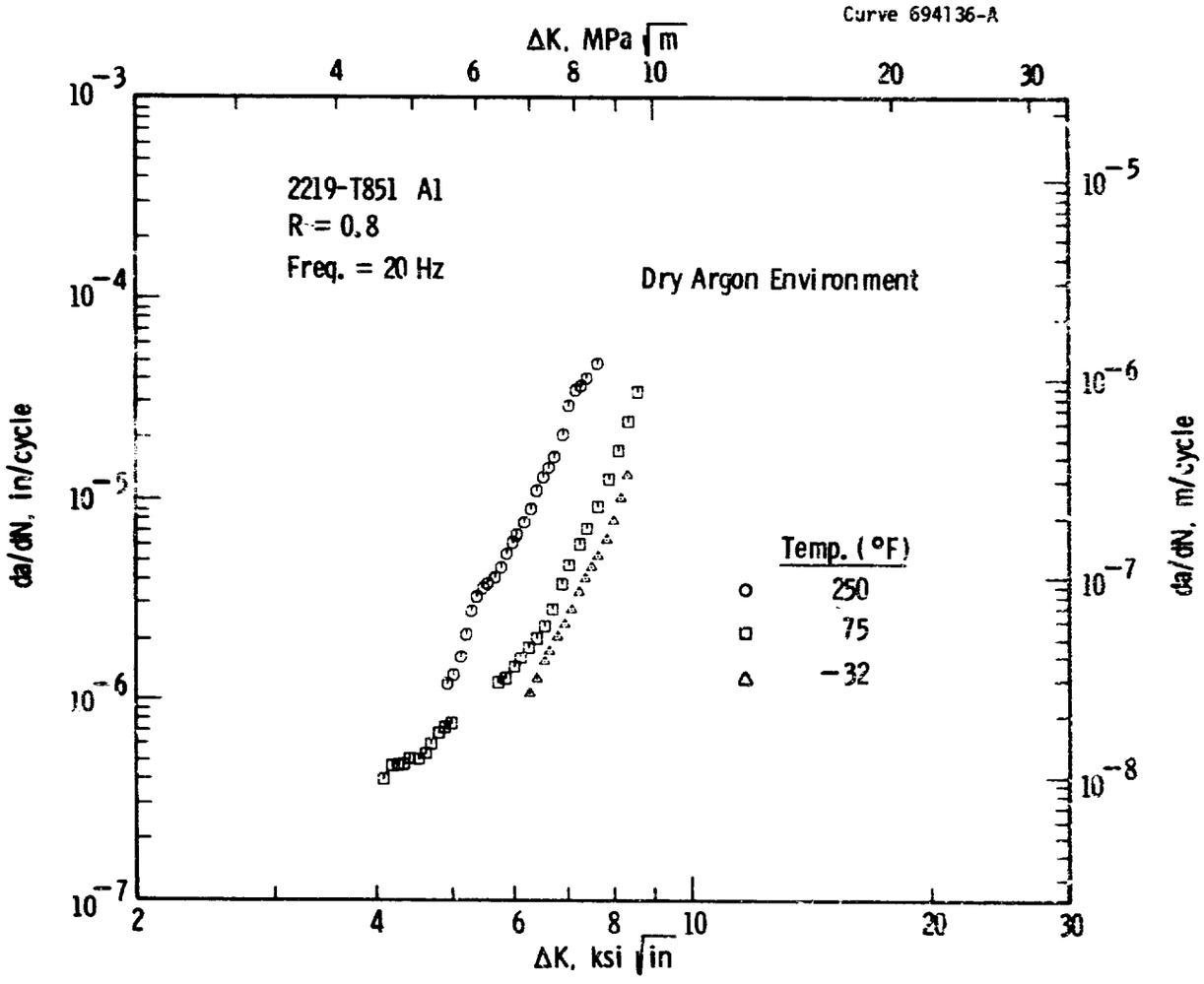

Fig. 4-20— Effect of temperature on fatigue crack growth rates in 2219-T851 aluminum tested in dry argon

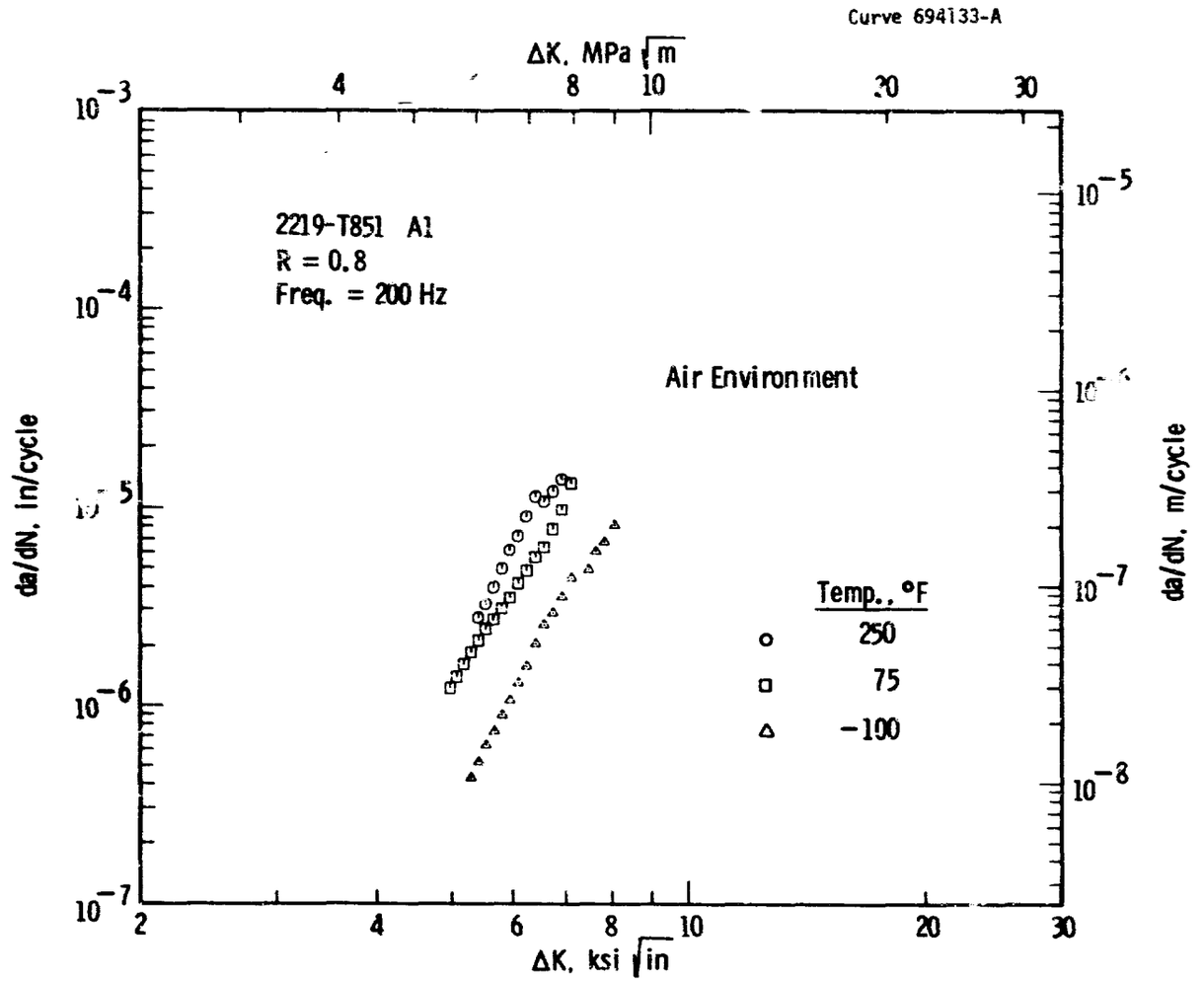

Fig. 4-21— Effect of temperature on fatigue crack growth rates in 2219-T851 aluminum tested in air at R = 0.8, freq. = 200 Hz

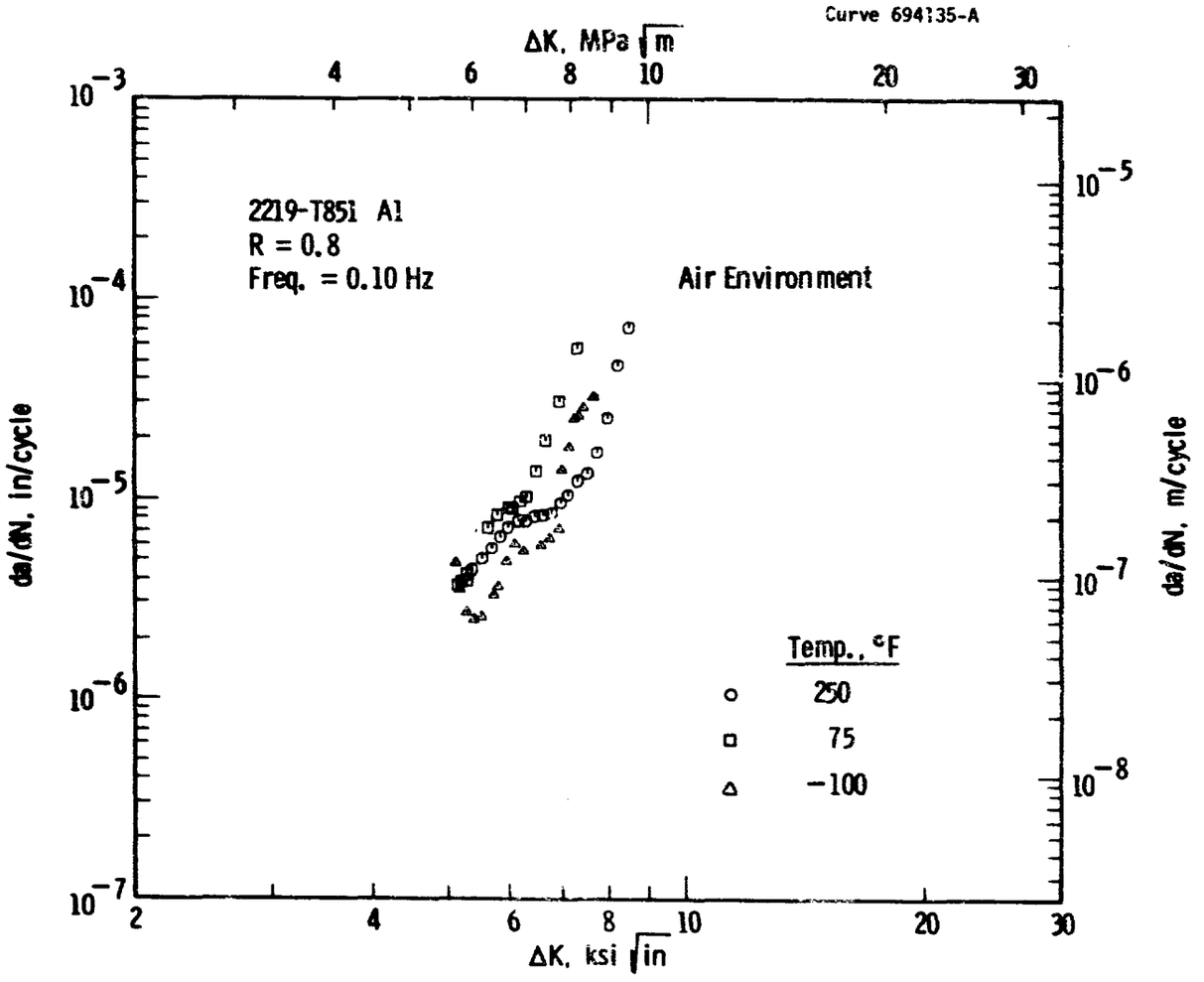

Fig. 4-22— Effect of temperature on fatigue crack growth rates in 2219-T851 aluminum tested in air at R = 0.8, Freq. = 0.10 Hz

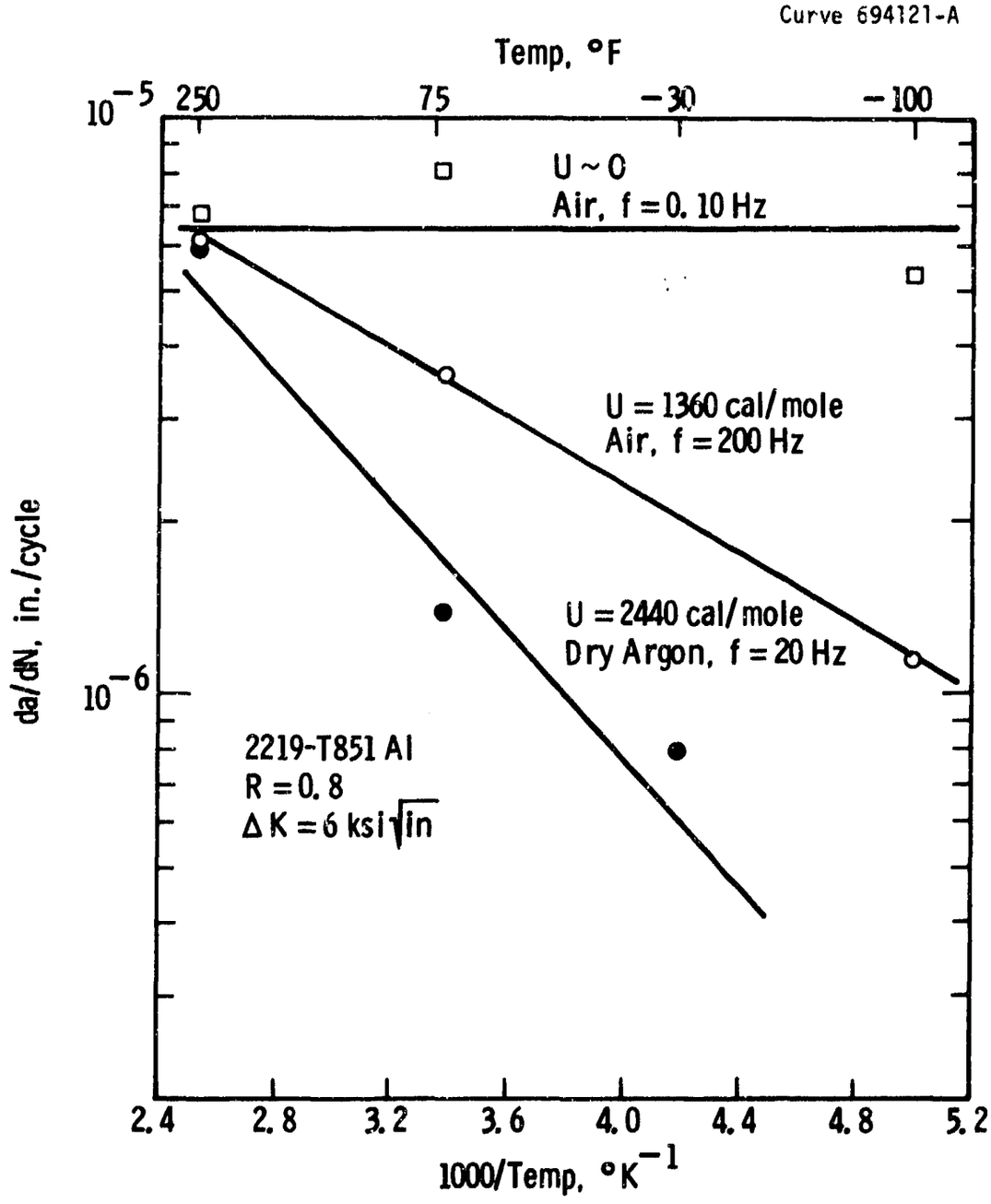

Fig. 4-23 – Effect of test frequency (f) and environment on the temperature dependence of fatigue crack growth rates in 2219-T851 aluminum

The influence of cyclic frequency on the temperature dependence of fatigue crack growth rates in air is a factor that must be taken into account in design. However, since this temperature-frequency interaction is due to a changing environmental condition, the corresponding activation energies provide little information about the underlying mechanism which controls crack growth. Hence, the formulation of mechanisms of fatigue crack growth should be based on data under constant environmental conditions.

The temperature dependence in air at R = 0.1 was observed to have the same characteristics as those observed at R = 0.8. As shown in Fig. 4-24, the temperature dependence at R = 0.1 also varies with test frequency — the lower frequency being much less sensitive to changes in temperature. Comparing these data with the R = 0.8 of Fig. 4-21 provides an assessment of the influence of load ratio on the temperature dependence of the fatigue crack growth rates. This comparison is given in Fig. 4-25, again in the form of an Arrhenius plot, for ΔK = 6 ksi$\sqrt{\text{in.}}$ and a frequency of 200 Hz. As indicated, increasing the load ratio from R = 0.1 to R = 0.8 causes a nearly uniform factor of four increase in the growth rates. The corresponding activation energies of 1440 cal/mole and 1360 cal/mole, which were determined from linear regression, are interpreted as being equivalent considering the inherent variability in the rate data. Thus, an average apparent activation energy of 1400 cal/mole characterizes the temperature dependence over this temperature range in spite of the fact that data at R = 0.1 represent Region II behavior and data at R = 0.8 represent Region III behavior. This result suggests that, for a given test frequency, changes in temperature causes a parallel shift of data along the da/dN axis which can be described by

$$da/dN = A(R) \exp\left(-\frac{U(f)}{RT}\right) \qquad (4\text{-}2)$$

where A(R) = function defining the load ratio dependence of da/dN as discussed in Section 7.6.

U(f) = frequency dependent apparent activation energy.

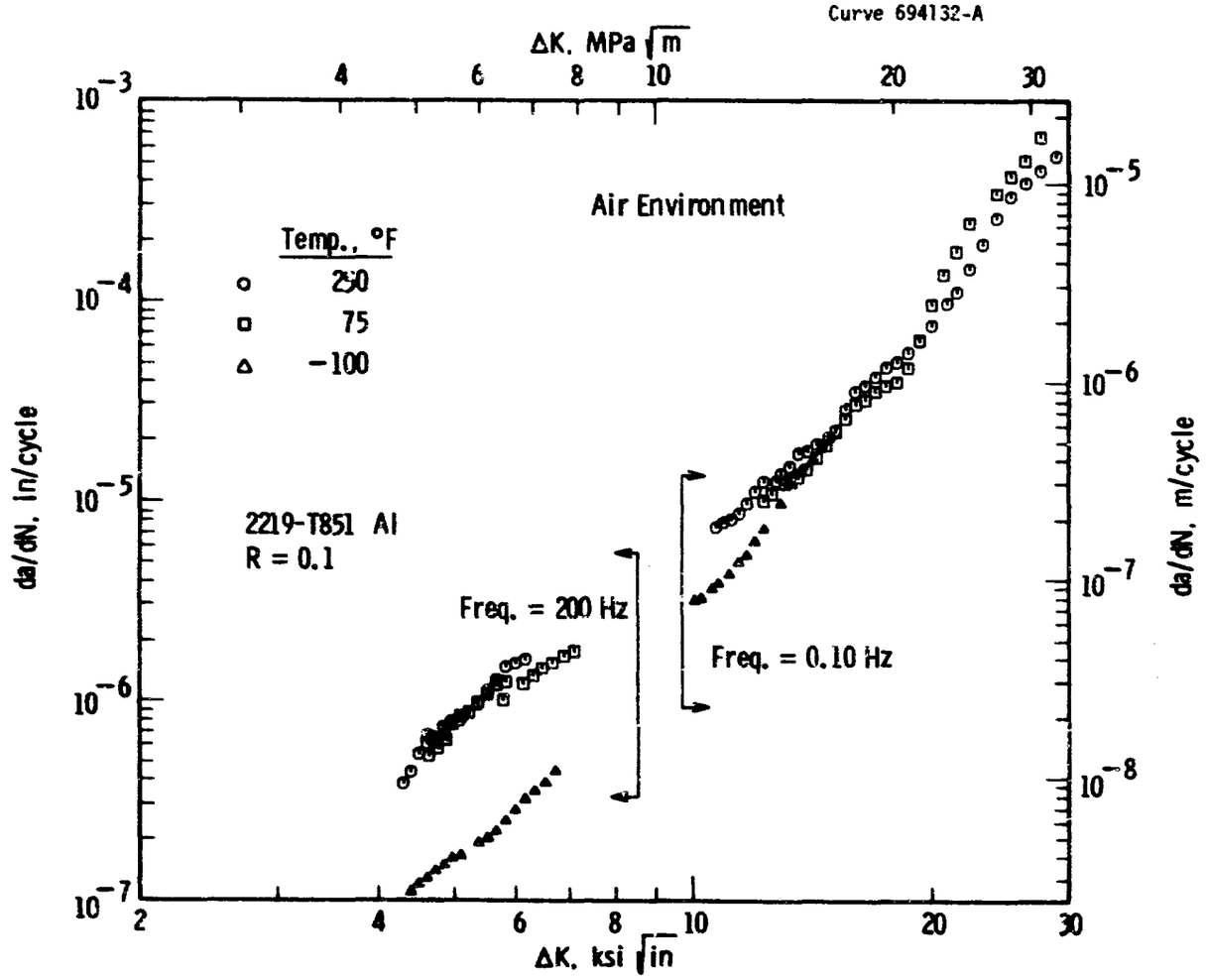

Fig. 4-24— Effect of temperature on fatigue crack growth rates in 2219-T851 aluminum tested in air at R = 0.1, freq. = 0.10, 200 Hz

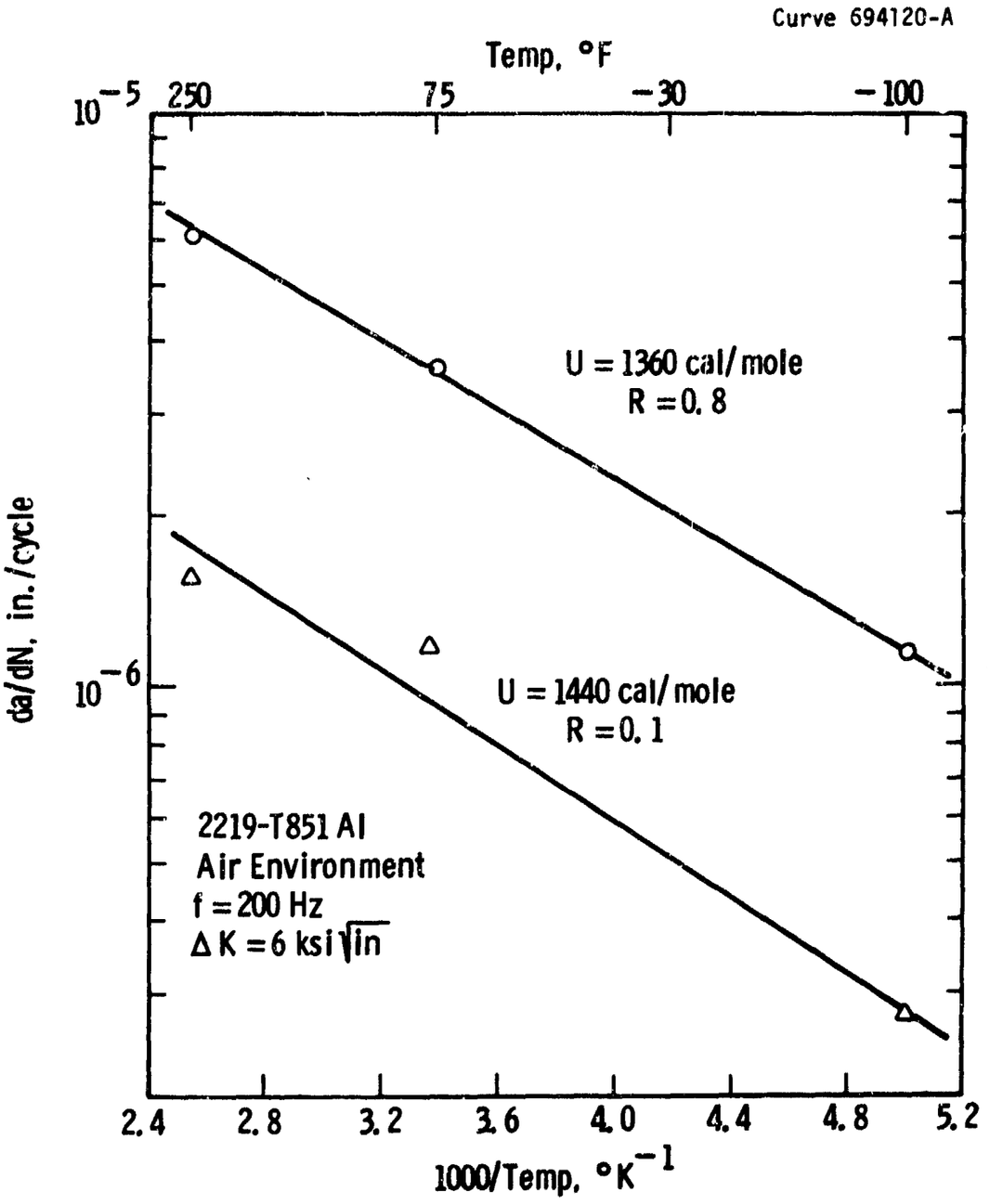

Fig. 4-25 — Effect of load ratio (R) on the temperature dependence of fatique crack growth rates in 2219-T851 aluminum

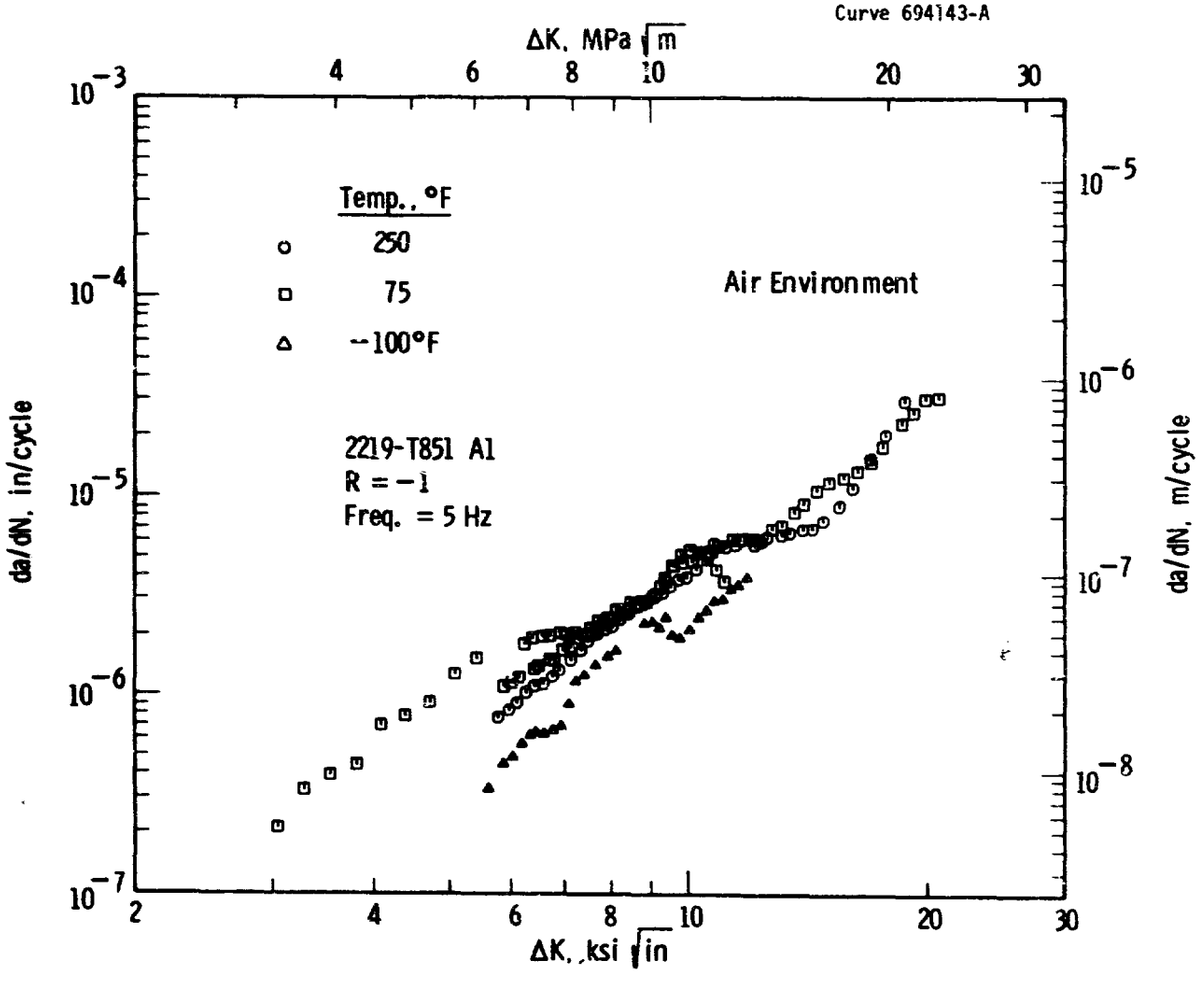

Fig. 4-26— Effect of temperature on fatigue crack growth rates in 2219-T851 aluminum tested in air at R = −1, Freq. = 5 Hz

Although the frequency dependence of the apparent activation energy is clearly shown by the data on 2219-T851, additional testing would be required to specifically define the function U(f). However, it should be noted that since U(f) appears to be environmentally controlled, and since air growth rates in 2219-T851 converge with dry argon results at 250°F, growth rates above this temperature would be expected to follow the inert environment rates and thus exhibit a single, frequency-independent activation energy.

It should also be pointed out that Eq. (4-2) implies that the apparent activation energy is independent of ΔK. Some data from this study, notably Figs. 4-20 and 4-21, indicate that this is a reasonable assumption. However, it has been reported that the activation energy for fatigue crack growth decreases with increasing ΔK for aluminum alloys exposed to distilled water and various gaseous environments.[48,49]

Additional data showing the influence of test temperature on fatigue crack growth rates in 2219-T851 aluminum exposed to laboratory air are shown in Fig. 4-26 for R = -1 and a frequency of 5 Hz. These data exhibit generally more scatter than that observed at R > 0, nevertheless, the observed temperature dependence is consistent with the effects at positive load ratios.

4.3.5.2 10Ni Steel

Figure 4-27 provides a comparison of fatigue crack growth rates in 10Ni steel exposed to laboratory air (40-60% RH) and dry argon (< 1 ppm water vapor) at 75°F. Data at a common test frequency of 5 Hz indicate that the presence of moisture in the laboratory air enhances the growth rates slightly over the inert environment rates. However, the sensitivity is less than that observed in the 2219-T851 aluminum alloy.

As in the aluminum alloy, the air rates at 0.10 Hz are consistently less than those at 5 Hz — again, this is attributed to transient effects accompanying test interruptions during the long duration 0.10 Hz tests. The influence of test frequency on the growth rates in dry argon is minimal.

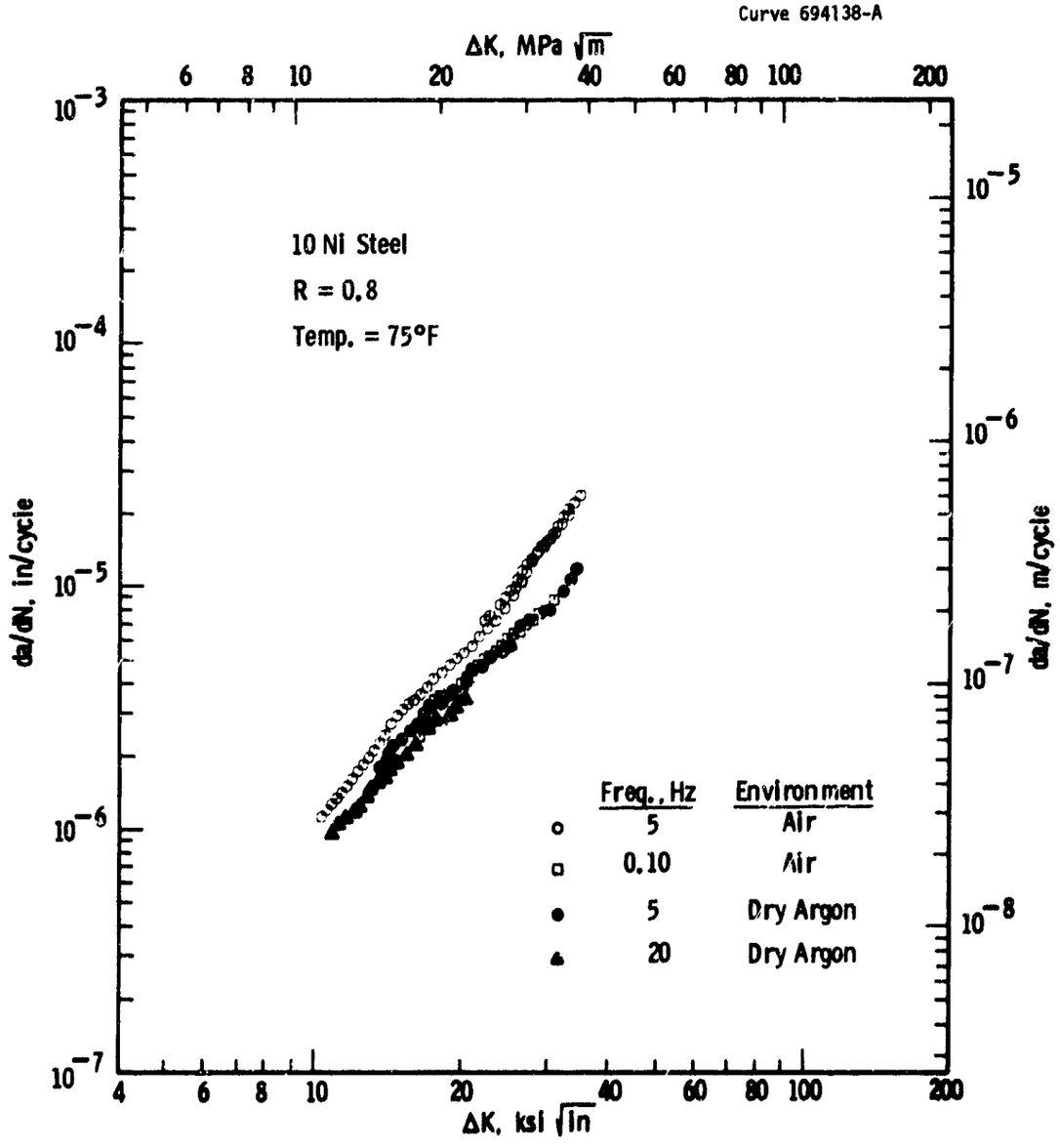

Fig. 4-27 — Influence of a laboratory air environment (40 - 60% RH) on fatigue crack growth rates in a 10 Ni steel

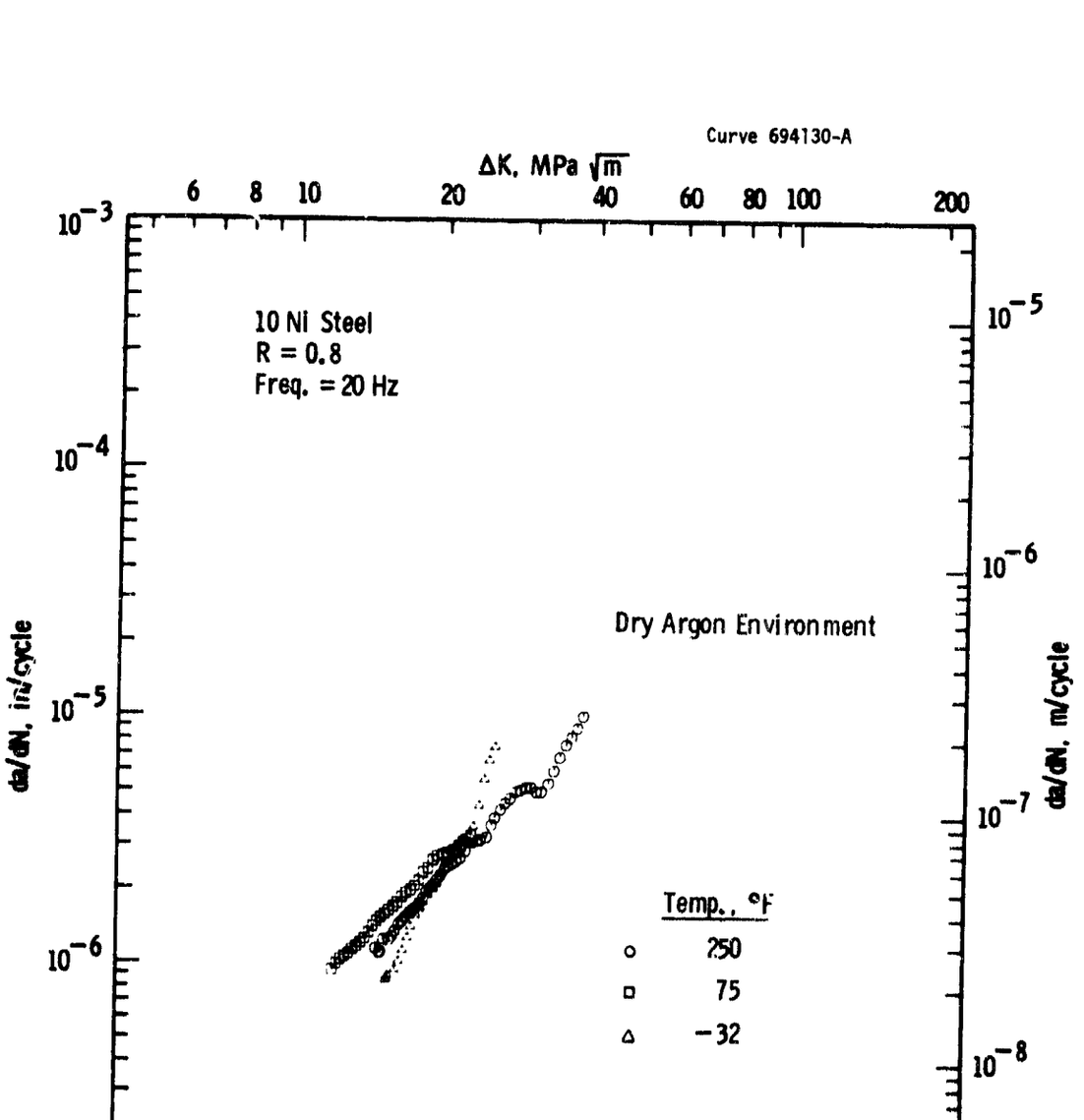

Fig. 4-28— Effect of temperature on fatigue crack growth rates in 10 Ni steel tested in dry argon at R = 0.8, freq. = 20 Hz

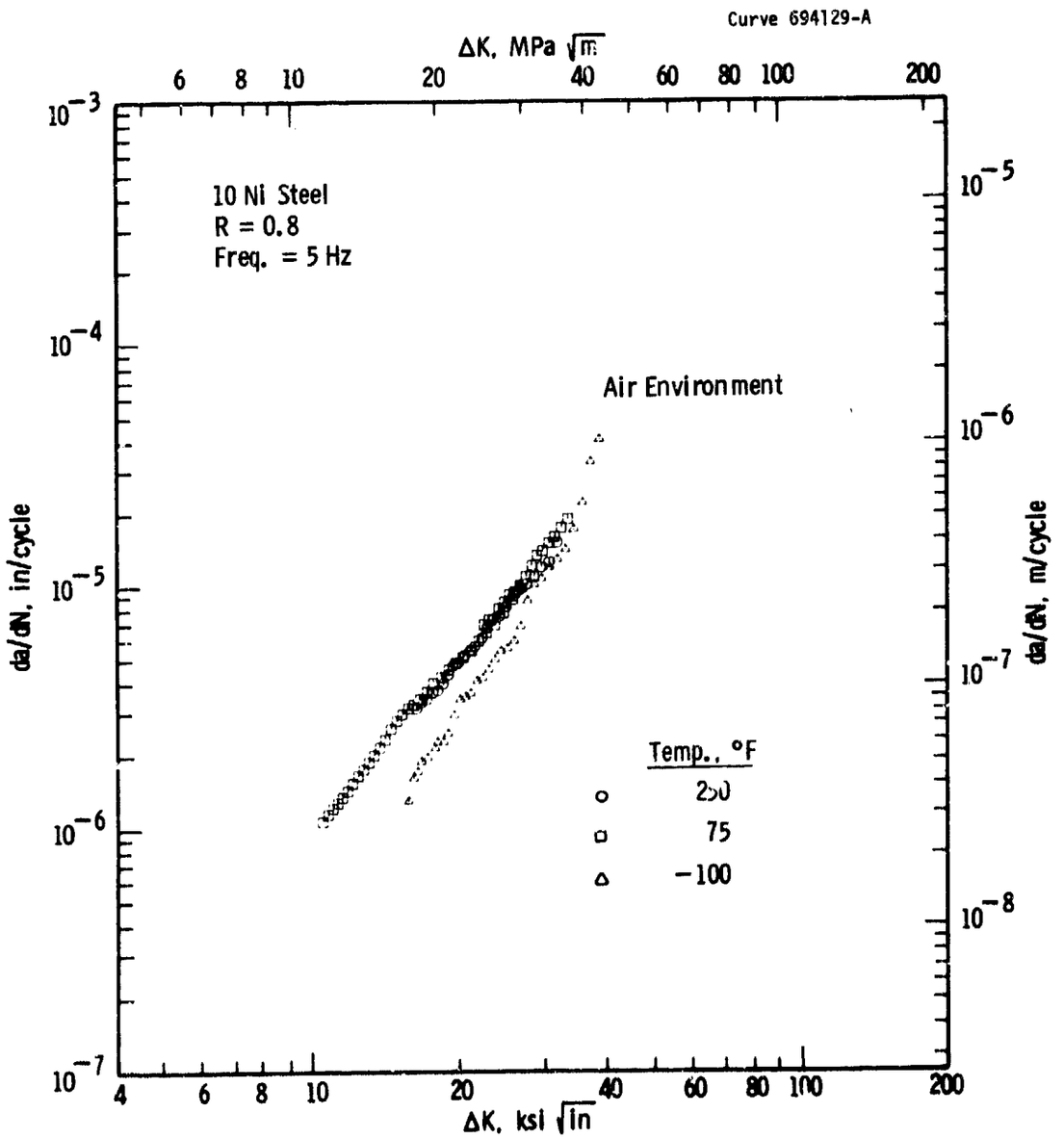

Fig. 4-29— Effect of temperature on fatigue crack growth rates in 10 Ni steel tested in laboratory air at R = 0.8, freq. = 5 Hz

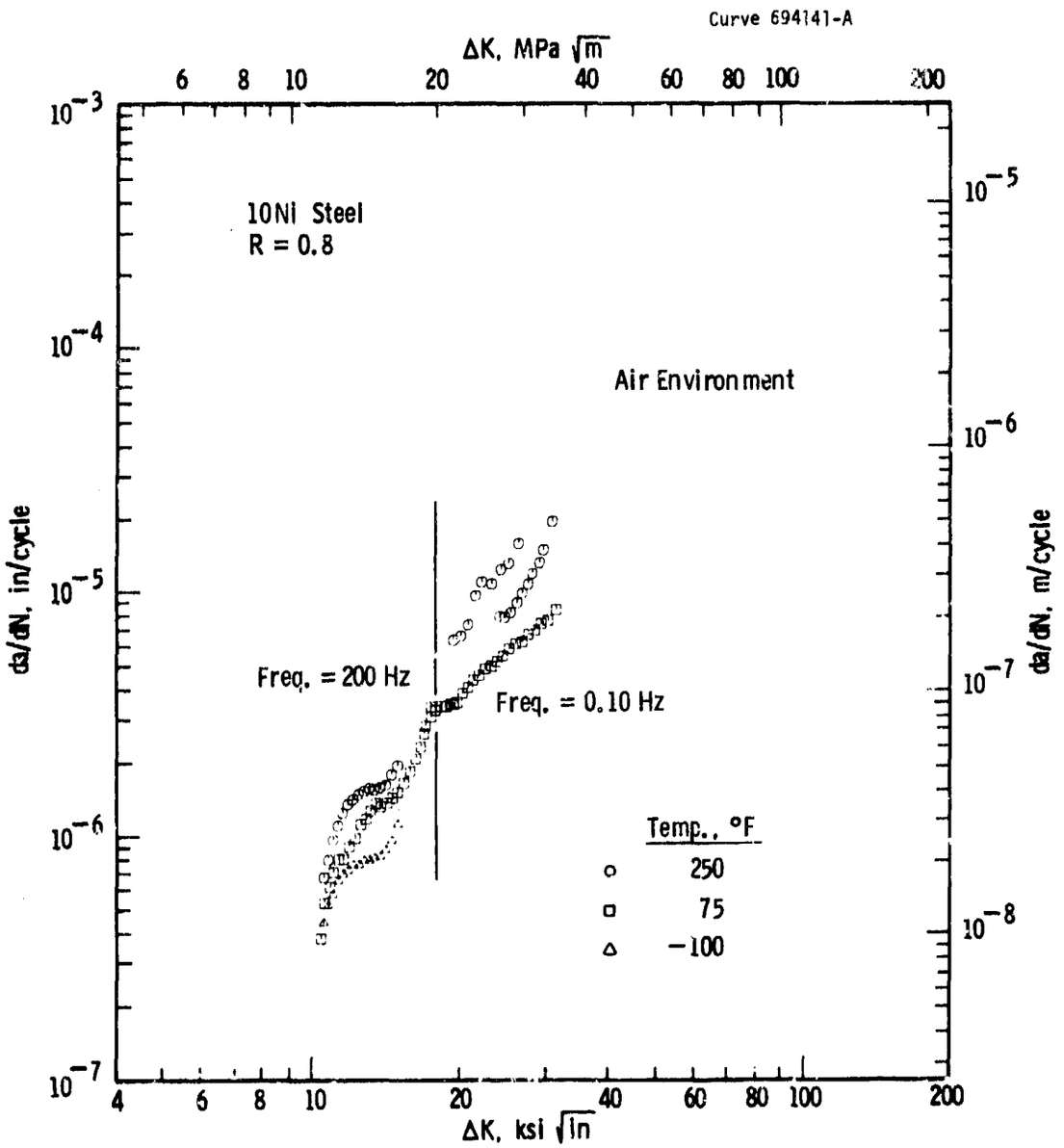

Fig. 4-30— Effect of temperature on fatigue crack growth rates in 10Ni steel tested in laboratory air at R = 0.8, Freq. = 0.10, 200 Hz

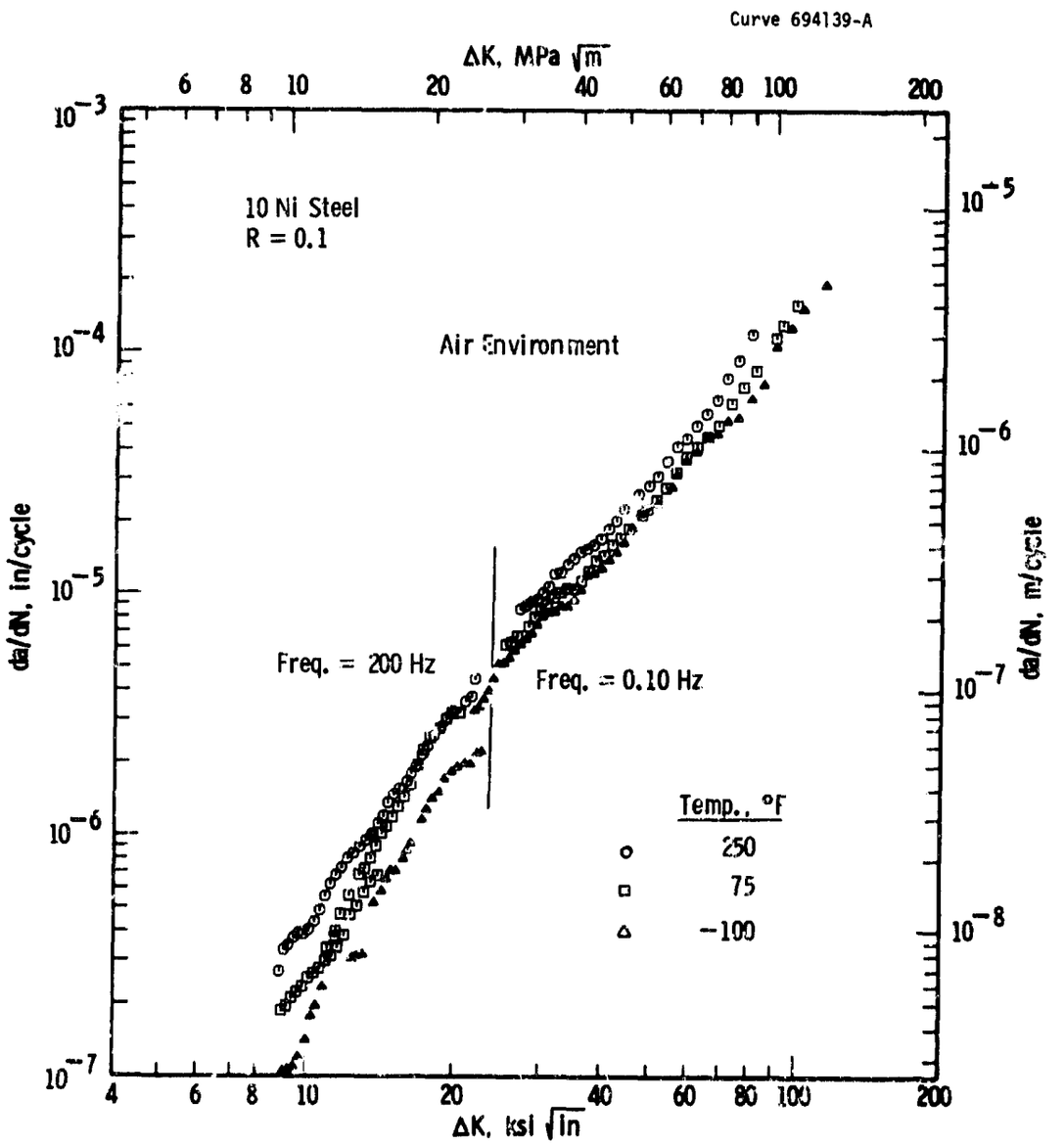

Fig. 4-31— Effect of temperature on fatigue crack growth rates in 10 Ni steel tested in laboratory air at R = 0.1, Freq. = 0.10, 200 Hz

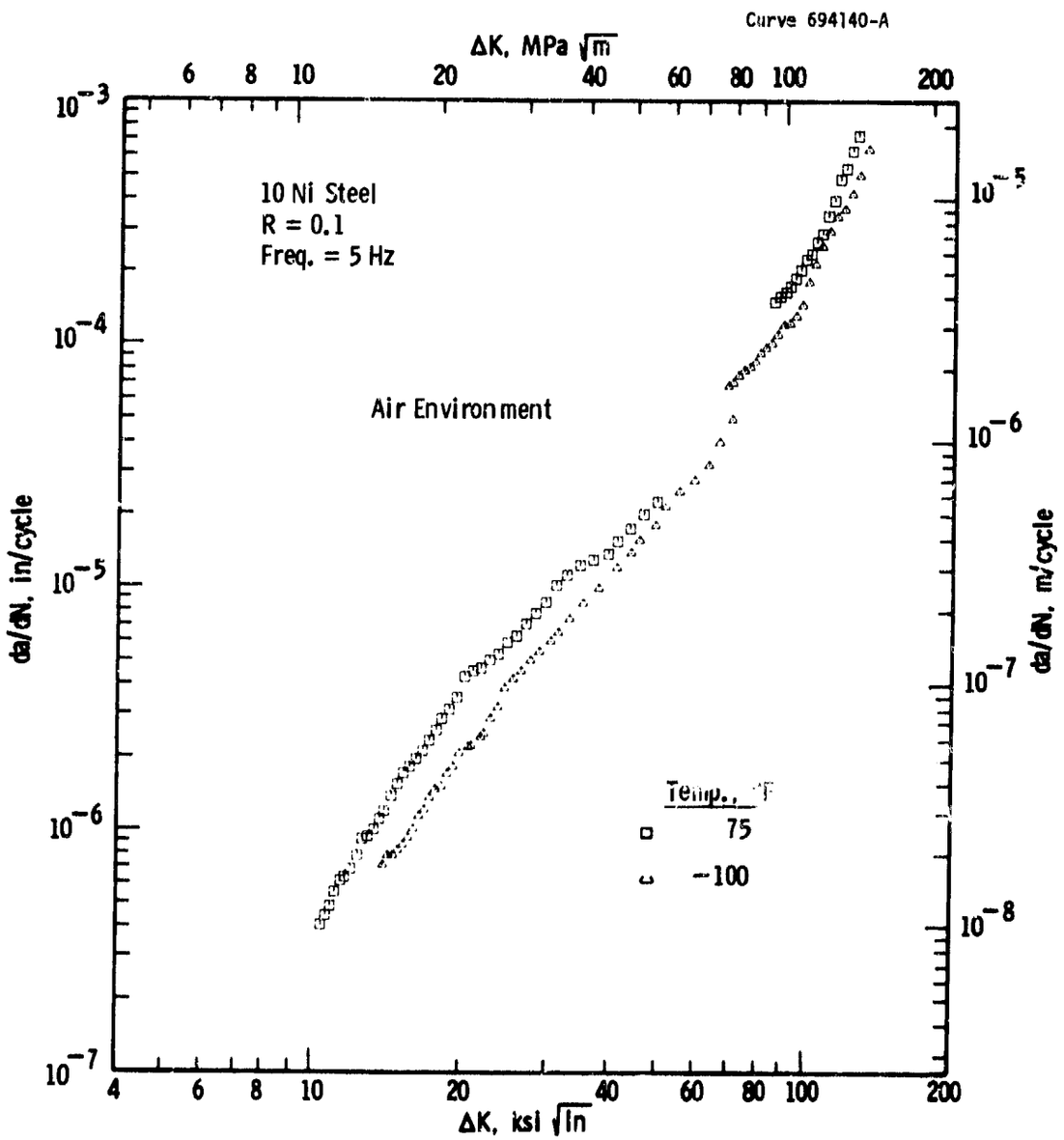

Fig. 4-32 -- Effect of temperature on fatigue crack growth rates in 10Ni steel tested in laboratory air at R = 0.1, Freq. = 5 Hz

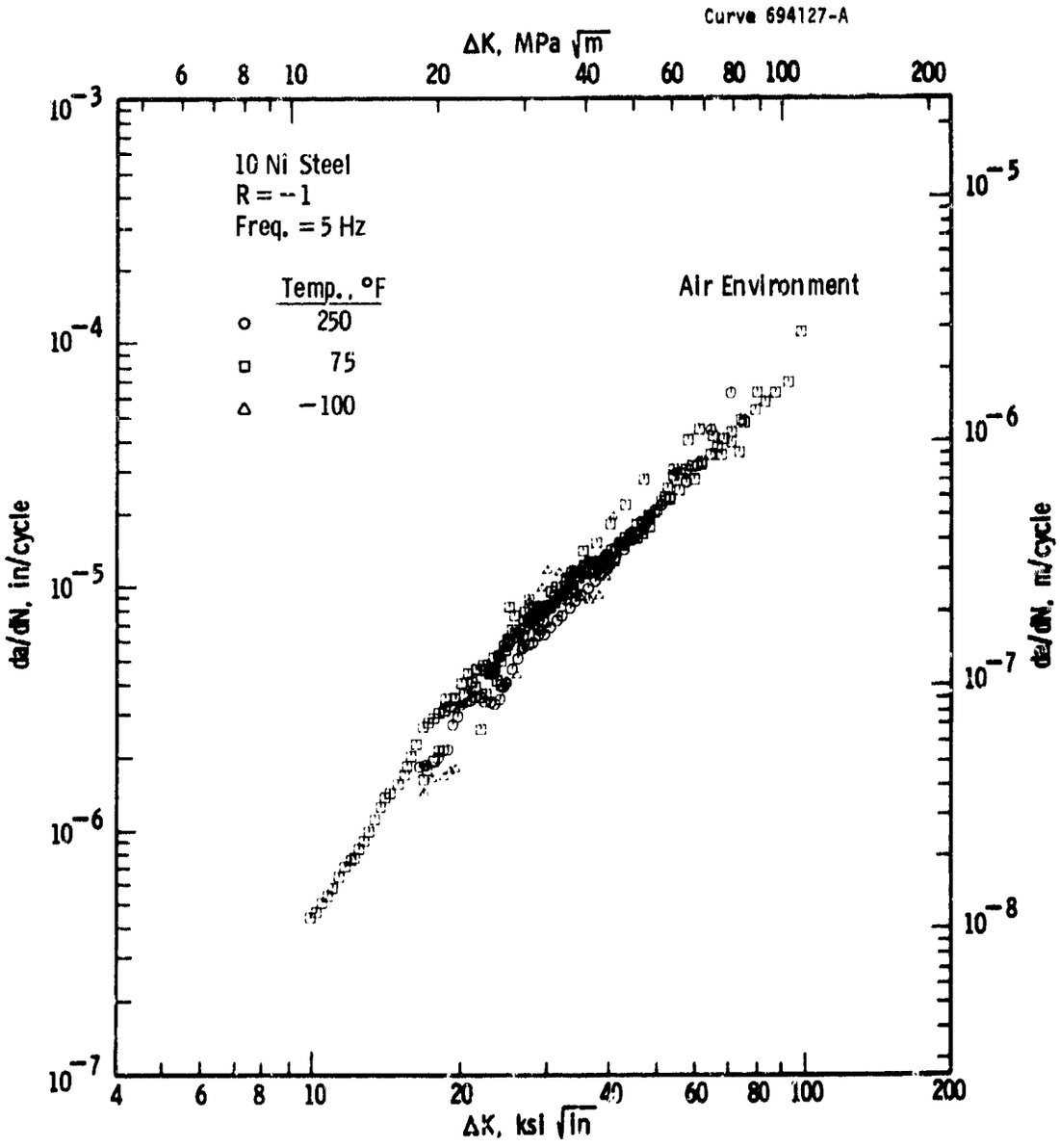

Fig. 4-33— Effect of temperature on fatigue crack growth rates in 10 Ni steel tested in laboratory air at R = −1, freq. = 5 Hz

Figure 4-28 shows that temperature changes over the range from -32°F to 250°F result in no discernable trends in the growth rates in dry argon. Growth rate data obtained in laboratory air at temperatures ranging from -100°F to 250°F are given in Figs. 4-29 and 4-33 for a variety of load ratios. These data show a consistent increase in the growth rates in the 10Ni steel as temperature is increased. However, the effect is in some cases barely discernable and never increases the growth rates by more than a factor of two. For this reason, additional analyses in terms of a Arrhenius representation was not undertaken. Data in Fig. 4-31 show a slight decrease in the temperature dependence as the test frequency is decreased and thus are consistent with the general explanation of the temperature dependence formulated for 2219-T851 aluminum.

4.3.6 Effect of Crack Straightness

During the acquisition of data on the influence of loading and environmental variables on fatigue crack growth rates, ancillary information was obtained on the influence of crack straightness on measured fatigue crack growth rates. Crack straightness, which differs from crack tunneling, is defined in terms of differences in crack length measured on the front and back surfaces of a specimen. The allowable extent of crack non-straightness is specified in Section 8.7.4 of Appendix I.

Figure 4-34 provides an example of the effect of non-straight cracks on the fatigue crack growth rates measured at several test temperatures. The anomalous rates which are shown as solid data points correspond to violations of the proposed straightness requirements (Section 8.7.4, Appendix I). These data were generated on 1/4-in.-thick CT specimens (W = 2 in.). The invalid rate measurements are based on front and back surface crack length measurements which differed by more than 0.050 in. and thus exceeded the 0.025W requirement. This difference was primarily the result of unsymmetrical initiation of cracking along the machined notch during precracking.

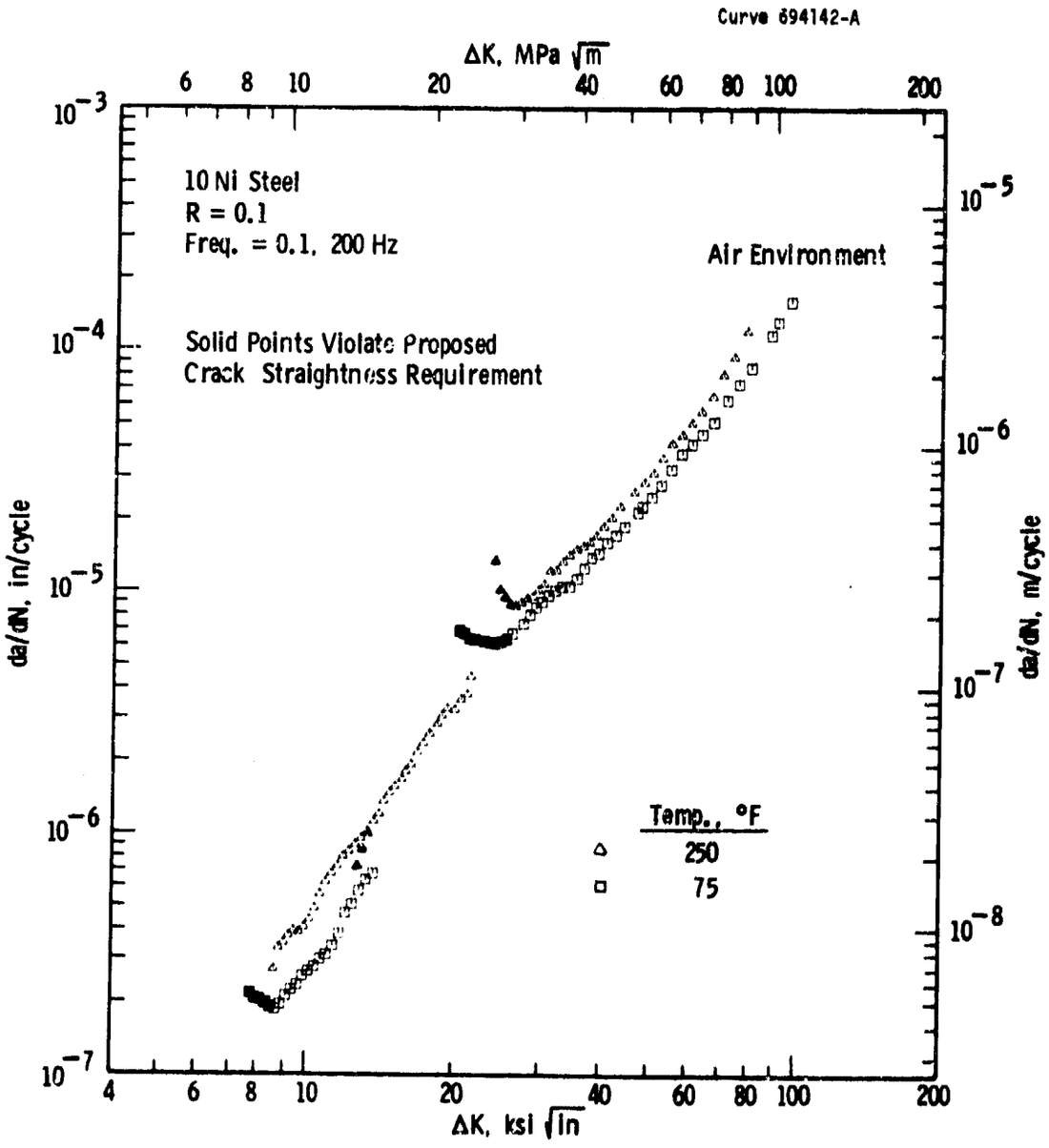

Fig. 4-34– Influence of crack straightness on fatigue crack growth rates in 10Ni steel tested in laboratory air at various temperatures

These problems are inevitable, in spite of the notch preparation procedures recommended in Section 7.3 of Appendix I.

The above results clearly demonstrate the need for a limitation on crack non-straightness and attest to the utility of the proposed straightness requirements. Recognization of this problem should help to explain — and hopefully eliminate — some of the anamolous data reported in the literature, particular those at the start of a test.

4.4 Establishment of Specimen Size Requirements

The purpose of a requirement on specimen size in fatigue crack growth rate testing is to maintain predominately elastic conditions in the test specimen, thereby allowing results to be interpreted in terms of the crack-tip stress intensity which is defined by linear-elastic theory. The size requirement is not intended to maintain a plane strain state of stress at the crack-tip as is the case for size requirements in ASTM E399 on fracture toughness testing. Specimen thickness (and thus stress state) is considered to be a controlled test variable in fatigue crack growth rate testing.

Current recommended size requirements for fatigue crack growth rate testing (Section 7.2 of Appendix I) are as follows:

CT Specimens

$$W-a \geq \frac{4}{\pi}\left[\frac{K_{max}}{\sigma_{YS}}\right]^2 \tag{4-3}$$

CTT Specimens

$$\sigma_N \leq \sigma_{YS} \tag{4-4}$$

where

$$\sigma_N = \frac{P}{BW(1 - 2a/W)} \tag{4-5}$$

In terms of a requirement on the specimen's uncracked ligament, Eqs. (4-4) and (4-5) give

$$(W-2a) \geq \frac{P_{max}}{B\,\sigma_{YS}} \tag{4-6}$$

These requirements are specific to specimen geometry because as discussed previously the loading modes of these specimens differ significantly.[4] For the CCT specimen, which is loaded in a tensile

mode, the conditions of $\sigma_N = \sigma_{YS}$ and fully plastic limit load are achieved at nearly the same applied loads. On the other hand, due to a bending mode in the CT specimen these two conditions occur at significantly different applied loads. Thus, a broader range of possible requirements exist for the CT specimen. For this reason data on the general utility of the size required for the CT specimen are reviewed and discussed in the following sections. Addition questions are also addressed in these sections; namely,

1) Should size requirements be formulated in terms of the monotonic or cyclic plastic zone size?
2) If the monotonic plastic zone is appropriate, how should it be estimated for strain-hardening materials?

4.4.1 Results on 10 Ni Steel

The high toughness of the 10 Ni steel examined in this program provided the opportunity to generate results which give information on the current size requirements. Fatigue crack growth rates obtained at R = 0.8 using CT specimens (B = 1/4 in., W = 2.0 in.) are shown in Fig. 4-35; results violating the current size requirement are given as solid data points. Data obtained at a test frequency of 0.1 Hz are up to a factor of two slower than those obtained at 5 Hz and are believed to be related to transient effects accompanying test interuptions during these long duration test at 0.1 Hz.[2] Note also that invalid data tend to exhibit upturns or accelerations -- particularly in specimen 10N-9.

Specimen deflections, measured at a location 0.19 in. from the front surface of these specimens, were monitored throughout the tests. Figures 4-36 and 4-37 give both the maximum deflection, V_{max}, and the deflection range, ΔV as a function of fatigue crack length. The maximum deflections calculated from elastic compliance*, V^e_{max}, is also provided for comparison. As shown values of V_{max} for both

*Equations for calculation of elastic compliance are given in Section 3.4.

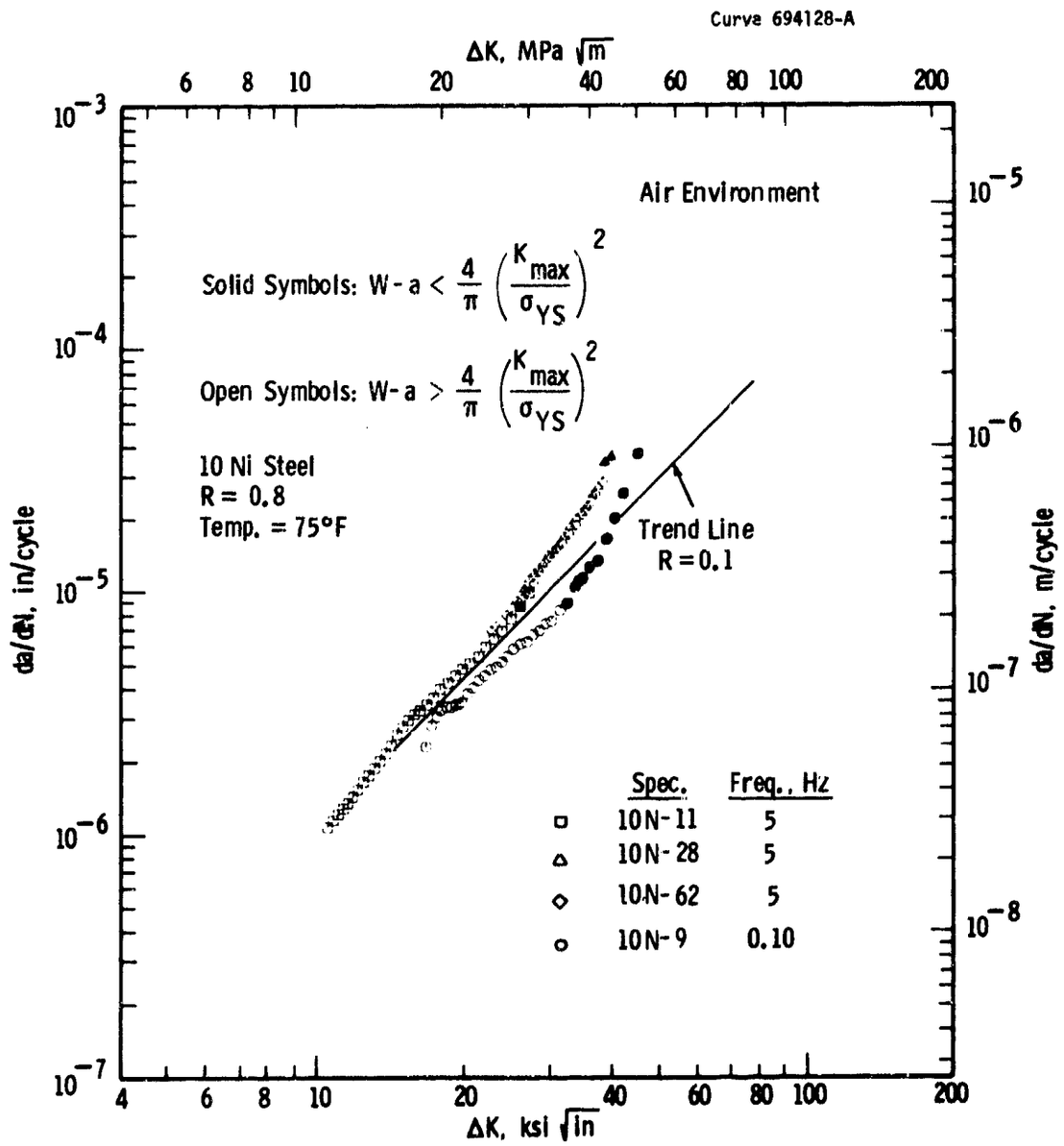

Fig. 4-35 – Effect of specimen size requirement violations on fatigue crack growth rates in 10 Ni steel

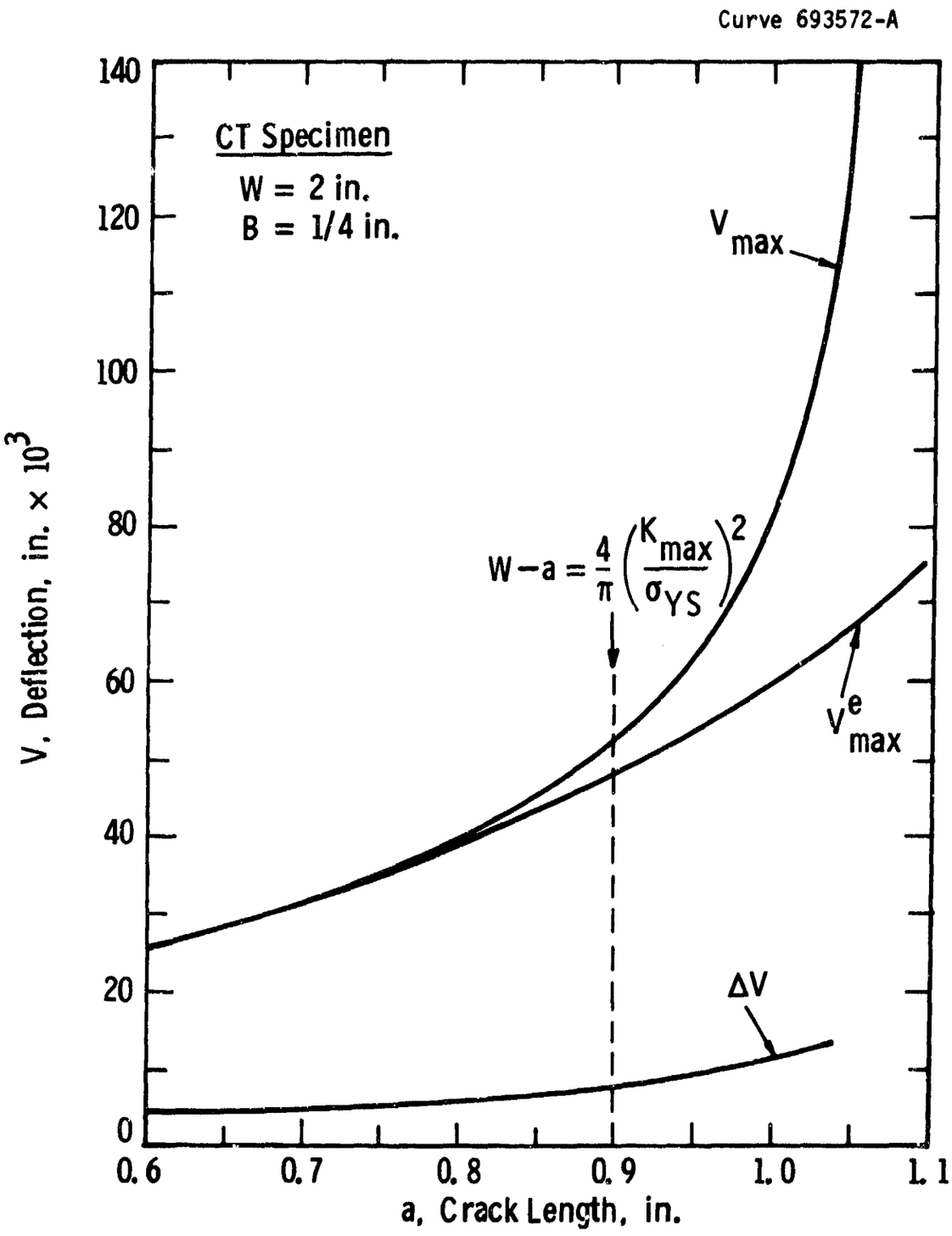

Fig. 4-36— Measured versus elastically calculated specimen deflections during fatigue crack growth test on 10 Ni steel (Specimen 10N-28)

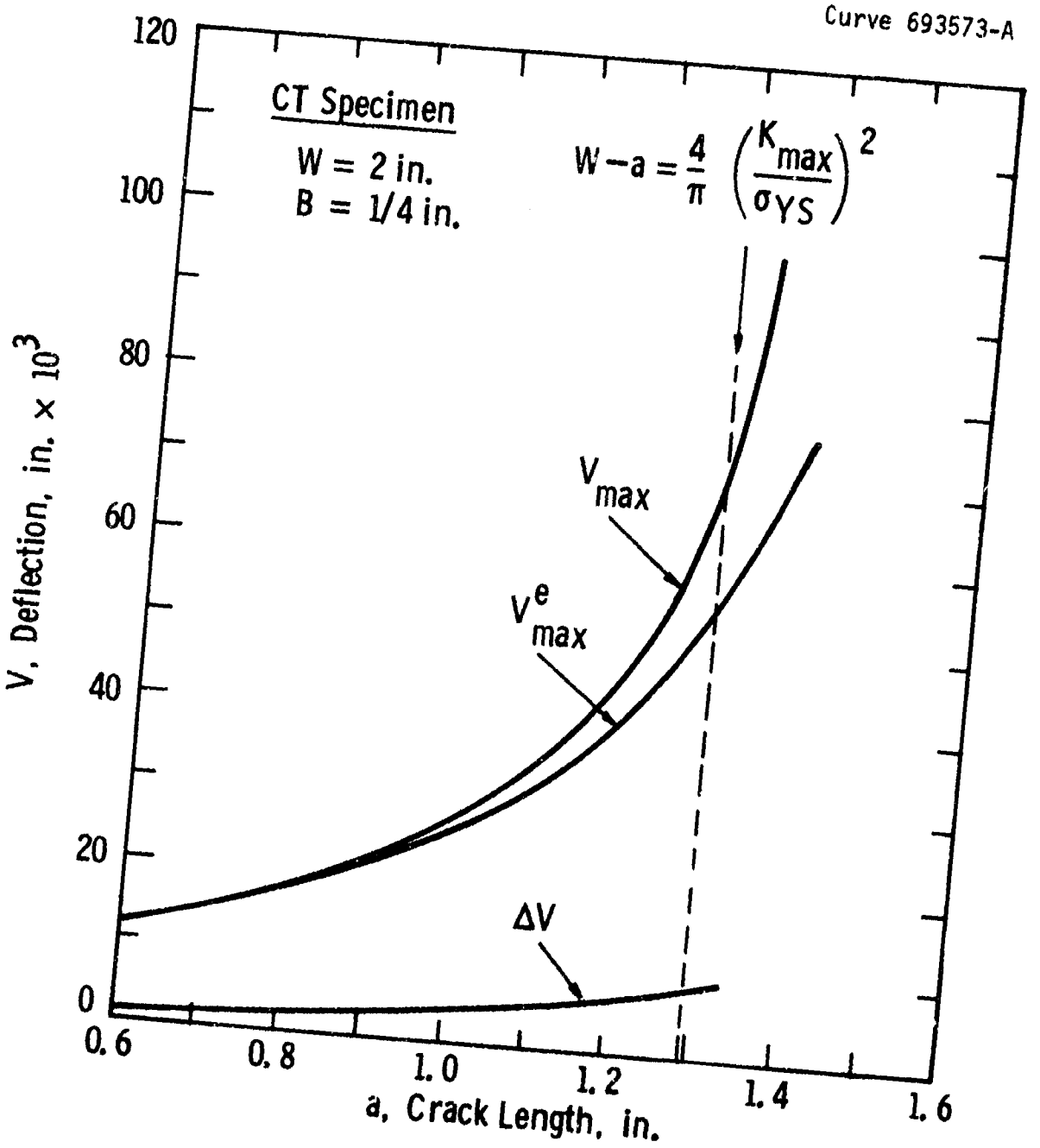

Fig. 4-37 — Measured versus elastically calculated specimen deflections during fatigue crack growth test on 10 Ni steel (Specimen 10N-11)

specimens 10N-11 and 10N-28 become increasingly larger than V^e_{max} as the fatigue crack extends. This deviation (V_{max}-V^e_{max}) is due to plasticity development in the uncracked ligament and defines a plastic component of the specimen deflection, $V_{plastic}$. Furthermore, the deflection range remains essentially unaffected by this plasticity development as evidenced by: 1) no hysteresis in periodic autographic recordings of load versus deflection during the test and 2) compliance values obtained from measured ΔV values were consistent with calculated elastic compliance values.

Figures 4-36 and 4-37 also identify the maximum crack length values from Eq. (4-3). As indicated in these figures, meeting the specimen size requirement limits $V_{plastic}$ to about 10 to 20 percent of V_{max}. The increase $V_{plastic}$ for data not satisfying Eq. (4-3) appears to be the cause of the accelerated growth rates in Fig. 4-35.*

The deflection data in Figs. 4-36 and 4-37 also illustrate that fracture of the 10 Ni steel test specimens is controlled by fully plastic limit load behavior rather than by a K_{max}-controlled instability. Terminal values of crack length agree with predictions based on fully plastic limit load while terminal K_{max} values of about 200 ksi$\sqrt{in}$. are estimated to be significantly below the fracture toughness of this material.[28]

4.4.2 Survey of Results on Other Materials

A survey of fatigue crack growth rate data from the literature which provides additional insight on the specimen size requirement for CT specimens is presented in this section. This information primarily relates to the applicability of the current size requirement to low strength materials.

James has summarized room temperature fatigue crack growth rate data on annealed 304 stainless steel (σ_{YS} = 30 ksi) which was

*Unfortunately, due to X-Y recorder problems, deflection measurements were not obtained near the end of the test for specimen 10N-9 which exhibited the most accelerated growth rates.

obtained using ten widely differing specimen geometries.[9] As illustrated in Fig. 4-38 these data are within a scatter band of a factor of 3 to 4 and are considered to be in reasonable agreement considering the fact that they were generated by different laboratories and include small variations in such variables as relative humidity, cyclic frequency, and load ratio. Unfortunately, detailed information on test loads and crack lengths are not available for many of these data to check whether or not Eq. (4-3) is violated. However, data on the CT (W = 2 in. and 4 in.) and WOL (W = 2.55 in.) specimens are certain to be in violation of Eq. (4-3) -- particularly those data above 60,000 psi$\sqrt{\text{in.}}$. In spite of this fact, CT and WOL data agree with results from the other specimen geometries. This geometry independence of the data suggests that the assumption of small scale yielding is not violated, and thus the crack-tip stress intensity represents a proper driving-force for fatigue crack growth under these conditions.

Figure 4-39 includes additional data on annealed 304 stainless steel.[50,51] These data were obtained at 1000°F (where σ_{YS} = 17 ksi) using CT (W = 2.0 in.) and single-edge-notched (SEN, W = 5.0 in.) specimens. From information on applied loads and crack lengths, specific data points for these tests were checked against the requirement of Eq. (4-3). Solid points in Fig. 4-39 represent data which violates Eq. (4-3) while open points are valid.* Interestingly, data differentiated on this basis exhibit growth rates which are in agreement (within a factor of two) when results are analyzed in terms of linear-elastic fracture mechanics. The implication of these results is that Eq. (4-3) results in conservative size requirements for annealed 304 stainless steel.

Additional information on this point is provided by data from Dowling[29] and Paris, et al.[52] on an A533B steel (σ_{YS} = 70 ksi) and

*Since deeply cracked SEN specimens experience a loading mode similar to that for CT specimens, it is assumed that Eq. (4-3) is equally applicable to SEN specimens.

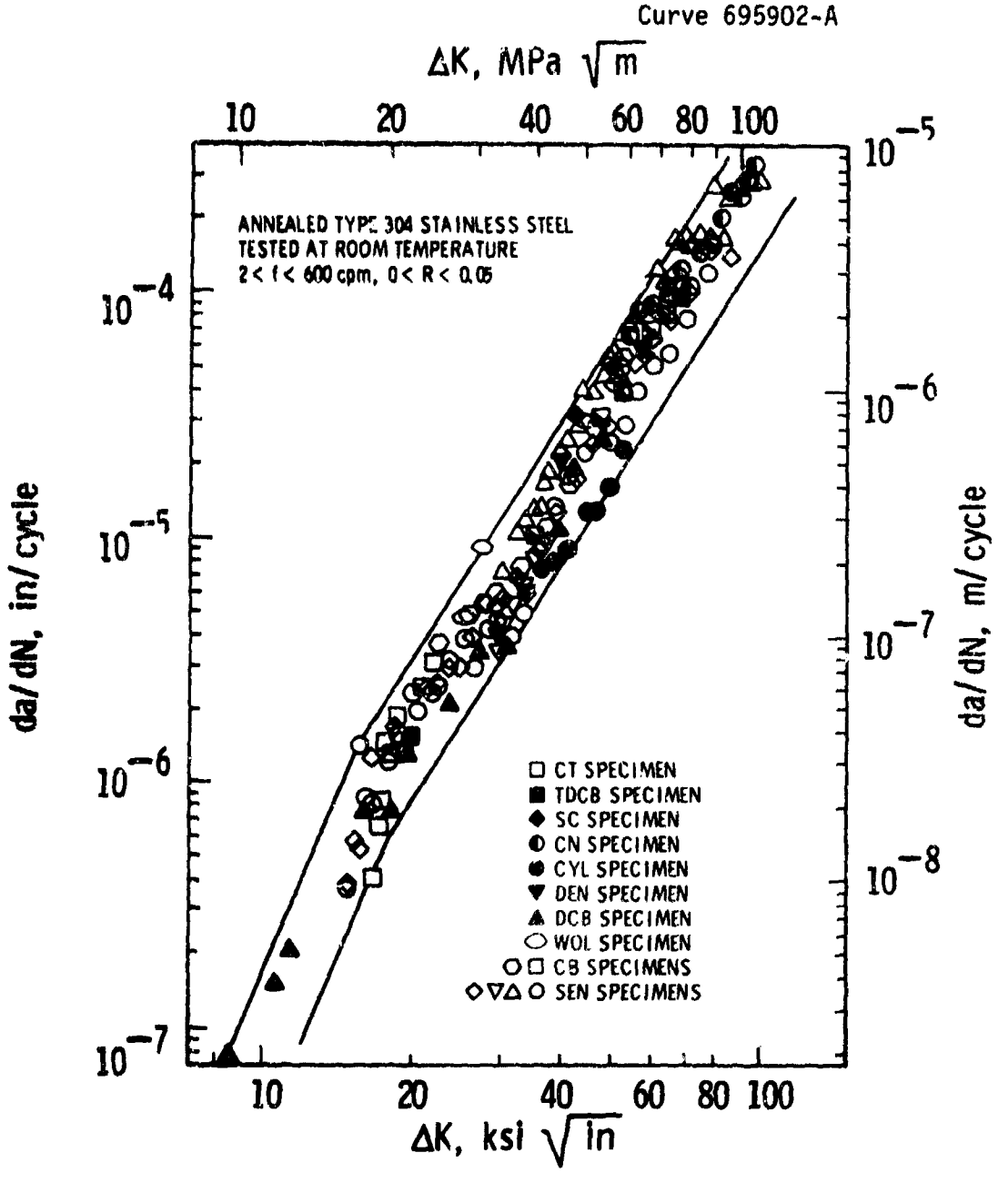

Fig. 4-38—Fatigue crack growth rate data on annealed 304 stainless steel illustrating geometry independence

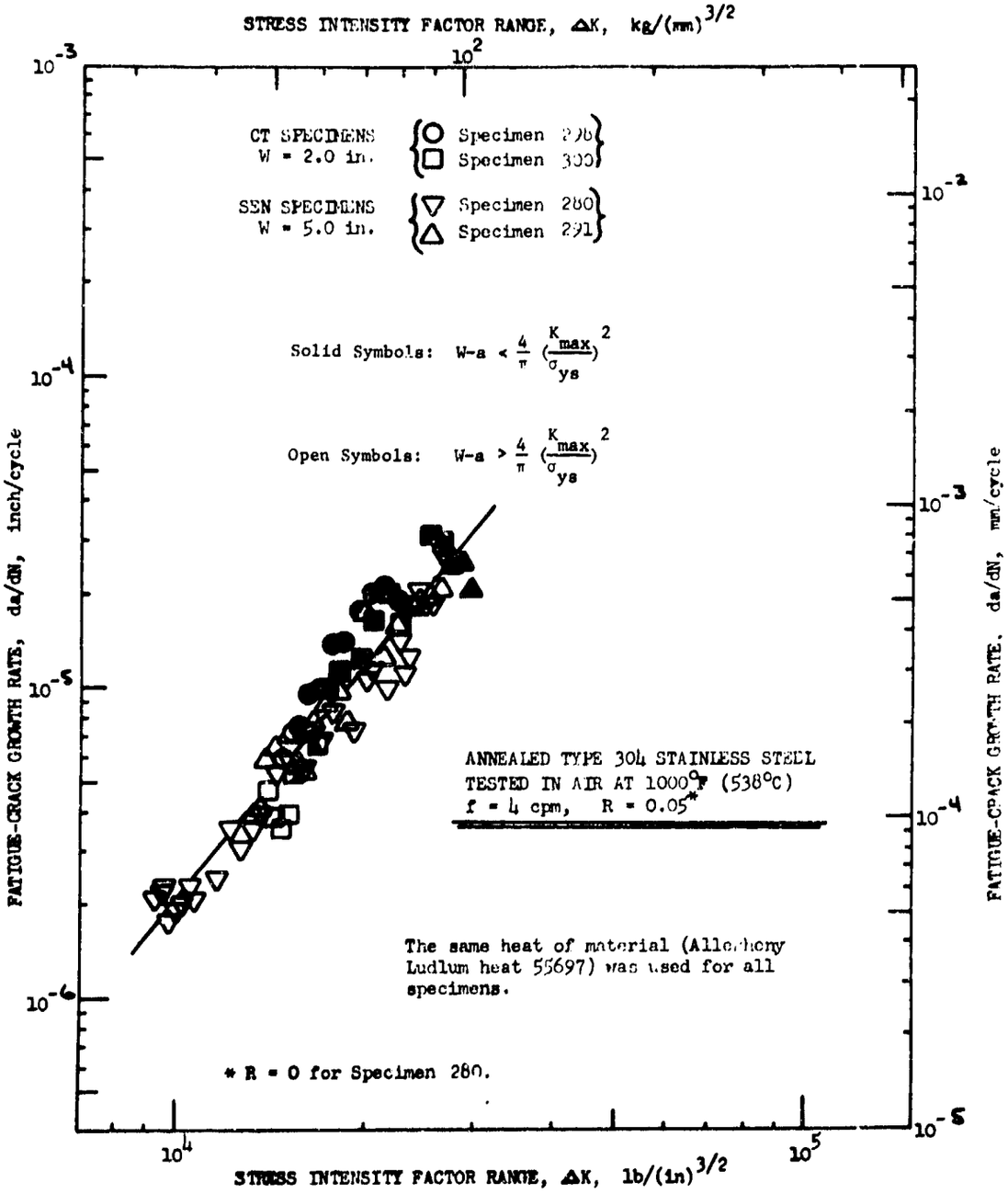

Fig. 4-39 - Fatigue crack growth rate data on annealed 304 stainless steel tested at 1000°F

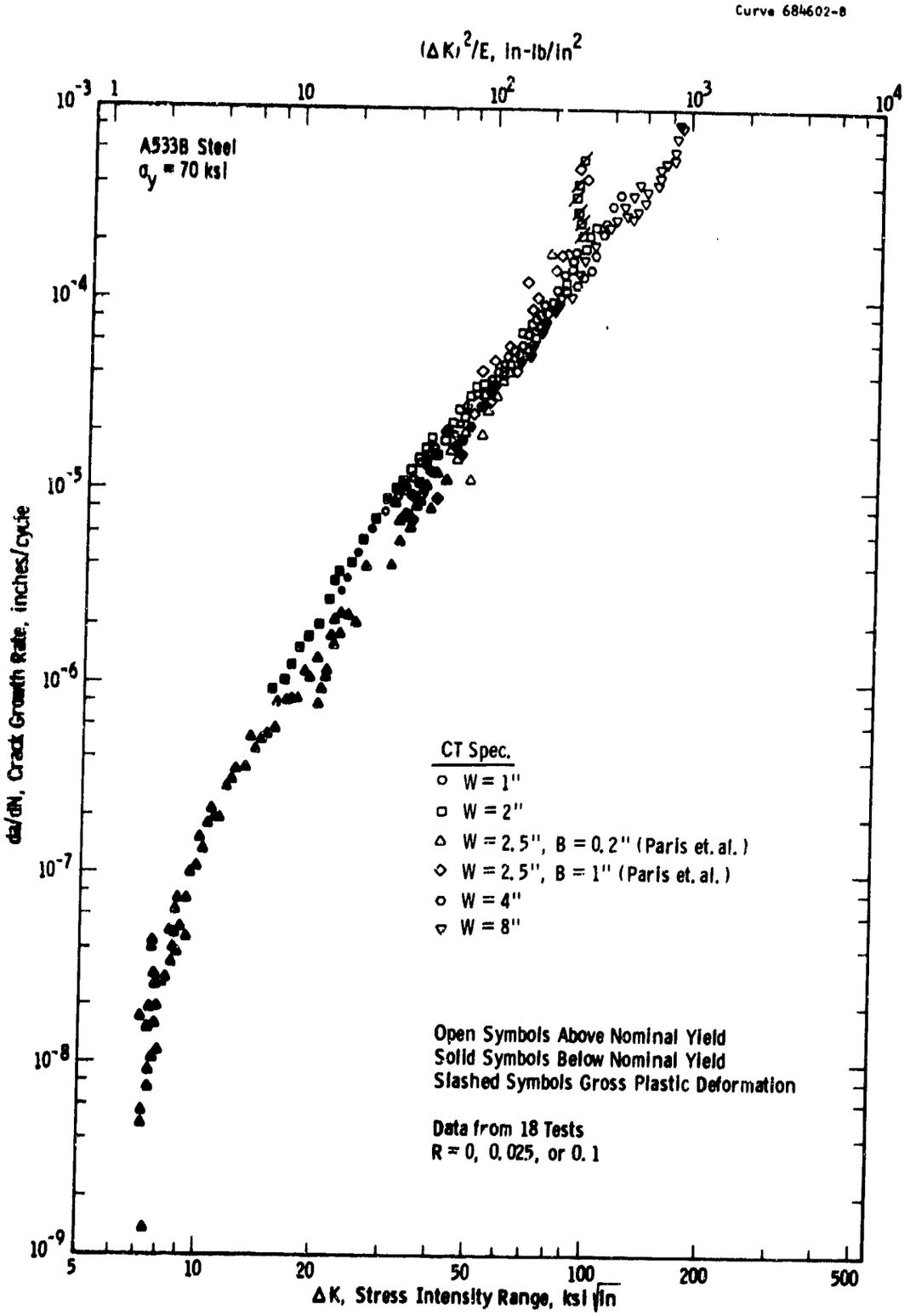

Fig. 4-40—Fatigue crack growth rate versus stress intensity for various size specimens of A533B steel

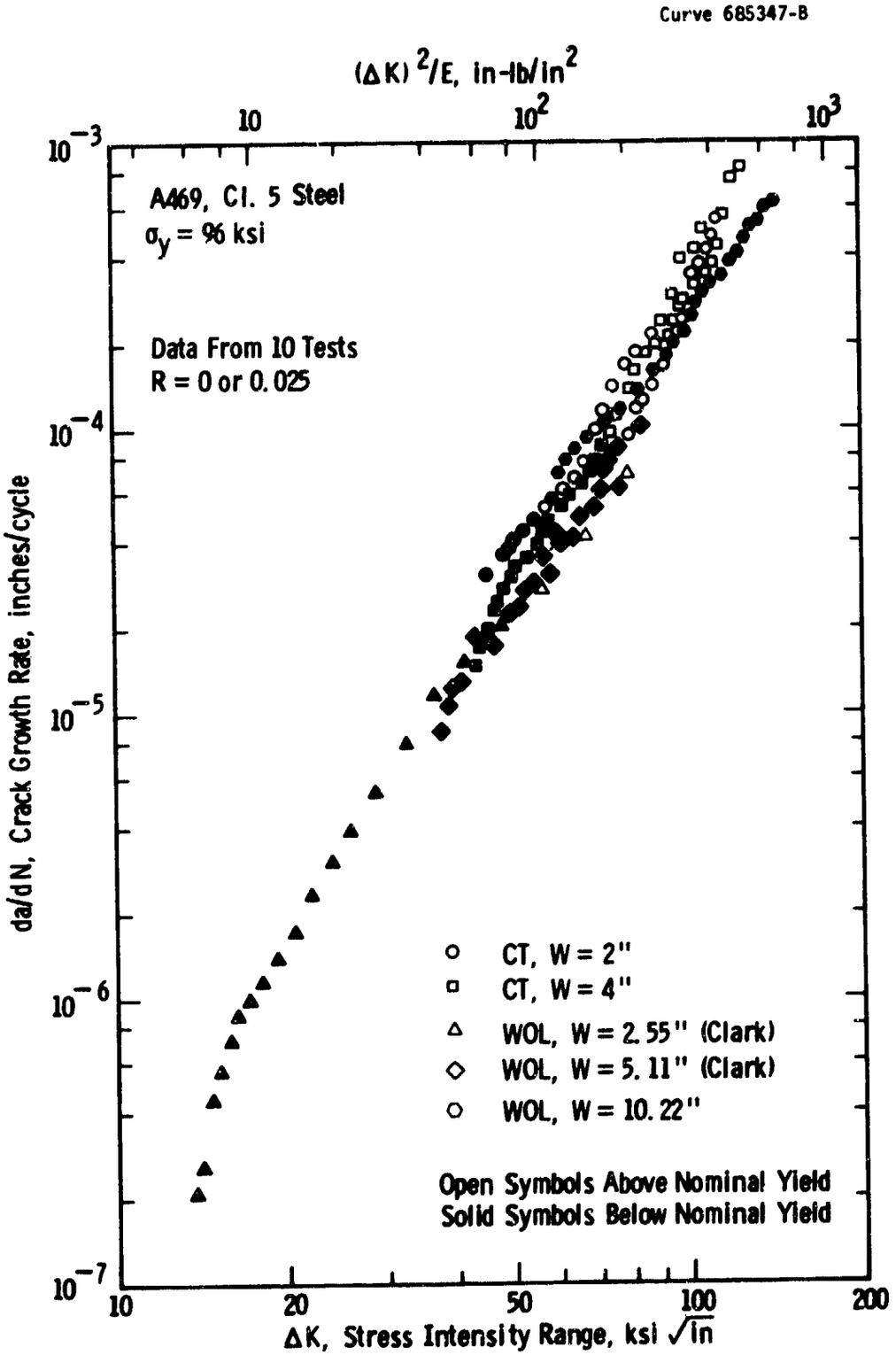

Fig. 4-41– Fatigue crack growth rate versus stress intensity for various size specimens of A469, Cl. 5 steel

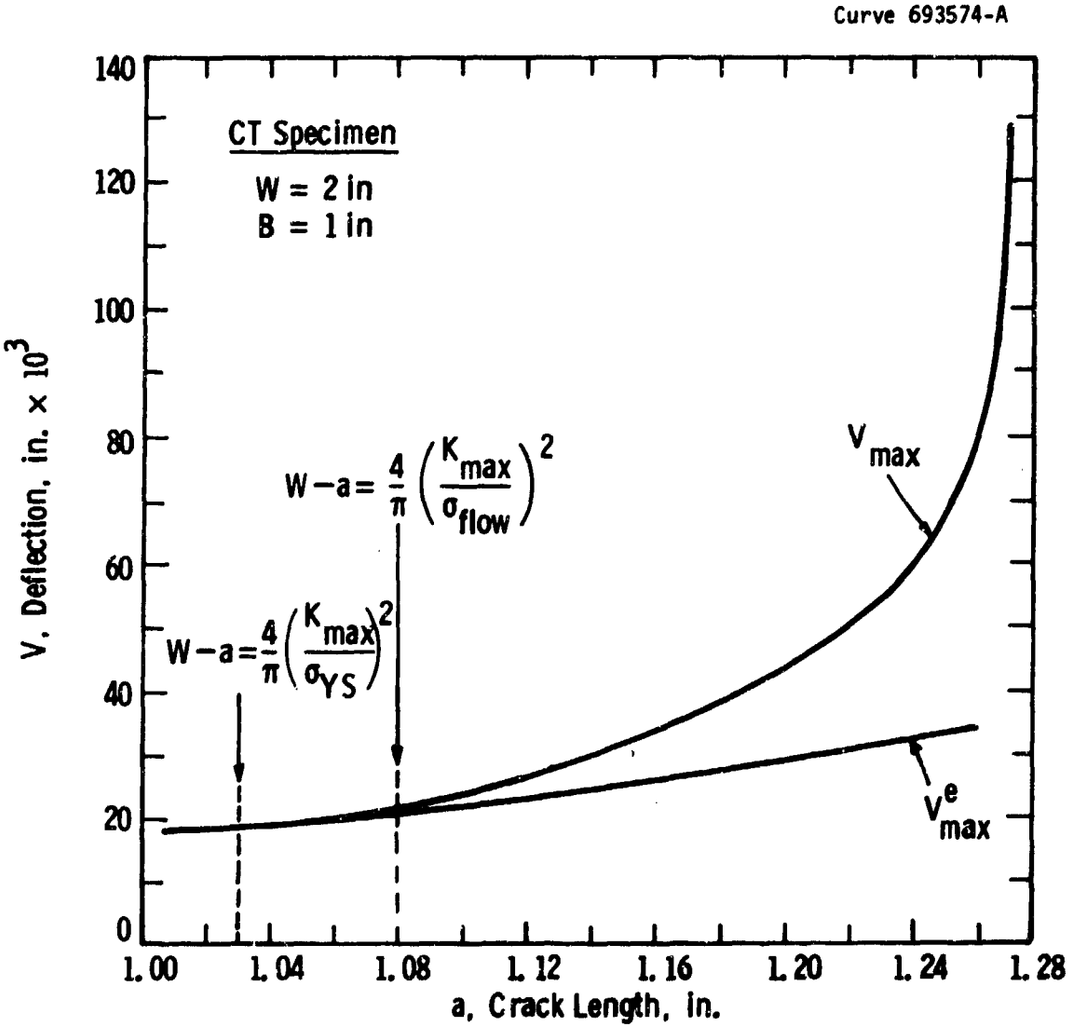

Fig. 4-42—Measured versus elastically calculated specimen deflections during fatigue crack growth test on A533B steel

by Dowling [29] and Clark [53] on an A469 steel (σ_{YS} = 96 ksi). These data which were obtained on a wide-range of CT and WOL specimen sizes are shown in Figs. 4-40 and 4-41; solid symbols represent data obtained under conditions where the nominal stress (including tension plus bending) in the uncracked ligament, σ_N, was less than the materials' yield strengths, while open symbols are for $\sigma_N > \sigma_{ys}$. Terminal data points in these tests coincide with fully plastic limit load conditions. Equation (4-3) is violated about midway (in terms of ΔK) between $\sigma_N = \sigma_{YS}$ and fully plastic behavior. In spite of this fact data (Figs. 4-40 and 4-41) which are both valid and invalid by Eq. (4-3) are in agreement.

Deflection measurements are also available for specimens used to obtain data above 10^{-5} in./cycle in Figs. 4-40 and 4-41. For example, Fig. 4-42 shows the maximum deflection as a function of fatigue crack length. As indicated in Fig. 4-42, Eq. (4-3) is violated for crack lengths beyond 1.03 in., however, unlike behavior in the 10 Ni steel (Figs. 4-36 and 4-37) the measured and elastically calculated deflections remain equal at this point. This behavior is probably due to the fact that the A533B steel is capable of considerably more monotonic strain hardening than is the 10 Ni steel. Using the flow stress, i.e., $\sigma_{flow} = 1/2(\sigma_{YS} + \sigma_{ult})$, in place of σ_{YS} in Eq. (4-3) is a simple means of accounting for strain hardening, nevertheless, it predicts a limiting crack length of 1.08 in. which coincides with the onset of a measurable plastic deflection component. Another interesting point is the fact that this plastic deflection appears not to cause acceleration in the data as was the case in the 10 Ni steel.

4.4.3 Discussion and Recommendations on Specimen Size Requirements

Results presented in previous sections indicate that for high strength, low monotonic strain hardening materials (e.g., 10 Ni steel) the current size requirement for CT specimens corresponds to the onset of a measurable plastic deflection in the specimen which are accompanied by accelerations in growth rate. Thus, for these materials the size requirement of Eq. (4-3) appears both appropriate and necessary. On

the other hand, the same size requirement appears to be conservative for low strength materials which exhibit significant monotonic strain hardening (e.g., annealed 304 stainless steel).

Several alternatives are worth considering to alleviate the conservative requirement for low strength materials. Since most of these materials also exhibit cyclic hardening, it has been proposed that Eq. (4-3) be simply modified by replacing σ_{YS} by the 0.2% offset cyclic yield, σ_{YS}^{c}.[54] Another alternative, which was considered in the previous section, is to replace σ_{YS} by $\sigma_{flow} = 1/2(\sigma_{YS} + \sigma_{ult})$ in Eq. (4-3). The impact of each of these changes on size requirements for various materials is given in Table 4-4. Both the monotonic and cyclic flow properties are given for a variety of materials; the last two columns give factors by which the current remaining ligament (W-a) requirement would be changed by the above modifications. For several materials these changes are quite large; for example, in hot rolled and annealed SAE AM-350, replacing σ_{YS} by σ_{flow} requires a (W-a) which is 25% of the current requirement and replacing σ_{YS} by σ_{YS}^{c} requires (W-a) which is only 11% of the current requirement. For higher strength materials the impact of these same changes is much different; for example, in quenched and tempered SAE 4340 steel replacing σ_{YS} by σ_{flow} would alter the (W-a) requirement by only a few percent, while replacing σ_{YS} by σ_{YS}^{c} would require a (W-a) of 2.8 times the current requirement due to the fact that this material cyclicly hardens. However, an increase in the size requirement for high strength materials such as SAE 4340 is not consistent with general testing experience.

It is helpful to further consider the above alternatives in terms of simple physical models. The current size requirement for CT specimens is equivalent to restricting the monotonic plastic zone size ($2r_y$) to a fixed percentage of the specimen's uncracked ligament. For plane stress conditions $2r_y$ is estimated by[55]*

*The arguments which follow apply equally well for plane strain conditions.

TABLE 4-4

POTENTIAL INFLUENCE OF VARIOUS FLOW PROPERTIES ON CURRENT SIZE REQUIREMENTS FOR CT SPECIMENS

Material	Condition	σ_{YS} (ksi)	σ_{ult} (ksi)	σ_{flow} (ksi)	σ_{YS}^{c} (ksi)	Factors by Which Current (W-a) Requirement Changes	
						$\sigma_{flow} \rightarrow \sigma_{YS}$	$\sigma_{YS}^{c} \rightarrow \sigma_{YS}$
SAE AM-350	Hot Rolled and Annealed	64	191	128	196	0.25	0.11
RQC-100	Hot Rolled Plate	128	135	131	87	0.95	2.2
SAE 1045	Quenched and Tempered	198	210	204	120	0.94	2.7
SAE 4340	Quenched and Tempered	199	213	206	120	0.93	2.8
SAE 30304	Hot Rolled and Annealed	37	108	72	104	0.26	0.13
AISI 316 SS (@ 800°F)	Annealed	19	67	43	42	0.20	0.20
2014-T6	Sol. Treat. and Artificial Age	67	74	71	60	0.89	1.12
7075-T6	Sol. Treat. and Artificial Age	68	84	76	76	0.80	0.80
5456-H311	Strain Hardened	34	58	46	52	0.55	0.43

$$2r_y = \frac{1}{\pi}\left[\frac{K_{max}}{\sigma_{YS}}\right]^2 \tag{4-7}$$

thus, the requirement of Eq. (4-3) allows

$$\frac{2r_y}{(W-a)} = 1/4 \tag{4-8}$$

Hence, the current size requirement limits the monotonic plastic zone to about 25% of the uncracked ligament.

For cyclic loading the plane stress plastic zone size ($2r_y^c$) can similarly be estimated by[56,57]

$$2r_y^c = \frac{1}{4\pi}\left(\frac{\Delta K}{\sigma_{YS}}\right)^2 \tag{4-9}$$

In addition, since reversed yielding occurs in the cyclic plastic zone it is appropriate to use σ_{YS}^c in place of σ_{YS} in the above equation, giving

$$2r_y^c = \frac{1}{4\pi}\left[\frac{\Delta K}{\sigma_{YS}^c}\right]^2 \tag{4-10}$$

The ratio of cyclic to monotonic plastic zone sizes is from Eqs. (4-7) and (4-10) is given by

$$\frac{r_y^c}{r_y} = \frac{(1-R)^2}{4}\left(\frac{\sigma}{\sigma_{YS}^c}\right)^2 \tag{4-11}$$

where $R = K_{min}/K_{max}$. As indicated by Eq. (4-11) this ratio becomes very small for large R values and for much cyclic hardening. A schematic of relative plastic zone sizes is given in Fig. 4-43 for R = 0 and R = 0.8 and for various degrees of cyclic hardening. As illustrated both cyclic and monotonic plastic zones are present during fatigue crack growth rate testing.

The above relative size estimates are consistent with the deflection measurements presented previously, Section 4.4.1.

Measurable plastic deflections occur when the monotonic plastic zone size is about 25% of the uncracked ligament and these plastic deflections continue to increase as the fully plastic limit load condition is approached. The lack of hysteresis in load versus deflection recordings is due to the relatively small size of the cyclic plastic zone. In view of this behavior it is apparent that although deformation processes in the cyclic plastic zone may control crack extension, the specimen size requirement should be based on restricting the monotonic plastic zone size. (This is especially so at large R values, Fig. 4-43, where a size requirement is most needed). It also follows that it is physically unrealistic to simply replace σ_{YS} by σ_{YS}^{c} in the current size requirement, Eq. (4-3). The use of σ_{flow} in Eq. (4-3) to account for monotonic strain hardening, however, appears to be a viable alternative.

With respect to the disposition of the current size requirement, it is recommended that it be left unaltered in the current test method for the following reasons. First, it serves a necessary purpose for high strength, high toughness materials. Secondly, the following questions need to be answered before a size requirement which is equally applicable to all materials is formulated: 1) Does the condition defined by $W-a = 4/\pi\ (K_{max}/\sigma_{flow})^2$ correspond the onset of plastic deflections for most materials, particularly those with much monotonic strain hardening? and 2) How are fatigue crack growth rates in various materials affected by these plastic deflections? 3) Are the calculated stress intensities affected by plastic deflections?

The proposed test method contains a caveat which describes the limitations of the current size requirement and contains a provision whereby previously generated data can be validated by empirically demonstrating that equivalent da/dN-ΔK results are obtained for larger specimens which satisfy the current size requirement. In addition, a recommended, but optional, procedure is provided to monitor specimen deflections during tests which violate the current size requirement — this type of information is necessary to resolve the above questions.

Dwg. 6425A14

$$r_Y^c/r_Y = \frac{(1-R)^2}{4}\left(\frac{\sigma_{YS}}{\sigma_{YS}^c}\right)^2$$

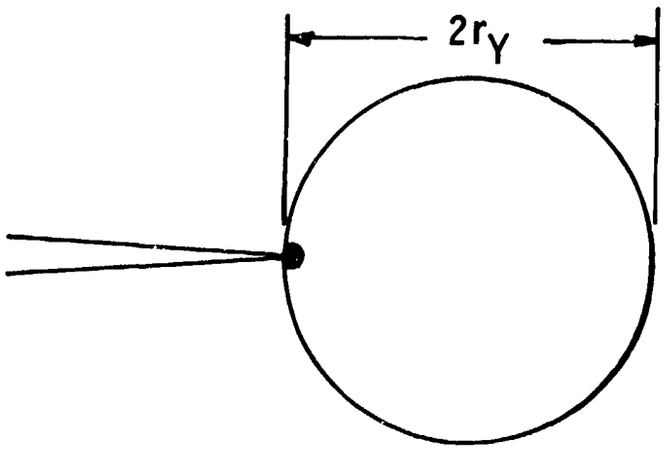

R = 0.8

$\sigma_{YS}^c/\sigma_{YS}$	r_Y^c/r_Y
1.0	0.01
2.0	0.002

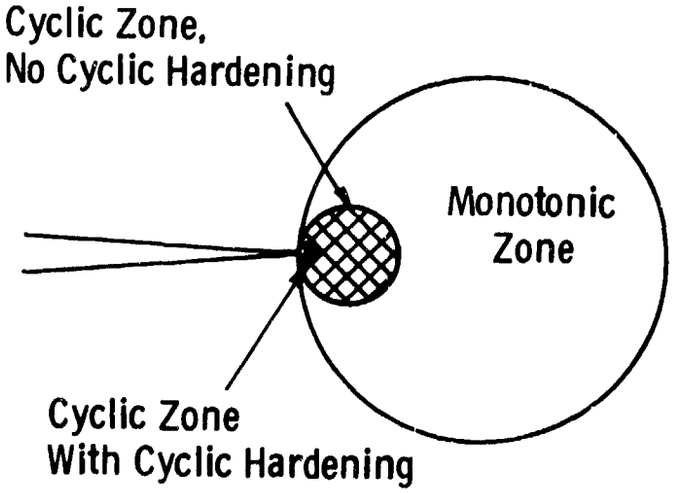

R = 0.1

$\sigma_{YS}^c/\sigma_{YS}$	r_Y^c/r_Y
1.0	0.25
2.0	0.06

Fig. 4-43 — Schematic of idealized cyclic and monotonic plastic zone sizes for various load ratios (R) and degrees of cyclic hardening

Several test programs are underway at various laboratories to generate sufficient data, using a wide range of specimen sizes, to answer the questions put forth in this section, and thereby attempt to establish a size requirement which is equally applicable to all materials. ASTM's Task Group on Fatigue Crack Growth Rate Testing (E24.04.01) is serving as a clearinghouse for this information and will subsequently work to update the size requirements in future versions of ASTM Standards.

5. SPECIALIZED PROCEDURES FOR LOW GROWTH RATE TESTING

5.1 Overview of Proposed Methods

Many low crack growth rate test method guidelines parallel those of the recommended high and intermediate crack growth rate test practice. These include requirements on grips and fixtures, specimen configuration and sizes, measurement of crack length vs. cycles information, data processing and reporting. Low crack growth rates are, in general, more sensitive to R-value and small variations in ΔK than at intermediate crack growth rates, for example, see Fig. 4-16. Data variability at low da/dN may be amplified (relative to variability at high da/dN) by increased sensitivity to material differences, local residual stresses, crack front irregularities and load precision. Moreover, the detection of anomalous low crack growth rate data is generally made more difficult by the greater length of time required between measurements and by limited data. Consequently, several precautions were introduced into the proposed method to control variability of low crack growth rate measurements. Procedures were also developed to ensure that low crack growth rate measurements would be representative of the materials true steady state characteristics, and that artifacts attributed to transient crack growth are minimized. The most notable modifications to the proposed practice to ensure reliable data in the low crack growth rate regime are: (1) precracking requirements, (2) use of specialized K-decreasing techniques, and (3) inclusion of an operational definition of the fatigue crack growth threshold, ΔK_{th}.

5.2 K-Increasing Vs. K-Decreasing Test Methods

Crack growth rate data below 10^{-7} m/cycle may be generated by K-increasing or K-decreasing test procedures. When load amplitude is held

constant, ΔK values increase as the crack extends in most specimen geometries. This constant-load amplitude, K-increasing technique is the preferred method of data acquisition for intermediate and high crack growth rate regimes (see Section 8.5, Appendix I). However, when very low rates of crack growth are to be established by K-increasing methods, precracking becomes very time consuming and causes the method to be inefficient. For these situations, a K-decreasing method becomes more desirable since precracking can either be minimized or eliminated.

In K-decreasing tests, conventional precrack procedures are employed to initiate the crack, whereupon valid crack growth rate data are established as load and stress intensity factor are decreased according to some predetermined schedule. For low crack growth rate measurements, this approach is most attractive since significant time spent precracking at low ΔK is eliminated. Moreover, the K-decreasing process may be halted at any crack length, the load range fixed, and the test continued as a K-increasing test according to requirements of Section 8.5, Appendix I. Conducting K-increasing and K-decreasing tests within a single experiment provides a reasonable method for assessing reproducibility of data and is a viable approach for detection and elimination of anomalous results. Also, under K-decreasing test conditions the specimen size requirement of Section 7.2, Appendix I, becomes less restrictive since K is lowest when the remaining uncracked specimen ligament (W-a) is smallest. Planning the load schedule and processing data for a K-decreasing test is more complex than that for a K-increasing test. In addition special precautions are necessary to ensure valid data which are free of transient behavior. These latter considerations, however, are readily overcome with added testing experience. For low crack growth rate measurement, the greater efficiency offered by the K-decreasing test approach seems to far outweigh the added complexity. Consequently, after some initial exploratory testing, this part of the program focused on establishing acceptable low crack growth rate test procedures which utilize a K-decreasing technique.

For the standard CT and CCT specimen configurations, testing in which K decreases with crack extension can be provided by programmed shedding of load (or deflection) or by constant deflection. A third possible K-decreasing test technique considers specimens loaded by wedge opening forces[58], however, fixturing for this method is cumbersome, and in fact, prohibitive at high test frequencies. In this investigation the primary K-decreasing approach employed was manual shedding of loads in discrete steps as illustrated by Fig. 7, Appendix I. (Programmed load shedding can also be accomplished in a relatively continuous manner by employing computer controlled techniques as discussed in Ref. (59). Tests under constant deflection conditions were used for a limited number of K-decreasing experiments in this study. Experience indicated that it was usually easier and more accurate to control and monitor stress intensity factor from load measurements made remote from the specimen by a load cell, than from deflection measurement at the specimen. Furthermore, programmed shedding of load affords traversal of a much broader range of K than does the constant deflection test method. For example, K decreases by less than a factor of two under constant deflection over an a/W range of 0.3 to 0.7 for the CT geometry. However for the same configuration, programmed load shedding permits a much braoder range of K over the same a/W range. For these reasons, programmed load shedding was the preferred K-decreasing test method used in this study.

Valid low and intermediate fatigue crack growth rate data obtained by K-increasing (constant-load-amplitude) and K-decreasing (programmed load shedding) test methods at various R-values are shown in Figs. 5-1 and 5-2 for the 2219-T851 aluminum alloy, and in Fig. 5-3 for the 10Ni steel. Also shown in Fig. 5-1 are limited K-decreasing intermediate crack growth rate data obtained from constant-deflection-amplitude tests. For many tests the K-decreasing portion of the test was followed by a K-increasing portion in which fatigue crack propagation data at low and intermediate growth rates were determined. In these tests the K-decreasing (load shedding) process was terminated after obtaining the desired low crack growth rate, the loads fixed, and the test

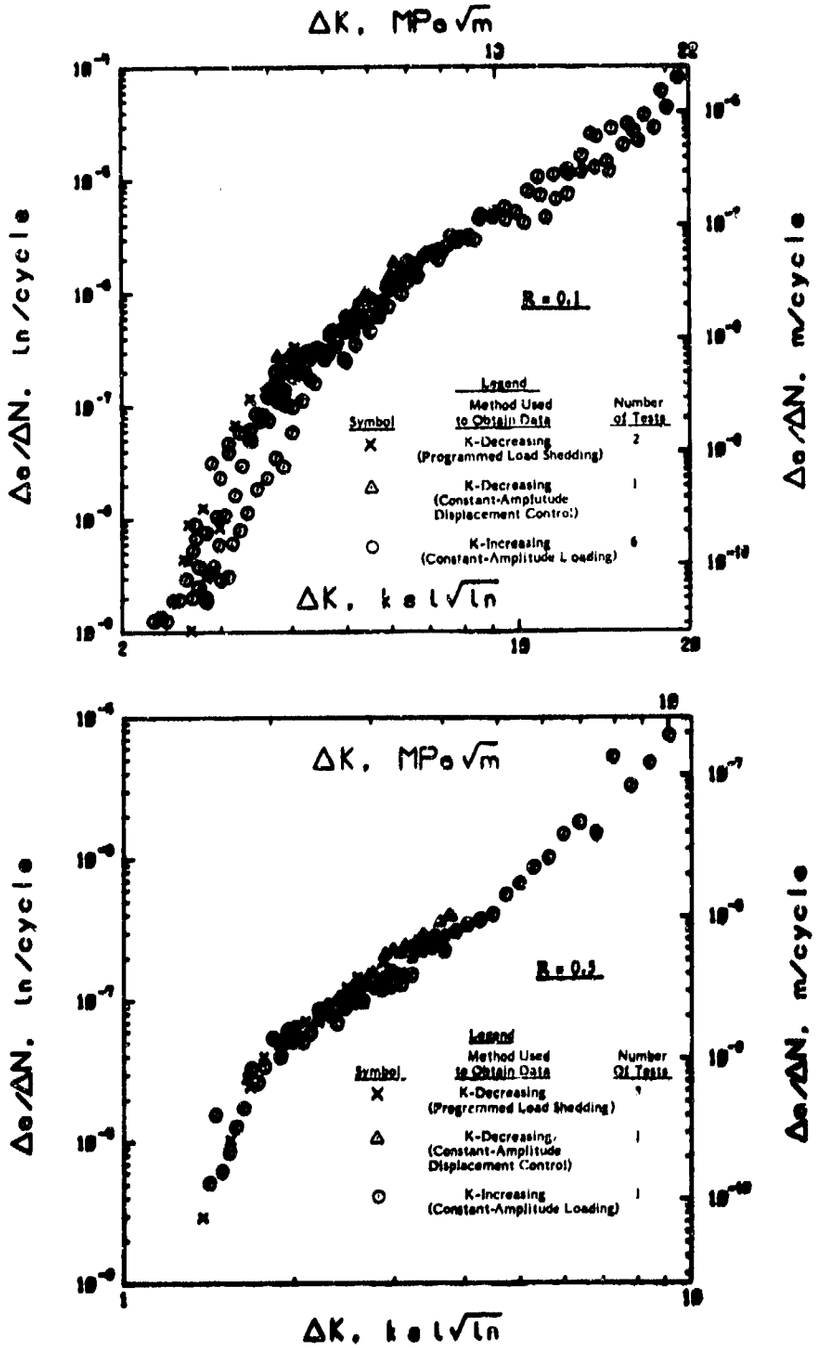

Material: 2219-T851 Aluminum Plate, 3.188 in. (81 mm) Thickness
Specimens: CT, B=0.25 in. (6.4 mm), W=2 in. (51 mm)
Orientation: L-T
Environment: Ambient Air

Fig. 5-1 Comparison of K-Increasing and K-Decreasing Test Methods on Aluminum Alloy 2219-T851 at R=0.1 and 0.5

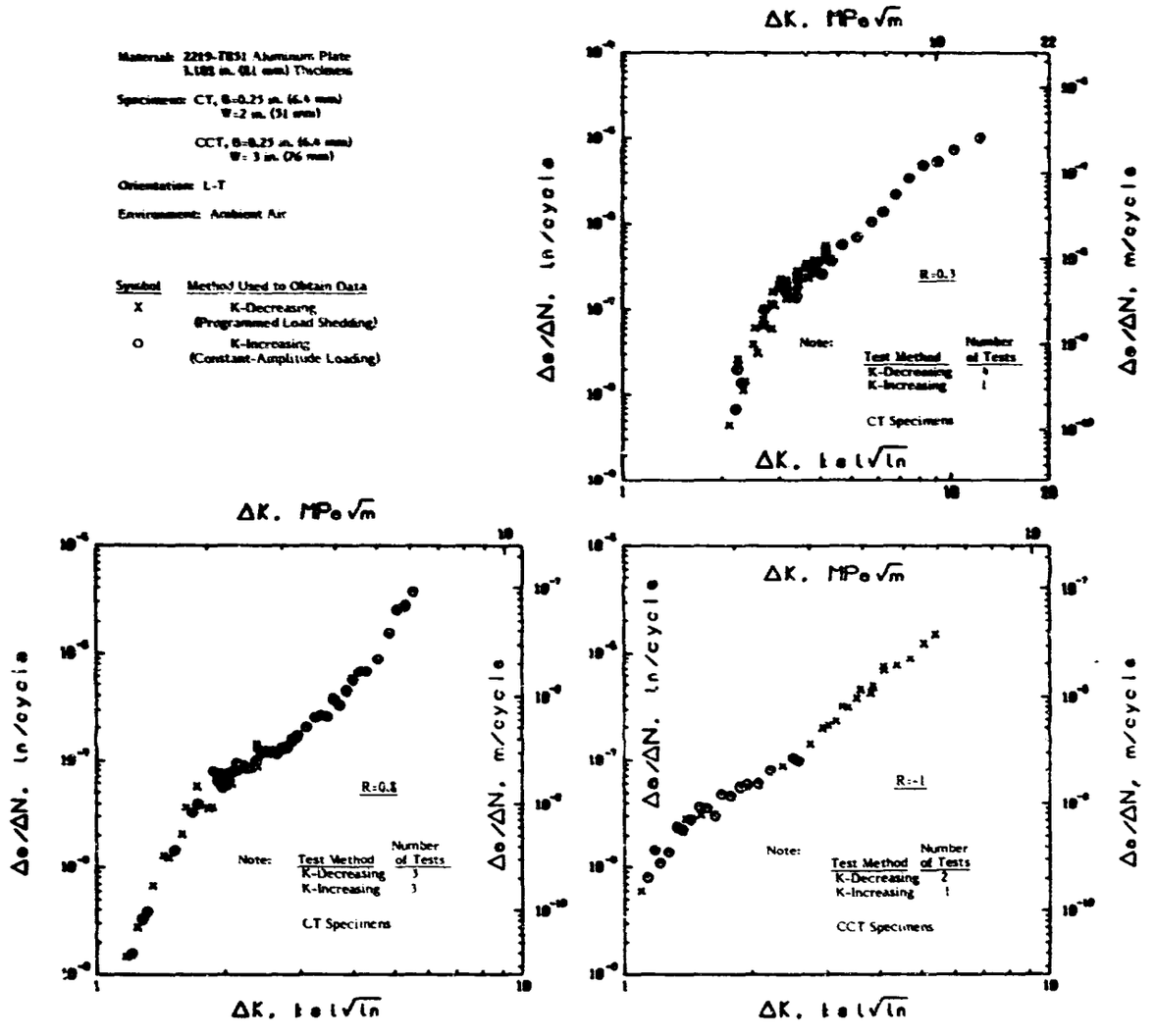

Fig. 5-2 Comparison of K-Increasing and K-Decreasing Test Methods on Aluminum Alloy 2219-T851 at R=0.3, 0.8 and -1

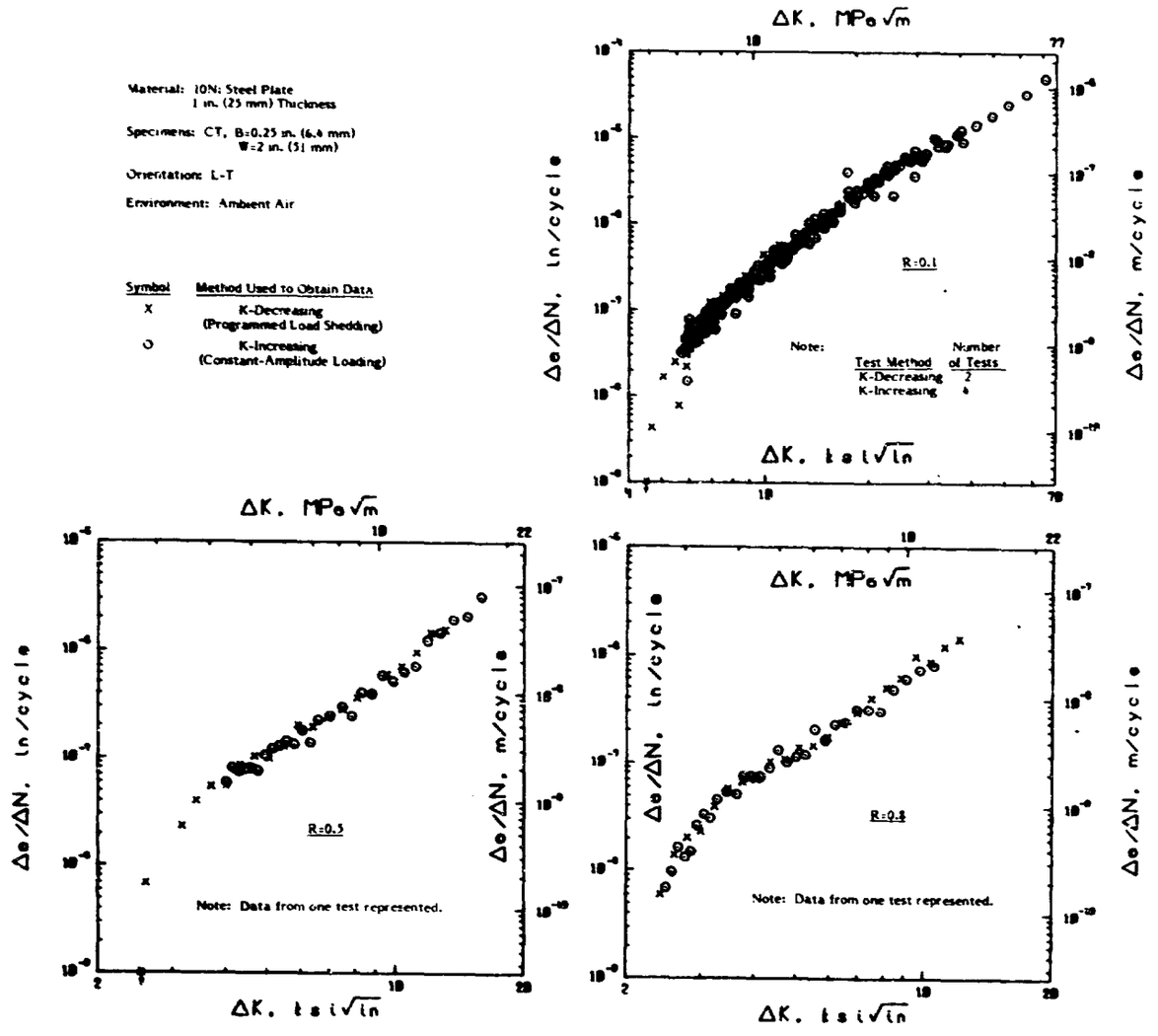

Fig. 5-3 Comparison of K-Increasing and K-Decreasing Test Methods on 10Ni Steel Alloy at R=0.1, 0.5 and 0.8

continued to completion as a K-increasing test. Thus, the K-increasing test data provided a check on the validity of the K-decreasing test data determined on the same test specimen, thus transient and anomalous data, if present, were readily detected and eliminated. When validity requirements and procedures of Appendix I were met, K-increasing and K-decreasing data established for both alloys were found to be in good agreement. Agreement between K-increasing and K-decreasing data was even better when results were generated using the two techniques on the same specimen. This is best illustrated by test data determined on single specimens from 10Ni steel alloy at R = 0.5 and R = 0.8 shown in Fig. 5-3.

5.3 Detecting and Eliminating Transient Effects

Transient crack growth phenomena are likely to occur during the course of a test, particularly when loading and/or environmental variables are changed, or when crack front irregularities develop. Optimum test procedures should be designed to recognize and minimize potential sources of test method variability so that established crack growth rate data are representative of true steady-state characteristics of the material-environment combination being considered. The following sections provide a discussion of the procedures and requirements of Appendix I which are designed to eliminate transient data, particularly those requirements related to low growth rate testing.

5.3.1 Precracking Procedure

The importance of precracking is to provide a sharp, straight (also symmetrical for the CCT specimen) fatigue crack of adequate length which ensures that (1) the effect of the machined starter notch is removed from the specimen K-calibration, (2) crack-tip conditions have become stable with respect to conditions of the material and environment under test, and (3) any permanent or transient fatigue crack growth characteristics caused by crack front irregularities and/or precrack load history are minimized. These assurances are basically satisfied by the testing requirements of Section 8.3, Appendix I.

An example for the need for a minimum precrack length requirement is illustrated by the crack growth rate data for aluminum alloy 2024-T351

shown in Fig. 5-4[60]. These data were developed from tests on identical specimen geometries tested at various fixed ΔP values. It was found that regardless of initial loads, a crack length on the order of 0.15 in. (3.8 mm) from the notch tip was required for data to fit the general trend line shown. The imminent danger of a "false" interpretation of threshold is rather obvious from these results. Experience gained at precracking many specimens for the low crack growth rate tests in this investigation indicated that a minimum precrack extension of 0.10 in. (2.5 mm) from the machined notch was generally sufficient to ensure elimination of crack growth transients, provided other requirements of Section 8.3, Appendix I, were also met.

When the precracking procedure involves a series of stepped decreases in stress intensity factor it is important that crack growth retardation, or other transient crack growth characteristics, have negligible effect on crack growth measurement at the beginning of the test. Transient characteristics of overload-retardation phenomena have been well documented in the literature[61]. It was observed on several occasions during this program, particularly when the stepped load reduction was significant (~20% of the previous load), that a period of crack growth stabilization extended over several plastic zone diameters following the overload. However, when the overload plastic zone size was small relative to the crack growth increment, Δa, over which crack growth rate was established, no measurable transient crack growth could be detected. It has been demonstrated for several materials that retardation in the growth rates caused by overloads, in the form of either a single spike or a 10 cycle block, only occurs over a crack extension interval of less than three times the overload plastic zone size[62]. Other data, shown in Fig. 5-5, illustrate that small overloads, consisting of less than about a 20 percent increase over the maximum load of base line cycles, have a negligible effect on the apparent fatigue crack growth threshold[63]. The aforementioned observations provided guidelines for the precracking requirements in Section 8.3.2., Appendix I; specifically, that (1) reduction in K_{max} be in increments no greater than 20 percent, and (2) the final precrack

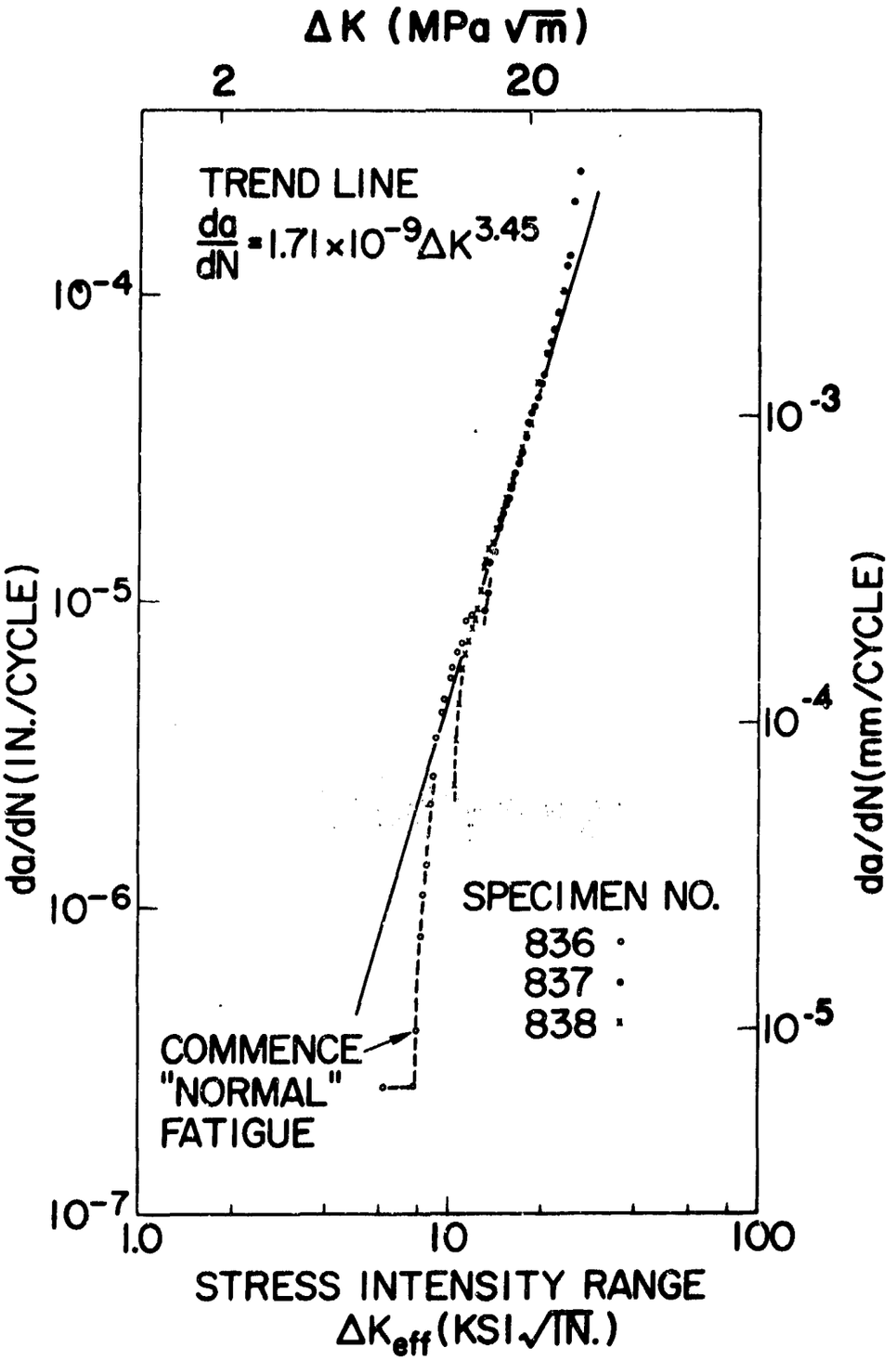

Fig. 5-4 Anamalous Crack Growth Rate Data
(Sullivan and Crooker, NRL Report 7912)

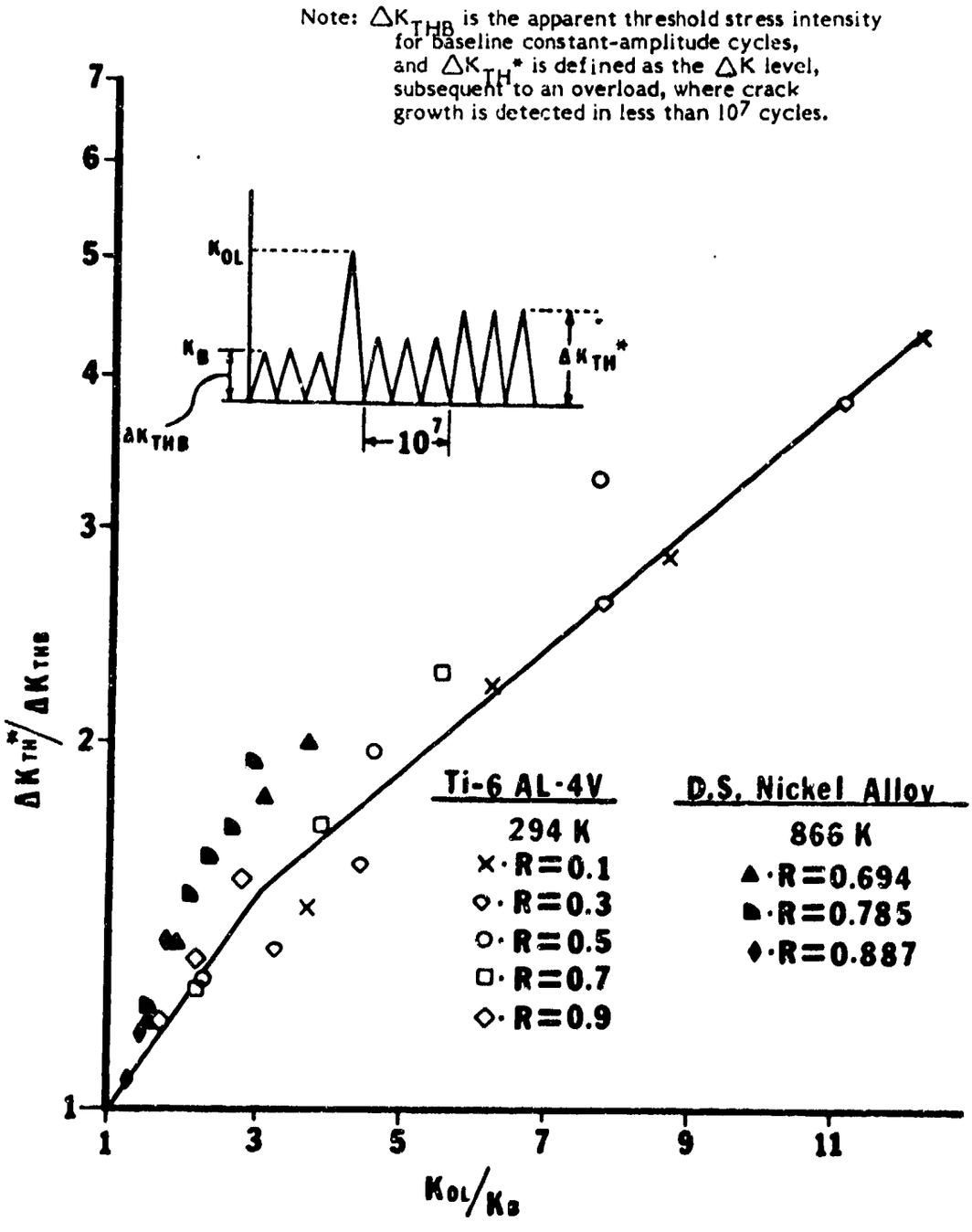

Fig. 5-5 Relative Change in Fatigue Crack Growth Threshold After Single Cycle Overloads as a Function of the Relative Overload for Two Alloys and Various Stress Ratios (Hopkins et al, ASTM STP 595)

length, a_o, shall be greater than $(3/\pi)\cdot(K_{max_i}/\sigma_{YS})^2+a_i$, where K_{max_i} is the terminal value of K_{max} at any prior load step and a_i is the corresponding crack length. The latter requirement ensures that the final precrack length is separated from the largest overload plastic zone boundry by at least three plastic zone diameters. Since low crack growth rate behavior is also known to be highly sensitive to R-values, Section 8.3.2 of Appendix I also recommends that the R-value during the final stages of precracking be kept the same as that of subsequent testing.

5.3.2 K-Increasing Test Procedures

Guidelines for elimination of several forms of transient crack growth phenomena for the K-increasing test are specified in the general procedure for high and intermediate crack growth rate testing, Section 8.5, Appendix I. Under this form of testing, transient crack growth is introduced primarily when load and/or environmental conditions are changed during the test, thus testing an entire specimen at a constant ΔP is preferred. If load range must be varied, it is suggested that P_{max} increase rather than decrease to avoid retardation-delay phenomena. Transient fatigue crack growth behavior is also known to depend on environmental considerations. For example, transient crack growth phenomena associated with long duration test interruptions have been reported in the literature for various material-environment systems [4]. Therefore minimizing both the number and durations of test interruptions is desirable. The test procedure also specifies that data should be discarded if growth rates following an interruption are less than those before the interruption, Section 8.5.3 in Appendix I. In summary, it is always good practice, when test conditions are changed, to critically examine data following the change to identify non-steady state crack growth, since these data are dependent on the specific test history and do not represent material or material-environment properties.

5.3.3 K-Decreasing Test Procedures

As discussed previously the K-decreasing technique represents an optimum method for determining very slow rates of crack growth.

Specific procedures for the K-decreasing testing are given in Section 8.6, Appendix I. The magnitude and rate at which the stress intensity factor is shed as the crack extends must be selected with caution since various forms of crack growth transients may result in anomalous data. Stepping from a high-to-low constant amplitude load block must eventually result in a decrease in the crack growth rate from the steady-state value of da/dN associated with the high load block to the steady-state value associated with the low load block. Three general types of crack growth transition phenomena might be envisioned as shown in Fig. 5-6. These are: (1) instantaneous transition with no interaction between load blocks, (2) crack growth retardation attributed to overload-delay phenomena, and (3) transition of crack growth rate from the respective steady-state values of high-to-low block cycles. The first type transition represents the idealized situation, while the latter two types which involve transient behavior may be somewhat more realistic. Both types 2 and 3 transient phenomena were observed in this investigation. The standard K-decreasing test procedure has been developed to assure that transient crack growth takes place over an interval of crack extension which is negligible compared to the total crack growth increment, Δa, over which a valid da/dN measurement is made, that is, such that the above case 1 represents a good approximation. The principal requirements to adequately approximate case 1 during the K-decreasing test procedure are: (1) a 10 percent maximum limit on the magnitude of the load shed, (2) a minimum required increment of crack growth per data point, and (3) a bound on the normalized rate of load shed, that is $(1/K_{max})\cdot(dK_{max}/da)$. Justification for these requirements is based on equivalency of results from K-increasing and K-decreasing test, Figs. 5-1 to 5-3. These requirements and supporting data are further discussed in the following paragraphs.

It has been shown in overload-retardation studies that the affected region over which retardation occurs is related to relative difference in the monotonic plastic zone sizes of the overload and baseline cycles[64-67]. Restricting the magnitude of the load shed

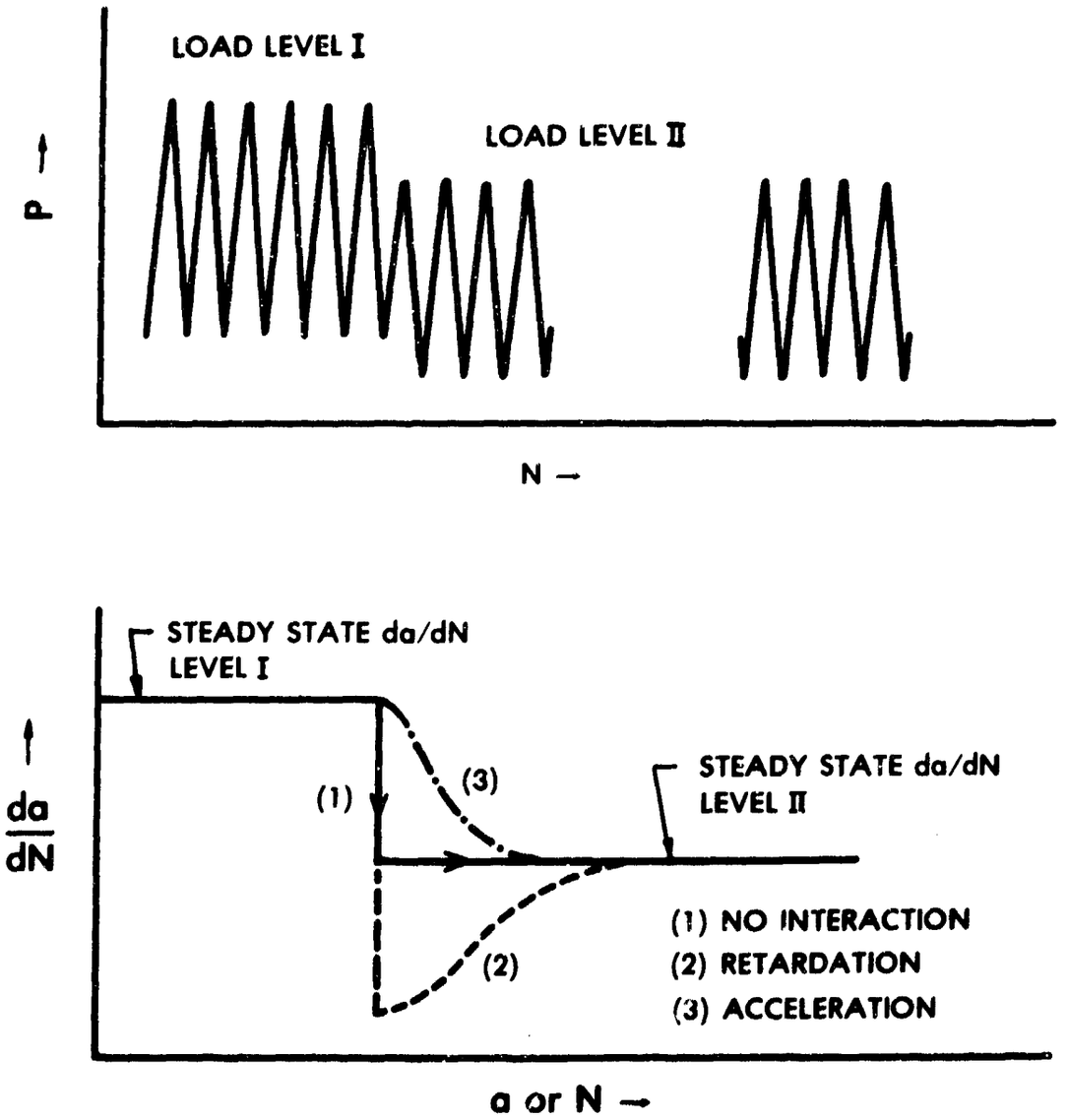

FIG. 5-6 POSSIBLE CRACK GROWTH RATE TRANSIENT PHENOMENA FOR HIGH TO LOW BLOCK LOADING SEQUENCE

to 10 percent, limits the change in the plastic zone size to approximately $(0.01/2\pi)(K_{max}/\sigma_{YS})^2$. Data of Fig. 5-5 indicates no detectable overload-retardation effect on the apparent threshold stress intensity factor when the magnitude of the overload is within 10 percent of the maximum load during the baseline cycles. It follows, therefore, that it is desirable during testing to maintain the nominal K-gradient such that the fractional change in the monotonic plastic zone size remains constant as the crack grows. It has been demonstrated mathematically[59] that this condition is approximated by the expression;

$$K_{max} = K_{max_o} \exp[C(a-a_o)] \tag{5-1}$$

where K_{max_o} is the initial stress intensity corresponding to the initial crack length, a_o; "a" is the instantaneous crack length, and C is a constant with dimensions of 1/length. For a constant R-value test the stress intensity factors K_{min} and ΔK follow the same relationship; namely,

$$K_{min} = K_{min_o} \exp[C(a-a_o)] \tag{5-2}$$

$$\Delta K = \Delta K_o \exp[C(a-a_o)] \tag{5-3}$$

From the above, a normalized K gradient for the K-decreasing test at constant R-value may be written as:

$$(1/\Delta K) \cdot (d\Delta K/da) = (1/K_{max}) \cdot (dK_{max}/da) = (1/K_{min}) \cdot (dK_{min}/da) = C \tag{5-4}$$

Section 8.6.2 of Appendix I recommends that the normalized K-gradient for the K-decreasing test denoted as $C = (1/K) \cdot (dK/da)$, be controlled within perscribed limits. For a stepped load shed test this may be accomplished beforehand by specifying a targeted nominal stress intensity factor vs. crack length, relationship (K vs. "a")

according to Eqs. (5-1) to (5-3). Load steps are then selected to follow the nominal relationship according to requirements of the method, e.g., Fig. 7, Appendix I. The optimum value of C must be chosen with consideration given to alloy type, load ratio, and environment. Usable values of C should be established by demonstrating agreement between K-decreasing and valid K-increasing test results. The experience of this investigation and that reported by Saxena, et al. [59] has shown that C values of greater than -2.0 in.$^{-1}$ (-0.08 mm^{-1}) are acceptable at positive R-values for a variety of alloys. A comparison of valid K-increasing da/dN measurements and K-decreasing da/dN results established at various values of C are shown for the 2219 aluminum alloy and the 10Ni steel of this study in Figs. 5-7 and 5-8, respectively. The C values shown in these figures comprise data established from a large number of individual load sheds which encompass a wide range of growth rates (Figs. 5-7A and 5-8A) as well as a range of R-values (Figs. 5-7B and 5-8B). Equivalency of K-increasing and K-decreasing data are shown for C value greater than -3.8 in.$^{-1}$ (-0.15 mm^{-1}) and -2.4 in.$^{-1}$ (-0.095 mm^{-1}) for the aluminum and steel, respectively. As indicated by the data contained in these figures, the recommended limit on the normalized K gradient, namely $C \geq -2$ in.$^{-1}$ ($C \geq 0.080$ mm^{-1}), may be conservative in certain cases. For example, considerable K-decreasing data established using C-values significantly less than -2.0 in.$^{-1}$ (-0.0080 mm^{-1}) are shown to compare favorably with valid K-increasing data — this is particularly true for high positive R values as shown in Figs. 5-7B and 5-8B. The recommended band on C which is specified in Appendix I can probably be modified to further optimize testing, however, any modification must await further testing experience on additional materials, environments and loading variables. Thus, Appendix I suggests that, when the bounds on C are not met, the crack growth rate data be validated by demonstrating equivalence between K-decreasing and K-increasing data.

For the materials examined in this study, tests employing large decreasing K-gradients (that is, small C values) resulted in growth rates which were faster than the steady-state rates obtained in

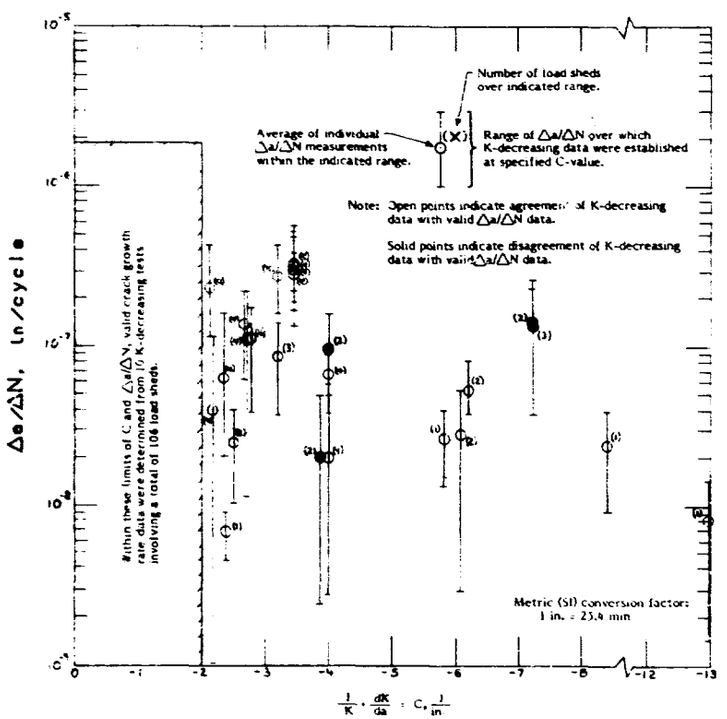

Fig. 5-7A Effect of Normalized K-Gradient to Determine Valid K-Decreasing Test Data for Aluminum Alloy 2219-T851

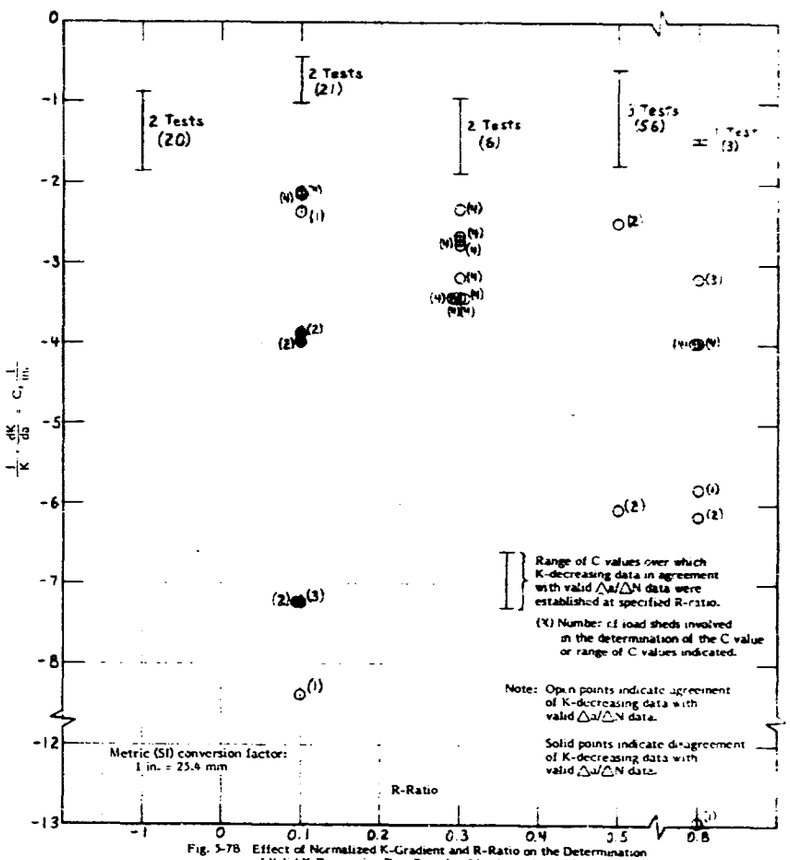

Fig. 5-7B Effect of Normalized K-Gradient and R-Ratio on the Determination of Valid K-Decreasing Test Data for Aluminum Alloy 2219-T851

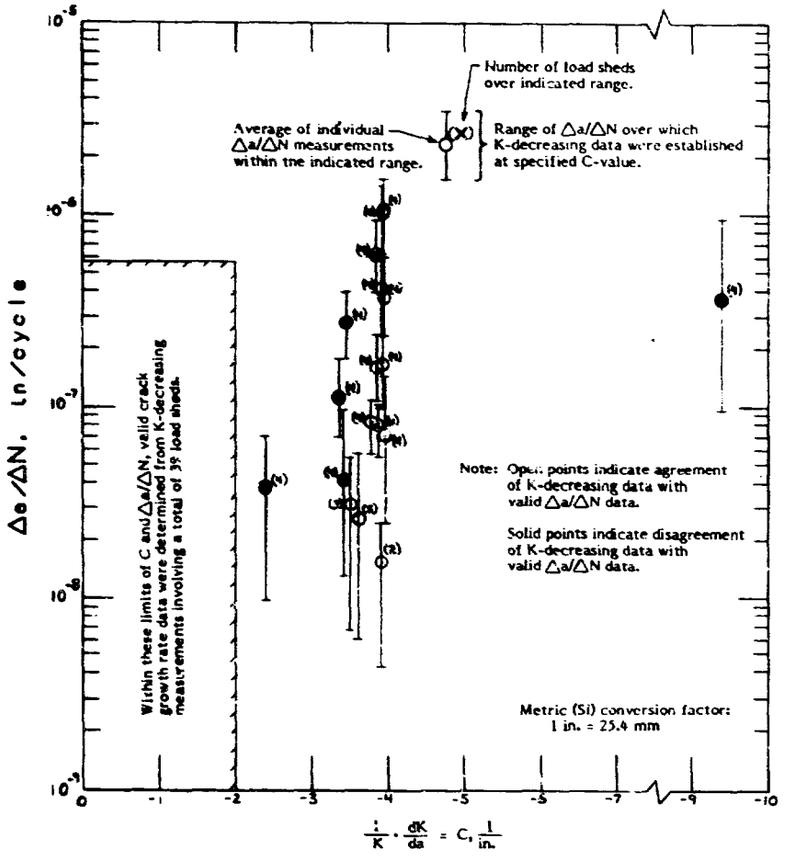

Fig. 5-8A Effect of Normalized K-Gradient to Determine Valid K-Decreasing Test Data for 10 Ni Steel Alloy

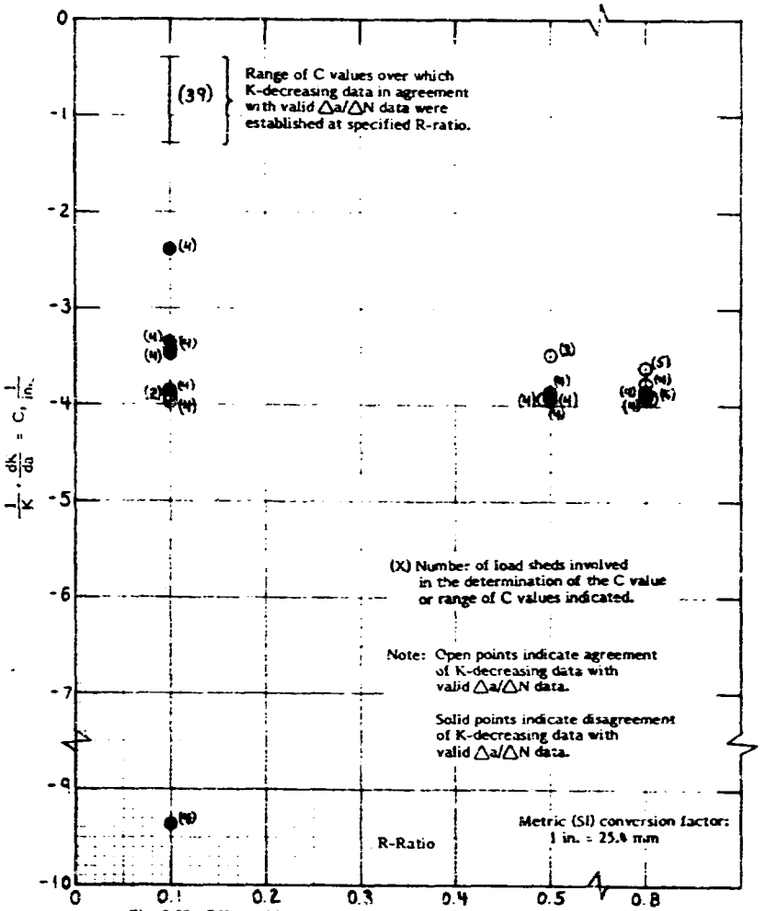

Fig. 5-8B Effect of Normalized K-Gradient and R-Ratio on the Determination of Valid K-Decreasing Test Data for 10 Ni Steel Alloy

K-increasing, constant-load-amplitude tests. This behavior is indicative of the type 3 transient illustrated in Fig. 5-6 and is surprisingly opposite to what one would expect from overload-retardation consideration. These results are shown in Figs. 5-9 to 5-11 which contain data from three programmed load shed tests conducted at R = 0.1 on 2219 aluminum. The accelerated growth rates for large decreasing K-gradients ($C < -2$ in.$^{-1}$) occurred predominantly at the lower positive R values. Similar, though less extensive, observations were made with the 10Ni steel, also at R = 0.1. Maintaining the nominal value of C within the limits recommended in Appendix I appears to be an effective means of eliminating this anomalous behavior.

The mechanism for the anomalous acceleration of very low crack growth rates caused by a large decreasing K-gradient is not well understood. This phenomenon may be related to time-dependent corrosion processes. Crack arrest in aluminum alloys exposed to an aqueous environment and low ΔK values has been linked to gradual buildup of corrosion product on the crack surface [68]. Experimental evidence indicated that in the presence of an aggressive environment the time-dependent buildup causes the crack to reach a closed position at increasingly higher loads, thereby decreasing the effective ΔK at the crack-tip as well as the crack growth rate. Alternatively, in inert environments, growth rates as much as an order of magnitude faster were observed at comparable stress intensity factor values in some materials. Analagous to the crack closure caused by residual crack-tip deformations, this mechanism would be more prominant at low positive R-values, where contact forces of the corrosion products would be more significant than at high R-values where the crack remains open during most or all of the loading cycle. In this investigation all low crack growth rate tests were conducted in ambient laboratory air. Evidence of environmental moisture interaction with both alloys was noted by markings on specimen fracture surfaces. It was not determined from these observations when these markings occurred in the history of the experiment. It is postulated that since a rapid K reduction promotes crack advance at

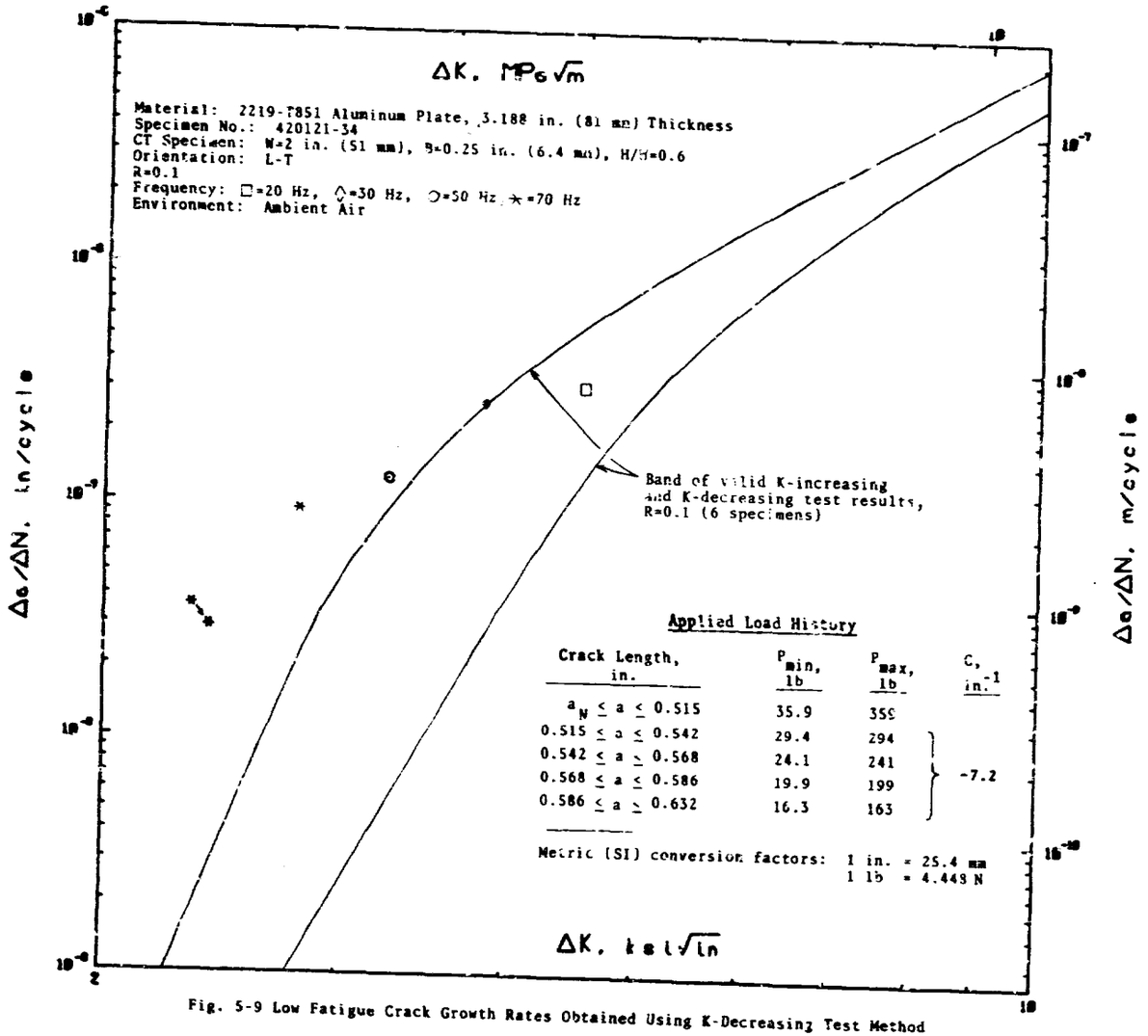

Fig. 5-9 Low Fatigue Crack Growth Rates Obtained Using K-Decreasing Test Method

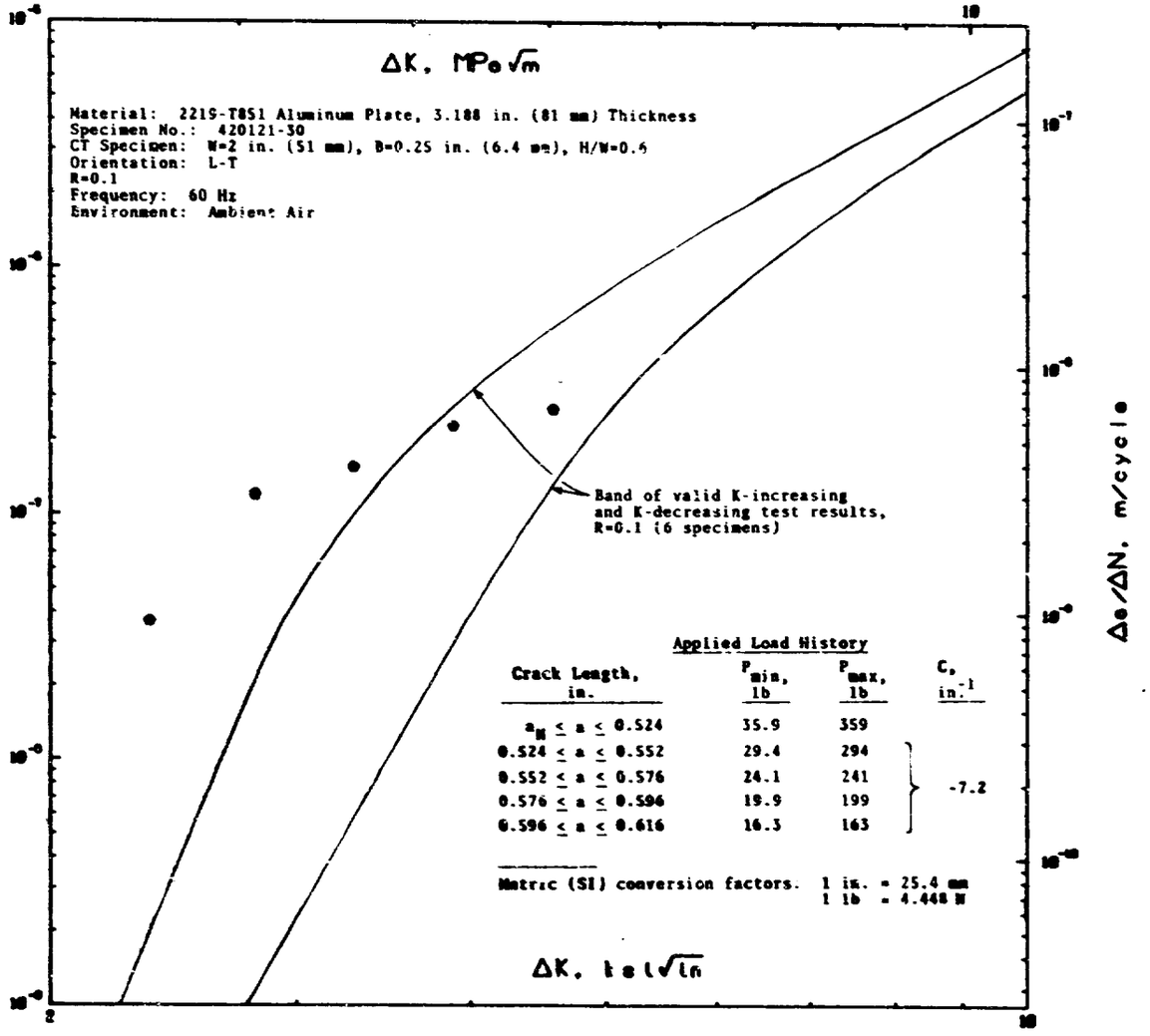

Fig. 5-10 Low Fatigue Crack Growth Rates Obtained Using K-Decreasing Test Method

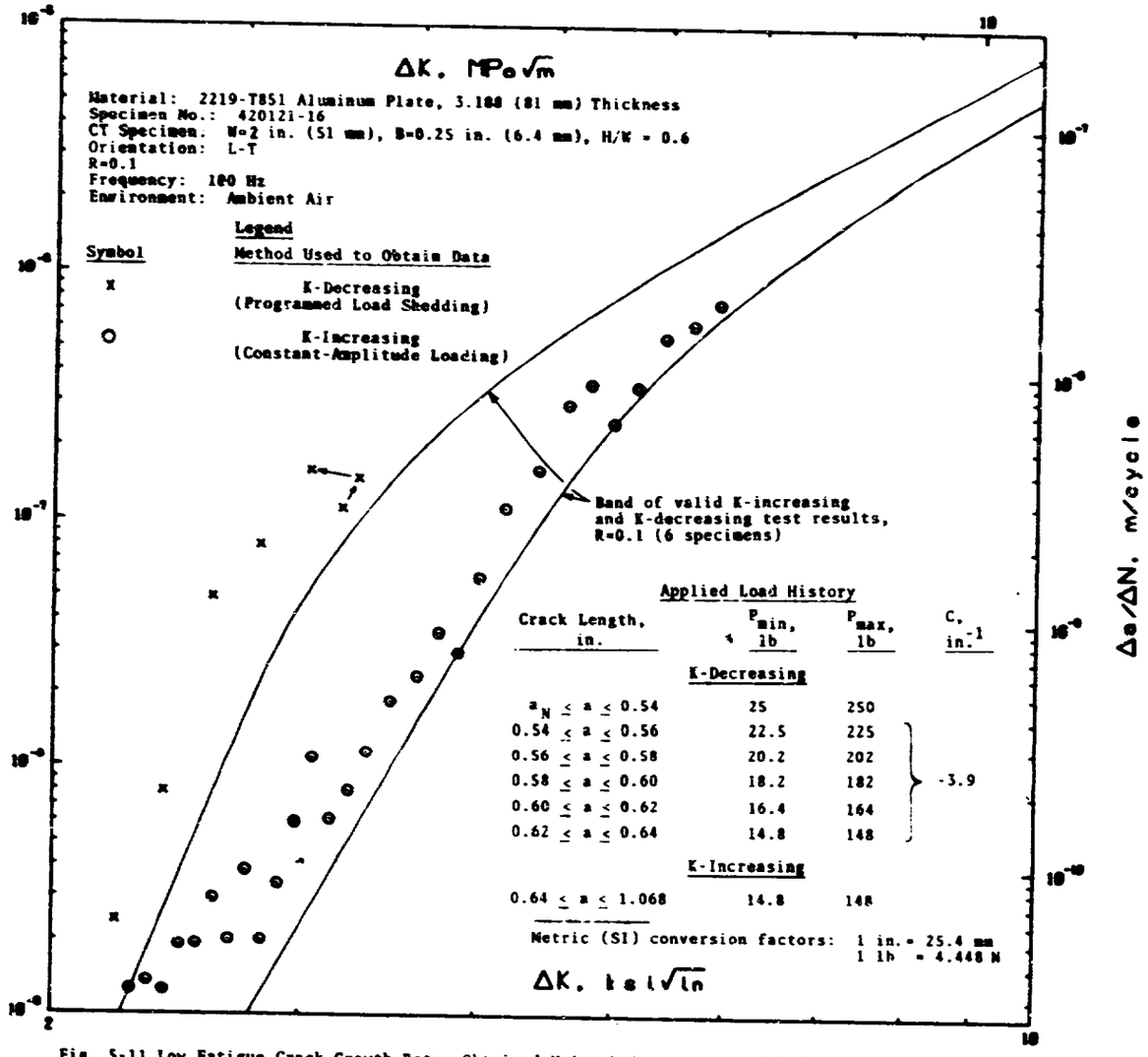

Fig. 5-11 Low Fatigue Crack Growth Rates Obtained Using K-Increasing and K-Decreasing Test Methods

rates which lessen the time, and therefore the buildup of corrosion products to equilibrium levels, that would be approached under more gradual rates of K decrease. Hence, non-equilibrium conditions of environment interaction may exist. Moreover the observation that the acceleration effect was confined to R = 0.1 but was unnoticed at higher R-values supports this argument. Additional work is required to better understand this phenomenon.

5.4 Frequency Independence of da/dN at High Frequencies

Figure 5-12 contains fatigue crack growth rate data on 2219-T851 aluminum for test frequencies ranging from 10 Hz to 150 Hz and load ratios from 0.1 to 0.8. These data demonstrate that low growth rates in this material are independent of test frequency for these relatively high frequencies. Similar results were observed for the 10Ni steel. These results enable low growth rate data to be generated using an optimum test frequency, thereby minimizing the required test times. This frequency independence would be expected to apply until environmental effects occurred at lower frequencies or temperature effects due to adiabatic crack-tip heating occurred at higher frequencies.[35] Frequencies of an order of magnitude greater than the highest frequencies in Fig. 5-12 would be required to cause significant crack-tip heating in metals.

The frequency independence of the growth rates in Fig. 5-12 implies that environmental effects due to the moisture in laboratory air are absent. These results are consistent with low growth rate data and threshold determinations for other material-environment systems, for example see Ref. (52). Environmental effects are likely to influence low growth rates and ΔK_{th} at low cyclic frequencies, although this fact has not been demonstrated due to the prohibatively long test times which are required. Fortunately, most applications where low growth rate and ΔK_{th} information is important also experience relatively high cyclic frequencies.

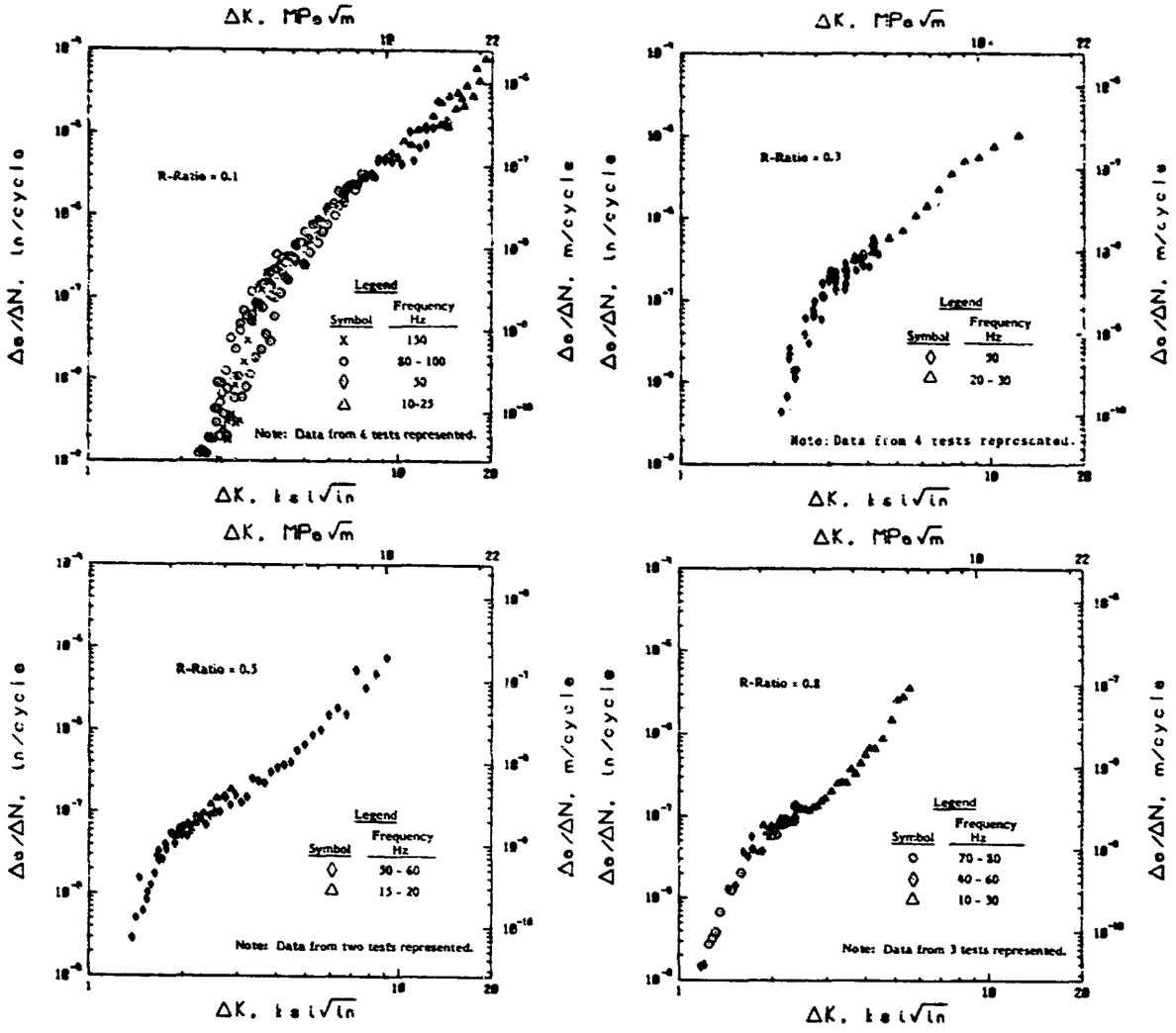

Fig. 5-12 - Effect of frequency on fatigue crack growth rates of 2219-T851 plate

5.5 Operational Definition of the Fatigue Crack Growth Threshold

Very slow rates of fatigue crack growth decrease rapidly with small reductions in ΔK. A value of ΔK above which fatigue crack growth has been observed, but below which crack growth has not been observed has been termed a fatigue crack growth threshold, ΔK_{th}. Values of da/dN generally associated with a fatigue crack growth threshold correspond to an increment of crack growth (averaged along the total crack front) which is less than one atomic spacing per cycle. Thus crack growth at these levels occurs discontinuously along the flaw periphery and makes the task of defining a "true" crack arrest threshold difficult. The measurement of the threshold is a function of sensitivity of the measurement technique, length of observation time, and test procedure. Furthermore, the definition of ΔK_{th} may have a different connotation for different alloy-environment systems and for different design situations. In certain cases the concept of a "true" arrest threshold has been provisionally accepted until better methods to quantify low da/dN fatigue crack growth resistance are available, for example, see Ref. (52). For some alloys, such as 2219-T851 aluminum and 10Ni steel, a continuous finite rate of da/dN decrease with decreasing ΔK is noted down to very low crack growth rates on the order of 10^{-10} m/cycle, as shown in Figs. 5-1 to 5-3. In this case a practical definition of ΔK_{th} corresponding to some arbitrary, but low, crack growth rate provides a practical means of characterizing a material's resistance to low rate fatigue crack growth. Caution should be exercised not to arbitrarily utilize the latter operational definition of the threshold for design purposes. Section 9.4, Appendix I, presents a procedure for describing an operational fatigue crack growth threshold as that ΔK corresponding to a fatigue crack growth rate of 10^{-10} m/cycle. The proceudre gives specific requirements on the range of crack growth data and analysis procedure to be used to determine the ΔK value corresponding to a da/dN value of 10^{-10} m/cycle.

6. DATA ANALYSIS PROCEDURES

Two separate computational procedures are necessary to analyze fatigue crack growth data so that results can be expressed in a useful, geometry-independent form. One of these procedures is the computation of the range of stress intensity factor, ΔK, from discrete crack length measurements and loading variables for the specific test specimen geometry employed; the other involves computing the fatigue crack growth rate from discrete measurements of crack length and elapsed fatigue cycles. Typically, both of these operations are conducted on 20 to 40 data points per test. Various aspects of these computations are discussed below, particularly as they relate to the proposed methods of Section 9, Appendix I.

6.1 Computation of ΔK

The wide-ranged analytical K-calibrations which are provided in the proposed test method to calculate ΔK are valid for all practical values of crack length which will be encountered in using the test method.[69,71] These calibrations thereby represent an improvement over the various expressions — particularly for the CT specimens — which were previously in use, since they eliminate potential errors due to extrapolation of previous equations beyond their applicable ranges.

An additional consideration related to using the K-calibrations to analyze fatigue crack growth rate data involves the definition of ΔK for tests which include compressive loading, that is, for tests where $R < 0$. The issue which needs to be resolved here is whether or not to include the compressive portion of the loading cycle into the computation. Values of ΔK which include, as well as exclude, the compressive loading can be found in data from the literature. The existence of two different computational procedures often leads to confusion — particularly when data is extracted from its original source for summary papers, data handbooks, or design usage.

In order to promote consistency in analyzing and reporting data, Sections 5.2 and 9.3 of Appendix I define ΔK using only the positive portion of the loading cycle. This recomendation is based on: 1) the theoretical fact that the stress intensity factor is undefined for compressive loading and 2) the common physical conception that the stress intensity factor is equal to zero when the crack faces are closed. The definition of ΔK in Section 5.2 of Appendix I can be viewed as an operational definition, since it makes no attempt to account for local crack-tip phenomena such as blunting, residual stress or crack closure at positive R values. Furthermore, it is important to realize that this operational definition of ΔK in no way influences the effect of compressive loading on fatigue crack growth behavior since the materials' intrinsic response to compressive loading will be incorporated in the measured crack growth rate.

6.2. Computation of da/dN

During the course of developing the test method numerous requests were made by ASTM members and others to recommend techniques for determining da/dN from "a" versus N, and also, to provide details of these techniques in the test method. Two recommended techniques are contained in Appendix A of the proposed test method. A summary and discussion of various processing techniques are given below; considerations which led to recommending the techniques provided in the test method are also given.

6.2.1 Summary and Evaluation of Data Processing Techniques

The general problem encountered in processing data from any crack growth test is that of determining the derivative of a function, $a = f(N)$ which is not completely defined, but is only approximated at certain discrete points which correspond to periodic measurements of crack length and elapsed cycles (a_i, N_i). Since crack length measurement is a stochastic process, successive measurements of a_i on different specimens of the same geometry, each subjected to the same loading history, will vary at any given N_i. This variability can arise from two sources — measurement error and intrinisic differences in the fatigue crack growth resistance of the test pieces. Measurement errors

have several different, but often related, sources: 1) human factors — particularly in visual measurements where human perception plays a role in determining the crack-tip location which is often masked by localized plastic deformation, 2) technique factors — for example, microscope magnification, specimen surface finish, and lighting source in visual measurements; selection of a proper applied current in potential drop measurements; instrument characteristics and calibration equations in a variety of other automated measurements, 3) material factors — these can arise from differences in crack-tip deformations for different materials, or for the same material at different strength levels. Often the above sources of variability overshadow those due to intrinsic differences in fatigue crack growth rate of a given material.

A variety of different views exist on what constitutes the "best" technique for processing fatigue crack growth data. One view is that the variability in a_i should be preserved so as to illustrate the variability in da/dN_i. From this view one concludes that the secant or point-to-point, technique is ideal. This technique involves simply calculating the slope of a straight line which connects two adjacent data points, that is

$$da/dN = \frac{a_{i+1} - a_i}{N_{i+1} - N_i}$$

It is important, however, to recognize that although this technique preserves the variability in a_i, this variability is dominated by errors in measuring a_i and thus provides little information on the inherent material variability of da/dN. The latter can only be determined by extensive replicate testing. Nevertheless, the secant technique is expedient for a number of reasons. First, it is a straightforward and easily applied technique. Secondly, and perhaps most importantly, it is uniquely suited to analyze K-decreasing data which are established using load shedding and results in only a few data points at each load level. For these reasons, the secant method is provided as a recommended processing technique in the proposed test method.

Another view of what constitutes the "best" data processing technique recognizes the measurement error in a_i and seeks to minimize its influence on da/dN_i. A variety of methods, most of which involve least squares fitting, have been employed to accomplish this goal. These methods can be separated into those that fit the entire "a" versus N curve, and those that fit the "a" versus N curve locally in increments. In addition, graphical techniques have been used which contain ingredients of each of the above two approaches.

The graphical technique usually consists of visually fitting a smooth curve through plotted (a_i, N_i) data and then estimating da/dN_i by measuring the slope of a straight line drawn tangent to the fitted curve. Although this technique can produce results which are comparable to those obtained using other techniques, its success depends on the skill of the user. Based on this fact, and the relative inefficiency of the methods, graphical techniques could not be recommended in a general test method.

Methods for fitting the entire "a" versus N curve have employed polynomials[72], orthogonal polynomials[73], logarithmetic functions[74], spline functions[75,76], and combinations of the above.

Simple polynomials of the form

$$a = \sum_{j=0}^{k} \alpha_j N^{\beta_j}$$

having k+1 terms and kth order have been used to process data. Polynomials of 6th and 7th order are often required to adequately fit typical "a" versus N curves. Davies and Fedderson[77] have demonstrated that, although these functions provide a reasonable fit to the data, their derivatives can give erroneous results due to the k-1 inflections in a kth order function. These inflections can lead to improper interpretations of the fatigue crack growth behavior.[72]

More complex polynomials have been utilized[78] to avoid the above problem and can be represented by the following general form

$$a = \sum_{j=0}^{\ell} \gamma_j h_j(N)$$

where $h_j(N)$ are power functions whose exponents can be as large as 240. For each $(a_i N_i)$ data set, a large number of potential power functions are examined and a small subset is selected using the methods of linear programming. The coefficients, γ_j are then determined using the least squares technique. The optimum fitting functions , $h_j(N)$, can be selected so that the composite function is monotonic, thus eliminating one of the major problems encountered with simple polynomials. However, experience with this technique has shown that, in spite of the high order terms that can be used, inadequate fits can occur near the upper end of some "a" versus N curves. This is particularly true for data generated using CT specimens under constant amplitude loading, since growth rates can increase rapidly due to the relatively large positive K-gradient in this specimen for deep cracks.

The problem of achieving a good overall fit is one that is always present for those data processing techniques which attempt to represent the entire "a" versus N curve. This problem stems from the basic nature of most crack growth curves — they contain a very flat initial portion and a very steep final portion. Furthermore, the specific shape of the "a" versus N curve depends on the particular specimen geometry used to generate these data. Thus, the general utility of processing techniques which are based on an overall fit of the crack growth curve cannot be demonstrated using a limited number of data from one specific test specimen geometry.

Techniques which attempt to represent the entire crack growth curve also add unnecessary complexities to the task of data processing. For example, the case of orthagonal polynomials[73] and spline functions[75,76] require decisions on certain input parameters — no

completely general criteria are available for making these decisions, thus subjectivity is introduced into the method. Furthermore, the spline functions exhibit the same problem related to inflection points which were previously discussed for simple polynomials. In addition, the orthogonal polynomial method requires that crack length measurements be equally spaced. In practice this does not always occur — in fact, varying crack length measurement intervals are recommended and are dependent on the specimen K-gradient as specified in Section 8.7.2 in Appendix I.

The difficulties associated with attempting to fit the entire "a versus N curve have motivated the use of incremental techniques to process fatigue crack growth rate data. These techniques are based on the fact that all that is required to process the data is a local assessment of the slope of the "a" versus N curve and not a complete description of the functional dependence of "a" on N. In addition to their simplicity, incremental techniques have the advantage of identifying local perturbations in the growth rate which may be associated with material inhomogenities or test problems.

Incremental techniques consist of fitting a low order polynomial — typically a parabola — to successive subsets of the total data set. These subsets generally contain an odd number of data points and da/dN is estimated from the derivative of the fitted curve at the central point. The local fit can be obtained using finite difference procedures or the least squares procedure. However, the least squares procedure is preferred since finite difference procedures can exhibit numerical difficulties for unevenly spaced data points, thereby resulting larger aberations in the growth rate.(1)

The incremental polynomial technique provided in Appendix A of the proposed test method utilizes the least-squares procedure to fit a parabola to successive subsets of three-to-nine data points. This technique is illustrated in Fig. 6-1 for the case of a seven-point subset; comparisons are also shown with the previously discussed secant and graphical techniques. Although the incremental polynomial technique does smooth the data, the smoothing is localized and thus does not

Curve 680804-E

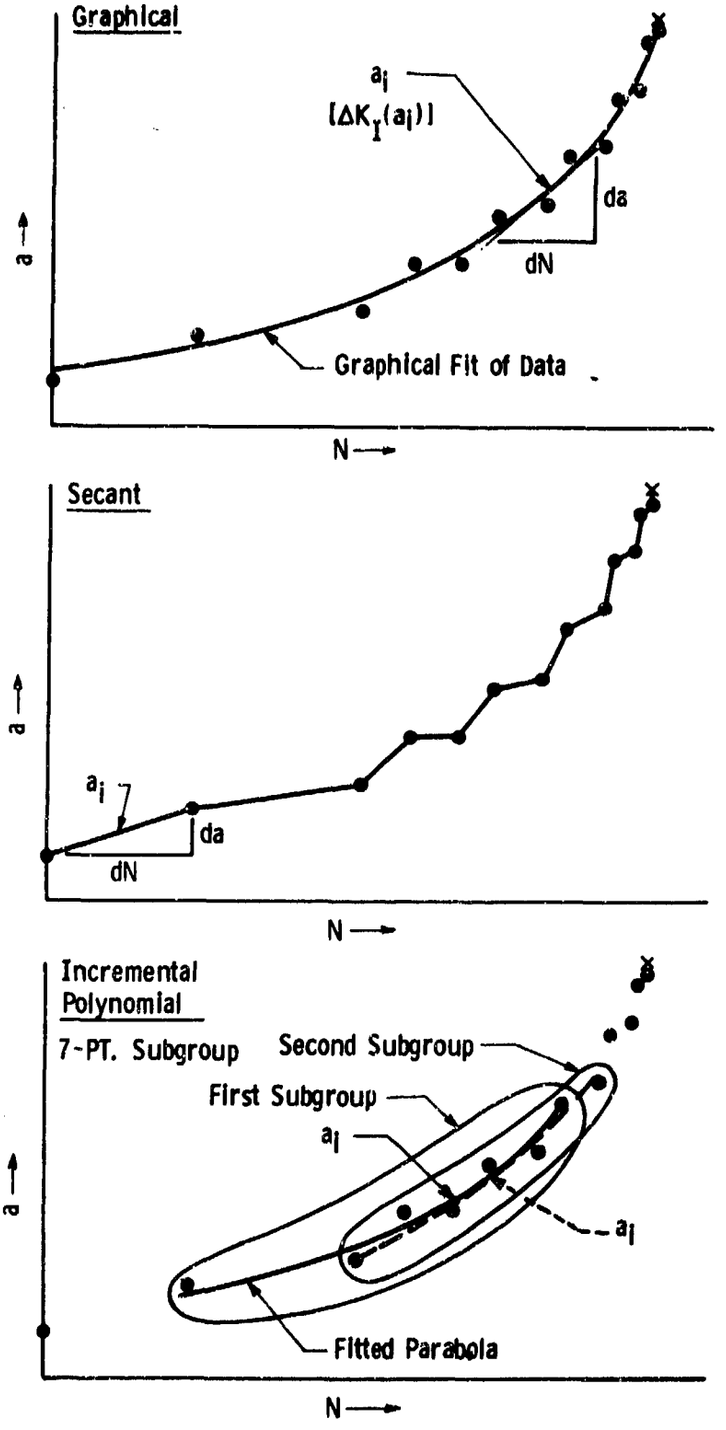

Fig. 6-1—Schematic illustration of various data processing techniques

eliminate discontinuities in the crack growth curve which may provide important information. This feature of the technique is demonstrated by the data in Fig. 6-2. These data were generated using 1-inch thick CT specimens of 1045 steel which contained void-like, artificial defects. The locations of the defects in the specimen and along the ΔK axis are as indicated. When the data were analyzed using the seven point, incremental polynomial technique, the local perturbations in the growth rates, caused by the defects, were readily detectible in spite of the fact that they were barely discernable in the "a" versus N curve. (The solid line represents measured growth rates for defect-free material).

The main disadvantage of the incremental techniques, as they are often employed, is that they do not provide growth rates for the first and last $(m-1)/2$ data points in the total data set (where m is the number of data points in the incremental subset). However, this disadvantage is overridden by the advantages of incremental techniques relative to other fitting techniques — particularly their simplicity, reproduciability, and accurate representation of local perturbations. Moreover, incremental techniques, such as the incremental polynomial method, could easily be modified to supply the first and last $(m-1)/2$ rates from derivatives of the first and last fitted parabolas, since these functions accurately represent the crack growth curve in their respective regions.

6.2.2 Contributions of Crack Length Measurement Accuracy and Measurement Interval to Variability in da/dN

An analysis has been conducted to examine the influence of interactions between crack length measurement accuracy and measurement interval on the accuracy and variability of fatigue crack growth rates determined using the recommended secant and incremental polynomial (Inpoly) techniques.

When attempting to evaluate variables which influence data processing using empirical (a_i, N_i) data the following question arises — how do the processed $(da/dN, \Delta K)$ results compare to the "true" $(da/dN, \Delta K)$ results? In order to overcome this difficulty, synthetic (a, N) data

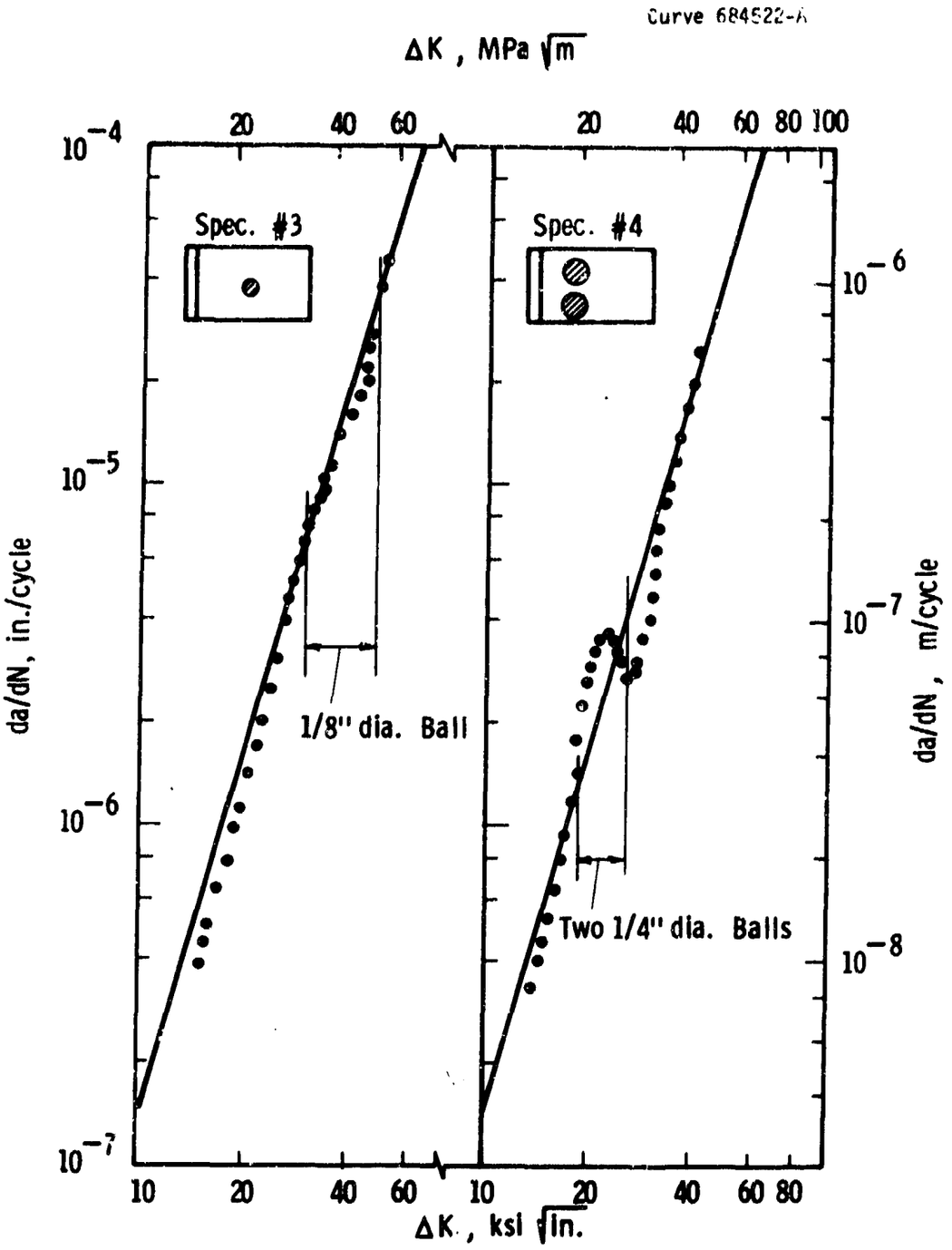

Fig. 6-2—Fatigue crack growth rates in compact specimens containing artificial defects (data analyzed using incremental polynomial method)

were generated from arbitrarily defined "true" (da/dN, ΔK) results as follows:

1) The "true" (da/dN, ΔK) results were defined by the following relationship which is typical of Region II growth rates in steels

$$da/dN = 4.0 \times 10^{-9} (\Delta K)^{2.25} \qquad (6\text{-}1)$$

where da/dN = fatigue crack growth rate in in./cycle.
ΔK = stress intensity factor range in ksi$\sqrt{in}$.

2) The above relationship was integrated, for the case of a CT specimen (B = 1 in., W = 2 in.) over the a/W range from 0.3 to 0.8 and the ΔK range from 20 ksi$\sqrt{in}$. to 100 ksi$\sqrt{in}$., to establish an idealized "a" versus N curve.
3) Various synthetic "a" versus N curves were subsequently formulated from the idealized curve by selecting different crack length intervals, Δa, and applying various measurement errors, ε.
4) These synthetic crack growth were then processed and the resulting (da/dN, ΔK) data was compared with the true (da/dN, ΔK) data.

After processing the synthetic data using both the secant and incremental polynomial techniques, the crack growth rate results were characterized by performing a least squares fit to the following general expression

$$da/dN = C_o \Delta K^n \qquad (6\text{-}2)$$

A comparison the fitting parameters, C_o and n, with the "true" values of Eq. (6-1) was used to assess the influence of ε and Δa on the accuracy of the data processing technique.

The variability or scatter in da/dN data introduced by the processing techniques was characterized in terms of a variability factor[1] VF, define as

$$VF = \exp(4R) \qquad (6\text{-}3)$$

where R is the residual standard deviation defined as

$$R = \left[\frac{\Sigma(\ell n\ da/dN_i - \ell n\ d\hat{a}/dN_i)^2}{Z - 2}\right]^{1/2} \qquad (6\text{-}4)$$

da/dN_i = processed crack growth rate at ΔK_{Ii}

$d\hat{a}/dN_i$ = rate given by least squares fit at ΔK_{Ii}

Z = number of $(da/dN_i, \Delta K_{Ii})$ points

Thus, VF, the variability factor, is merely

$$(d\hat{a}/dN_i + 2 \text{ std. dev.}) \div (d\hat{a}/dN_i - 2 \text{ std. dev.}).$$

A slightly modified form of the variability factor, termed VF^*, was used as a combined index of accuracy and variability of the processed data. The computational form of VF^* is similar to that for VF, except that the true crack growth rate at ΔK_{Ii} is used in place of $d\hat{a}/dN_i$. Note that when the C_o and n values obtained by fitting the processed data are equal to those in Eq. (6-1), VF^* is identical to VF. However, when C_o and n differ from those in Eq. (6-1), VF^* is greater than VF.

A summary of results from this analysis is provided in Table 6-1 for both the secant and Inpoly data processing techniques and a variety of Δa and ε values. Results are given for zero error, uniform error, and random error. The uniform error consists of alternate values of $+\varepsilon$ and $-\varepsilon$ applied to successive points on the idealized crack growth curve. The random error was generated from a normal distribution of zero mean and standard deviation, S — the tabulated values of ε are equal to S and were also applied to the idealized crack growth curve.[79]

In cases 1 thru 4 no measurement error was applied and only Δa was varied. For these cases the variability associated with each processing technique, as characterized by VF, is nearly equal to one, thus indicating that the steps in generating the synthetic data have little contribution to VF. For the Inpoly technique, VF^* increases with increasing Δa and reflects the deviation between the regression and

TABLE 6-1

INFLUENCE OF CRACK LENGTH MEASUREMENT INTERVAL (Δa) AND MEASUREMENT ERROR (ε) ON ACCURACY AND VARIABILITY ASSOCIATED WITH DATA PROCESSING

				Secant/Incremental Polynomial			
Case	Δa (in.)	ε (in.)	Δa/ε	C_o (x 10^9)	n	VF	VF*
1	0.005	0	0	4.01/3.98	2.25/2.25	1.015/1.002	1.015/1.006
2	0.010	0	0	4.01/3.92	2.25/2.26	1.009/1.003	1.009/1.024
3	0.025	0	0	4.01/3.63	2.25/2.28	1.004/1.009	1.004/1.129
4	0.050	0	0	4.02/3.39	2.25/2.31	1.002/1.004	1.007/1.383
		±ε, alternating uniform error					
5	0.025	0.005	5	3.60/3.60	2/26/2.29	5.71/1.08	5.87/1.16
6	0.050	0.010	5	5.18/3.47	2.16/2.31	5.98/1.14	6.27/1.40
7		0.005	10	4.64/3.43	2.20/2.31	2.35/1.07	2.38/1.38
8	0.100	0.020	5	3.47/4.50	2.28/2.25	6.73/1.24	6.81/1.82
9		0.010	10	3.86/5.31	2.26/2.20	2.49/1.12	2.49/1.77
		ε∿(0,S), random error from normal distribution (Ref. 79)					
10	0.010	0.002	5	3.79/3.94	2.25/2.26	3.65/1.16	3.71/1.16
11	0.010	0.001	10	4.02/3.97	2.25/2.25	1.74/1.08	1.75/1.08
12	0.025	0.005	5	3.81/3.62	2.25/2.28	3.89/1.21	3.98/1.25
13	0.025	0.0025	10	3.96/3.66	2.25/2.28	1.73/1.10	1.74/1.15
14	0.025	0.00125	20	4.02/3.65	2.25/2.28	1.34/1.05	1.35/1.13
15	0.050	0.010	5	4.58/3.72	2.21/2.29	4.16/1.22	4.20/1.48
16	0.050	0.005	10	4.10/3.43	2.24/2.31	1.95/1.13	1.96/1.40
17	0.050	0.0025	20	4.02/3.43	2.25/2.31	1.36/1.05	1.36/1.37

"true" values of Eq. (6-1). The significance of this data processing bias will be examined later.

As expected the analysis using the uniform errors indicate that the data processing techniques are responsible for higher variability (VF) and inaccuracies (VF^*) than do the analyses using random errors. However, both analyses illustrate the same points. Note that both VF and VF^* increase significantly as $\Delta a/\varepsilon$ is decreased, especially for the secant technique. These results provide the basis for the specifications of Section 8.7.2 of Appendix I that require Δa to be at least ten times larger than ε. This provision is designed to maintain the variability introduced to da/dN, by the combination of measurement error and data processing, at a reasonable level.

The increase in VF^* with decreasing $\Delta a/\varepsilon$ indicates that inaccuracies, in terms of deviations between the processed and "true" (da/dN, ΔK) results, are occurring. A comparison of VF and VF^* for a given $\Delta a/\varepsilon$ shows that this processing bias is more significant for the Inpoly technique. In order to assess the practical significance of this bias, the difference between processed and true (da/dN, ΔK) results were converted to differences in cyclic life. Processed results, defined by C_o and n, were integrated for the case of a CT specimen (B = 0.25, W = 2) over an a/W range of 0.3 to 0.8 and a ΔK range of 20 ksi$\sqrt{\text{in}}$. to 100 ksi$\sqrt{\text{in}}$. These results are shown in Table 6-2 for several cases, defined in Table 6-1, which are most typical of fatigue crack growth rate testing. The total number of cycles required to propagate the crack from a/W of 0.3 to 0.8 in the test specimen are shown normalized with respect to the results from the ideal crack growth curves (N_{ideal} = 95,556 cycles). As indicated, the data processing bias influences the specimens' cyclic life by less than 5 percent — this influence is small compared to the variation in cyclic life observed when replicate specimens are tested.[1] Thus, although the bias from the secant and Inpoly data processing techniques may be statistically significant, it is of no practical significance in fatigue crack growth rate testing.

TABLE 6-2

INFLUENCE OF DATA PROCESSING BIAS ON CYCLIC LIFE

Case	$\Delta a/\varepsilon$	Processing Technique	N/N_{Ideal}
12	5	Secant	1.049
		InPoly	1.001
13	10	Secant	1.010
		InPoly	0.990
16	10	Secant	1.008
		InPoly	0.956
17	20	Secant	0.995
		InPoly	0.956

N_{Ideal} = cycles to grow a crack from a/W = 0.3 to 0.8 in a CT specimen (B = 1/4 in., W = 2.0 in.) with ΔP = 1.2 kips and fatigue crack growth rates defined by $da/dN = 4.0 \times 10^{-9} (\Delta K)^{2.25}$ (units of in./cycle and ksi$\sqrt{in.}$)

7. EVALUATION OF DATA PRESENTATION METHODS

This phase of the program deals with the development and evaluation of methods for presentation of fatigue crack growth rate data. The underlying considerations in examining these methods were: (i) they should be convenient for use in material selection and design, and (ii) they should provide for an unambiguous interpretation of the data by those not completely familiar with detailed test procedures or data analysis techniques.

Three primary methods of data presentation were considered: (1) graphical presentation — data are plotted in parametric form using suitable coordinate axes, (2) tabular presentation — data are tablulated along with testing variables, (3) mathematical presentation — data are represented by an equation which describes either the average behavior or some statistical bound on the average behavior. Appendix I, Section 10.10, includes specific requirements on the graphical presentation of data; tabular and mathematical presentations are considered supplementary and are not required as part of the test method.

The following sections contain detailed descriptions of the various methods considered, and where possible provide comparisons and define optimum methods.

7.1 Graphical Display

Graphical display of fatigue crack growth rate data represents a clear and concise method of reporting data, particularly when comparisons are being made between variables that affect fatigue crack growth. A graphical display also has the advantage of directly illustrating the extent of variability in the data. This feature is important since there is currently no universally accepted statistical method for characterizing variability in da/dN.

The graphical methods currently in use consist of either log-log or semi-log plots of da/dN as a function of ΔK or K_{max}. The log-log plots have greater utility in the sense that they can be employed to display wide-range data for which ΔK or K_{max} may vary by more than an order of magnitude. No fundamental arguments exist for the use of ΔK versus K_{max}, thus both are considered technically acceptable. However, there is an advantage to reporting data in a consistent manner to facilitate data comparisons and use of data in design — in fact this is one of the goals of any standardization effort. In view of the above considerations, this goal can best be achieved by a concensus of the technical community engaged in generating and using these data. The graphical display method specified in Section 10.10 of Appendix I, namely that data be plotted as log ΔK versus log da/dN, is based on such a concensus. This method is by far the most frequently used graphical display format according to input from the test methods survey which was conducted as part of this program in conjunction with ASTM Subcommittee E24.04 on Subcritical Crack Growth. Furthermore, E24's Task Group on Fatigue Crack Growth Rate Testing, at a meeting in October of 1976, strongly supported the specification of a single graphical display method in the test method and voted to include the log ΔK-log da/dN format.

Section 10.10 of Appendix I also recommends that the independent variable, ΔK, be plotted on the abscissa, and the dependent variable, da/dN, be plotted on the ordinate — this practice is consistent with the convention used in most scientific and engineering fields. In addition, to facilitate data comparisons and assessment of variability, it is suggested that the relative sizes of the log cycles upon which data are plotted be adjusted so that log ΔK versus log da/dN forms a line inclined at approximately 45° to the coordinate axes. For example, when plotting Region II da/dN values, this is adequately accomplished by using ΔK log cycles which are approximately two and four times larger than the da/dN log cycles for steels and aluminums, respectively. For data collections which focus on either Region I or Region III, expanded ΔK log cycles are advisable.

7.2 Tabular Presentation

Reporting data in tabular form is the most thorough, although not necessarily the most effective, method of data presentation. The tabulation of (a,N) and (ΔK,da/dN) data, along with pertinent test variables, is primarily helpful when users of the data wish to perform supplemental analyses such as statistical characterizations of variability. In spite of this advantage,tabular presentations of fatigue crack growth rate data are infrequently used due to several cumbersome features.

The extent of data generated in a fatigue crack growth rate test — typically consisting of from 20 to 40 data points for primary (a,N) data and processed (ΔK, da/dN) data — can easily exceed the space restrictions of many publications, particularly those of scientific and technical journals. Furthermore, even if reports and publications could accommodate this additional space requirement, the overall benefit would be marginal since most readers are satisifed by a graphical display of (ΔK,da/dN) data and are not interested in performing additional detailed analyses or manipulations of the data. This fact is especially true now that standard methods are available for fatigue crack growth rate testing.

The question of whether or not to require the tabulation of test data has been encountered in developing other test methods having similar features to the method under consideration here. ASTM Committee E09 on Fatigue has addressed this problem while developing ASTM test methods E468 and E606[80]. Following the precident established by these former efforts, Section 10.13 of Appendix I indicates the desirability of tabulating and storing data so that it can be made available upon request. When appropriate, this reporting option can be specified in contractual agreements on testing and research programs.

7.3 Mathematical Representation

An important aspect of this effort, particularly with respect to usage of data in design, deals with the evaluation of "models" which provide accurate analytical representations over wide ranges of fatigue crack growth rates.* Wide-range fatigue crack growth rate data, and mathematical representations of these data, are becoming increasingly important — even for many so-called "low-cycle fatigue" applications — since knowledge of low growth rates is an important input to overload-retardation models which are used to predict cyclic lives under variable amplitude loading [61].

One approach, that has been used to "model" fatigue crack growth rate data is to identify mathematical functions that inherently possess a shape similar to the often observed sigmodial character of wide-range log da/dN versus log ΔK results. Such functions generally incorporate several constants that can be determined by simple regression techniques for a particular set of experimental data. Three such models will be discussed in greater detail in subsequent sections.

Other models often referred to in the literature are the Forman equation [81] and the Walker equation [82] which have been demonstrated to adequately characterize the crack growth rate behavior in Regions II and III. Evaluation of such models was not considered in the present work due to their applicability to data over a limited range of growth rates.

7.3.1 Hyperbolic Sine Model

Annis, Wallace and Sims [83] have proposed the following equation to represent fatigue crack growth rates, da/dN, as a function of stress intensity factor range, ΔK.

---

*The use of the term "model" is not intended to imply that any of the mathematical representations have any fundamental physical significance.

$$\{\log\left(\frac{da}{dN}\right) - b_4\} = b_1 \sinh\left(b_2 \log(\Delta K) + b_3\right) \qquad (7\text{-}1)$$

where b_1 thru b_4 are regression parameters. The hyperbolic sine function is symmetric with respect to the origin. Thus, the purpose of constants b_3 and b_4 is to relocate the origin with respect to the log da/dN and log ΔK axes such that the function lies in the positive quadrant for all realistic values of ΔK. The constants b_1 and b_2 control the shape of the function to some extent. However, it should be noted that the function described by Eq.(7-1) is symmetric about the point of inflection which lies at coordinates given by (b_3, b_4) on the log ΔK and log da/dN axes, respectively. In other words, this means that da/dN versus ΔK data in Regions I and III should exhibit reflective symmetry — a constraint not justifiable on any empirical or physical grounds. The original data supporting the validity of Eq.(7-1) extends only over Regions II and III. If wider range data covering all three regions of fatigue crack growth had been available, it is not likely that a good correlation between the model and the data could have been obtained. Hence, no further work on evaluating this model was undertaken.

7.3.2 Inverse-Hyperbolic-Tangent Model

Collipriest[84] has proposed using the inverse hyperbolic tangent function to represent the sigmoidal shape of the log da/dN versus log ΔK curve. This model has been shown to provide a good representation[85] of wide-range fatigue crack growth behavior at constant load ratios. The general equation describing fatigue crack growth rates using this model is

$$\log\frac{da}{dN} = C_1 + C_2 \operatorname{arctanh}\left[\frac{\log[(1-R)K_c \cdot \Delta K_{th}/(\Delta K)^2]}{\log[\Delta K_{th}/(1-R)K_c]}\right] \qquad (7\text{-}2)$$

where ΔK_{th} is the threshold stress intensity range for fatigue crack growth and K_c is the critical stress intensity for the onset of unstable

crack extension.* Often fatigue crack growth data are only available over a limited ΔK versus da/dN range and the values of ΔK_{th} and K_c are no longer strictly defined as above. In such cases these limiting values are selected to provide an optimum fit to the data and therefore are reduced to fitting parameters rather than material properties. Thus, for clarity C_3 and C_4 will be used in place of ΔK_{th} and $K_c(1-R)$; the latter designations being reserved for material properties. Mathematically, the constants C_3 and C_4 represent the lower and upper ΔK asymptotes, respectively. Following this nomenclature Eq. (7-2) becomes

$$\log da/dN = C_1 + C_2 \operatorname{arctanh} \left[\frac{\log \left[(C_3)(C_4)/(\Delta K)^2 \right]}{\log \left[C_3/C_4 \right]} \right] \qquad (7\text{-}3)$$

The above equation can be simplified by employing the following mathematical identify,

$$\operatorname{arctanh} (x) = \frac{1}{2} \ln \frac{1+x}{1-x} \qquad (7\text{-}4)$$

Substitution of Eq. (7-4) into (7-3) gives

$$\frac{da}{dN} = C_5 \left[\frac{\log (\Delta K/C_3)}{\log (C_4/\Delta K)} \right]^{C_6} \qquad (7\text{-}5)$$

where C_5 and C_6 are constants for a given material, environment and load ratio (R). The simpler form of Eq. (7-5) relative to Eq. (7-2) facilitates computer analysis when determining the fitting constants by regression.

*K_c may be geometry dependent and thus is not necesarily a material property.

7.3.3 Three-Component Model

A model based on adding the material's resistance to fatigue crack growth (that is, $(da/dN)^{-1}$) in the three regions of log (da/dN) versus log (ΔK) has been developed in this program. This approach is conceptually similar to that employed by Williams to describe environment enhanced crack growth under static load.[86] The characterisitic equation describing da/dN for a constant load ratio and fixed environment is given by

$$\frac{1}{(da/dN)} = \frac{A_1}{(\Delta K)^{n_1}} + \frac{A_2}{(\Delta K)^{n_2}} - \frac{A_2}{(K_c(1-R))^{n_2}} \qquad (7\text{-}6)$$

where A_1, n_1, A_2, n_2 and K_c are constants that can be obtained from the data. The three terms in Eq.(7-6) correspond to the three regions of crack growth rates; transition regions are modelled by a combination of two adjacent terms. In Eq.(7-6) the exponents n_1 and n_2 can be estimated by equating them to the slopes in Regions I and II respectively from a plot of the data. The value of K_c, which is a parameter characterizing the onset of instability (primarily a fitting parameter and should not be confused with K_{Ic}) can also be determined from a plot of the data. For materials that do not exhibit Region III, or if growth rates are not characterized in that region, the last term in Eq.(7-6) is set equal to zero. Physically, this means that fatigue crack growth resistance does not require adjustment for the static component of cracking because it is either not important for the material being tested, or the K_{max} levels for which data exist are considerably below the fracture toughness of the material. In addition, it should be noted that also setting A_1 equal to zero reduces Eq.(7-6) to the familar Paris equation[87] in Region II.

7.4 Regression Analyses of Wide-Range da/dN-ΔK Data

A detailed evaluation of the inverse-hyperbolic-tangent model and the proposed three-component-model was undertaken by performing regression analyses on data sets of 2219-T851 aluminum and 10Ni steel at

TABLE 7-1

SPECIMEN NUMBERS AND THE FATIGUE CRACK GROWTH RATE RANGE COVERED IN THE VARIOUS DATA SETS USED FOR REGRESSION ANALYSES

Data Set No.	Material	R	Specimens Included	da/dN Range (in./cycle)
1	2219-T851 Al	0.1	CCP-2,3, CT-3,4,5,6,11,20	$2 \times 10^{-8} - 8 \times 10^{-4}$
2	2219-T851 Al	0.1	CCP-2,3, CT-3,4,5,6,7,11,20	$4 \times 10^{-9} - 8 \times 10^{-4}$
3	2219-T851 Al	0.1	CCP-2,3, CT-3,4,5,11,20	$10^{-7} - 8 \times 10^{-4}$
4	2219-T851 Al	0.1	CCP-2,3, CT-3,4,5,6,7,11,20, 28,45,49	$10^{-9} - 8 \times 10^{-4}$
5	2219-T851 Al	0.3	CT-53,57,71,79,56,58	$4 \times 10^{-9} - 6 \times 10^{-5}$
6	2219-T851 Al	0.5	CT-12,14,52,54,60	$3 \times 10^{-9} - 1.3 \times 10^{-4}$
7	2219-T851 Al	0.8	CT-8,51,77,19,27	$10^{-9} - 5 \times 10^{-5}$
8	10Ni Steel	0.1	10Ni-31,33,35,3,2,14,20,25	$10^{-9} - 10^{-4}$
9	10Ni Steel	0.8	10Ni-5,39,9S*,11,28S*,62S*	$6 \times 10^{-9} - 2 \times 10^{-5}$

*Only data satisfying the minimum uncracked ligament size requirement are included.

various R values. Table 7-1 identifies the data sets that were used for the regression analyses and the following sections summarize important results.

7.4.1 Regression with the Inverse-Hyperbolic-Tangent Model

A detailed description of all results obtained using this model have been reported previously.[88] Hence, only a brief description of results and important conclusions will be repeated here.

Two types of regression analyses were performed; namely, (1) linear regression — parameters C_3 and C_4 in Eq. (7-5) were estimated from data plots and best estimates for constants C_5 and C_6 were determined by linear regression and (2) nonlinear regression — initial estimates of all four parameters were provided and best estimates of the parameters were obtained by simultaneous iteration and regression. The results from these analyses are provided in Table 7-2 and Fig. 7-1 and can be summarized as follows:

TABLE 7-2

REGRESSION CONSTANTS FOR EQ.(7-5) OBTAINED FROM FATIGUE CRACK GROWTH RATE DATA ON 2219-T851 Al ALLOY (R = 0.1)

Data Set No.	Type of Regression Analysis	C_3 (ksi$\sqrt{in.}$)	C_4 (ksi$\sqrt{in.}$)	C_5	C_6	r†
1	linear	3.0	30.0	5.7×10^{-6}	1.66	0.98
2	non-linear	2.42	27.2	3.02×10^{-6}	1.89	0.99
3	non-linear	3.65	27.2	7.7×10^{-6}	1.52	0.98

†r = correlation coefficient (1 ksi$\sqrt{in.}$ = 1.1 MPa$\sqrt{m}$)

(1) For the nonlinear analysis, the estimated values of C_3 are about 5 to 10 percent less than the smallest value of ΔK in a particular data set, and the values of C_4 are about 5 to 10 percent greater than the largest value of ΔK in a data set.

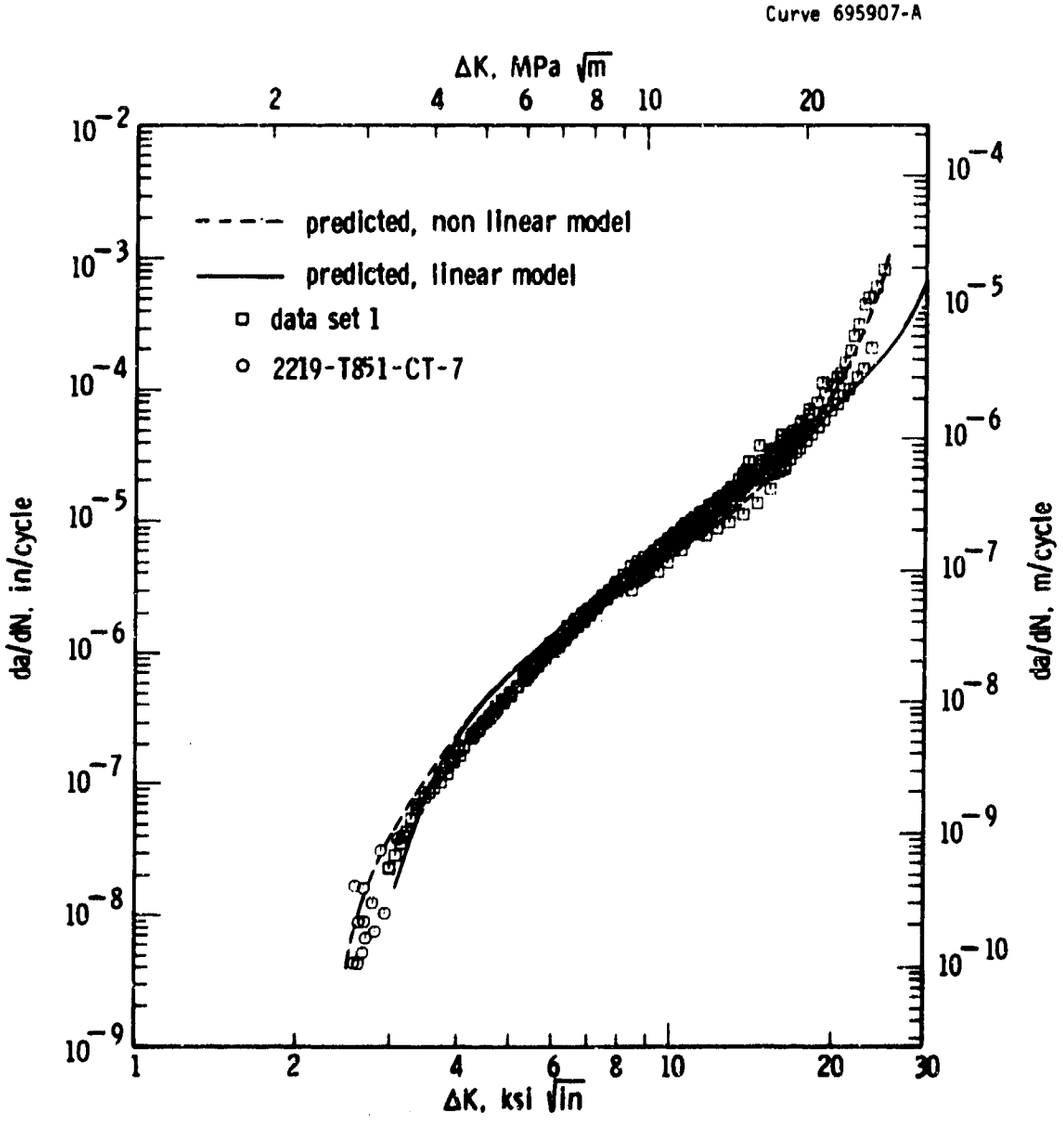

Fig. 7-1—Comparison of experimental and predicted crack growth rate behavior obtained from linear and non-linear regression analyses using the inverse-hyperbolic-tangent model

(2) Although the global fits, characterized by the correlation coefficients (r in Table 7-2), are very similar, there are differences in the local fits obtained using the linear and nonlinear analyses.* This difference is most evident in Region III where the two curves can differ by more than a factor of two (Fig. 7-1) as the result of relatively small errors (about 10%) in graphically estimating C_4. Obtaining a best estimate of C_4, using the nonlinear analysis, improves the fit in Region III as illustrated in Fig. 7-1.

(3) The inverse hyperbolic tangent model is capable of providing an adequate fit to wide-range da/dN data at a constant load ratio (R).

Further evaluations of this model in terms of the influence of its asymptotic nature on life predictions and its utility for representing load ratio (R) effects are considered in Sections 7.5.2 and 7.6, respectively.

7.4.2 Regression with the Three-Component Model

The evaluation of this model was limited to the simple linear regression analysis which involved inputing estimates for the exponents n_1, n_2 and the parameter K_c in Eq. (7-6); corresponding best estimates of parameters A_1 and A_2 were then obtained using multiple-linear-regression.

An alternate form for Eq. (7-6) which is convenient for computer analysis is

$$\frac{1}{(da/dN)} = \frac{A_1}{(\Delta K)^{n_1}} + A_2 \left[\frac{1}{(\Delta K)^{n_2}} - C'\right] \qquad (7\text{-}7)$$

where $C' = 1/(K_c(1-R))^{n_2}$. Exponents n_1 and n_2 were determined by estimating the slopes of the log da/dN vs. log ΔK plots in regions I and II, respectively. The value of C' can be determined from inspection of the Region III data.

---

*The term global fit refers to the fit over the entire range of data; local fit refers to the fit over a limited range of data.

Generally, when using multiple-linear-regression of the type required for obtaining best estimates of coefficients A_1 and A_2, the sum of the square of residuals (SSR), as given by Eq. (7-8) is minimized.[89]

$$SSR = \sum_{i=1}^{n} (y_i - \hat{y}_i)^2 \tag{7-8}$$

where y_i = i_{th} observed value of the dependent variable corresponding to the independent variable, x_i

$\hat{y}_i$ = predicted value of y_i

n = number of data points

Since $1/(da/dN)$ values ranged from 10^9 to 10^4 in a majority of the data sets analyzed, the contribution to the SSR is much larger for the higher $1/(da/dN)$ values in the data set. This would unnecessarily assign high weights to data in Region I and low weights to — and perhaps even ignore — data in Regions II and III. This problem was resolved by employing a value of SSR based on relative error, instead of absolute error, as follows

$$(SSR)_{rel} = \sum_{i=1}^{n} \left[\frac{y_i - \hat{y}_i}{y_i}\right]^2 \tag{7-9}$$

The input parameters and regression parameters obtained for data sets 2 thru 9 are presented in Table 7-3 along with the correlation coefficients.

It was observed that a significant amount of uncertainty was involved in graphically determining the input parameters n_1, n_2 and K_c from plots of the data. The amount of uncertainty depended on the region of crack growth rate and the scatter in the particular data set. The influence of this uncertainty on the global and local fits was investigated. The index used to evaluate the global fit was the correlation coefficient, r, and to evaluate the local fit was a visual comparison between the fitted curve and the data.

TABLE 7-3

SUMMARY OF DATA REGRESSION ANALYSIS RESULTS USING THE THREE COMPONENT MODEL

Data Set No.	Material	R	Input Parameters* n_1	n_2	K_c (ksi$\sqrt{in.}$)	Regression Parameters* A_1	A_2	r†
2	2219-T851 Al	0.1	12.5	4.0	33.0	1.085×10^{13}	1.375×10^{9}	0.965
2		0.1	12.5	3.7	33.0	1.36×10^{13}	7.2×10^{8}	0.972
2		0.1	12.5	3.3	33.0	1.66×10^{13}	2.8×10^{8}	0.954
3		0.1	12.5	3.3	33.0	1.06×10^{14}	2.72×10^{8}	0.964
4		0.1	12.5	3.7	33.0	1.49×10^{13}	6.86×10^{8}	0.97
4		0.1	12.5	3.3	33.0	1.84×10^{13}	2.77×10^{8}	0.951
5		0.3	12.5	3.3	33.0	7.3×10^{11}	2.69×10^{8}	0.965
6		0.5	11.5	3.3	35.0	1.39×10^{9}	2.04×10^{8}	0.964
6		0.5	12.5	3.3	35.0	2.63×10^{9}	2.04×10^{8}	0.965
6		0.5	15.0	3.3	35.0	9.61×10^{9}	2.04×10^{8}	0.965
7		0.8	12.5	3.3	35.0	5.83×10^{9}	9.25×10^{7}	0.900
7		0.8	12.5	3.3	33.0	5.29×10^{9}	1.11×10^{8}	0.847
7		0.8	12.5	3.3	30.5	7.2×10^{9}	4.54×10^{9}	0.540
8	10Ni Steel	0.1	10.0	2.8	0	6.51×10^{14}	1.47×10^{9}	0.953
8		0.1	10.0	2.0	0	1.077×10^{15}	1.058×10^{8}	0.910
9		0.8	10.0	2.8	0	1.60×10^{11}	8.52×10^{8}	0.960
9		0.8	10.0	2.0	0	1.42×10^{12}	3.86×10^{7}	0.760

*Values obtained when ΔK is expressed in ksi$\sqrt{in.}$ and da/dN in in./cycle (1 ksi$\sqrt{in.}$ = 1.1 MPa$\sqrt{m}$, 1 in./cycle = 2.5×10^{-2} m/cycle)

†r = Correlation coefficient

In data set 6 of Table 7-3, the value of n_1 was varied between 11.5 and 15 while holding imput parameters n_2 and K_c constant. This exercise is shown to result in an insignificant difference in the correlation coefficient while the local fit in Region I changed by as much as a factor of two in predicted growth rates, Fig. 7-2a. The influence of the value n_2 was investigated using data set 2. There were only marginal changes in the correlation coefficient for values of n_2 between 3.3 and 4.0. The local fit in Region II changed by less than the general scatter in the data, Fig. 7-2b. It was thus concluded that within the limits of accuracy with which n_1 and n_2 can be estimated graphically, there are insignificant differences in the accuracy of the local and global fits.

Varying the value of K_c is expected to influence the fit in Region III only. Hence, data set 7 which exhibited a large Region III, in terms of its ΔK range, was selected for study. Values of K_c ranging from 30.5 to 35.0 ksi$\sqrt{in}$. (33.55 to 38.5 MPa$\sqrt{m}$) were used while holding other input parameters constant. The significant influence of K_c on the corelation coefficient, Table 7-3, as well as the local fits in Regions II and III, Fig. 7-3, is evident. However, the differences in fit (both global and local) are not very significant between K_c values of 33 and 35 ksi$\sqrt{in}$. (36.3 and 38.5 MPa$\sqrt{m}$). It should be possible to estimate a value of K_c within the above limits from inspection of the data. Hence, picking an appropriate value of K_c from the plot of the data is not considered a limitation in using the linear analysis on the three-component model.

Additional comments on a comparison of the measured and fitted growth rates from the above analyses are appropriate. The factor of two disparity between fitted and measured rates in Region I of Fig. 7-2a and Region II of Fig. 7-3 is due to the relatively small number of data points in these particular regions. Thus, the use of a nonlinear analysis to further optimize the fitting parameters would not improve the fit significantly for these cases. These examples illustrate that an even distribution of (da/dN, ΔK) data is preferrable when

Curve 693697-A

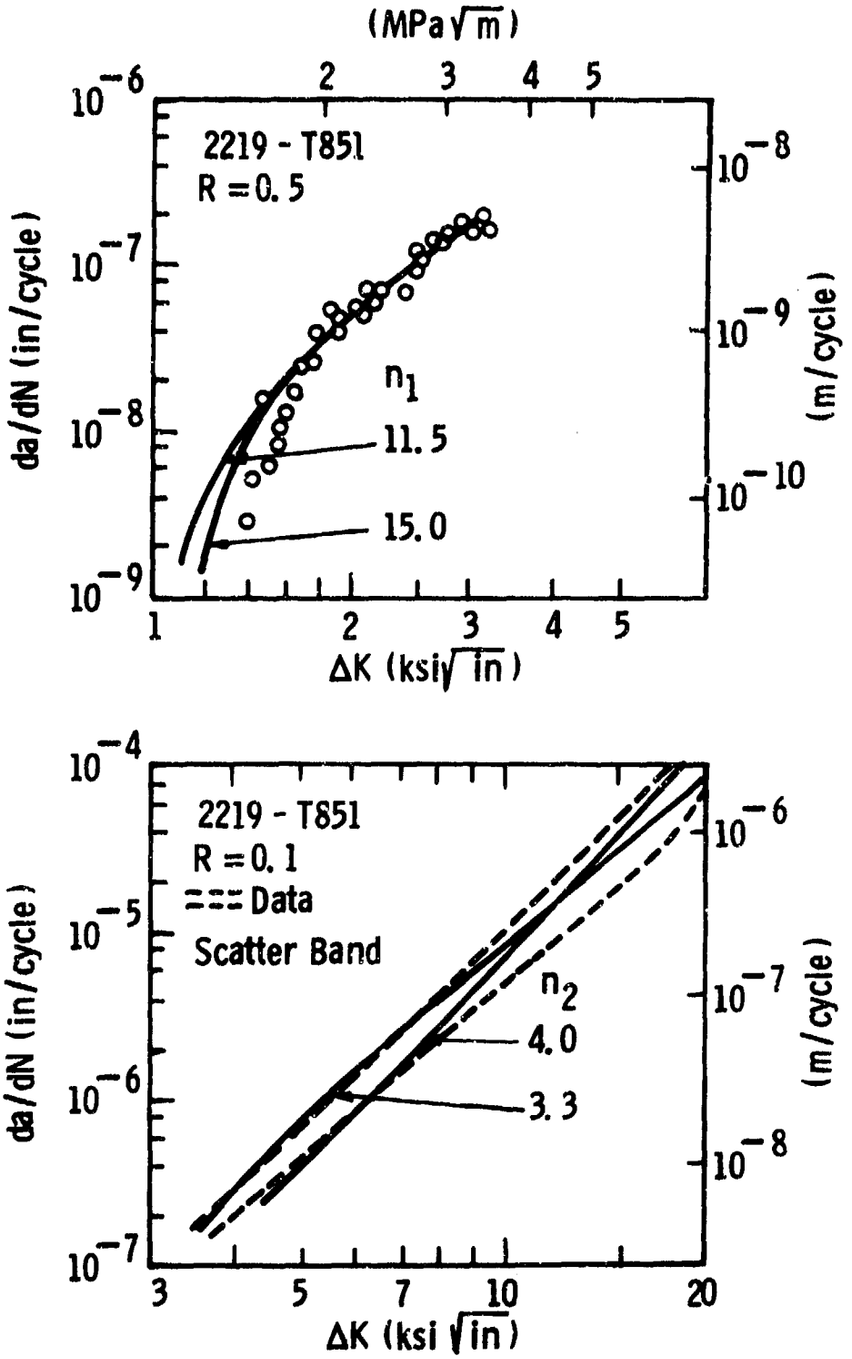

Fig. 7-2– Influence of the value of n_1 and n_2 on the fit obtained with the three-component Model

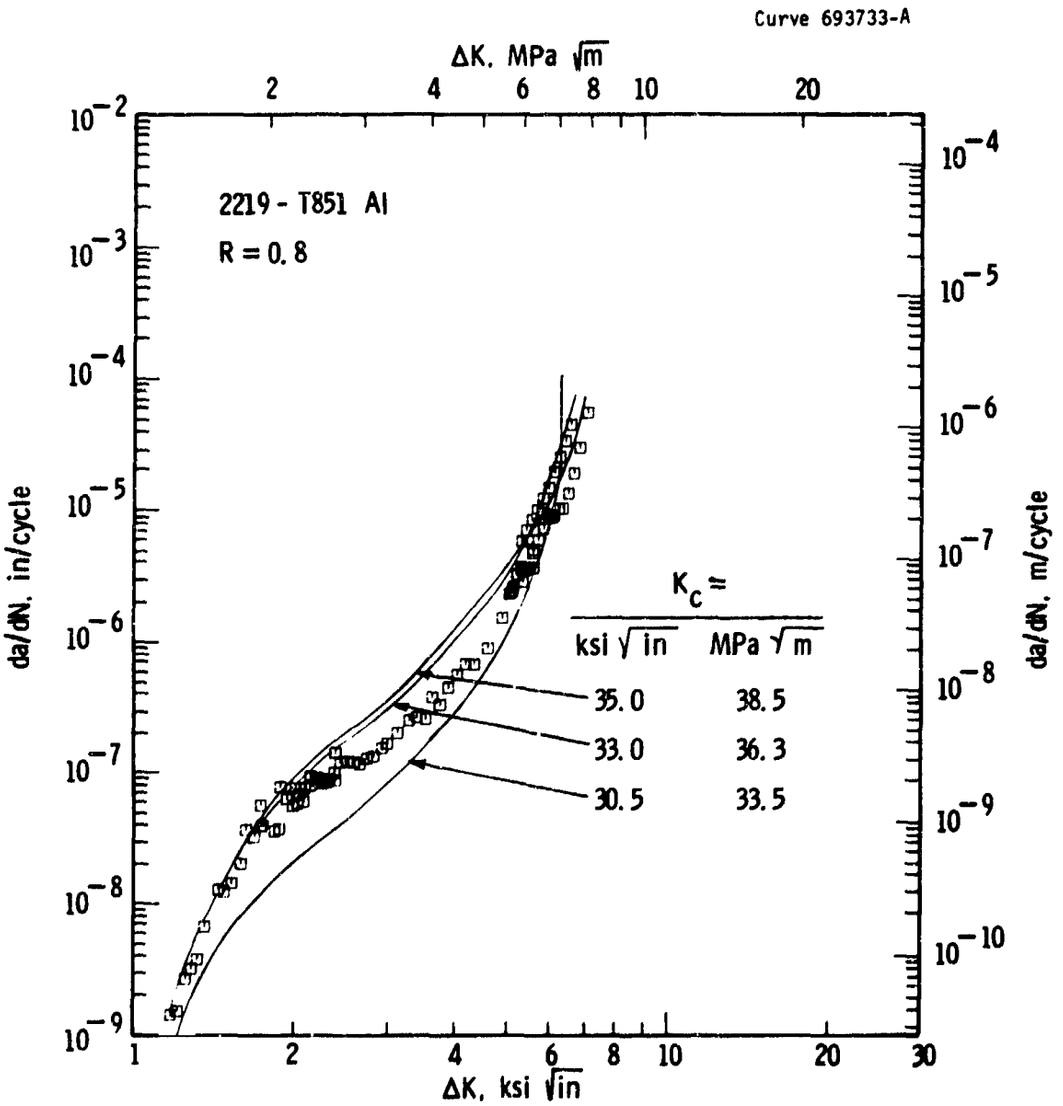

Fig. 7-3 – Influence of the value of K_c on the fit obtained for 2219-T851 aluminum alloy at a load ratio of 0.8 using the three component model

attempting to obtain optimum fits to wide-range fatigue crack growth rate behavior. The influence of this particular factor was not further explored, however, it is not expected to significantly influence the model comparisons in subsequent sections since this factor will have influenced all models in a similar fashion.

7.5 Cyclic Life Predictions from Wide Range da/dN-ΔK Models

7.5.1 Comparison of Predicted and Observed Cyclic Lives

In many cases the ultimate goal behind generating fatigue crack growth rate data, and representing it by mathematical equations, is to enable predictions of cyclic life ("a" versus N) of structures for which initial defect sizes, geometry and stress intensity expressions are available. Thus, a rational basis for evaluating mathematical expressions relating da/dN versus ΔK is to compare cyclic lives predicted from these expressions with those observed in experiments.

Predicted "a" versus N behavior for compact type specimens under loading conditions identical to those used for generating the original "a" versus N data were developed by integrating the various regression equations. Both the inverse-hyperbolic-tangent and three-component models were thus evaluated. Integration was performed numerically using Simpson's rule.[90] Specimens were selected from various crack growth regimes at stress ratios of 0.1 and 0.8 for both materials tested in this program. To facilitate comparison of observed and predicted results, the crack length and number of cycles were normalized with respect to the observed final crack length and the observed number of cycles to failure, respectively. This normalization provides a direct comparison in terms of percentage deviation. Detailed information on the particular specimens for which these comparisons were made are given in Table 7-4. Normalized cyclic lives are summarized in Figs. 7-4 thru 7-6 are are discussed below.

TABLE 7-4

LOAD AND CRACK LENGTH DETAILS FOR WHICH CYCLIC LIVES WERE PREDICTED

Specimen No.*	R	a_i (in.)	a_f (in.)	ΔP (kips)	N_f (cycles to failure)
			2219-T851 Aluminum		
2219-4	0.1	0.609	1.5	0.297	4.390×10^5
2219-5	0.1	0.635	1.55	0.180	3.505×10^6
2219-49	0.1	0.620	0.920	1.17	2.542×10^5
2219-8	0.8	0.680	0.800	0.09	2.136×10^6
2219-27	0.8	0.680	0.800	0.30	2.669×10^4
			10Ni Steel		
10Ni-33	0.1	1.430	1.75	0.085	3.319×10^6
10Ni-14	0.1	0.603	1.50	0.60	7.075×10^5
10Ni-39	0.8	0.97	1.60	0.091	15.28×10^6
10Ni-11	0.8	0.593	1.30	0.60	3.221×10^5

R = load ratio, a_i = initial crack length, a_f = final crack length, N_f = no. of cycles to failure, ΔP = load range ($P_{max} - P_{min}$)

*All specimens are CT specimens with W = 2 in., B = 1/4 in. with the exception of 2219-49 for which B = 1 in.
(1 in. = 25.4 mm, 1.0 kip = 4.45×10^3 Newtons)

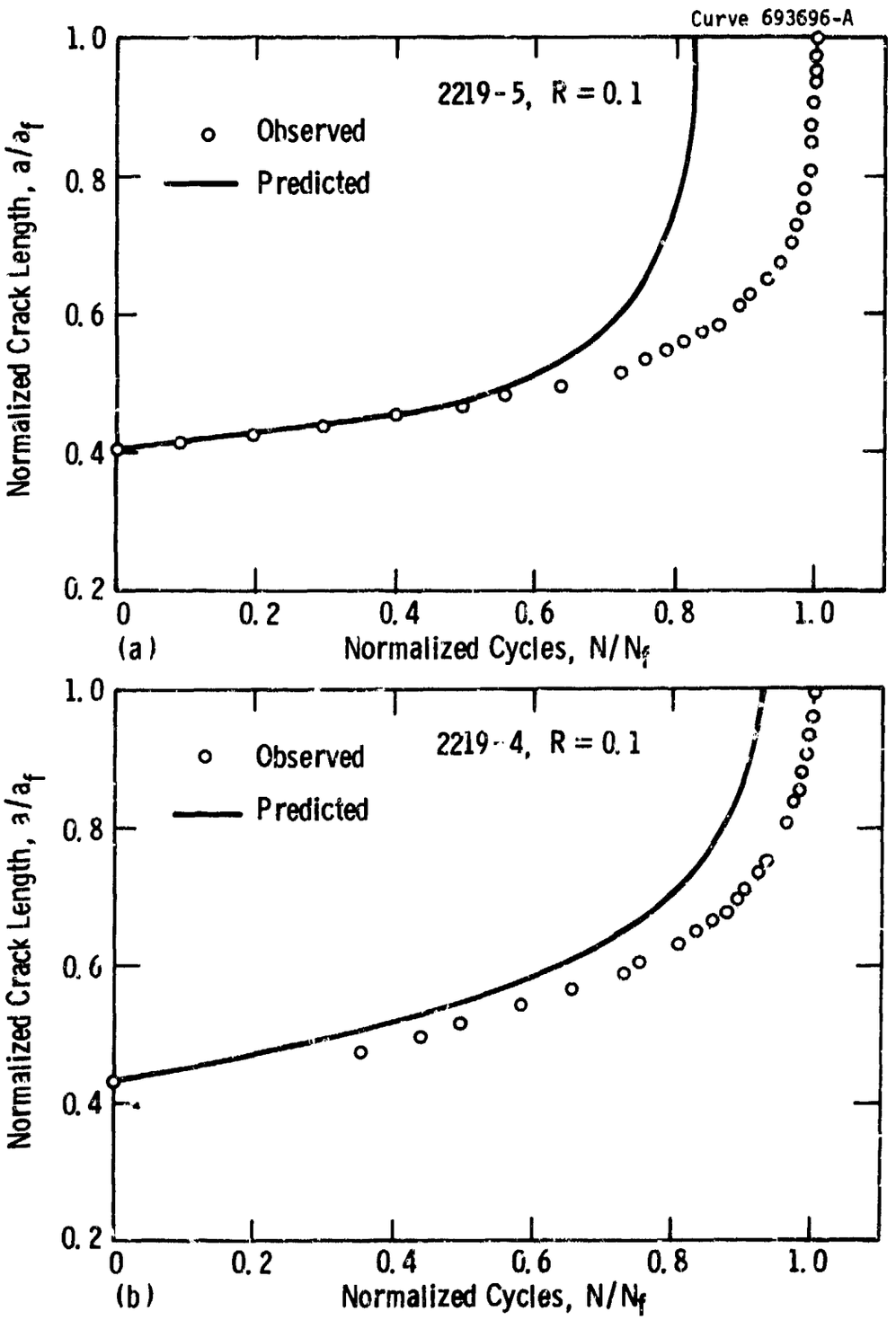

Fig. 7-4 — Comparison of the observed "a vs. N" behavior with that predicted by the integration of the growth rates as represented by the Inverse-Hyperbolic-Tangent model for 2219-T851A1

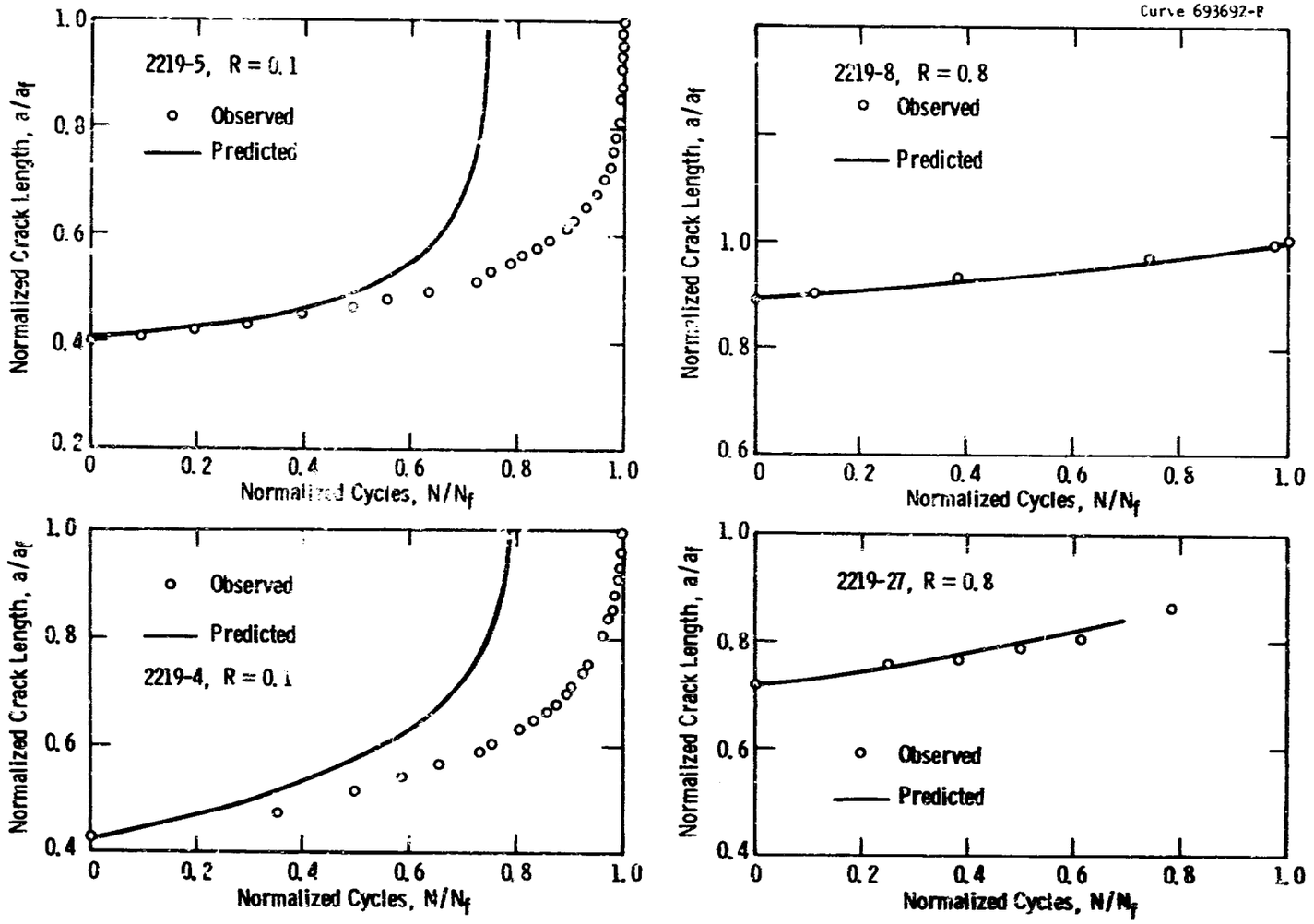

Fig. 7-5— Comparison of the observed " a vs N" behavior with that predicted by the integration of the growth rates as represented by the three component model for 2219-T851 aluminum

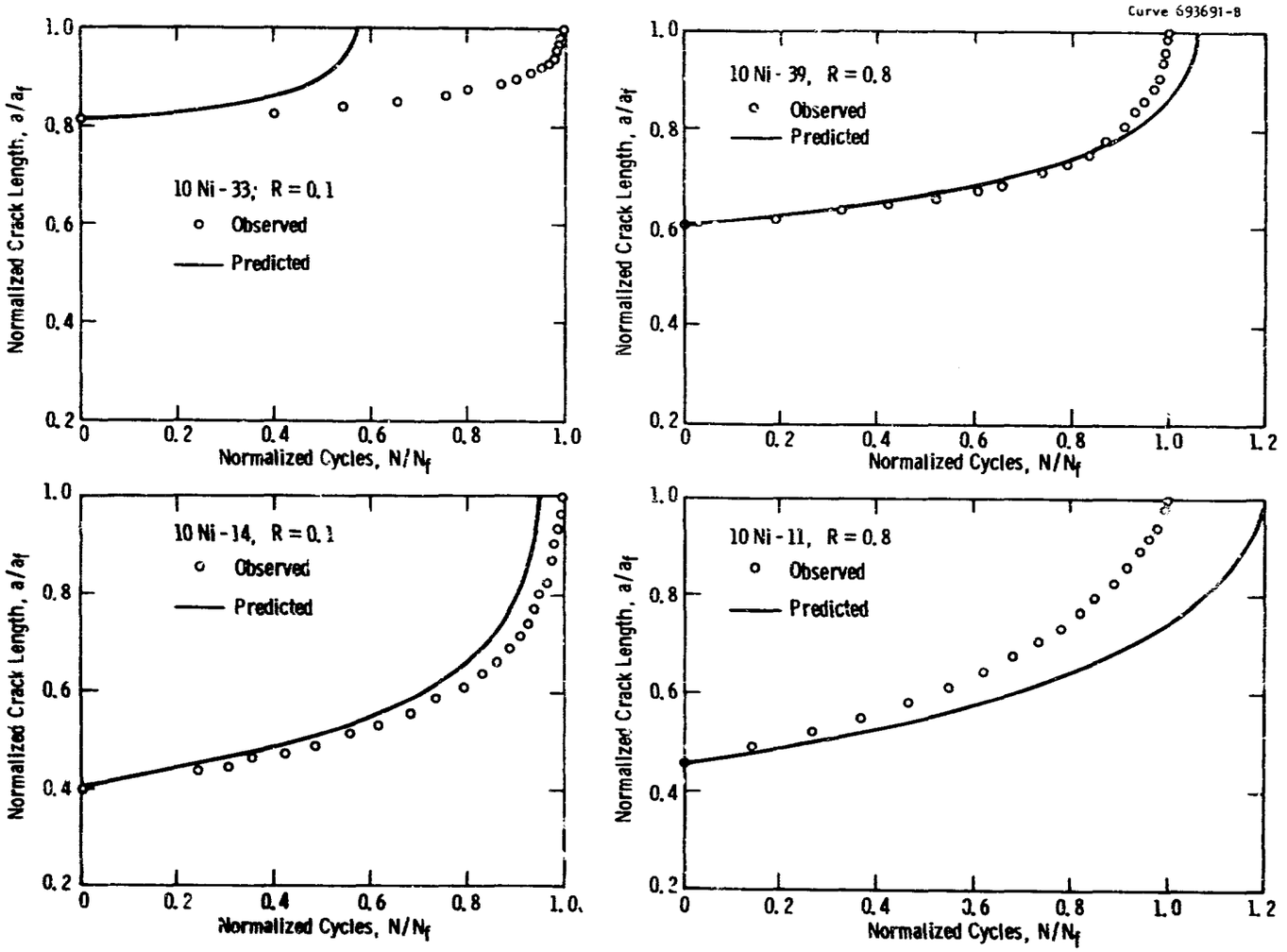

Fig. 7-6—Comparison of the observed "a vs. N" behavior with that predicted by the integration of the growth rates as represented by the three-component model for 10 Ni-steel

Figure 7-4 shows the predicted and observed cyclic lives obtained from integrating the regression equation developed using the nonlinear analysis and the inverse-hyperbolic-tangent-model (Table 7-1, data set 2). The observed "a" versus N results correspond to data from specimens 2219-4 and -5 which were tested at a load ratio of 0.1. The differences between observed and predicted cyclic lives are 10 to 20 percent. Comparison results obtained for these same cases by integrating the three component model are given in Figs. 7-5a and 7-5b — here differences between observed and predicted lives of 20 to 25 percent were obtained. In all cases the differences between observed and predicted lives are consistent with the inherent scatter in the (da/dN, ΔK) data. For example, these deviations are equivalent to a da/dN variability factor of 1.5, or $\pm$ 25%, which as illustrated in Fig. 7-1 is typical of the da/dN variability in data set 2. The above results indicate that both wide-range models provide comparable predictions for cases corresponding to (da/dN, ΔK) values which lie within the data set used to establish the regression equations.*

No particular significance is ascribed to the fact that these predictions from both models underestimated the observed cyclic lives. Since predictions are being made using regression equations which represent the average da/dN response at a given ΔK, both overestimates and underestimates of the observed lives will occur if enough cases are analyzed. Furthermore, if predictions are made for all specimens contained within a data set, one would expect the deviations between predicted and observed results to approach the typical scatter in da/dN.

To illustrate the above point, additional cases were analyzed using the three-component model and are summarized in Figs. 7-5 and 7-6. These analyses show that deviations between observed and predicted results range from essentially zero (Fig. 7-5c) to about

---

*Additional comparisons of the predictive capability of the two model are provided in Section 7.5.2 for cases correspond to (da/dN, ΔK) values near the ends of, and just beyond, the data set used to establish the regression equations.

45 percent (Fig. 7-6a). The 45 percent deviation is understandable since this particular case corresponds to Region I growth where the scatter in da/dN is a large as a factor of five.

7.5.2 Extrapolation Errors in Life Predictions

An important criterion for evaluating the utility of any mathematical representation of fatigue crack growth rate data is the ease with which these models can be misused and more importantly the consequences of any such misuse. Perhaps the most common misuse of models involves employing them beyond the (da/dN, ΔK) range for which their specific regression parameters were developed. Although the dangers of extraplation are generally recognized, it is inevitable that some extrapolation will occur when using models in design, particularly when Region I growth rates are involved. Thus, it is valuable to examine the errors that are incurred when extrapolating with each model.

Extrapolations in terms of ΔK are limited when employing the inverse-hyperbolic-tangent model since ΔK asymptotes are required. However, some extrapolation in terms of ΔK is a built-in feature of this model, since in order to establish a good fit, the ΔK asymptotes (C_3 and C_4) are typically 5 to 10 percent beyond the range of the data set (Section 7.4.1). This small extrapolation of ΔK corresponds to an extremely large extrapolation of da/dN since C_3 and C_4 force da/dN to zero and infinity, respectively. These built in extrapolations, combined with the dependence of C_3 and C_4 on the extent of available data are sources of significant errors in predicting cyclic lives. These errors are examined in the following analysis.

In a hypothetical example, the regression equations for both the inverse-hyperbolic-tangent model and the three-component model were extrapolated 10 percent beyond the lowest ΔK value in data set 2 (2.72 ksi$\sqrt{\text{in.}}$) and "a" versus N corresponding to this extrapolated growth rate regime was predicted. These predictions were subsequently compared with similar predictions from the three component model

Curve 693693-A

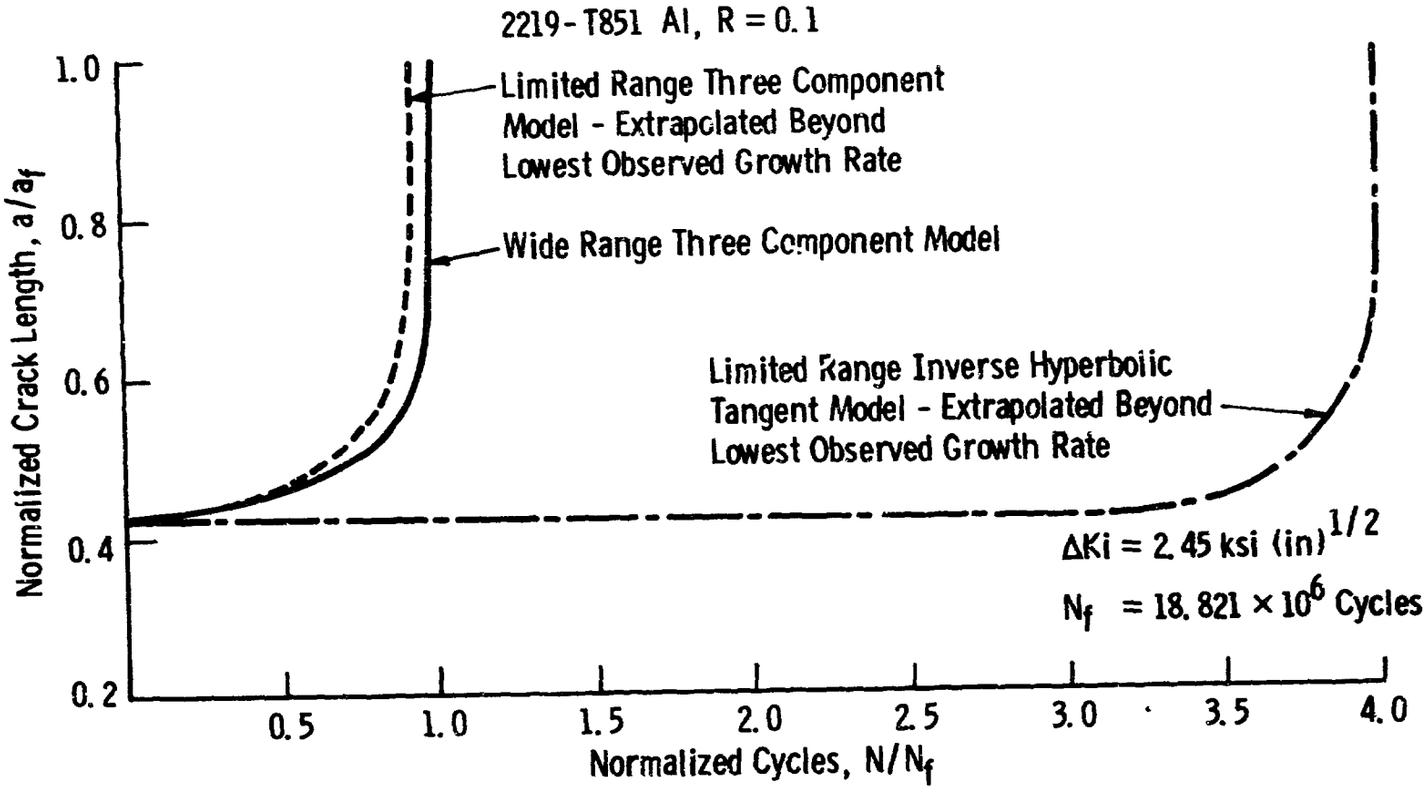

158

Fig. 7-7 — Comparison of predicted cyclic life behavior from extrapolating (≃ 10 % on ΔK) the fits obtained by the three component model and the inverse hyperbolic tangent model. The solid curve represents the predicted crack growth behavior obtained from a fit over a wider range of data using the three component model. 1 ksi $(in)^{1/2} = 1.1$ MPa $(m)^{1/2}$

which was fit to data set 4 and thereby included a wider range of growth rates than are included in data set 2 (see Table 7-1). As shown in Fig. 7-7 the predictions from extrapolating the narrower ranged three-component-model compare very well with those obtained from the wider-ranged three-component model. However, the predictions from the narrower ranged inverse-hyperbolic-tangent model are in error by a factor of four. When errors from the above source occur while using the inverse-hyperbolic-tangent model they will always overpredict the life. The three-component model by its nature is much less sensitive to this type of error; furthermore, the small errors that do occur will always underpredict the life.

As is clearly demonstrated by the above analysis, the asymptotic nature of the inverse-hyperbolic-tangent model can in some cases significantly overestimate cyclic life. In addition, the strong dependence of the lower ΔK asymptote on the range of available data can lead to the selection of a false threshold for fatigue crack growth, ΔK_{th}. Both of these factors can contribute to a nonconservative design.

7.6 Modeling Load Ratio Effects

The effect of load ratio (R) on fatigue crack growth rates were investigated in the present work and is discussed in Section 4.3.4. The intent of this section is to further examine these results and formulate a mathematical description of the influence of this loading variable on da/dN.

From a visual inspection of wide-range log (ΔK) versus log (da/dN) data for several R values, Figs. 4-16 and 4-17, the following observations are significant when attempting to formulate mathematical models: (1) the dependence of da/dN on R differs for each of the three growth rate regimes — thus, the effect of this variable is more complex than can be described by a parallel translation along either coordinate axis and (2) Region III growth rates, when observed, can in some cases be characterized by a single paramter, K_c, (for example, K_c remained

invariant between 33 and 35 ksi$\sqrt{in}$. for the 2219-T851 aluminum alloy at R-values between 0.1 and 0.8).

The various constants in the inverse-hyperbolic-tangent model (see Section 7.3.2) can conceivably be modified to incorporate the influence of R on da/dN as follows:

$$\log da/dN = C_5(R) \left[\frac{\log \frac{\Delta K}{C_3(R)}}{\log \frac{C_4(R)}{\Delta K}} \right]^{C_6(R)} \qquad (7\text{-}10)$$

where terms $C_3(R)$, $C_4(R)$, $C_5(R)$ and $C_6(R)$ are all functions of R. The functions $C_3(R)$ and $C_4(R)$ describe the load ratio dependencies in Region I and III, respectively. The function $C_4(R)$ for some alloys such as 2219-T851 is simply $K_c(1-R)$, where K_c is a constant as described previously. The functions $C_5(R)$ and $C_6(R)$ control the load ratio dependence in Regions II and in transition regions. In fact it may be possible to determine a common value of C_6 for data over a range of R-values.

The primary difficulty in attempting to utilize the above approach involves several practical problems in determining $C_3(R)$. As discussed previously the value of C_3, at any given value of R, is closely linked to the lowest value of ΔK in the particular data set one is attempting to model. Thus, for $C_3(R)$ to be exclusively a function of R, the lowest growth rate in the data set for each R value must be identical. Since this condition is rarely met in currently available data, some form of data extrapolation is necessary to define $C_3(R)$ at a constant da/dN. The asymptotic nature of the inverse-hyperbolic-tangent model inherently limits such extrapolations and furthermore, as discussed in Section 7.5.2, it can result in significant errors in both da/dN and C_3. These factors make the definition of $C_3(R)$ both complex and ambigious, thus limiting the usefulness of the inverse-hyperbolic tangent model to represent wide-range da/dN-ΔK data.

A mathematical representation of the R-dependence of da/dN using the three-component model is simplified — relative to the inverse-hyperbolic-tangent model — for several reasons. First, since each crack growth rate region is represented by a separate component, modeling the R-dependence, which is specific to growth rate regime, is more efficient and straightforward. Secondly, the procedure for defining the R-dependence in Region I is relatively insensitive to the range of available data at each R value and thus is unambigious.

Incorporating the influence of load ratio (R) into the three-component model takes the following form:

$$\frac{1}{(da/dN)} = \frac{A_1(R)}{(\Delta K)^{n1}} + \frac{A_2(R)}{(\Delta K)^{n2}} - \frac{A_2(R)}{(K_c(1-R))^{n2}} \qquad (7\text{-}11)$$

As indicated by Eq. 7-11 it is possible to identify common values of n_1, n_2 and K_c which are applicable to a range of R values. The functions $A_1(R)$ and $A_2(R)$ directly control the load ratio dependencies in Regions I and II, respectively. The onset of instability in Region III is again described by the term $K_c(1-R)$.

Since $A_1(R)$ values are inversely related to the intercepts on the da/dN axis, rather than ΔK asymptotes as in the inverse-hyperbolic-tangent model, the problem of the Region I R-dependence being sensitive to the range of available data is averted. The relative insensitivity of the A_1 values to the lowest da/dN value in a data set can be illustrated using data sets 2 and 4 for which the lowest da/dN values are 4×10^{-9} and 1×10^{-9} in./cycle, respectively. The corresponding regression values of A_1 for these data sets are 1.66×10^{13} and 1.84×10^{13} for equivalent values of n_1, n_2, and K_c. Since these values represent the inverses of the predicted growth rates of $\Delta K = 1$ ksi$\sqrt{\text{in.}}$, they therefore correspond to a 10% variation in predicted growth rates — an insignificant difference.

The functional form of $A_1(R)$ which describes the Region 1 R-dependence for the 2219-T851 alloy of this study is shown in Fig. 7-8a.

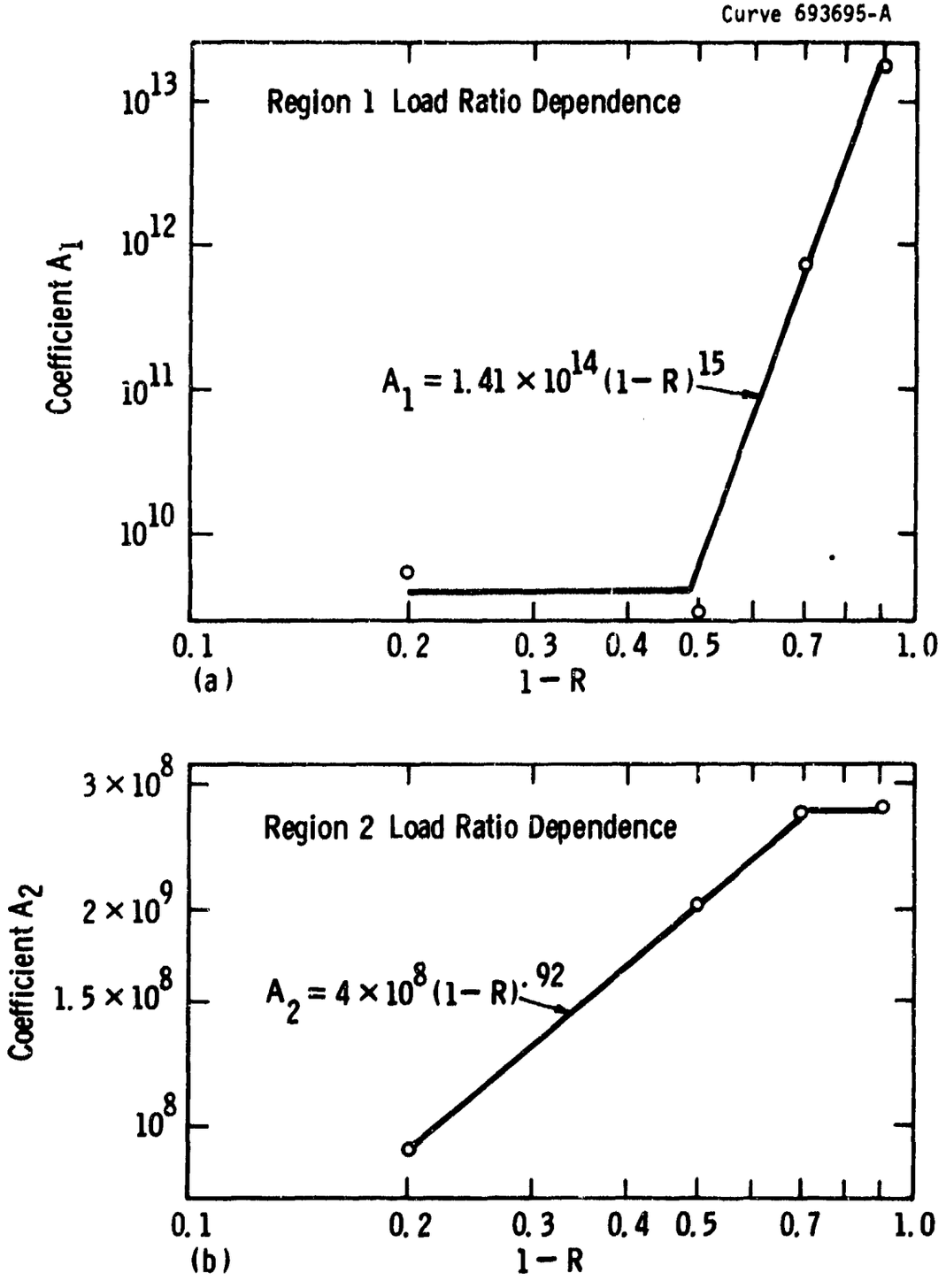

Fig. 7-8 – Coefficients A_1 and A_2 in the three-component model as a function of load ratio, R for 2219-T851 Al

The coefficient A_1 is very sensitive to load ratio for R values between 0.1 and 0.5 and can be described by the following equation:

$$A_1(R) = 1.41 \times 10^{14} \ (1-R)^{15} \qquad (7\text{-}12)$$

For R values between 0.5 and 0.8, A_1 remains constant within the limits of data scatter. For this same material in Region II, the R-dependence, as described by $A_2(R)$, is shown in Fig. 7-8b. Here A_2 varies by only a factor of three between R = 0.1 and 0.3. For values of R between 0.3 and 0.8, the variation in A_2 is described by

$$A_2(R) = 4 \times 10^{8} \ (1-R)^{0.92} \qquad (7.13)$$

The exponents in Eqs. 7-12 and 7-13 provide a direct measure of the strength of the R-dependence in Regions I and II, respectively. Higher exponents correspond to stronger R-dependencies.

It is appropriate to point out that, even for a single da/dN region, no simple, single function can adequately describe the R-dependence of crack growth rate. As indicated in Fig. 7-8, as well as in Section 4.3.4, R-effects appear to saturate at high R values in Region I and at low R values in Region II. This complexity, which is inherent in the data, makes a mathematical description of R-effects difficult, regardless of the specific model employed. Furthermore, it should be noted that data for $R < 0$ has not been considered in the above analysis. Based on the behavior observed at R = -1 for the materials examined in this work (Section 4.3.4), such a consideration would further complicate the mathematical modeling of R-effects. For the purposes of interpolating between R-values, the simple graphical representation using the piecewise-linear functions of Fig. 7-8 appears adequate. More complex functions, involving higher order terms in R, do not appear worthwhile.

A comparison of observed and predicted growth rates using the $A_1(R)$ and $A_2(R)$ values of Fig. 7-8 is provided in Fig. 7-9 for data on

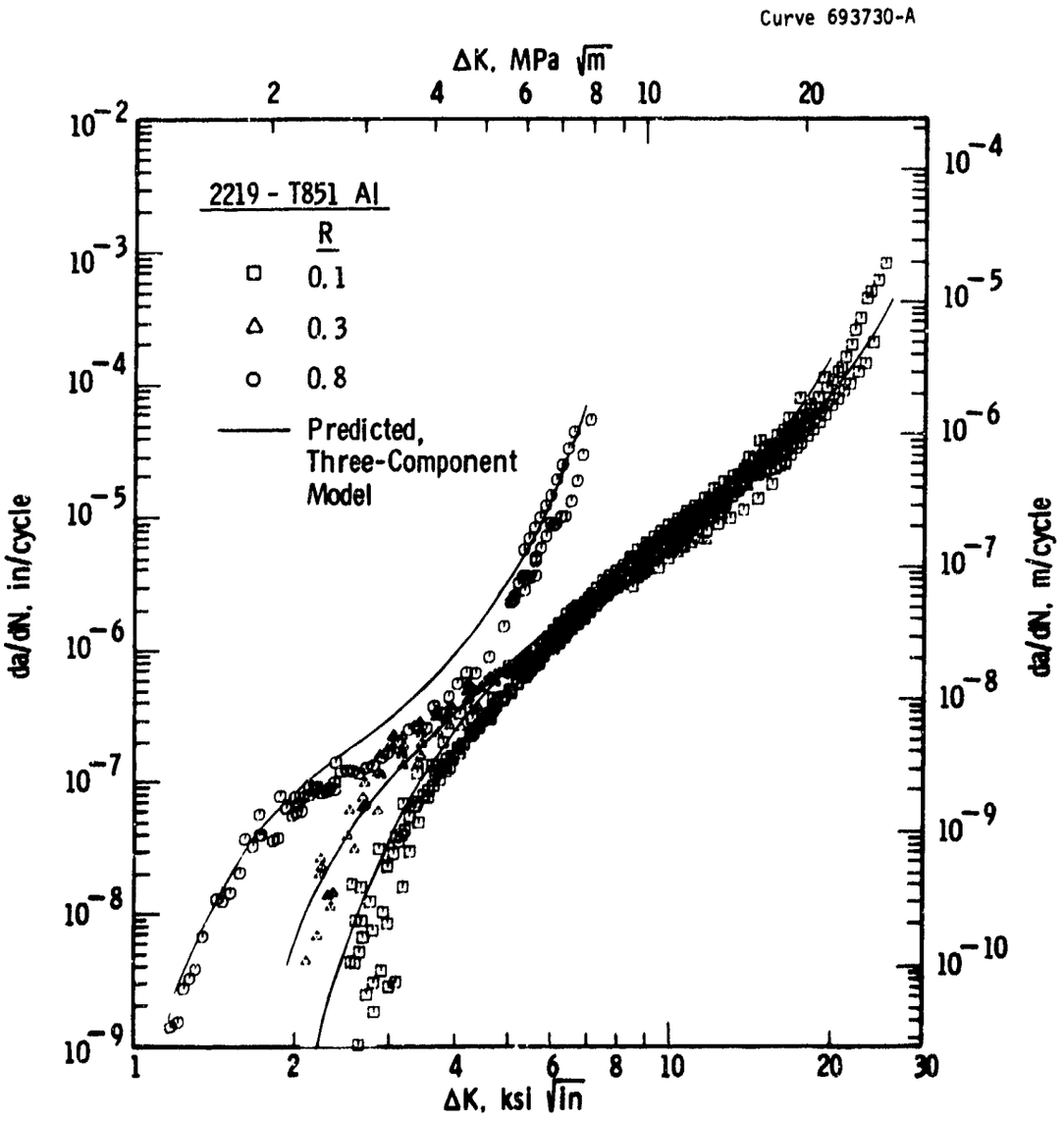

Fig. 7-9—Comparison of the fitted curves obtained from the three-component model with experimental crack growth rate data for 2219-T851 aluminum alloy at various load ratios

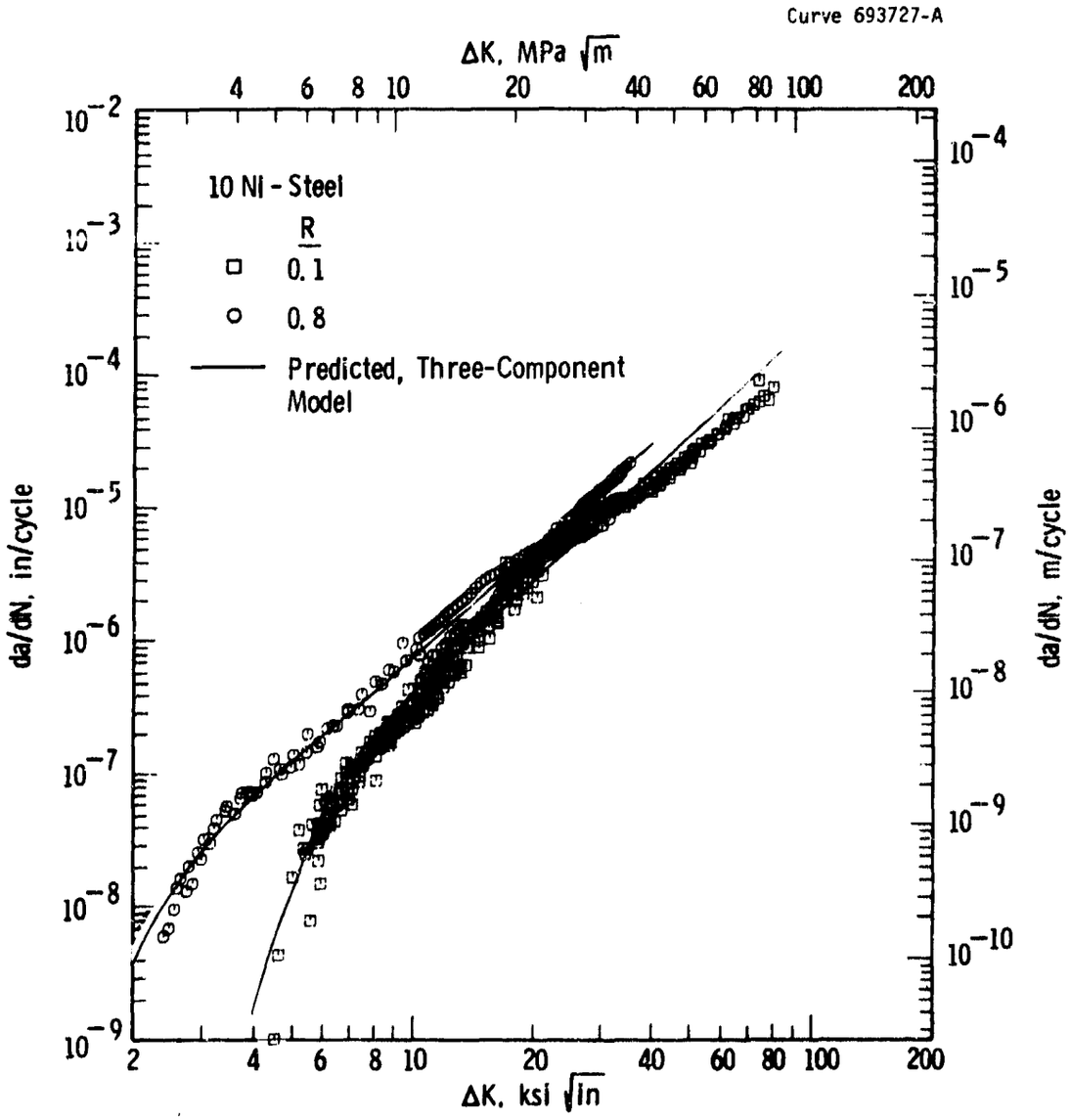

Fig. 7-10— Comparison of the fitted curves obtained from the three-component model with experimental data for a 10 Ni steel at load ratios of 0.1 and 0.8

2219-T851 at several R values. Due to the availability of less extensive data on the 10Ni steel, a precise definition of $A_1(R)$ and $A_2(R)$ is not possible for this material. However, predicted curves — using regression values of A_1 and A_2 from data at R values of 0.1 and 0.8 — are given in Fig. 7-10 along with the measured growth rates. Figures 7-9 and 7-10 indicate that the three-component model has the flexibility required to describe complex load ratio dependencies which vary with growth rate regime. In obtaining the fitted curves illustrated in Fig. 7-9 and 7-10, a linear regression analysis was employed and common values of n_1, n_2 and K_c were estimated using data at R = 0.1. It is felt that the fit to data over the entire R range would improve if a nonlinear regression analysis were used to optimize n_1, n_2 and K_c by considering the combined data from all R-values.

7.7 Mathematical Modeling — Summary and Recommendations

The work on wide-range fatigue crack growth rate modeling which is presented in the previous sections requires additional development in certain areas that were beyond the scope of the present program. Thus, recommendations for future efforts are provided in this summary.

The proposed three-component model has several attractive features, however further development and evaluation are advisable. This model has been demonstrated to have certain advantages over other wide-range models; namely, (1) its separate components provide for a straightforward description of varaibles, such as load ratio, which are specific to growth rate regime and (2) it does not lead to the selection of a false threshold for fatigue crack growth (ΔK_{th}) and concomitant overestimates of cyclic lives at low crack growth rates.

When employing the three-component model on data at a single load ratio, a graphical estimate of several imput parameters, followed by a simple multiple-linear-regression, appears adequate. However, when dealing with data at several load ratios, for which common values of fitting parameters n_1, n_2 and K_c are to be selected, a more

systematic procedure which considers data at all R values is desirable. However, an optimum procedure for carrying out such an evaluation needs to be defined and would be the next logical step to further extend this model. Work in this area should also contribute to improved methods for characterizing the variability in da/dN-ΔK data and thereby aid in the development of improved probabilistic methods for utilizing da/dN-ΔK information.

9. REFERENCES

1. W. G. Clark, Jr. and S. J. Hudak, Jr., "Variability in Fatigue Crack Growth Rate Testing," J. Testing and Evaluation, Vol. 3, No. 6, 1975, pp. 454-476.

2. S. J. Hudak, Jr. and R. J. Bucci, "Development of Standard Methods of Testing and Analyzing Fatigue Crack Growth Rate Data -— First Semi-Annual Report," Research Report 75-9D7-AFCGR-R1, AFML Contract F33615-75-C-5064, Westinghouse R&D Center, December 1975.

3. S. J. Hudak, Jr., R. J. Bucci, A. Saxena and R. C. Malcolm, "Development of Standard Methods of Testing and Analyzing Fatigue Crack Growth Rate Data -— Third Semi-Annual Report," Research Report 77-9E7-AFCGR-R1, AFML Contract F33615-75-C-5064, Westinghouse R&D Center, March 1977.

4. C. A. Miller, S. J. Hudak, Jr. and R. P. Wei, "The Influence of Loading Variables on Environment-Enhanced Fatigue Crack Growth in High Strength Steels," J. Testing and Evaluation, Vol. 1, No. 6, 1973, pp. 524-530.

5. P. S. Pao, W. Wei and R. P. Wei, "Effect of Frequency on Fatigue Crack Growth Response of AISI 4340 Steel in Water Vapor," Lehigh University Report IFSM-77-85, October 1977.

6. P. M. Scott and D. R. V. Silvester, "The Influence of Mean Tensile Stress on Corrosion Fatigue Crack Growth in Structural Steel Immersed in Seawater," Report UKOSRP 3/02, United Kingdom Atomic Energy Authority.

6a. P. C. Paris, "Testing for Very Slow Growth of Fatigue Cracks," MTS Closed Loop Magazine, Vol. 2, No. 5, 1970.

7. C. Y. Li and R. P. Wei, Material Research and Standards, Vol. 6, 1966, p. 392.

8. K. D. Unangst, T. T. Shih and R. P. Wei, "Crack Closure and Fatigue Crack Growth in 2219-T851 Aluminum Alloy," Report IFSM-76-77, Lehigh University, August 1976.

9. L. A. James, "Fatigue Crack Propagation in Austenitic Stainless Steels," Atomic Energy Review, Vol. 14, No. 1, 1976, pp. 37-86.

10. D. R. Donaldson and W. E. Anderson, "Crack Propagation Behavior of Some Air Frame Materials," Symp. Proc. on Crack Propagation, Cranfield, England, 1961, p. 375.

11. A. M. Sullivan and T. W. Crooker, "Analysis of Fatigue-Crack Growth in a High Strength Steel — Part I: Stress Level and Stress Ratio Effects at Constant Amplitude," J. Pressure Vessel Technology, Vol. 98, May 1976, pp. 179-184.

12. D. Brook and J. Schijve, "The Effect of Sheet Thickness on the Propagation of Fatigue-Cracks in 2024-T3 Alclad Sheet Material," Report MF 230, National Aerospace Laboratory NLR, Netherlands, 1964.

13. R. P. Wei, "Some Aspects of Environment-Enhanced Fatigue-Crack Growth," Engr. Fracture Mechanics, Vol. 1, 1970, pp. 633-651.

14. J. M. Barsom, E. J. Imhof and S. T. Rolfe, "Fatigue-Crack Propagation in High-Yield Strength Steels," Engr. Fracture Mechanics, Vol. 2, 1971, pp. 301-317.

15. W. G. Clark, Jr. and H. E. Trout, Jr., "Influence of Temperature and Section Size on Fatigue Crack Growth Behavior in Ni-Mo-V Alloy Steel," Engr. Fracture Mechanics, Vol. 2, 1970, pp. 107-123.

16. A. R. Jack and A. T. Price, "Effects of Thickness on Fatigue Crack Initiation and Growth in Notched Mild Steel Specimens," Acta. Met., Vol. 20, July 1972, pp. 857-866.

17. A. J. Brothers and S. Yukawa, "Fatigue Crack Propagation in Low-Alloy Heat-Treated Steels," Trans. ASME, Ser. D: J. Basic Engrg., March 1967, pp. 19-27.

18. J. R. Griffiths and C. E. Richards, "The Influence of Thickness on Fatigue Crack Propagation in a Low Alloy Steel Weld Metal Above and Below General Yield," Met. Sci. and Engr., Vol. 11, 1973, pp. 305-310.

19. A. M. Sullivan and T. W. Crooker, "Effect of Specimen Thickness on Fatigue Crack Growth Rate in 5Ni-Cr-Mo-V Steel:Comparison of Heat-Treated and Stress Relieved Specimens," NRL Report 7936, Naval Research Laboratory, Washington, D.C., December 1975.

20. C. M. Carman and J. M. Katlin, "Low Cycle Fatigue Crack Propagation Characteristics of High Strength Steels," Trans. ASME, Series D: J. Basic Engrg., December 1966, pp. 792-800.

21. J. Eftis and H. Liebowitz, "On the Modified Westergaard Equations for Certain Plane Crack Problems," Int. J. Fracture Mechanics, Vol. 8, No. 4, December 1972, pp. 383-391.

22. M. Isida, "Effect of Width and Length on Stress Intensity Factors of Internally Cracked Plates Under Various Boundary Conditions," Inter. Journal of Fracture Mechanics, Vol. 7, No. 3, September 1971, pp. 301-316.

23. L. Albertin and S. J. Hudak, Jr., "The Effect of Compressive Loading on Fatigue Crack Growth Rate and Striation Spacing in 2219-T851 Aluminum," Scientific Paper 77-1D9-FRTOG-P3, Westinghouse R&D Center, December 1977.

24. W. G. Clark, Jr., "Subcritical Crack Growth and its Effect upon the Fatigue Characteristics of Structural Alloys," Eng. Fracture Mechanics, Vol. 1, 1968, pp. 385-397.

25. T. W. Crooker, L. A. Cooley, E. A. Lange and C. N. Freed, Trans. Am. Soc. Metals, Vol. 61, 1968, p. 568.

26. C. E. Richards and T. C. Lindley, "The Influence of Stress Intensity and Microstructure on Fatigue Crack Propagation in Ferritic Materials," Eng. Fracture Mechanics, Vol. 4, 1972, pp. 951-978.

27. J. G. Kaufman, K. O. Bogardus, D. A. Mauney and R. C. Malcolm, "Creep Cracking of 2219-T851 Plate at Elevated Temperature", ASTM STP 590, 1976, pp. 149-168.

28. Private communication with S. R. Novak, U.S. Steel Corp. Research Laboratory, March 1977.

29. N. E. Dowling, "Fatigue-Crack Growth Rate Testing at High Stress Intensities," ASTM STP 631, 1977, pp. 139-158.

30. C. M. Hudson and J. T. Scardina, "Effect on Stress Ratio on Fatigue Crack Growth in 7075-T6 Aluminum Alloy Sheet," Engrg. Fracture Mechanics, Vol. 1, 1969, pp. 429-446.

31. R. O. Ritchie, "Influence of Microstructure on Near-Threshold Fatigue Crack Propagation in Ultra-High Strength Steel," Metal Science, Vol. 11, No. 8/9, August/September 1977.

32. L. P. Pook and N. E. Frost, Int. J. Fract., Vol. 9, 1973, p. 53.

33. R. J. Cooke, Ph.D. Thesis, Birmingham University, 1973.

34. W. Elber, "The Significance of Crack Closure," ASTM STP 486, 1971, p. 230.

35. R. A. Schmidt and P. C. Paris, "Threshold for Fatigue Crack Propagation and Effects of Load Ratio and Frequency," ASTM STP 536, 1973, p. 79.

36. T. C. Lindley and C. E. Richards, "The Relevance of Crack Closure to Fatigue," Proc. of Conf. on Mechanics and Mechanisms of Crack Growth, Cambridge, 1973.

37. M. Kikukawa, M. Jono and K. Tanaka, "Fatigue Crack Closure Behavior of Low Stress Intensity Level," Proc. of 2nd Int. Conf. on Mechanical Behavior of Materials, Boston, August 1976.

38. T. W. Crooker, Trans. ASME, Vol. 93, 1971, p. 893.

39. E. Sasaki, A. Ohta and M. Kosuge, "Fatigue Crack Propagation Rate and Stress Intensity Threshold Level of Several Structural Materials of Varying Stress Ratios," National Research Institute for Metals, Tokyo, Japan, 1977.

40. R. I. Stephens, "Fatigue Crack Growth Specimen Configuration with Compressive Loads Present," Int. J. Fracture, Vol. 12, 1976, p. 323.

41. N. E. Frost, L. P. Pook, and K. Denton, "A Fracture Mechanics Analysis of Fatigue Crack Growth Data for Various Materials," Eng. Fracture Mechanics, Vol. 3, 1971, pp. 109-126.

42. J. M. Barsom, Corrosion Fatigue, ed. O. Devereux, A. J. McEvily and R. W. Staehle, NACE, Houston, Texas, 1971, p. 424.

43. J. P. Gallagher and R. P. Wei, Corrosion Fatigue, ed. O. Devereux, A. J. McEvily, and R. W. Staehle, NACE, Houston, Texas, 1971, p. 409.

44. R. P. Wei, "Some Aspects of Environment-Enhanced Fatigue-Crack Growth," Eng. Fracture Mechanics, Vol. 1, 1970, pp. 633-651.

45. R. P. Wei and J. D. Landes, Int. J. Fracture Mechanics, Vol. 5, 1969, p. 69.

46. A. Hartman, Int. J. Fract. Mechanics, Vol. 1, 1965, p. 167.

47. F. J. Bradshaw and C. Wheeler, "The Effect of Environment on Fatigue Crack Growth in Aluminum and Some Aluminum Alloys," Applied Mat. Res., Vol. 5, 1966, pp. 112-120.

48. R. P. Wei, "Fatigue Crack Propagation in a High-Strength Aluminum Alloy," Int. J. Fracture Mechanics, Vol. 4, 1968, pp. 159-167.

49. T. Yokobori and T. Aizawa, "The Influence of Temperature and Stress Intensity Factor Upon the Striation Spacing and Fatigue Crack Propagation Rate of Aluminum Alloy," Int. J. Fracture Vol. 9, 1973, pp. 489-491.

50. L. A. James, "The Effect of Frequency Upon the Fatigue-Crack Growth of Type 304 Stainless Steel at 1000°F," ASTM STP 513, 1972, pp. 218-229.

51. L. A. James and E. B. Schenk, Jr., "Fatigue-Crack Propagation Behavior of Type 304 Stainless Steel at Elevated Temperature," Met. Trans., Vol. 2, February 1971, pp. 491-496.

52. P. C. Paris, R. J. Bucci, E. T. Wessel, W. G. Clark, Jr., and T. R. Mager, "Extensive Study of Low Fatigue Crack Growth Rates in A533 and A508 Steels," ASTM STP 513, 1972, pp. 141-176.

53. W. G. Clark, Jr., Unpublished fatigue crack growth rate data, Westinghouse R&D Center, Pittsburgh, PA, 1969.

54. L. A. James, Technical presentation and Task Group discussion, Meeting of ASTM Task Group E24.04.01, Philadelphia, PA, October 1976.

55. G. R. Irwin, "Plastic Zone Near a Crack Tip and Fracture Toughness," Mechanical and Metallurgical Behavior of Sheet Metals, Proceedings of 7th Sagamore Ordnance Material Research Conference, Part 4, 1960, pp. 63-71.

56. P. C. Paris, "The Fracture Mechanics Approach to Fatigue," Fatigue - An Interdisciplinary Approach, Syracuse University Press, 1964, pp. 107-127.

57. J. R. Rice, "Mechanics of Crack Tip Deformation and Extension by Fatigue," Fatigue Crack Propagation, ASTM STP 415, American Society for Testing and Materials, 1967, pp. 247-311.

58. I. E. Figge and J. C. Newman, "Fatigue Crack Propagation in Structures with Simulated Rivert Forces," ASTM STP 415, 1967, pp. 71-93.

59. A. Saxena, S. J. Hudak, Jr., J. K. Donald, D. W. Schmidt, "Computer Controlled K-Decreasing Test Technique for Low Rate Fatigue Crack Growth Testing," J. Testing and Evaluation, JTEVA, Vol. 6, May 1978.

60. A. M. Sullivan and T. W. Crooker, "Evaluation of Fatigue Crack-Growth-Rate Determination Using a Crack Opening Displacement Technique for Crack Length Measurement," NRL Report 7912, September 1975.

61. Fatigue Crack Growth Under Spectrum Loads, ASTM STP 595, American Society of Testing and Materials, 1976.

62. W. J. Mills, "Load Interaction Effects on Fatigue Crack Growth in 2024-T3 Aluminum and A514F Steel Alloys," Ph.D. Dissertation, Lehigh University, 1975.

63. S. W. Hopkins, C. A. Rau, G. R. Leverant, A. Yeun, "Effect of Various Programmed Overloads on the Threshold for High Frequency Fatigue Crack Growth," ASTM STP 595, 1976, pp. 125-141.

64. O. E. Wheeler, "Crack Growth Under Spectrum Loading," Journal of Basic Engineering Transactions, ASME, March 1972, pp. 181-186.

65. H. A. Wood in Fatigue Life Prediction for Aircraft Structures and Materials, AGARD Lecture Series No. 62, May 1973.

66. V. W. Trebules, R. Roberts, R. W. Hertzberg, "Effect of Multiple Overloads on Fatigue Crack Propagation in 2024-T3 Aluminum Alloy," ASTM STP 536, 1973, pp. 115-146.

67. R. W. Hertzberg and W. J. Mills, "Character of Fatigue Fracture Surface Micromorphology in the Ultra-Low Crack Growth Rate Regime," ASTM STP 600, 1976, pp. 220-234.

68. G. E. Nordmark and W. G. Fricke, "Fatigue Crack Arrest at Low ΔK in Corrosive Environment," Report No. 57-78-02, Alcoa Laboratories, February 1978.

69. J. C. Newman, Jr., "Stress Analysis of Compact Specimen Including the Effects of Pin Loading," Fracture Analysis, ASTM STP 560, 1974, pp. 105-121.

70. J. E. Srawley, "Wide Range Stress Intensity Factor Expressions for ASTM 399 Standard Fracture Toughness Specimens," NASA TMX-71881, NASA-Lewis Research Center, 1976.

71. C. E. Feddersen, ASTM STP 410, 1966, pp. 77-79.

72. B. Mukherjee, "A Note on the Analysis of Fatigue Crack Growth Data," Int. J. Fracture Mechanics, Vol. 8, 1972, pp. 449-452.

73. H. G. Munro, "The Determination of Fatigue Crack Growth Rates by a Data Smoothing Technique," Int. J. Fracture, Vol. 9, 1973, pp. 366-368.

74. R. A. Smith, "The Determination of Fatigue Crack Growth Rate from Experimental Data," Int. J. Fracture, Vol. 9, 1973, pp. 352-355.

75. J. Polak and Z. Knesl, "On the Fatigue Crack Growth Rate Evaluation from Experimental Data," Int. J. Fracture, Vol. 11, 1975.

76. L. N. McCartney and P. M. Cooper, "Computerized Processing of Fatigue Crack Propagation Data," NPL Report Mat. App. 23, National Physical Laboratory, October 1972.

77. K. B. Davies and C. E. Fedderson, "Evaluation of Fatigue-Crack Growth Rates by Polynominal Curve Fitting," Int. J. Fracture, Vol. 9, 1973, pp. 116-118.

78. A. J. Federowicz and B. A. Powell, "A Computer Program to Obtain a Min-Max Regression Model by Linear Programming," Research Report 68-1C3-COMP-R2, Westinghouse R&D Center, July 1968.

79. R. P. Wei and W. Wei, unpublished results, Lehigh University, August 1976.

80. Annual Book of ASTM Standards, Part 10, American Society for Testing and Materials, Philadelphia, PA 1977.

81. R. G. Forman, V. E. Kearney and R. M. Engle, "Numerical Analysis of Crack Propagation in Cyclic Loaded Structures," J. Basic Eng., Series D, Vol. 89, September 1967.

82. K. Walker, "The Effect of Stress Ratio during Crack Propagation and Fatigue for 2024-T3 and 7075-T6 Aluminum," Effects of Environment and Complex Load History on Fatigue Life, ASTM STP 462, 1970.

83. C. G. Annis, Jr., R. M. Wallace and D. L. Suns, "A Interpolative Model for Elevated Temperature Fatigue Crack Propagation," AFML-TR-1976, Wright Patterson Air Force Base, November 1976.

84. J. E. Collipriest, "An Experimentalist's View of the Surface Flaw Problem. The Surface Crack: Physical Problems and Computational Solutions," ASME, 1972, pp. 43-62.

85. C. E. Jaske, C. E. Fedderson, K. B. Davies and R. C. Rice, "Analysis of Fatigue, Fatigue Crack Propagation and Fracture Data," Battelle Columbus Lab., NASA CR-132332, November 1973.

86. D. P. Williams, "A New Criterion for Failure of Materials by Environment-Induced Cracking," Int. J. Fracture, Vol. 9, 1973, pp. 63-74.

87. P. Paris and F. Erdogan, "A Critical Analysis of Crack Propagation Laws," Trans. ASME, Ser. D: J. Basic Engrg., December 1963, p. 528.

88. S. J. Hudak, Jr., A. Saxena, R. J. Bucci and R. C. Malcolm, "Development of Standard Methods of Testing and Analyzing Fatigue Crack Growth Data — Third Semi-Annual Report," Research Report 77-9E7-AFCGR-R1, Westinghouse R&D Center, March 1977.

89. R. W. Walpole and R. H. Myers, "Probability and Statistics for Engineers and Scientists," The Macmillan Co., New York, 1972.

90. E. Kreyszig, "Advanced Engineering Mathematics," John Wiley and Sons, New York, 1964.

APPENDIX 1

PROPOSED METHOD OF TEST FOR MEASUREMENT OF FATIGUE CRACK GROWTH RATES

ASTM E647-78T, "Tentative Test Method for Constant-Load-Amplitude Fatigue Crack Growth Rates Above 10^{-8} m/cycle" appears in the 1978 Annual Book of ASTM Standards, Vol. 10.

The following proposed method of test combines procedures for fatigue crack growth rate testing above and below 10^{-8} m/cycle into one document. This document is intended as a working document for ASTM E24.04 subcommittee use. Recommended procedures for establishment of fatigue crack growth rates above 10^{-8} m/cycle are identical to those of ASTM E647-78T. Paragraphs denoted with asterisk (*) contain modifications to ASTM E647-78T for the purpose of incorporating guidelines for establishment of fatigue crack growth rates below 10^{-8} m/cycle. The reader should consult ASTM E647-78T for specific changes made in noted paragraphs.

PROPOSED METHOD OF TEST FOR MEASUREMENT OF FATIGUE CRACK GROWTH RATES[1]

1. SCOPE

1.1* This method covers the determination of steady-state fatigue crack growth rates using either compact type (CT) or center-cracked-tension (CCT) specimens. Results are expressed in terms of the crack-tip stress intensity range, defined by the theory of linear elasticity.

1.2* Several different test procedures are provided, the optimum test procedure being primarily dependent on the magnitude of the fatigue crack growth rate to be measured.

1.3 Materials that can be tested by this method are not limited by thickness or by strength so long as specimens are of sufficient thickness to preclude buckling and of sufficient planar size to remain predominantly elastic during testing.

1.4 A range of specimen sizes with proportional planar dimensions is provided, but size is variable to be adjusted for yield strength and applied load. Specimen thickness may be varied independent of planar size.

1.5 Specimen configurations other than those contained in this method may be used provided that well established stress intensity calibrations are available and that specimens are of sufficient size to remain predominantly elastic during testing.

2. APPLICABLE DOCUMENTS

2.1 ASTM Standards

E4, Verification of Testing Machines[2]

E8, Tension Testing of Metallic Materials[2]

---

[1] This method is under the jurisdiction of ASTM E24 on Fracture Testing.

[2] Annual Book of ASTM Standards, Parts 6, 7, and 10.

E337, Determining Relative Humidity by Wet-and-Dry Bulb Psychrometer[2]

E338, Sharp-Notch Tension Testing of High-Strength Sheet Materials[1]

E399, Plane Strain Fracture Toughness of Metallic Materials[1]

E467, Recommended Practice for Verification of Constant Amplitude Dynamic Loads in an Axial Load Fatigue Testing Machine[1]

E561-75T, Recommended Practice for R-Curve Determination[1]

2.2 ASTM Data File

Research Report E24-1001

3.* SUMMARY OF METHOD

The method involves cyclic loading of notched specimens which have been acceptably precracked in fatigue. Crack length is measured, either visually or by an equivalent method, as a function of elapsed fatigue cycles and these data are subjected to numerical analysis to establish the rate of crack growth. Crack growth rates are expressed as a function of the stress intensity factor range, ΔK, which is calculated from expressions based on linear elastic stress analysis.

4. SIGNIFICANCE

4.1 Fatigue crack growth rate expressed as a function of crack-tip stress intensity factor range, da/dN vs. ΔK, characterizes a materials resistance to stable crack extension under cyclic loading. Background information on the rationale for employing linear elastic fracture mechanics to analyze fatigue crack growth rate data is given in Refs. (1) and (2).

4.1.1* In innocuous (inert) environments fatigue crack growth rates are primarily a function of ΔK and load ratio (R), or K_{max} and R.

Note 1: ΔK, K_{max}, and R are not independent of each other. Specification of any two or these variables is sufficient to define the loading condition. It is customary to specify one of the stress intensity parameters (ΔK or K_{max}) along with the load ratio (R).

[1]Annual Book of ASTM Standards, Parts 6, 7 and 10.

[2]Annual Book of ASTM Standards, Parts 5, 20, 32 and 41.

Temperature and aggressive environments can significantly affect da/dN vs. ΔK, and in many cases accentuate R-effects and also introduce effects of other loading variables such as cyclic frequency and waveform. Attention needs to be given to the proper selection and control of these variables in research studies and in generation of design data.

4.1.2 Expressing da/dN as a function of ΔK provides results which are independent of planar geometry, thus enabling exchange and comparison of data obtained from a variety of specimen configurations and loading conditions. Moreover, this feature enables da/dN vs. ΔK data to be utilized in the design and evaluation of engineering structures.

4.1.3 Fatigue crack growth rate data are not always geometry-independent in the strict sense since thickness effects sometimes occur. However, data on the influence of thickness on fatigue crack growth rate is mixed. Fatigue crack growth rates over a wide range of ΔK have been reported to either increase, decrease or remain unaffected as specimen thickness is increased. Thickness effects can also interact with other variables such as environment and heat treatment. In addition, materials may exhibit thickness effects only over the terminal range of da/dN vs. ΔK which are associated with either nominal yielding[1] or a K_{max} - controlled instability. The potential influence of specimen thickness should be considered when generating data for research or design.

4.2 This method can serve the following purposes:

4.2.1 To establish the influence of fatigue crack growth on the life of components subjected to cyclic loading, provided data are generated under representative

[1] This condition will be avoided in tests which conform to the specimen size requirements of this method.

conditions, and combined with appropriate fracture toughness data (e.g., see ASTM E399), defect characterization data, and stress analysis information (e.g., see Refs. 3 and 4).

Note 2: Fatigue crack growth can be significantly influenced by load-history. During variable amplitude loading, crack growth rates can be either enhanced or retarded (relative to steady-state, constant-amplitude growth rates at a given ΔK) depending on the specific loading sequence. This complicating factor needs to be considered in using constant amplitude growth rate data to analyze variable amplitude fatigue problems (for example, see Ref. 5).

4.2.2 To establish material selection criteria, design allowables, and non-destructive inspection requirements for quality assurance.

4.2.3 To analyze failures and formulate appropriate remedial measures.

4.2.4 To establish in quantitative terms, the individual and combined effects of metallurgical, fabrication, environmental and loading variables on fatigue crack growth.

5. DEFINITIONS

5.1 Cycle, one complete sequence of values of applied load that is repeated periodically in fatigue. The symbol N represents the number of cycles.

5.1.1 Maximum Load, P_{max} (F) - the greatest algebraic value of applied load in a fatigue cycle. Tensile loads are considered positive and compressive loads negative.

5.1.2 Minimum Load, P_{min} (F) - the least algebraic value of applied load in a fatigue cycle.

5.1.3 Load Range, ΔP (F) - the algebraic difference between the maximum and minimum loads in a fatigue cycle.

5.1.4 Load Ratio (also called "stress ratio"), R - the algebraic ratio of the minimum to maximum load in a fatigue cycle, i.e., $R = P_{min}/P_{max}$.

5.2 Stress Intensity Factor, K $(FL^{-3/2})$ - the magnitude of the ideal-crack-tip stress field in a linear-elastic body. In this method, mode 1 is assumed. Mode 1 corresponds to loading such that the crack surfaces are displaced apart, normal to the crack plane.

5.2.1 K_{max} $(FL^{-3/2})$ - the maximum value of stress-intensity factor in a fatigue cycle. This value corresponds to P_{max}.

5.2.2 K_{min} $(FL^{-3/2})$ - the minimum value of stress-intensity factor in a fatigue cycle. This value corresponds to P_{min} when $R > 0$ and is taken to be zero when $R \leq 0$.

5.2.3 ΔK $(FL^{-3/2})$ - the variation in stress-intensity factor in a fatigue cycle, that is, $K_{max} - K_{min}$.

Note 3: The loading variables R, ΔK, and K_{max} are related such that specifying any two uniquely defines the third according to the following relationship: $\Delta K = (1-R)K_{max}$ for $R \geq 0$ and $\Delta K = K_{max}$ for $R \leq 0$.

Note 4: These operational stress intensity factor definitions do not include local crack-tip effects; for example, crack closure, residual stress and blunting.

5.3* Normalized K-Gradient, $C = \frac{1}{K} \cdot \frac{dK}{da}$, (L^{-1}) - the fractional rate of change of K with increasing crack length.

Note 5: When C is held constant the percentage change in K is constant for equal increments of crack length. The following identity is true for the normalized K-gradient in a constant-load ratio test:

$$\frac{1}{K} \cdot \frac{dK}{da} \equiv \frac{1}{K_{max}} \cdot \frac{dK_{max}}{da} \equiv \frac{1}{K_{min}} \cdot \frac{dK_{min}}{da} \equiv \frac{1}{\Delta K} \cdot \frac{d\Delta K}{da}$$

5.3.1* K-Increasing Test - a test in which the value of C is nominally positive. For the standard specimens in this method the constant-load-amplitude test will result in a K-increasing test where the C value changes but is always positive.

5.3.2* K-Decreasing Test - a test in which the value of C is nominally negative. In this method K-decreasing tests are conducted by shedding load, either continuously or by a series of decremental steps, as the crack grows.

5.4 Stress Intensity Calibration, K-Calibration - a mathematical expression, based on empirical or analytical results, which relates stress intensity factor to load and crack length for a specific specimen planar geometry.

5.5 Crack Length, a (L) - the physical crack size used to determine crack growth rate and stress-intensity factor in fatigue. For the CT specimen, "a" is measured from the line connecting the bearing points of load application (Fig. 1); for the CCT specimen, "a" is measured from the perpendicular bisector of the central crack (Fig. 2).

5.6* Fatigue Crack Growth Rate, da/dN or $\Delta a/\Delta N$, (LT^{-1}) - crack extension caused by fatigue loading and expressed in terms of crack extension per cycle of fatigue.

5.7* Fatigue Crack Growth Threshold, ΔK_{th} $(FL^{-3/2})$ - that value of ΔK at which da/dN approaches zero. For most materials it is practical to define ΔK_{th} as ΔK which corresponds to a fatigue crack growth rate of 10^{-10} m/cycle. The procedure for determining this ΔK_{th} is given in Sec. 9.4.

6. APPARATUS

6.1 Grips and Fixtures for CT Specimen - a clevis and pin assembly (Fig. 3) is used at both the top and bottom of the specimen to allow in-plane rotation as the specimen is loaded. This specimen and loading arrangement is to be used for tension-tension loading only.

6.1.1 Suggested proportions and critical tolerances of the clevis and pin are given (Fig. 3) in terms of either the specimen width, W, or the specimen thickness, B, since these dimensions may be varied independently within certain limits.

6.1.2 The pin-to-hole clearances are designed to minimize friction, thereby eliminating unacceptable end-moments which would invalidate the specimen K-calibrations provided herein. The use of a lubricant (e.g., MoS_2) on the loading pins is also recommended to minimize friction.

6.1.3 Using a 1000 MN/m^2 (~ 150 ksi) yield strength alloy (e.g., AISI 4340 steel) for the clevis and pins provided adequate strength and resistance to galling and to fatigue.

6.2 Grips and Fixtures for CCT Specimens - the type of grips and fixtures to be used with the CCT specimens will depend on the specimen width, W (defined in Fig. 2), and the loading conditions (i.e., either tension-tension or tension–compression loading). The minimum required specimen gage length varies with the type of gripping, and is specified so that a uniform stress distribution is developed in the specimen gage length during testing. For testing of thin sheets, constraining plates may be necessary to minimize specimen buckling (see ASTM E561–75T for recommendations on buckling constraints).

6.2.1 For tension-tension loading of specimens with $W \leq 75$ mm (3 in.) a clevis and single pin arrangement is suitable for gripping provided that the specimen gage length (i.e., the distance between loading pins) is at least 2W, Fig. 2. For this arrangement it is also helpful to either use brass shims between the pin and specimen or to lubricate the pin to prevent fretting-fatigue cracks from initiating at the specimen loading hole. Additional measures which may be taken to prevent cracking at the pin-hole include

attaching reinforcement plates to the specimen (for example, see ASTM E338) or employing a "dog-bone" type specimen design. In either case, the gage length is defined as the uniform section and shall be at least 1.7W. This gage length requirement is for all dog-bone designs regardless of methods of gripping.

6.2.2 For tension-tension loading of specimens of uniform width and $W \geq$ 75 mm (3 in.) a clevis with miltiple bolts is recommended (for example, see ASTM E561-75T). In this arrangement the loads are applied more uniformly, thus, the minimum specimen gage length (that is the distance between the innermost rows of bolt holes) is relaxed to 1.5W.

6.2.3 The CCT specimen of uniform width may also be gripped using a clamping device instead of the above arrangements. This type of gripping is necessary for tension-compression loading. An example of a specific bolt and keyway design for clamping CCT specimens is given in Fig. 4. In addition, various hydraulic and mechanical-wedge systems which supply adequate clamping forces are commercially available and may be used. The minimum gage length requirement for clamped specimens is relaxed to 1.2W.

6.3 Alignment of Grips - it is important that attention be given to achieving good alignment in the load train through careful machining of all gripping fixtures. For tension-tension loading, pin or gimbal connections between the grips and load frame are recommended to achieve loading symmetry. For tension-compression loading the length of the load train (including the hydraulic actuator) should be minimized and rigid, non-rotating joints should be employed to reduce lateral motion in the load train.

7. SPECIMEN CONFIGURATION, SIZE AND PREPARATION

7.1 Standard Specimens - the geometry of standard compact type (CT) and center-cracked-tension (CCT) specimens are given in Figs. 1 and 2, respectively. The specific geometry of center-cracked-tension (CCT) specimens depends on the method of gripping as specified in section 6.2. Notch and precracking details for both specimens are given in Fig. 5. The CT specimen is not recommended for tension-compression testing, because of uncertainties introduced into the K-calibration.

7.1.1 It is required that the machined notch, a_n, in the CT specimen be at least 0.2W in length so that the K-calibration is not influenced by small variations in the location and dimensions of the loading-pin holes.

7.1.2 The machined notch, $2a_n$, in the CCT specimen shall be centered with respect to the specimen centerline to within $\pm$ 0.001W. The length of the machine notch in the CCT specimen will be determined by practical machining considerations and is not restricted by limitations in the K-calibration.

Note 6: It is recommended that $2a_n$ be at least 0.2W when using the compliance method to monitor crack extension in the CCT specimen so that accurate crack length determinations can be obtained.

7.1.3 For both specimens, the thickness (B) and width (W) may be varied independently within the following limits which are based on specimen buckling and crack-front-curvature considerations:

i) For CT specimens it is recommended that thickness be within the range: $W/20 \leq B \leq W/4$. Specimens having thicknesses up to and including W/2 may also be employed, however, data from these specimens will often require through-thickness crack curvature corrections (Sec. 9.1). In addition, difficulties may be encountered

in meeting the through-thickness crack straightness requirements of Sec. 8.3.3 and Sec. 8.7.4.

ii) Using the above rationale, the recommended upper limit on thickness in CCT specimens is W/8, although W/4 may also be employed. The minimum thickness necessary to avoid excessive lateral deflections or buckling in CCT specimens is sensitive to specimen gage length, grip alignment and load ratio (R). It is recommended that strain gage information be obtained for the particular specimen geometry and loading condition of interest and that bending strains not exceed 5 percent of the nominal strain.

7.2 Specimen Size- in order for results to be valid according to this method it is required that the specimen be predominantly elastic at all values of applied load. The minimum in-plane specimen sizes to meet this requirement are based primarily on empirical results and are specific to specimen configuration.[6]

7.2.1 For the CT specimen it is required that the uncracked ligament, (W-a), be equal to or greater than $(4/\pi)(K_{max}/\sigma_{YS})^2$ where σ_{YS} is the 0.2% offset yield strength of the test material (measured by ASTM-E8) at the temperature for which fatigue crack growth rate data are to be obtained.

7.2.2 For the CCT specimen it is required that the nominal stress in the uncracked ligament, given by

$$\sigma_N = \frac{P_{max}}{B\,W(1 - \frac{2a}{W})},$$

be less than σ_{YS}.

Note 7: The above criteria are likely to be restrictive, that is, they may require overly large specimens sizes for materials which exhibit a high degree of strain hardening (e.g., annealed low-alloy ferritic steels, annealed austenitic stainless steels, etc.). Currently there are insufficient data on these materials to formulate easily calculable size requirements which are analogous to those given above. However, data from specimens smaller than those allowed by Section 7.2 may be validated by demonstrating that da/dN versus ΔK results are equivalent to results from larger specimens which meet the requirements of Section 7.2. Supplementary information on the extent of plastic deformation encountered in any given test specimen can be obtained by measuring specimen deflections as described in Appendix B.

7.2.3 Figure 6 gives the limiting K_{max} values, designated K_{maxL}, which are defined by the above specimen size criteria. This information is expressed in dimensionless form so that the curves can be used to calculate either: (i) the value of K_{maxL} for a given combination of specimen size, W, and material yield strength, σ_{YS}, or (ii) the minimum specimen size required to obtain valid data up to a desired K_{max} value for a given material strength level. (However, it should be noted that the desired K_{max} value cannot be achieved if it is greater than the K value for unstable fracture.) All values of $K_{max}/(\sigma_{YS}\sqrt{W})$ which fall below the respective curves for the two specimens satisfy the specimen size requirements of this method.

7.3 Notch Preparation - the machined notch for either of the standard specimens may be made by electrical-discharge machining (EDM), milling, broaching or sawcutting. The following notch preparation procedures are suggested to facilitate fatigue precracking in various materials:

a) EDM, ρ < 0.25 mm (0.010 in.) (ρ = notch root radius) - high strength steels, $\sigma_{YS} \geq 1172$ MPa (170 ksi); titanium and aluminum alloys.

b) Mill or broach, $\rho \leq$ 0.08 mm (0.003 in.) - low/medium strength steels, $\sigma_{YS} \leq$ 1172 MPa (170 ksi), aluminum alloys.

c) Grind, $\rho \leq$ 0.25 mm (0.010 in.) - low/medium strength steels.

d) Mill or broach, $\rho \leq$ 0.25 mm (0.010 in.) - aluminum alloys

e) Sawcut - aluminum alloys.

Examples of various machined notch geometries and associated precracking requirements are given in Fig. 5 (Section 8.3).

8. PROCEDURE

8.1* Number of Tests - at crack growth rates greater than 10^{-8} m/cycle, range in da/dN at a given ΔK may vary by about a factor of two.[7] At rates below 10^{-8} m/cycle, the variability in da/dN may increase to a value of about five due to increased sensitivity of da/dN on small variations in ΔK. This scatter may be further increased by variables such as, material differences, residual stresses, load precision, and data processing techniques which take on added significance in the low crack growth rate regime. It is good practice to conduct replicate tests; when this is impractical, tests should be planned such that regions of overlapping da/dN vs. ΔK data are obtained. Since confidence in inferences drawn from the data increases with number of tests, the desired number of tests will depend on the end use of the data.

8.2 Specimen measurements - the specimen dimensions shall be within the tolerances given in Figs. 1 and 2.

8.3* Fatigue Precracking - the importance of precracking is to provide a sharpened fatigue crack of adequate size and straightness (also symmetry for the CCT specimen) which ensures (1) the effect of the machined starter notch is removed from the specimen K-calibration, (2) elimination of effects on subse-

quent crack growth rate data caused by changing crack front shape or precrack load history.

8.3.1 Fatigue precracking shall be conducted with the specimen in the same metallurgical condition in which it is to be tested. The precracking equipment shall be such that the load distribution is symmetrical with respect to the machine notch and K_{max} during precracking is controlled to within $\pm$ 5 percent. Any convenient loading frequency that enables the required load accuracy to be achieved can be used for precracking. The machined notch plus fatigue precrack must lie within the envelope, shown in Fig. 5, that has as its apex the end of the fatigue precrack. In addition the fatigue precrack length shall not be shorter than 0.10 B or h, whichever is greater (Fig. 5).

8.3.2 The final K_{max} during precracking shall not exceed the initial K_{max} for which test data are to be obtained. If necessary, loads corresponding to K_{max} values higher than initial test values may be used to initiate cracking at the machined notch. In this event the load range shall be stepped-down to meet the above requirement. It is suggested that reduction in P_{max} for any step be no greater than 20 percent, and that measureable crack extension occur before proceeding to the next step. To avoid transient effects in the test data, the load range in each step shall be applied over a crack length increment of at least $(3/\pi)(K_{max_i}/\sigma_{YS})^2$; where K_{max_i} is the terminal value of K_{max} from the previous load step. If P_{min}/P_{max} during precracking differs from that used during testing, see precautions of Sec. 8.5.1.

8.3.3 Measure the fatigue precrack length from the tip of the machined notch to the crack tip on the front and back surfaces of the specimen to within 0.10 mm (.004 in.) or 0.002W, whichever is greater. Measure both cracks, front and back, in the CCT specimens. If any two crack length measurements differ by more than 0.025W or by more than 0.25B, whichever is less, the precracking operation is not suitable and subsequent testing would be invalid under this method. If a fatigue crack departs more than ± 5 degrees from the plane of symmetry the specimen is not suitable for subsequent testing. In either case, check for potential problems in alignment of the loading system and/or details of the machined notch before continuing to precrack to satisfy the above requirements.

8.4 Test Equipment - the equipment for fatigue testing shall be such that the load distribution is symmetrical to the specimen notch.

8.4.1 The load cell in the test machine shall be verified according to ASTM E4 and ASTM E467. Testing shall be conducted such that both ΔP and P_{max} are controlled to within $\pm$ 2 percent throughout the test.

8.4.2 An accurate digital device is required for counting elapsed cycles. A timer is a desirable supplement to the counter and provides a check on the counter. Multiplication factors (e.g., X10 or X100) should not be used on counting devices when obtaining data at growth rates above 10^{-5} m/cycle since they can introduce significant errors in the growth rate determination.

8.5* K-Increasing Test Procedure For $da/dN > 10^{-8}$ m/cycle - this test procedure is well suited for fatigue crack growth rates above 10^{-8} m/cycle; however, it becomes increasingly difficult to use as growth rates decrease below 10^{-3} m/cycle because of precracking considerations (Sec. 8.3.3). (A K-decreasing

test procedure which is better suited for rates below 10^{-8} m/cycle is provided in Sec. 8.6). When using the K-increasing procedure it is preferred that each specimen be tested at a constant ΔP and a fixed set of loading variables. However, this may not always be feasible when it is necessary to generate a wide range of information with a limited number of specimens. When loading variables are changed during a test, potential problems arise from several types of transient phenomenon. The following procedures should be followed to minimize or eliminate transient effects while using this K-increasing test procedure.

8.5.1 If load range, ΔP, is to be incrementally varied it should be done such that P_{max} is increased rather than decreased. This is to preclude retardation of growth rates caused by overload effects; retardation being a more pronounced effect than accelerated crack growth associated with incremental increase in P_{max}. Transient growth rates are also known to result from changes in P_{min} or R. Sufficient crack extension should be allowed following changes in load to enable the growth rate to establish a steady-state value. The amount of crack growth that is required depends on the magnitude of load change and on the material.

8.5.2 When environmental effects are present, changes in load level, test frequency or wave form can result in transient growth rates. Sufficient crack extension should be allowed between changes in these loading variables to enable the growth rate to achieve a steady-state value.

8.5.3 Transient growth rates can also occur, in the absence of loading variable changes, due to long-duration test interruptions, e.g., during work stoppages. In this case data should be discarded if the growth rates following an interruption are less than those before the interruption.

8.6* K-Decreasing Procedure for da/dN $<10^{-8}$ m/cycle - this procedure is started by cycling at a ΔK and K_{max} level equal to or greater than the terminal precracking values. Subsequently, loads are shed (decreased) as the crack grows and test data are recorded until the lowest ΔK or crack growth rate of interest is achieved. The test may then be continued at constant load limits to obtain comparison data under K-increasing conditions.

8.6.1* Load shedding during the K-decreasing test may be conducted as decreasing load steps at selected crack length intervals, as shown in Fig. 7. Alternatively, the load may be shed in a continuous manner by an automated technique, for example, by use of an analog and/or digital computer[8].

8.6.2* The rate of load shedding with increasing crack length shall be gradual enough to (i) preclude anamolous data resulting from reductions in the stress intensity factor and concomitant transient growth rates, and (ii) allow the establishment of about five (da/dN, ΔK) data points of approximately equal spacing per decade of crack growth rate. The above requirements can be met by limiting the normalized K-gradient, $C = \frac{1}{K} \cdot \frac{dK}{da}$, to a negative value having a magnitude equal to or less than 0.08 mm^{-1} (2 $in.^{-1}$). That is,

$$|C| = \left|\frac{1}{K} \cdot \frac{dK}{da}\right| \leq 0.08 \text{ mm}^{-1} \text{ (2 in.}^{-1}\text{)}$$

When loads are incrementally shed, the requirements on C correspond to the nominal K-gradient depicted in Fig. 7.

Note 8: Acceptable values of C may depend on load ratio, alloy type and environment. Negative values of C less than the magnitude indicated above have been demonstrated as acceptable for several steel alloys and aluminum alloys tested in laboratory air over a wide range of load ratios[6,8].

8.6.3* If the magnitude of a negative value C exceeds that prescribed in Sec. 8.6.2, the procedure shall consist of decreasing K to the lowest growth rate of interest followed by a K-increasing test at a constant ΔP (conducted in accordance with Sec. 8.5). Upon demonstrating that data obtained using K-increasing and K-decreasing procedures are equivalent for a given set of test conditions, the K-increasing testing may be eliminated from all replicate testing under these same test conditions.

8.6.4* It is recommended that the load ratio (R) and C be maintained constant during K-decreasing testing.

8.6.5* The K-history and load history for a constant C test is given as follows:

(i) $\Delta K = \Delta K_o \exp [C(a-a_o)]$, where ΔK_o is the initial ΔK at the start of the test and a_o is the corresponding crack length. Because of the identity given in Sec. 5.3 (Note 5), the above relationship is also true for K_{max} and K_{min}.

(ii) The load histories for the standard specimens of this method are obtained by substituting the appropriate K-calibrations given in Sec. 9.3 into the above expression.

8.6.6* When employing step shedding of load, as in Fig. 7, the reduction in P_{max} of adjacent load steps shall not exceed 10 percent of the previous P_{max}. Upon adjustment of maximum load from P_{max1} to a lower value, P_{max2}, a minimum crack extension of 0.50 mm (0.02 in.) is recommended.

8.6.7* When employing continuous shedding of load the requirement of Sec. 8.6.6 is waived. Continuous load shedding is defined as

$$(P_{max1} - P_{max2}) / P_{max1} \leq 0.02.$$

8.7 Measurement of Crack Length - fatigue crack length measurements are to be made as a function of elapsed cycles by means of a visual, or equivalent, technique capable of resolving crack extensions of 0.10 mm (0.004 in.), or 0.002W, whichever is greater. For visual measurements, polishing the test area of the specimen and using indirect lighting aid in the resolution of the crack tip. It is recommended that, prior to testing, reference marks be applied to the test specimen at predetermined locations along the direction of cracking. Crack length can then be measured using a low power (20 to 50X) traveling microscope. Using the reference marks eliminates potential errors due to accidental movement of the traveling microscope. If precision photographic grids or Mylar scales are attached to the specimen, crack length can be determined directly with any magnifying device which gives the required resolution.

8.7.1 It is preferred that measurements be made without interrupting the test. When tests are interrupted to make crack length measurements, the interruption time should be minimized (e.g., less than 10 min.) since transient growth rates can result from interruptions of long duration. To enhance resolution of the crack tip, a static load not exceeding the maximum load of the previously applied load cycle may be applied during measurement interruptions. This procedure is permissible provided that it does not cause static-load crack extension or creep deformation.

8.7.2 Crack length measurements shall be made at intervals such that da/dN data are nearly evenly distributed with respect to ΔK. The following measurement intervals are recommended according to specimen type:

(i) CT specimen; $\Delta a \leq 0.02W$ for $0.25 \leq a/W \leq 0.60$

$\Delta a \leq 0.01W$ for $a/W > 0.60$

(ii) CCT specimen; $\Delta a \leq 0.03W$ for $2a/W < 0.60$

$\Delta a \leq 0.02W$ for $2a/W > 0.60$

In any case the minimum Δa shall be 0.25 mm (0.01 in.) or ten times the crack length measurement precision[1], whichever is greater.

8.7.3 If crack length is monitored visually the following procedure applies. For specimens with $B/W \leq 0.15$, the length measurements need only be made on one side of the specimen. For specimens with $B/W \geq 0.15$, measurements are to be made on both front and back sides of the specimen and the average value of these measurements (2 values for the CT specimen, 4 values for the CCT specimen) used in subsequent calculations.

8.7.4 If at any point in the test the average through-thickness fatigue crack departs more than ± 5 degrees from the plane of symmetry of the specimen, the data are invalid according to the method. In addition, data are invalid where any two surface crack lengths at a given number of cycles differ by more than 0.025W or by more than 0.25B, whichever is less.

9. CALCULATIONS AND INTERPRETATION OF RESULTS

9.1 Crack Curvature Correction - after completion of testing the fracture surfaces shall be examined, preferably at two locations (for example, at the precrack and terminal fatigue crack lengths), to determine the extent of through-thickness crack curvature. If a crack contour is visible, calculate a five point, through-thickness average crack length per ASTM E399, Sec. 8.2.3. The difference between the average through-thickness crack length and the corresponding crack length recorded during the test (for example, if visual measurements were obtained this might be the average of the surface crack length measurements) is the crack curvature correction.

9.1.1 If the crack curvature correction results in a greater than 5 percent difference in calculated stress intensity at any crack length, then the correction shall be employed when analyzing the recorded test data.

[1] The crack length measurement precision is herein defined as the standard deviation on the mean value of crack length determined for a set of replicate measurements.

9.1.2 If the magnitude of the crack curvature correction either increases or decreases with crack length, a linear interpolation shall be used to correct intermediate data points. This linear correction shall be determined from two distinct crack contours separated by a minimum spacing of 0.25W or B, whichever is greater. When there is no systematic variation of crack curvature with crack length, a uniform correction determined from an average of the crack contour measurements shall be employed.

9.1.3 When employing a crack length monitoring technique other than visual, a crack curvature correction is generally incorporated in the calibration of the technique. However, since the magnitude of the correction will probably depend on specimen thickness, the above correction procedures may also be necessary.

9.2 * Determination of Crack Growth Rate - the rate of fatigue crack growth is to be determined from the crack length versus elapsed cycles data ("a" versus N). Recommended approaches which utilize the secant or incremental polynomial methods are given in Appendix A. Either method is suitable for the K-increasing, constant ΔP test. For the K-decreasing tests where load is shed in decremental steps, as in Fig. 7, the secant method is recommended. Where shedding of K is performed continuously with each cycle by automation, the incremental polynomial technique is applicable. A crack growth rate determination shall not be made over any increment of crack extension which includes a load step.

Note 9: Both recommended methods for processing "a" versus N data are known to give the same average da/dN response. However, the secant method often results in increased scatter in da/dN relative to the incremental polynomial method, since the latter numerically "smooths" the data.[7,9] This apparent difference in variability introduced by the two methods needs to be considered, especially in utilizing da/dN vs. ΔK data in design.

9.3 Determination of Stress Intensity Range, ΔK - use the crack length values of Sec. 9.1 and Appendix A to calculate the stress intensity range corresponding to a given crack growth rate from the following expressions:

9.3.1 For the CT specimen calculate ΔK as follows:

$$\Delta K = \frac{\Delta P}{B\sqrt{W}} \frac{(2+\alpha)}{(1-\alpha)^{3/2}} (0.886 + 4.64\alpha - 13.32\alpha^2 + 14.72\alpha^3 - 5.60\alpha^4)$$

where $\alpha = a/W$; expression valid for $a/W > 0.2$.[10,11]

9.3.2 For the CCT specimen calculate ΔK consistent with the definitions of Sec. 5.2, that is

$$\Delta P = P_{max} - P_{min} \text{ for } R > 0$$

$$\Delta P = P_{max} \text{ for } R \leq 0$$

in the following expression [12]

$$\Delta K = \frac{\Delta P}{B} \sqrt{\frac{\pi\alpha}{2W} \cdot \sec\left(\frac{\pi\alpha}{2}\right)}$$

where $\alpha = 2a/W$; expression valid for $2a/W < 0.95$.

Note 10: Implicit in the above expressions are the assumptions that the test material is linear-elastic isotropic and homogeneous.

9.3.3 Check for violation of the specimen size requirement by calculating K_{maxL} (see Sec. 7.2, Fig. 6). Data are considered invalid according to this method when $K_{max} > K_{maxL}$.

9.4* Determination of a Fatigue Crack Growth Threshold - the following procedure provides an operational definition of the threshold stress intensity factor range for fatigue crack growth, ΔK_{th}, which is consistent with the general definition of Sec. 5.8:

(i) Determine the best-fit straight line from a linear regression of log da/dN versus log ΔK using a minimum of five (da/dN, ΔK) data points of approximately equal spacing between growth rates of 10^{-9} and 10^{-10} m/cycle.

(ii) Calculate the ΔK value which corresponds to a growth rate of 10^{-10} m/cycle using the above fitted line—this value of ΔK is defined as ΔK_{th} according to the operational definition of this method.

10. REPORT

The report shall include the following information:

10.1 Specimen type including thickness, B, and width, W. Provide figures of the specific CCT specimen design and grips used; also, provide a figure if a specimen type not described in this method is used.

10.2 Description of the test machine and equipment used to measure crack length. Also, state the precision with which crack length measurements were made.

10.3 Test material characterization in terms of heat treatment, chemical composition and mechanical properties (include at least the 0.2% offset yield strength and either elongation or reduction in area measured according to ASTM E8). Product size and form (e.g., sheet, plate, forging, etc.) shall also be identified.

10.4 The crack plane orientation according to the code given in ASTM E399. In addition, if the specimen is removed from a large product form give its location with respect to the parent product.

10.5 The terminal values of ΔK, R, and crack length from fatigue precracking. If precrack loads were stepped-down state the procedure employed and give the amount of crack extension at the final load level.

10.6 Test loading variables including ΔP, R, cyclic frequency and cyclic waveform.

10.7 Environmental variables including temperature, chemical composition, pH (for liquids), and pressure (for gases and vacuum). For tests in air report the relative humidity as determined by ASTM E337. For tests in "inert" reference environments, such as dry argon, give estimates of residual levels of H_2O and O_2 of the test environment (generally this differs from the analysis of residual impurities in the gas supply cylinder). Report nominal values for all of the above environmental variables, as well as maximum deviations throughout the duration of testing. Also, describe the material employed in the chamber used to contain the environment and steps taken to eliminate chemical/electrochemical reactions between the specimen - environment system and the chamber.

10.8 Analysis methods applied to the data including technique used to convert "a" versus N to da/dN, specific procedure used to correct for crack curvature and magnitude of crack curvature correction.

10.9 The specimen K-calibration and size criterion to ensure predominantly elastic behavior (for specimens not described in this method).

10.10 Plot da/dN as a function of ΔK. (It is recommended that the independent variable, ΔK, be plotted on the abscissa and the dependent variable, da/dN, on the ordinate. Log-log coordinates are commonly used. For optimum data comparisons the size of the ΔK-log cycles should be two-to-four times larger than the da/dN-log cycles.) Identify all data which violate the size requirements of Sec. 7.2 and Appendix B.

10.11 Description of any occurrences which appear to be related to anomalous data (e.g., transients following rest interruptions or changes in loading variables).

10.12* For K-decreasing tests, report C and also initial values of K and α. Indicate whether or not the K-decreasing data were verified by K-increasing data. Report ΔK_{th}, the equation of the fitted line (Sec. 9.4) used to establish ΔK_{th}, and any procedures used to establish ΔK_{th} which differ from those of Sec. 9.4.

10.13 It is desirable, but not required, to tabulate test results. When using this method of presentation, tabulate the following information for each test: a, N, ΔK, da/dN, and where applicable, the test variables of Sections 10.3, 10.6, 10.7 and 10.12. Also, identify all data determined from tests on specimens which violate the size requirements of Sec. 7.2 and Appendix B.

REFERENCES

1. P. C. Paris and F. Erdogan, "A Critical Analysis of Crack Propagation Laws", Trans. ASME, Ser. D: J. Basic Engrg., December 1963, p. 528-534.
2. P. C. Paris, "The Fracture Mechanics Approach to Fatigue", pp. 107-132, Proceedings - 10th Sagamore Army Materials Research Conf., Syracuse Univ. Pres., 1964.
3. W. G. Clark, Jr., "Fracture Mechanics in Fatigue", Experimental Mechanics, September 1971, pp. 1-8.
4. D. W. Hoeppner and W. E. Krupp, "Prediction of Component Life by Application of Fatigue Crack Growth Knowledge", Engineering Fracture Mechanics, Vol. 6, 1974, pp. 47-70.
5. Fatigue Crack Growth Under Spectrum Loads, ASTM STP 595, American Society for Testing and Materials, 1976.
6. S. J. Hudak, Jr., R. J. Bucci, A. Saxena, and R. C. Malcolm, "Development of Standard Methods of Testing and Analyzing Fatigue Crack Growth Rate Data -- Third Semi-Annual Report", Westinghouse Research Report 77-9E7-AFCGR-R1, Westinghouse Research Laboratories, Pittsburgh, PA., AFML Contract F33615-75-C-5064, March 1977.
7. W. G. Clark, Jr. and S. J. Hudak, Jr., "Variability in Fatigue Crack Growth Rate Testing", J. of Testing and Evaluation, JTEVA, Vol. 3, No. 6, 1975, pp. 454-476.
8. A. Saxena, S. J. Hudak, Jr., J. K. Donald, and D. W. Schmidt, "Computer Controlled K-Decreasing Technique for Low-Rate Fatigue Crack Growth Testing", Westinghouse Scientific Paper 77-1E7-FANWL-P1, May 5, 1977 (to be published in ASTM's Journal of Testing and Evaluation, May 1978).
9. W. G. Clark, Jr. and S. J. Hudak, Jr., "The Analysis of Fatigue Crack Growth Rate Data", Westinghouse Scientific Paper 75-9E7-AFCGR-P1, Westinghouse Research Laboratories, Pittsburgh, PA., to be published in Proceedings - 22nd Sagamore Army Materials Research Conference on Application of Fracture Mechanics to Design.

10. J. C. Newman, Jr., "Stress Analysis of the Compact Specimen Including the Effects of Pin Loading", Fracture Analysis, ASTM STP 560, 1974, pp. 105-121.

11. J. E. Srawley, "Wide Range Stress Intensity Factor Expressions for ASTM E399 Standard Fracture Toughness Specimens", Int. Journ. of Fracture, Vol. 12, June 1976, pp. 475-476.

12. C. E. Feddersen, "Discussion in Plane Strain Crack Toughness Testing of Metallic Materials", ASTM STP 410, American Society for Testing and Materials, 1976, pp. 77-79.

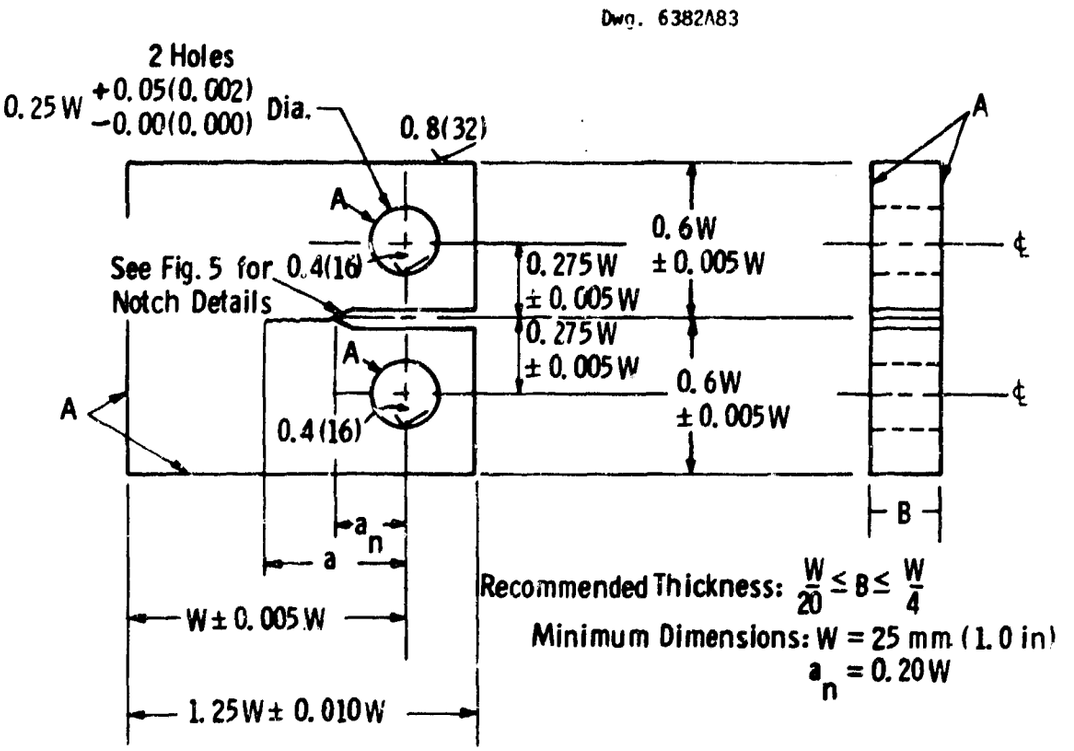

Notes: 1 - Dimensions are in millimeters (inches)
2 - A - surfaces shall be perpendicular and parallel as applicable to within 0.002 W, TIR.
3 - The intersection of the tips of the machined notch (a_n) with the specimen faces shall be equally distant from the top and bottom edges of the specimen to within 0.0005 W

Fig. 1 - Standard compact-type (CT) specimen for fatigue crack growth rate testing.

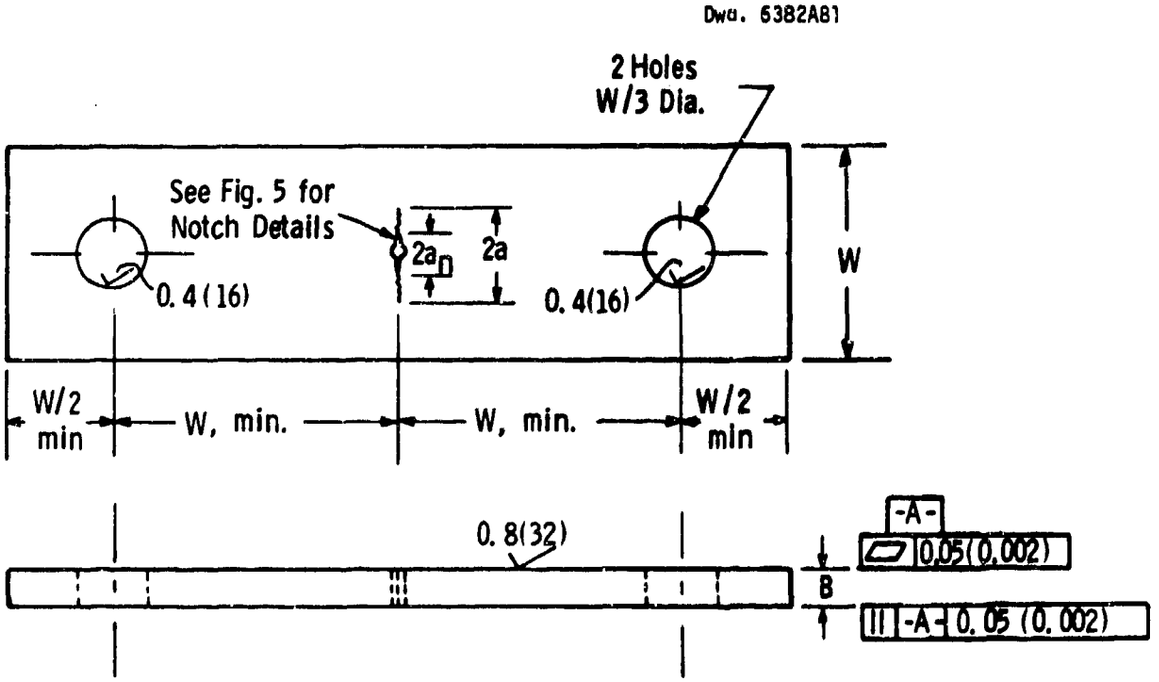

Notes: 1 - Dimensions are in millimeters (inches)
2 - The machined notch ($2a_n$) shall be centered to within $\pm$ .001W

Fig. 2 - Standard center-cracked-tension (CCT) specimen for fatigue crack growth rate testing when W ≤ 75 mm (3 in).

Dwg.6382A84

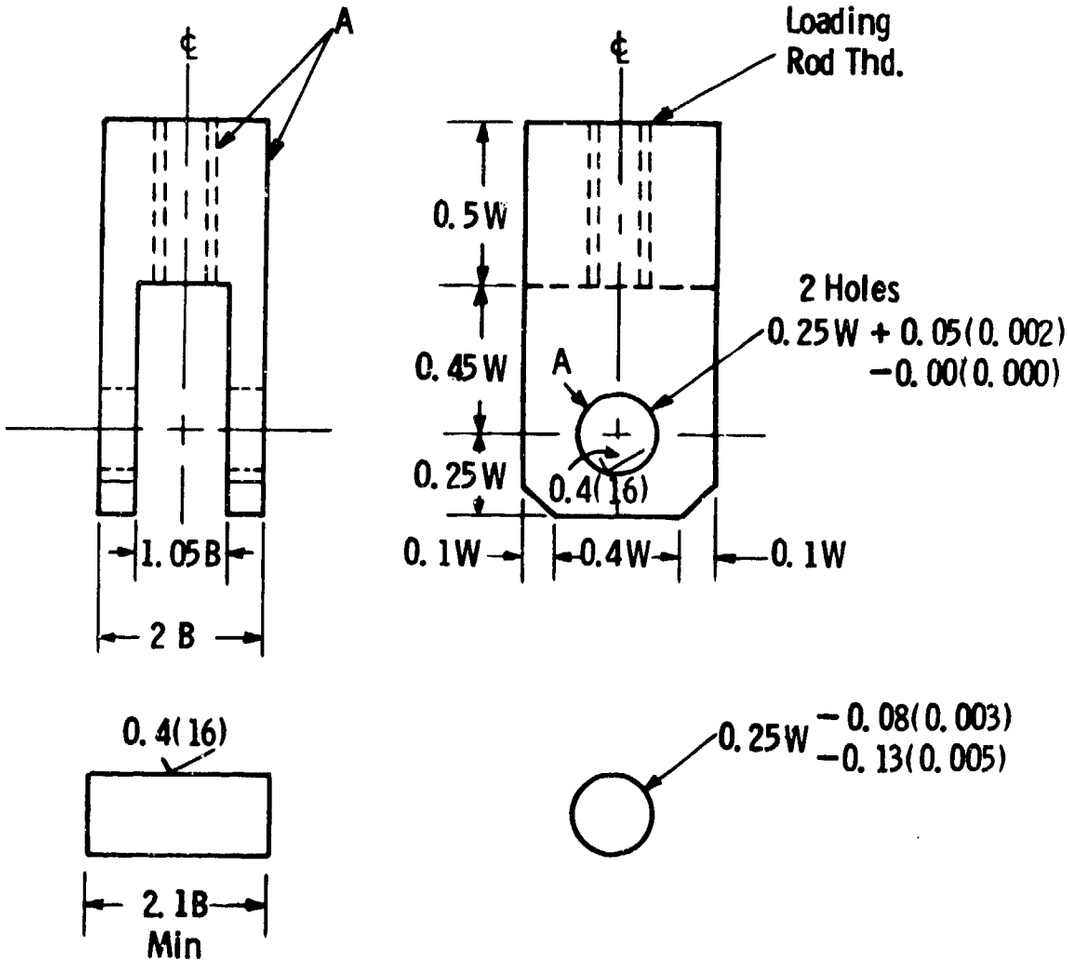

Notes: 1 - Dimensions are in millimeters (inches)
2 - A - surfaces shall be perpendicular and parallel as applicable to within 0.05 (0.002), TIR

Fig. 3 - Clevis and pin assembly for gripping CT specimens

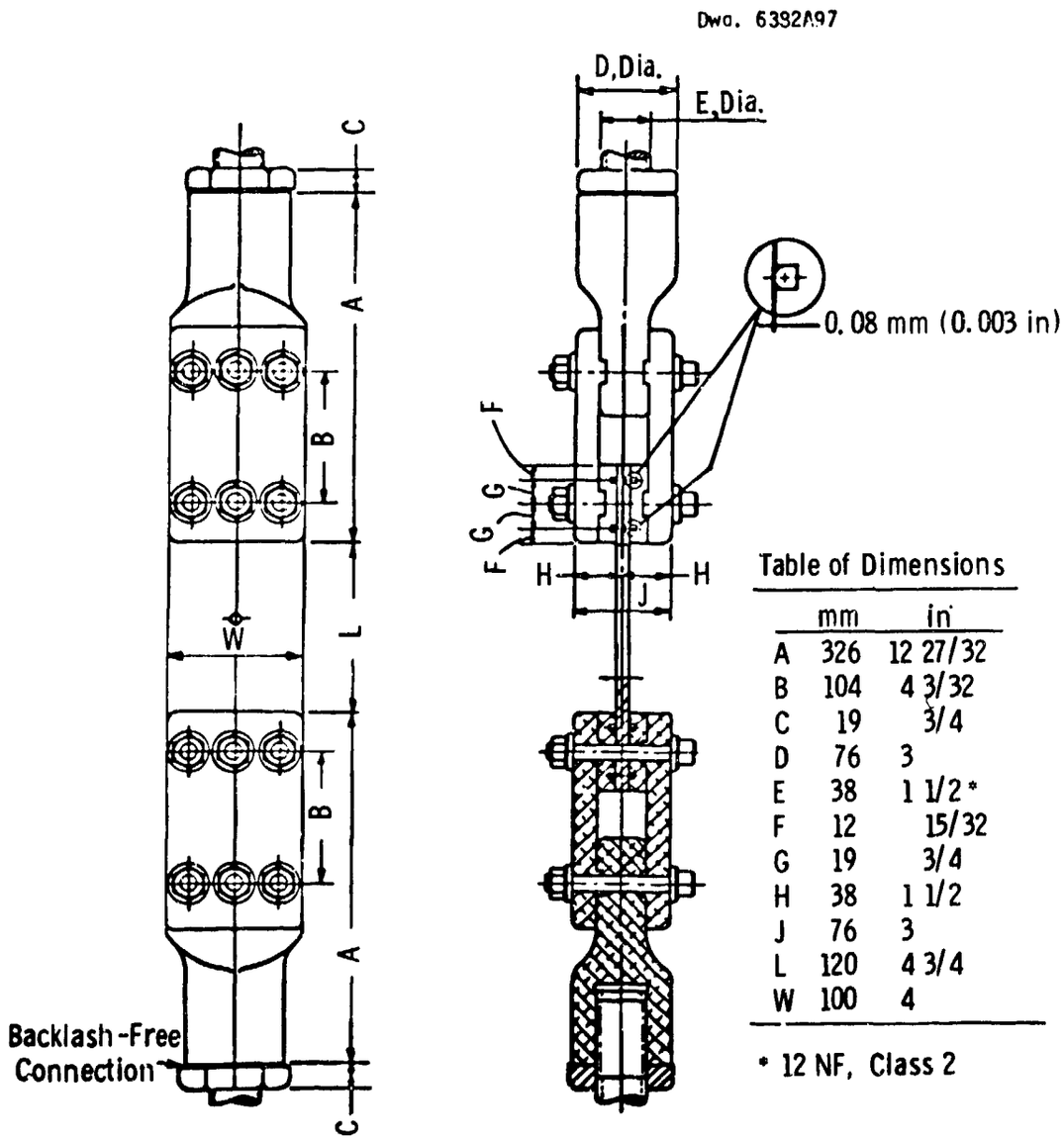

Table of Dimensions

	mm	in
A	326	12 27/32
B	104	4 3/32
C	19	3/4
D	76	3
E	38	1 1/2 *
F	12	15/32
G	19	3/4
H	38	1 1/2
J	76	3
L	120	4 3/4
W	100	4

* 12 NF, Class 2

Fig. 4 - Example of bolt and keyway assembly for gripping 100 mm (4 in) - wide CCT specimen.

Dwg. 6405A43

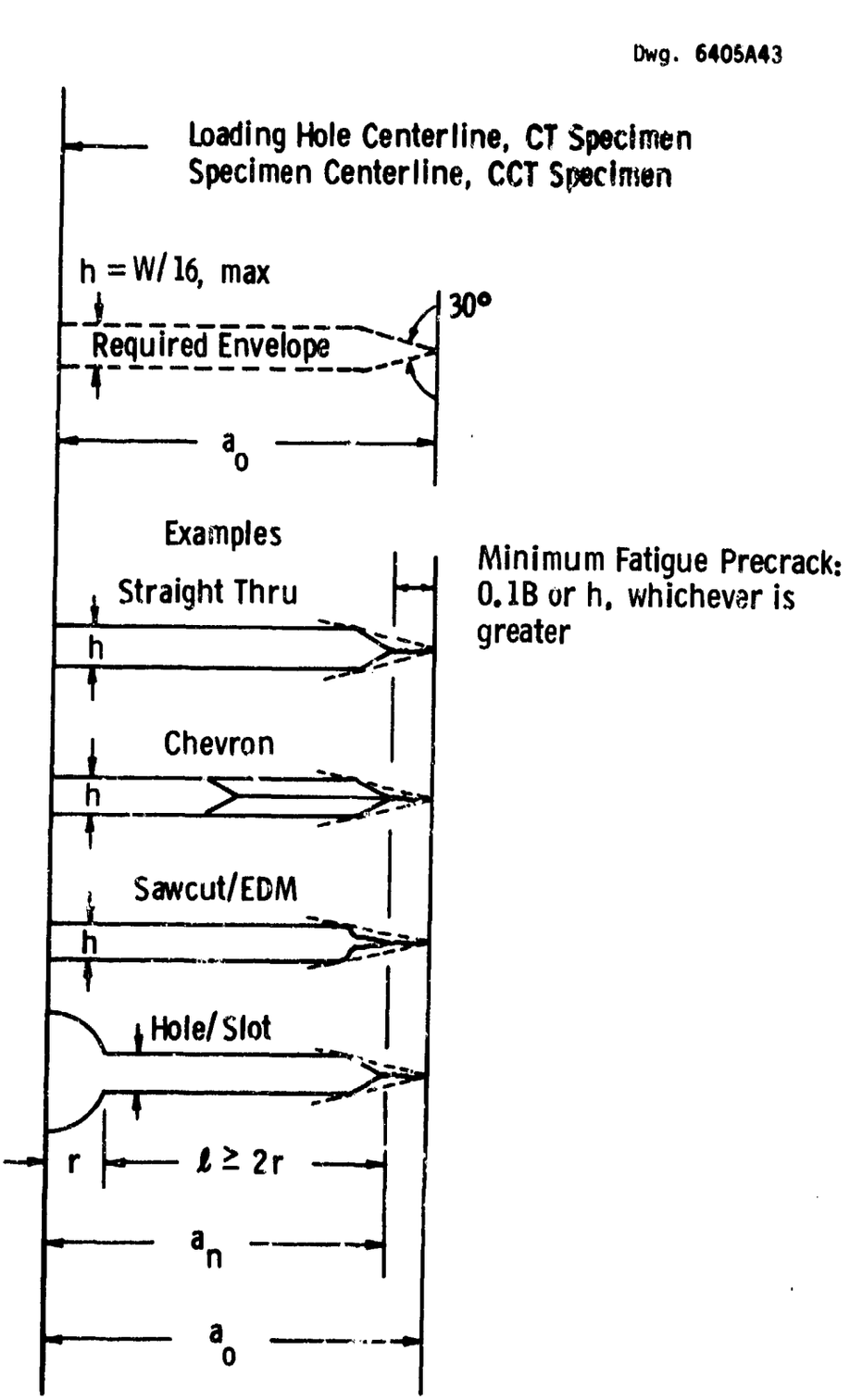

Fig. 5 – Notch details and minimum fatigue precracking requirements

Curve 685646-A

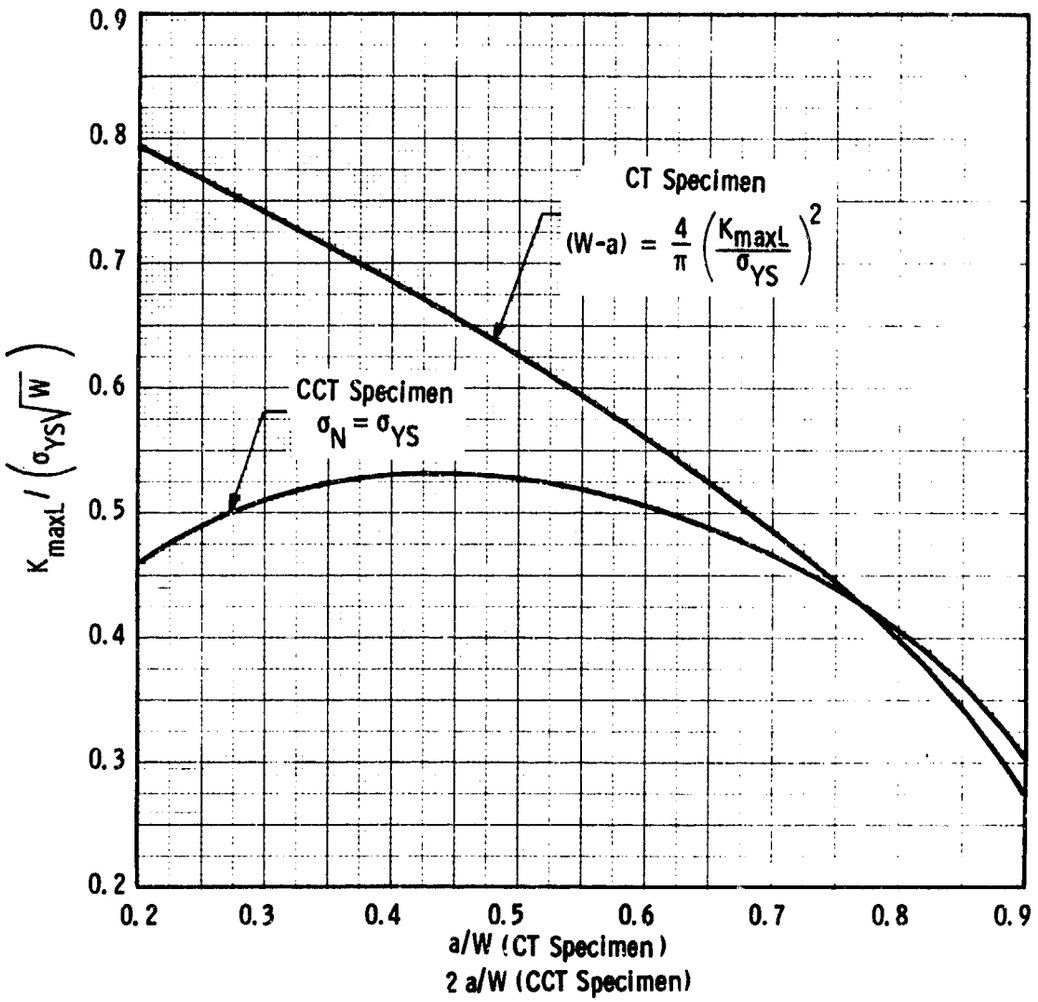

Fig. 6 – Normalized size requirements for standard fatigue crack growth specimens.

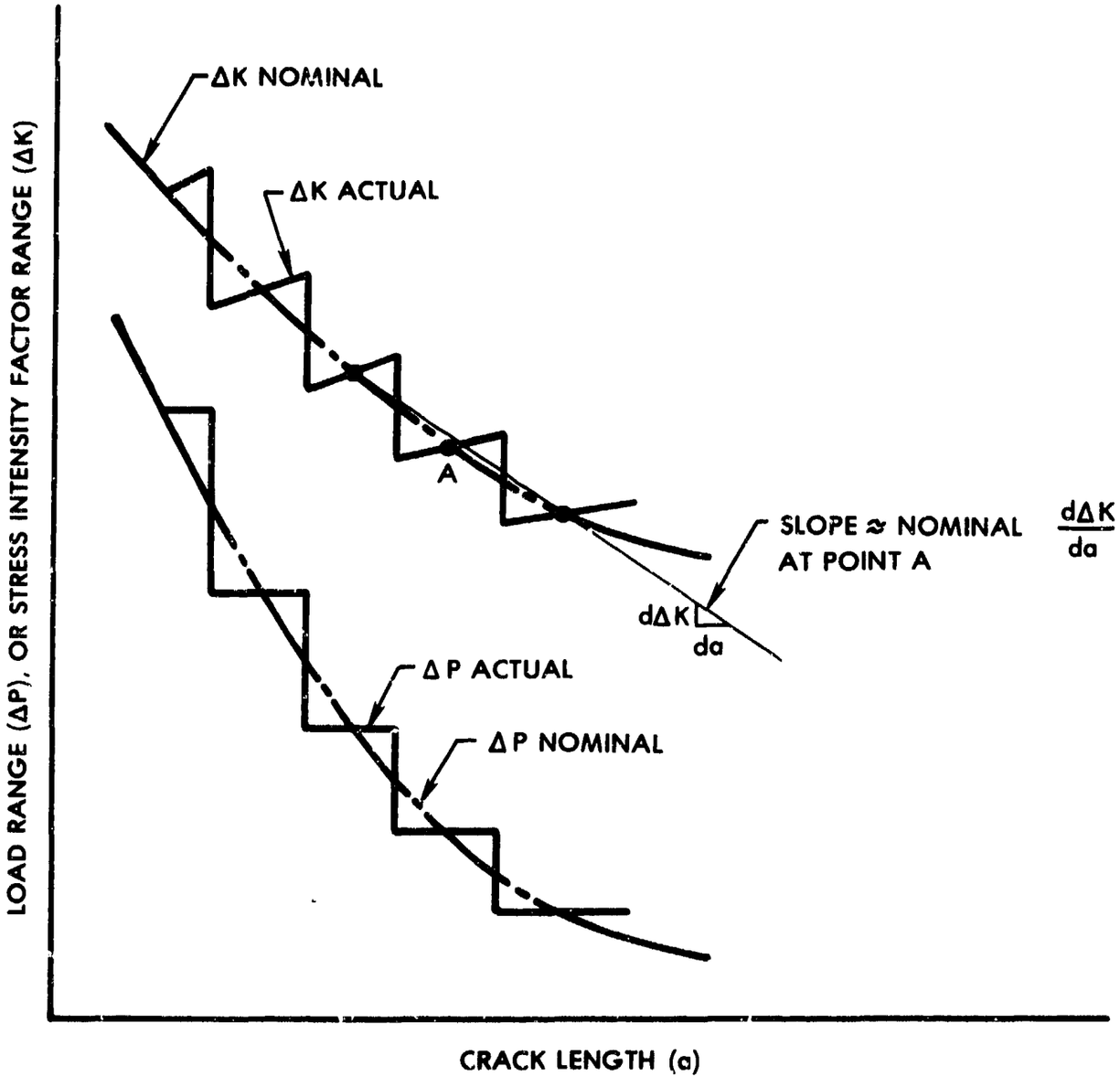

FIG. 7 TYPICAL K DECREASING TEST BY STEPPED LOAD SHEDDING

APPENDIX A

RECOMMENDED DATA REDUCTION TECHNIQUES

Secant Method - The secant or point-to-point technique for computing the crack growth rate simply involves calculating the slope of the straight line connecting two adjacent data points on the "a" versus N curve. More formally expressed as:

$$(da/dN)_{\bar{a}} = \frac{a_{i+1} - a_i}{N_{i+1} - N_i} \tag{A1}$$

Since the computed da/dN is an average rate over the $(a_{i+1} - a_i)$ increment, the average crack length, $\bar{a} = 1/2\,(a_{i+1} + a_i)$, is normally used to calculate ΔK.

Incremental Polynomial Method - This method for computing da/dN involves fitting a 2nd-order polynomial (parabola) to sets of (2n+1) successive data points, where n is usually 1, 2, 3 or 4. The form of the equation for the local fit is as follows:

$$\hat{a}_i = b_0 + b_1 \left(\frac{N_i - C_1}{C_2}\right) + b_2 \left(\frac{N_i - C_1}{C_2}\right) \tag{A2}$$

where

$$-1 \leq \left(\frac{N_i - C_1}{C_2}\right) \leq +1$$

and b_0, b_1 and b_2 are the regression parameters which are determined by the least squares method (that is, minimization of the square of the deviations between observed and fitted values of crack length) over the range $a_{i-n} \leq a \leq a_{i+n}$. The value $\hat{a}_i$ is the fitted value of crack length at N_i. The parameters $C_1 = 1/2(N_{i-n} + N_{i+n})$, and $C_2 = 1/2\,(N_{i+n} - N_{i-n})$, are used to scale the input data; thus, avoiding numerical difficulties in determining the regression parameters. The rate of crack growth at N_i is obtained from the derivative of the above parabola which is given by the following expression,

$$(da/dN)_{\hat{a}_i} = \frac{b_1}{C_2} + 2b_2\,(N_i - C_1)/C_2^2 \tag{A3}$$

The value of ΔK associated with this da/dN value is computed using the fitted crack length, $\hat{a}_i$, corresponding to N_i.

A Fortran computer program which utilizes the above scheme for n=3, i.e., 7 successive data points, is given in Table A1.[1] This program uses the specimen K-calibrations given in Sec. 9.3 and also checks the data against the size requirements given in Sec. 7.2.

An example of the output from the program is given in Table A2. Information on the specimen, loading variables and environment are listed in the output along with tabulated values of the raw data and processed data. A(MEAS.) and A(REG.) are values of total crack length obtained from measurement and from the regression equation (eq. A2), respectively. Goodness of fit of this equation is given by the multiple correlation coefficient, MCC. Values of DELK (ΔK) and DA/DN (da/dN) are given in the same units as the input variables (for the example problem these are ksi$\sqrt{\text{in.}}$ and in./cycle, respectively). Values of da/dN which violate the specimen size requirement appear with an asterick and note as shown in Table A2 for the final nine data points.

The definition of input variables for the program and formats for these inputs are given in Table A3.

---

[1] It should be noted that the basic regression equations which are used to calculate da/dN can also be solved on a programmable calculator, thus large electronic computer facilities are not required to use this technique.

Table A1 - Fortran Computer Program for Data Reduction by the Seven Point Incremental Polynomial Technique

```
      DIMENSION A(200),N(200),EE(3),DADN(200),DELK(200),ID(7)
      DIMENSION AA(10),NN(10)
      REAL K
      REAL NN
      INTEGER CO
      INTEGER TYPE
   10 FORMAT(/A6,' SPECIMEN',5X,2HB=,F6.3,5H IN.,5X,2HW=,F6.3,5H IN.
     *  ,5X,3HAN=,F6.3,5H IN.)
   15 FORMAT(1H1,' SEVEN POINT INCREMENTAL POLYNOMIAL METHOD FOR DETERMI
     *NING DA/DN ')
   17 FORMAT(/)
   20 FORMAT(/6H PMIN=,F6.3,4HKIPS,5X,5HPMAX=,F6.3,4HKIPS,5X,2HR=,F6.3,5
     *X,10HTEST FREQ=,F6.3,3HHZ.)
   22 FORMAT(/7H TEMP.=,F4.0,1HF,5X,12HENVIRONMENT=,A10)
   25 FORMAT (A6,9X,F8.1,F8.3,A6,9X)
   30 FORMAT(6A6,A4,2I6)
   35 FORMAT (////11H SPEC. NO.    ,6A6,A4,10X,14H NO.POINTS  = ,I3)
   40 FORMAT(4 (F6.4, F9.0))
   55 FORMAT(/8H OBS.NO.,  5X,6HCYCLES,1X,8HA(MEAS.),8X,7HA(REG.),5X,6HM
     *.C.C.,14X,4HDELK,14X,5HDA/DN)
   92 FORMAT(I4,9X,F8.0,7X,F8.3,8X,F8.3,8X,F8.6,11X,F8.2,12X,E8.3)
   95 FORMAT(I4,9X,F8.0,7X,F8.3)
   98 FORMAT(I4,9X,F8.0,7X,F8.3,8X,F8.3,8X,F8.6,11X,F8.2,12X,E8.3,2H *)
   99 FORMAT(F6.3,F6.3,F6.1,F6.3,F6.3,F6.3)
  200 FORMAT(////10H                )
  300 FORMAT(/45H *  - DATA VIOLATE SPECIMEN SIZE REQUIREMENTS )
C     TYPE=1 FOR CI AND 2 FOR A CCP
  500 READ(5,30,END=1000) (ID(I),I=1,7),NPTS,TYPE
      READ(5,99) PMIN,PMAX,F,W,AM
C     KIND=CI,CCP,ETC.
      READ (5,25) ENV,TEM,Y5,KIND
      READ(5,40)(A(I),N(I),I=1,NPTS)
      PRINT 15
      PRINT 35,(ID(II),II=1,7),NPTS
      PRINT 10,KIND,B,W,AM
      R=PMIN/PMAX
      PRINT 20 ,PMIN,PMAX,R,F
      PRINT 22 , TEM , ENV
      PRINT 55
      PRINT 200
      DO 31 I=1,NPTS
      A(I)=A(I) * AM
   31 CONTINUE
      K=0
      PI=3.1416
      PP=PMAX-PMIN
      DO 110 I=1,3
      PRINT 95,I,N(I),A(I)
  110 CONTINUE
      NPTS=NPTS-6
      DO 100 I=1,NPTS
      L=0
      K=K+1
      K1=K+6
      DO 60 J= K,K1
      L=L+1
      AA(L) = A(J)
      NN(L) = N(J)
   60 CONTINUE
      C1 = 0.5*(NN(1)+NN(7))
      C2 = 0.5*(NN(7)-NN(1))
      SX=0
      SX2=0
      SX3=0
      SX4=0
      SY=0
      SYX=0
      SYX2=0
```

Table A1 - (continued)

```
      DO 70 J=1,7
      X = (NN(J)-C1)/C2
      YY = AA(J)
      SX = SX + X
      SX2 = SX2 + X**2
      SX3 = SX3 + X**3
      SX4 = SX4 + X**4
      SY = SY + YY
      SYX = SYX + X*YY
      SYX2 = SYX2 + YY*X**2
   70 CONTINUE
      DEN=7.0*(SX2*SX4-SX3**2)-SX*(SX*SX4-SX2*SX3)+SX2*(SX*SX3-SX2**2)
      T2=SY*(SX2*SX4-SX3**2)-SYX*(SX*SX4-SX2*SX3)+SYX2*(SX*SX3-SX2**2)
      BB(1) = T2/DEN
      T3=7.0*(SYX*SX4-SYX2*SX3)-SX*(SY*SX4-SYX2*SX2)+SX2*(SY*SX3-SYX*SX2
     *)
      BB(2) = T3/DEN
      T4=7.0*(SX2*SYX2-SX3*SYX)-SX*(SX*SYX2-SX3*SY)+SX2*(SX*SYX-SX2*SY)
      BB(3) = T4/DEN
      YB = SY/7.0
      RSS = 0
      TSS = 0
      DO 75 J=1,7
      X = (NN(J)-C1)/C2
      YHAT = BB(1)+BB(2)*X+BB(3)*X**2
      RSS = RSS+(AA(J)-YHAT)**2
      TSS = TSS+(AA(J)-YB)**2
   75 CONTINUE
      R2 = 1.0-RSS/TSS
      DADN(I)= BB(2)/C2 + 2.0*BB(3)*(NN(4)-C1)/C2**2
      X=(NN(4)-C1)/C2
      AR=BB(1)+BB(2)*X+BB(3)*X**2
      S=1E+10
      SNET=0
      GO=Y+3
      GO TO (1,2)  ,TYPE
    1 CONTINUE
      W = AR/W
      FT=(2*T)*(0.886+4.64*T-13.32*T**2+14.72*T**3-5.6*T**4))/(1-T)**1.
     *5
      S = YS*SQRT(PI*W*(1-T))/2
      GO TO 100
    2 CONTINUE
      T= 2*AR/W
      SEC = 1.0/(COS(PI*T/2))
      FT = SQRT((PI*Y*SEC)/2.0)
      SNET=PMAX/(B*W*(1-T))
  100 DELK(I)=(FT*PP)/(B*SQRT(W))
      AR=DELK(I)/(1-R)
      IF(AR.GE.S) GO TO 97
      IF(SNET.GE.YS)GO TO 97
   91 PRINT 92,GO,N(GO),A(GO),AR,R2,DELK(I),DADN(I)
      GO TO 100
   97 PRINT 92,GO,N(GO),A(GO),AR,R2,DELK(I),DADN(I)
  100 CONTINUE
      J=NP1+1
      K=NP1+6
      DO 120 I=J,K
      PRINT 93,I,N(I),A(I)
  120 CONTINUE
      PRINT 94
      PRINT 95
      PRINT 100
      GO TO 500
 1000 CALL EXIT
      END
```

Table A2 - Example Output from Incremental Polynomial Computer Program

SEVEN POINT INCREMENTAL POLYNOMIAL METHOD FOR DETERMINING DA/DN

SPEC. NO. 10N-9 NO.POINTS = 37

CT SPECIMEN B= .250 IN. W= 2.000 IN. AN= .500 IN.

PMIN= 4.000KIPS PMAX= 5.000KIPS R= .800 TEST FREQ= .100HZ.

TEMP.= 75.F ENVIRONMENT= AIR

OBS.NO.	CYCLES	A(MEAS.)	A(REG.)	M.C.C.	DELK	DA/DN	
1	0.	.539					
2	15480.	.631					
3	22070.	.656					
4	30240.	.674	.677	.996911	17.56	.323-05	
5	36090.	.698	.698	.996347	18.03	.337-05	
6	41370.	.718	.715	.995268	18.44	.337-05	
7	46850.	.735	.736	.998739	18.93	.344-05	
8	50090.	.746	.746	.998733	19.17	.345-05	
9	54380.	.759	.760	.999740	19.53	.350-05	
10	60320.	.781	.781	.999713	20.08	.382-05	
11	65160.	.801	.801	.999411	20.60	.403-05	
12	70240.	.821	.822	.999473	21.19	.433-05	
13	74690.	.843	.842	.999451	21.76	.453-05	
14	80070.	.865	.866	.999436	22.51	.480-05	
15	83860.	.886	.885	.999299	23.11	.493-05	
16	88080.	.906	.906	.999176	23.75	.517-05	
17	91460.	.925	.924	.999120	24.41	.545-05	
18	95620.	.945	.946	.999483	25.21	.583-05	
19	99000.	.967	.967	.999173	25.99	.611-05	
20	102360.	.988	.988	.998500	26.84	.623-05	
21	105110.	1.008	1.006	.997105	27.58	.668-05	
22	108440.	1.028	1.028	.997266	28.55	.693-05	
23	111660.	1.047	1.051	.997266	29.60	.741-05	
24	113410.	1.067	1.064	.997552	30.23	.759-05	
25	116810.	1.090	1.091	.996303	31.65	.843-05	
26	118730.	1.108	1.108	.995912	32.55	.898-05	•
27	121220.	1.128	1.130	.998627	33.91	.105-04	• •
28	121880.	1.138	1.137	.998593	34.32	.111-04	• •
29	122830.	1.146	1.148	.998087	35.00	.114-04	• •
30	124280.	1.166	1.166	.999287	36.20	.127-04	• •
31	125820.	1.187	1.185	.999156	37.54	.138-04	• •
32	127480.	1.207	1.208	.999290	39.20	.165-04	• •
33	128700.	1.226	1.227	.994844	40.79	.201-04	• •
34	129760.	1.245	1.249	.977629	42.69	.279-04	•
35	130790.	1.277					
36	131480.	1.298					
37	131550.	1.323					

• - DATA VIOLATE SPECIMEN SIZE REQUIREMENTS

Table A3 - Definition of Input Variables for Fortran Program

Input Card	Program Line	Fortran Code	Variable Definition	Card Columns
1	28	ID(I)	Specimen identification, e.g. specimen number, heat number, material	1-40+
	28	NPTS	Number of paired (a,N) data points	40-46*
	26	TYPE	TYPE=1 for CT specimen TYPE=2 for CCT specimen	47-52*
2	29	PMIN	Minimum load, P_{min}, in kips	1-6°
	29	PMAX	Maximum load, P_{max}, in kips	7-12°
	29	F	Test frequency	13-18°
	29	B	Specimen thickness, B	19-24°
	29	W	Specimen width, W	25-30°
	29	AM	Machine notch length, a_n	31-36°
3	31	ENV	Test environment	1-6+
	31	TEM	Test temperature, °F	7-11°
	31	YS	0.2% yield stress of specimen	12-19°
	31	KIND	Specimen type, i.e. "CT" or "CCT"	20-25+
4,5,6, etc.	32	A(I)	Crack length "a" measured from machine notch, a_n	A(1) 1-6° N(1) 7-15°
	32	N(I)	Elapsed cycles, N	A(2) 16-21° N(2) 22-30° A(3) 31-36° N(3) 37-45° A(4) 46-51° N(4) 52-60° (4 paired (a,N) data points per card) A(5) 1-6° N(5) 7-15° etc. (next card)

+ alphanumeric

* integer, entered to far right of available columns

° use decimal point

APPENDIX B

RECOMMENDED PROCEDURE FOR SPECIMENS VIOLATING SECTION 7.2

This appendix presents a recommended empirical procedure for use when test specimens do not meet the size requirements of Section 7.2.* This procedure is of greatest utility for low strength materials, especially those exhibiting much monotonic and cyclic strain-hardening. Currently there are insufficient data on these materials to formulate an easily calculatable size requirement which would be analogous to those specified in Section 7.2. For this reason it is recommended, but not required, that specimen deflections be measured during testing in order to provide quantitative information on the extent of plastic deformation in the specimen.

During a constant-load-amplitude fatigue crack growth test with commonly used specimen geometries the specimen load-deflection behavior is influenced by plastic deformation as illustrated in Fig. B1. As the fatigue crack grows from length a_1 to a_3 the mean specimen deflection, as well as the compliance (that is, inverse slope of the curves in Fig. B1), increases in a manner predictable from linear-elastic theory. However, as the fatigue crack continues to grow, the mean specimen deflection can eventually become larger than the elastically calculated mean deflection. This difference is due to a plastic deflection, $V_{plastic}$, which is depicted for crack length a_4 in Fig. B1.

The plasticity phenomenon described above develops and increases continuously as the fatigue crack grows. This development is illustrated in Fig. B2 where both the measured and elastically calculated deflections, corresponding to minimum and maximum load, are given. The increasingly larger plastic deflection causes the measured deflections, V_{min} and V_{max}, to become increasingly larger than the elastically calculated deflections,

* The purpose of the size requirements of Section 7.2 is to limit the extent of plastic deformation during testing so that results can be analyzed using linear-elastic theory.

V^e_{min} and V^e_{max}. However, for any given crack length the measured and elastically calculated deflection ranges remain approximately equal (Fig. B2) since the cyclic plasticity remains small (Fig. B1).

Although the cyclic plasticity remains small, it would appear necessary to limit $V_{plastic}$. Limited data on A533-B steel[1] indicate that crack growth rates can be properly analyzed using linear elastic theory provided

$$V_{plastic} \leq V^e_{max} \tag{B1}$$

This condition can be more conveniently expressed in terms of directly measurable quantities by using the following relationships which are consistent with Fig. B2. Equation B1 is equivalent to

$$V_{max} \leq 2V^e_{max} \tag{B2}$$

and

$$\Delta V = V_{max} - V_{min} = V^e_{max} - V^e_{min} \tag{B3}$$

thus

$$V^e_{max} = \frac{\Delta V}{1-R} \tag{B4}$$

combining Equations (B2) and (B4) yields

$$V_{max} \leq \frac{2\Delta V}{1-R} \tag{B5}$$

When it is necessary to generate data using specimens which do not meet the size cirteria of Section 7.2, it is suggested that specimen deflections be measured and that data which violate equation B5 be so labeled. Information of this type will provide data to further test equation B5 and will hopefully lead to the formulation of an easily calculatable size requirement which would be appropriate for all materials.

---

[1] N. E. Dowling, "Fatigue-Crack Growth Rate Testing at High Stress Intensities", Flaw Growth and Fracture, ASTM STP631, American Society for Testing and Materials, 1977, pp. 139-158.

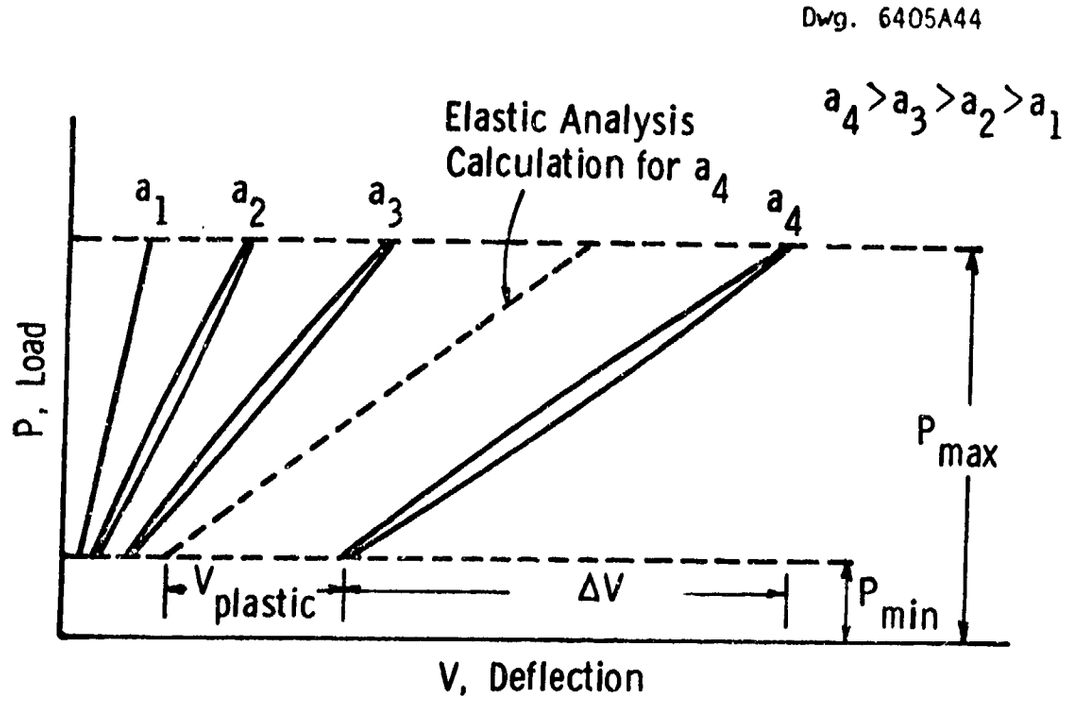

Fig. B1 – Effect of plastic deformation on specimen load - deflection behavior during fatigue crack growth rate testing at constant - load - amplitude.

Curve 689346-A

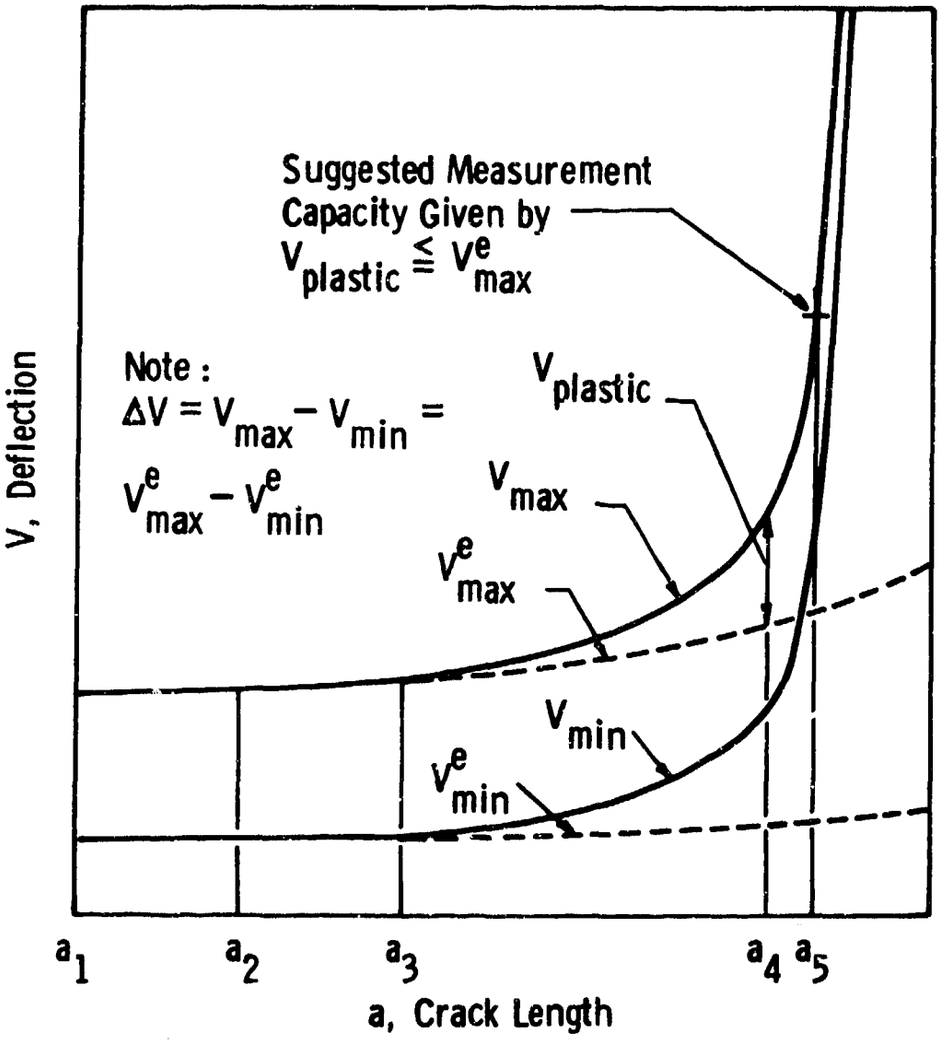

Fig. B2 — Suggested specimen measurement capacity based on comparison of measured (elastic plus plastic) and elastic deflections during a constant - load - amplitude fatigue crack growth rate test.

APPENDIX II

Scientific Paper 77-9D3-AFCGR-P1 December 6, 1977

ROLE OF CRACK-TIP STRESS RELAXATION IN FATIGUE CRACK GROWTH

A. Saxena and S. J. Hudak, Jr.
Structural Behavior of Materials
Westinghouse R&D Center
Pittsburgh, PA 15235

ABSTRACT

This study constitutes an effort to identify underlying processes which contribute to load ratio (R) effects in fatigue crack growth. Approximate analytical expressions are developed for crack-tip strains during steady-state cyclic loading. Using these expressions, the strain history of an element of material which is being approached by the tip of a fatigue crack — growing at a constant rate of either 10^{-7} or 10^{-5} in./cycle (2.5×10^{-9} or 2.5×10^{-7} m/cycle) was calculated for load ratios of 0 and 0.8. Applying these strain histories to smooth axial fatigue specimens of 10Ni steel and 2219-T851 aluminum simulated the material's mean stress relaxation behavior at the crack-tip and associated cyclic lives. The number of cycles to failure correlated with the simulated growth rates. Also, mean stress relaxation characteristics in the crack tip region qualitatively explain the load ratio effects on da/dN which depend on material type and growth rate regime. This information is likely to be important to alloy development and material selection for fatigue resistance as well as for proper modelling of fatigue crack growth data at several load ratios.

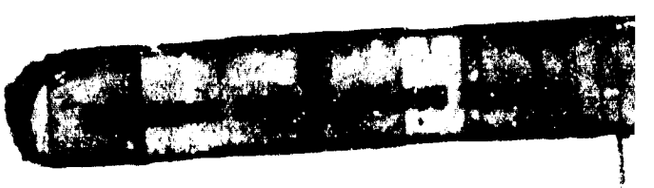

INTRODUCTION

The fracture mechanics approach to the characterization of the rate of growth of pre-existing, sharp defects in engineering metals subjected to fatigue loading is used widely. As identified by Paris and Erdogan[1], the primary parameter controlling the rate of fatigue crack growth, (da/dN), is the stress intensity range, ΔK, which characterizes the elastic stress and strain range in the vicinity of the crack-tip. Another loading variable which can influence the fatigue crack growth rate is the load ratio (R = minimum load/maximum load).[2]

In a recent study[3], the influence of load ratio was fully characterized in a 2219-T851 aluminum alloy and a 10Ni-steel for positive R values, Figs. 1 and 2. The wide range growth rates for which data were obtained, included the full three region behavior for the aluminum alloy and the first two regions for the steel. This sigmoidal shape is characterized by increases in slopes of the log (da/dN) versus log (ΔK) plot in the low (region I) and high (region III) growth rates compared to the intermediate growth rates (region II). The main conclusions of this previous study can be summarized as follows: (i) In region I, the load ratio is an important loading variable in both materials. (ii) In region II, the aluminum alloy shows a significant effect of R, although not to the extent observed in region I. (iii) In 10Ni-steel the influence of load ratio on da/dN in region II could not be distinguished from the general scatter in the data. (iv) In region III, (behavior influenced by the onset of static mode fracture — examined here only

for the aluminum alloy), the load ratio was again an important factor. These trends are in agreement with observations noted by Ritchie[4] on a 300M steel. Such results demonstrate that the influence of load ratio on fatigue crack growth rate is dependent on both material type and the growth rate regime being considered.

Attempts have been made to rationalize the effect of load ratio on da/dN by using the phenomenon of crack closure proposed by Elber[5]. This phenomenon, attributed to a zone of residual deformation left in the wake of a growing fatigue crack, assumes the crack surface to be closed even during a portion of the tensile loading cycle. It is postulated that the portion of the loading cycle during which the crack remains closed is ineffective in propagating the crack. If crack closure is a dominant factor in load ratio effects, then measuring the closure load as a function of R and accounting for the reduced load range in terms of an "effective ΔK" should normalize data generated at different load ratios. Despite some degree of normalization that has been demonstrated[5-8], the extent to which crack closure influences fatigue crack growth remains a controversial subject.[9]

The intent of this paper is to focus attention on alternate or supplementary crack-tip plasticity phenomena which are likely to influence fatigue crack growth. The individual and combined effects of these underlying phenomena need to be addressed in order to formulate a more complete understanding of the fatigue crack growth process and ultimately aid in material selection and alloy development for preventing fatigue failures.

The specific objectives of this study were to 1) estimate how cyclic plasticity at the crack-tip dictates the magnitude of mean stress ahead of a growing fatigue crack, using analysis and measurements on a 10Ni steel and a 2219-T851 aluminum alloy and 2) relate these mean stress characteristics to measured load ratio effects on da/dN in these same materials. A similar approach has previously been used in attempts to correlate strain-life data obtained on smooth specimens to fatigue crack growth rates as a function of ΔK[10,11] obtained on precracked fracture mechanics specimens.

CRACK-TIP STRESSES AND STRAINS

In this section a simple analysis to estimate the maximum and minimum strains in the plastic zone ahead of a fatigue crack growing at a constant rate and given load ratio is described. The strain history thus obtained can be applied to smooth axial fatigue specimens and corresponding stress response recorded as described in the next section. From the combination of the above analysis and experiment a complete stress-strain characterization of an element of material being approached by a propagating fatigue crack can be obtained. Consider a cracked body loaded with a remote fatigue stress, ΔS, which is applied normal to the plane of crack as shown in Fig. 3. ΔS results in a crack tip stress intensity range, ΔK, and a crack growth rate, da/dN. Figure 4 shows a schematic of the stress-strain behavior experienced by an infinitesimal element, dx (such as shown in Fig. 3), which is located at a distance x from the crack tip. The element locations chosen for illustration are: (a) beyond the monotonic plastic zone, $x > 2r_y$; (b) between the monotonic and cyclic plastic zones, $2r_y^c < x < 2r_y$, (c) at the cyclic plastic zone boundary, $x = 2r_y^c$; and (d) within the cyclic plastic zone, $x < 2r_y^c$. The "elastic" stress distribution along the x axis is analogous to the sustained loading case solved by Irwin.[12]

$$\Delta\sigma_y = \Delta\sigma_x \propto \frac{\Delta K}{x^{\frac{1}{2}}} \qquad (1a)$$

$$\Delta\tau_{xy} = 0 \tag{1b}$$

Since considerable plasticity occurs at the crack tip, the elastic stress field, Eqs. 1, must be modified. This modification can be simply estimated using Neuber's rule[13] as follows:

$$k_t = (k_\sigma \cdot k_\varepsilon)^{\frac{1}{2}} \tag{2}$$

where: k_t = elastic stress concentration factor

k_σ = stress concentration factor

k_ε = strain concentration factor

Combining the above definitions and Eq. 1a, we have

$$k_t = \frac{\Delta\sigma_y}{\Delta S} \propto \frac{1}{\Delta S} \frac{\Delta K}{(x)^{\frac{1}{2}}} \tag{3a}$$

$$k_\sigma = \frac{\Delta\sigma}{\Delta S} \tag{3b}$$

$$\text{and } k_\varepsilon = \frac{\Delta\varepsilon \cdot E}{\Delta S} \tag{3c}$$

where $\Delta\sigma$ and $\Delta\varepsilon$ are the actual stress and strain ranges in the crack-tip region. From Eqs. 2 and 3 it can easily be shown that,

$$\Delta\sigma \cdot \Delta\varepsilon = c \frac{(\Delta K)^2}{x \cdot E} \qquad \text{for } x < 2r_\gamma \tag{4}$$

c is a constant of proportionality which will be determined later. The 1/x - type singularity predicted for the product of stress and strain ranges in Eq. 4 is similar to that suggested in the work of Hutchinson[14], Rice and Rosengren[15] and McClintock[16] who have

related crack-tip stresses and strains to the path-independent line integral, J, for sustained loading conditions beyond nominal yield.

Alternate forms of Eq. 4 are as follows

$$\sigma_{max} \cdot \varepsilon_{max} = \frac{c_1 (K_{max})^2}{x \cdot E} \tag{5a}$$

$$\text{and } \sigma_{min} \cdot \varepsilon_{min} = \frac{c_1 (K_{min})^2}{x \cdot E} \tag{5b}$$

$$\text{where } c_1 = c \frac{1-R}{1+R} \quad \text{for } (R > 0) \tag{5c}$$

σ_{max}, ε_{max} and σ_{min}, ε_{min} are the maximum and minimum crack tip stresses and strains corresponding to stress intensity factors K_{max} and K_{min}, respectively.

The constant c_1 (Eq. 5) is obtained from the monotonic plastic zone boundary conditions

$$\varepsilon_{max} = \left(\frac{\sigma_{YS}}{E}\right)$$

$$\text{when } x = \frac{1}{\pi} \left(\frac{K_{max}}{\sigma_{YS}}\right)^2$$

for non-hardening materials, the above equation can be substituted into Eq. 5a to give

$$c_1 = \frac{1}{\pi \sigma_{YS}}$$

Thus, the final set of equations describing the estimated maximum, minimum, and range of crack-tip strains as a function of distance from the crack tip is given by

$$\varepsilon_{max} = \frac{(K_{max})^2}{\pi \sigma_{YS} \cdot E \cdot x} \tag{6a}$$

$$\varepsilon_{min} = \frac{(K_{min})^2}{\pi \sigma_{YS} \cdot E \cdot x} \tag{6b}$$

$$\Delta\varepsilon = \frac{(1+R)}{1-R} \frac{(\Delta K)^2}{\pi \sigma_{YS} \cdot E \cdot x} \tag{6c}$$

Simulating the Strain History of a Crack-Tip Element

The strain versus distance relationship defined by Eq. 6 can be used to specify a test history in terms of strain versus fatigue cycles. This strain history, when applied to an axial fatigue specimen, can be considered to simulate the cyclic deformation behavior experienced by an element of material being approached by a fatigue crack. The strain vs. cycles behavior is obtained by recognizing that the strain history of a material element, dx, located at a distance x from the crack tip, being approached by a fatigue crack growing at a constant rate, da/dN, is equivalent to that of an element moving towards a stationary crack tip at a rate, -dx/dN. That is,

$$-\frac{dx}{dN} = \frac{da}{dN} \tag{7a}$$

and

$$-\int_{2r_y}^{x} \frac{dx}{(da/dN)} = \int_{0}^{N} dN \tag{7b}$$

Note that, Eq. 7b is written for an element which is initially located at the monotonic plastic zone boundary; in other words, $x = 2r_y$ when $N = 0$; thus carrying out the integration in Eq. 7b we get,

$$x = 2r_y - N\left(\frac{da}{dN}\right) \tag{7c}$$

Substituting Eq. 7c into Eqs. 6a and 6b we get

$$\varepsilon_{max} = \frac{K_{max}^2}{\pi \sigma_{YS} \cdot E(2r_y - N(da/dN)} \tag{8a}$$

$$\text{and } \varepsilon_{min} = \frac{K_{min}^2}{\pi \sigma_{YS} \cdot E(2r_y - N(da/dN)} \tag{8b}$$

Using Eq. 8, strain histories were calculated for growth rates of 10^{-7} and 10^{-5} in./cycle (2.5×10^{-9} and 2.5×10^{-7} m/cycle) for load ratios of 0 and 0.8 for both materials investigated in this study. Figure 5 shows a schematic of such a strain history. The above strain histories were each applied to smooth axial fatigue specimens while the mean stress relaxation behavior was observed using procedures described in the next section.

EXPERIMENTAL PROCEDURE

Material Characterization

The materials investigated in this program were a 10Ni-steel and a 2219-T851 aluminum alloy. An extensive characterization of wide range fatigue crack growth rates as a function of stress intensity range for several load ratios is available for these materials from an earlier study[3], Figs. 1 and 2. The steel and aluminum was obtained in the form of 1 in. (25.4 mm) and 3 in. (76.1 mm) thick plates, respectively. The chemical composition of these materials is given in Table I. Both materials exhibited uniformity in conventional tensile properties with respect to location as well as orientation, Table II.

Cyclic stress-strain properties, as described by Eq. 10, of the two materials were characterized using the incremental step test. The strain-life curve, Eq. 11, was estimated by Dowling[17] using a modification of the procedures suggested by Landgraf[18] and Morrow[19]. These properties are represented as follows:

$$\Delta\sigma/2 = A(\Delta\varepsilon_p/2) \tag{10}$$

$$\Delta\varepsilon/2 = \frac{\sigma_f'}{E}(2N_f)^b + \varepsilon_f'(2N_f)^c \tag{11}$$

where A, n', σ_f', ε_f', b and c are fitting constants and $\Delta\varepsilon_p/2$ = plastic strain amplitude. Table III lists the values of the above fitting constants for 2219-T851 Al and 10Ni-steel.

Simulation Tests

A cylindrical specimen, ¼ in. (6.2 mm) in diameter and ½ in. (12.7 mm) in gage length was used for the simulation tests. Table IV summarizes the growth rates, load ratios and the corresponding ΔK values for which the strain histories were simulated. The maximum and minimum strain on the smooth specimen was increased as a function of the number of cycles according to a schedule determined by Eq. 8 using step increments of 0.5 percent on maximum strain. Standard MTS servohydraulic equipment was used for these tests. Stress-strain hysteresis loops were recorded periodically to measure the mean stress relaxation behavior. The number of cycles to failure were also recorded.

RESULTS AND DISCUSSION

Prior to interpreting mean stress relaxation results obtained from the crack-tip simulation tests, an experimental justification of the strain history developed in an earlier section is perhaps in order. The intent of the simulation tests was to duplicate the strain history of an element which is initially at the monotonic plastic zone boundary and is subsequently approached by the tip of a fatigue crack growing at a constant rate. If the above strain history is in fact a good approximation, the number of cycles it takes for the smooth specimen to fail should ideally be equal to the number of cycles required for the crack to extend one monotonic plastic zone size in a crack growth test. Alternatively, the monotonic plastic zone size divided by the number of cycles to failure on the corresponding simulation smooth specimen should be equal to the simulated rate of fatigue crack growth. These data are tabulated in Table V and demonstrate the suitability of the estimated strain histories.

Mean Stress Relaxation Behavior

In a constant amplitude, strain controlled test, when the strain ratio $(\frac{\varepsilon_{min}}{\varepsilon_{max}})$ is other than -1, the mean stress during fatigue cycling is initially non-zero. In the low-cycle-fatigue regime, which is associated with considerable cyclic plasticity, the initial non-zero mean stress relaxes and quickly attains a value nearly equal to zero. However, in the high cycle fatigue regime which does not involve cyclic

plasticity the mean stress remains approximately constant. The presence of a tensile mean stress is associated with a significant decrease in fatigue life[20]. It thus appears rational to characterize the mean stress behavior in the crack tip region by means of simulation tests for various growth rates and load ratios and then attempt to correlate these results with trends observed in the response of da/dN to load ratio, R.

Figures 6 and 7 show the residual mean stress, σ_o (normalized with respect to the 0.2% yield strength) plotted as a function of number of fatigue cycles, N (normalized with respect to the cycles to failure, N_f) for tests simulating various growth rates and R values for 2219-T851 Al and 10Ni steel, respectively. The same mean stress data can alternatively be plotted against percent fatigue damaage. This representation is more realistic because a large number of total fatigue cycles in each of the simulative tests were accumulated at low strain ranges, and thus do not account for a substantial fraction of the damage as may wrongly be interpreted from Figs. 6 and 7.

Fatigue damage was calculated by using Miner's linear damage summation rule[21] given by:

$$\sum_{i=1}^{N} \frac{\Delta N_i}{N_{fi}} = D \qquad (12)$$

where D = damage, ΔN_i = number of fatigue cycles at a given strain range $\Delta\varepsilon_i$, N_{fi} = number of fatigue cycles to failure at a constant strain range $\Delta\varepsilon_i$. For a particular strain range, N_{fi} was obtained from

a modified form of Eq. 11 which accounts for the influence of mean stress (σ_o)[22] on the cyclic life of smooth axial fatigue specimen.

$$\frac{\Delta\varepsilon_i}{2} = \frac{\sigma_f' - \sigma_o}{2} (2N_{fi})^b + \varepsilon_f' (2N_{fi})^c \qquad (13)$$

Percent fatigue damage was subsequently calculated using the following equation

$$\text{Percent Damage} = \left(\sum_{i=1}^{N} \frac{\Delta N_i}{N_{fi}}\right) / \left(\sum_{i=1}^{N_f} \frac{\Delta N_i}{N_{fi}} \times 100\right) \qquad (14)$$

Figures 8 and 9 present the normalized mean stress as a function of percent fatigue damage for 2219-T851 Al and 10Ni steel, respectively. The following observations are made from the figures: (i) a high level of mean stress is present for a substantial fraction of the fatigue life, (ii) the level of mean stress is strongly dependent on R value, (iii) at equivalent R values, the mean stress relaxes more readily in tests simulating growth rates of 10^{-5} in./cycle (2.5×10^{-7} m/cycle) as compared to those corresponding to a growth rate of 10^{-7} in./cycle (2.5×10^{-9} m/cycle), and (iv) in general, the 10Ni steel specimens were able to relax mean stress more readily as compared to the 2219-T851 aluminum specimens at equivalent growth rate levels and R values.

To further illustrate the last two observations, the difference in the normalized mean stresses at R values of 0.8 and 0, that is $(\sigma_o/\sigma_{YS})_{R=0.8} - (\sigma_o/\sigma_{YS})_{R=0}$, were plotted as a function of percent fatigue damage for the two materials at the two growth rate levels investigated, Fig. 10. For both materials, it is observed that the

change in normalized mean stress levels due to an increase in load ratio is significantly larger for growth rates of 10^{-7} in./cycle (2.5×10^{-9} m/cycle) than for growth rate of 10^{-5} in./cycle (2.5×10^{-7} m/cycle). Also, the change in mean stress level due to an increase in stress ratio for 10Ni steel was significantly less than for 2219-T851 aluminum at both growth rates investigated. Based on the above observations it is postulated that the load ratio effects in fatigue crack growth are directly linked to the extent of mean stress relaxation in the crack tip region. In region II of the da/dN vs. ΔK relationship the strain histories in the crack tip regions consist of a high degree of cyclic plasticity and thus, the potential for relaxing mean stresses is also high. Hence, fatigue crack growth rates are not expected to be very sensitive to load ratio. On the contrary, in region I the extent of cyclic plasticity is limited, thus causing high mean stresses to be retained and consequently the fatigue crack growth rates are very sensitive to load ratios.

It has been demonstrated here in that the ability to relax mean stresses is specific to material type. These differences are more significant in region II of da/dN vs. ΔK relationship which is associated with considerable cyclic plasticity. The 10Ni steel was shown to be more capable of relaxing mean stresses than 2219-T851 aluminum, hence it would be expected to exhibit smaller changes in growth rates as a function of R in region II. The differences in the behavior of the aluminum alloy and steel investigated can be linked to the slip character of the two materials. High strength aluminum alloys generally possess a planar slip character[23] while ferritic

steels are expected to exhibit a wavy slip mode associated with extensive cross-slip on secondary planes. During fatigue loading, deformation is localized in intense slip bands in planar slip materials and is relatively dispersed and homogeneous in wavy slip materials. During strain controlled cycling, the wavy slip materials tend to stabilize stresses more readily compared to planar slip materials[11,23,24] and thus would be expected to possess a higher capability to relax mean stresses in the crack tip region during fatigue crack growth. Additional work with different type of materials, including substructure characterization of the fatigued specimens, is needed to confirm this point.

All of the above observations are consistent with data on load ratio effects on da/dN in regions I and II[3,4]*. Additional research is necessary to further quantify the importance of crack-tip residual stresses for a better understanding of the mechanisms of fatigue crack growth. Although, this relaxation behavior and other local crack tip phenomena such as crack closure, are all related to the plasticity which occurs at the crack tip, the unique contribution of each must be considered in formulating realistic physical models for fatigue crack growth.

*As discussed in Ref. 4, load ratio effects in region III are likely to be determined by the presence of an additional mode of cracking as critical stress intensity for instability is approached.

SUMMARY AND CONCLUSIONS

Approximate analytical relationships for crack-tip stresses and strains within the monotonic and fatigue plastic zones were developed for cyclic loading. The strain histories thus derived as a function of number of fatigue cycles were imposed on smooth axial specimens of 10Ni steel and 2219-T851 aluminum to study the relaxation of mean stress as a function of fatigue damage. The following conclusions were derived from these results.

(1) It was demonstrated, from the fatigue life data obtained on the simulation tests, that the applied strain vs. elapsed fatigue cycles are good approximations.

(2) Load ratio effects commonly observed in fatigue crack growth rate data are related directly to the extent of mean stress relaxation behavior at the crack tip.

(3) The extent of mean stress relaxation at a given R value depends on the fatigue crack growth regime. Mean stresses were observed to relax more readily in tests simulating growth rates of 10^{-5} in./cycle (2.5×10^{-7} m/cycle) compared to growth rates of 10^{-7} in./cycle (2.5×10^{-9} m/cycle) thus explaining why load ratio effects are stronger at the lower growth rate.

(4) 10Ni steel was shown to be more capable of relaxing mean stresses in the crack tip region as opposed to 2219-T851 aluminum. This trend was linked to differences in slip character of the two materials.

(5) Further work is needed to quantify the crack tip residual stresses to develop a better understanding of fatigue mechanisms. Ultimately this can also be used in developing more realistic models for fatigue crack growth and would be valuable information for material selection and alloy development leading to improved materials for fatigue resistance.

ACKNOWLEDGMENTS

Gratitude is expressed to N. E. Dowling for helpful discussions during the course of this study. The fatigue crack growth data used in this paper were developed under the sponsorship of the U.S. Air Force, AFML Contract F33615-75-C-5064, project FY-1457-75-02110/7381. The efforts of L. W. Burtner and R. B. Hewlett in conducting the simulation tests are also gratefully acknowledged.

REFERENCES

1. P. C. Paris and F. Erdogan, "A Critical Analysis of Crack Propagation Laws", Trans. ASME, Series D, J. Basic Eng., Vol. 85, 1963, p. 528.
2. C. M. Hudson, "Effect of Stress Ratio on Fatigue Crack Growth in 7075-T6 and 2024-T3 Aluminum-Alloy Specimens", NASA Langley Research Center Report, NASA-TN-D-5390, August 1969.
3. S. J. Hudak, A. Saxena, R. J. Bucci and R. C. Malcolm, "Development of Standard Methods of Testing and Analyzing Fatigue Crack Growth Rate Data — Final Contract Report", AFML Contract F33615-75-C-5064, Westinghouse R&D Center, 77-9D3-AFCGR-R2, December 1977.
4. R. O. Ritchie, "Influence of Impurity Segregation on Temper Embrittlement and on Slow Fatigue Crack Growth and Threshold Behavior in 300M-High Strength Steel", Met. Trans. A, Vol. 8A, 1977, p. 1131.
5. W. Elber, "The Significance of Crack Closure", Damage Tolerance in Aircraft Structures, ASTM STP 486, 1971, p. 230.
6. R. A. Schmidt and P. C. Paris, "Threshold for Fatigue Crack Propagation and Effects of Load Ratio and Frequency", ASTM STP 536, 1973, p. 79.
7. M. Kikukawa, M. Jono and K. Tanaka, "Fatigue Crack Closure Behavior at Low Stress Intensity Level", Proc. of 2nd Int. Conf. on Mechanical Behavior of Materials, August 1976, Boston.

8. T. C. Lindley and C. E. Richards, "The Relevance of Crack Closure to Fatigue", Proc. of Mechanics and Mechanisms of Crack Growth, 1973, Cambridge.

9. K. T. Uganst, T. T. Shih and R. P. Wei, "Crack Closure in 2219-T851 Al Alloy", Eng. Fracture Mechanics, Vol. 9, 1977.

10. S. D. Antolovich, A. Saxena and G. R. Chanani, "A Model for Fatigue Crack Propagation", Engrg. Fracture Mechanics, Vol. 7, 1975, p. 649.

11. A. Saxena and S. D. Antolovich, "Low Cycle Fatigue, Fatigue Crack Propagation and Substructures in a Series of Polycrystalline Cu-Al Alloys", Metallurgical Transactions A, Vol. 6A, 1975, p. 1809.

12. G. R. Irwin, "Analysis of Stresses and Strains Near the End of a Crack Traversing a Plate", Trans. ASME, Journal of Applied Mechanics, 1957.

13. H. Neuber, "Theory of Stress Concentration for Shear-Strained Prismatical Bodies with Arbitrary Nonlinear Stress-Strain Law", Journal of Applied Mechs., Trans. ASME, Vol. 28, December 1961, p. 544.

14. J. W. Hutchinson, "Singular Behavior at the End of a Tensile Crack in a Hardening Material", Journal of Mechanics and Physics of Solids, Vol. 16, 1968, p. 13.

15. J. R. Rice and G. F. Rosengren, "Plane Strain Deformation Near a Crack Tip in a Power Law Hardening Material", Journal of Mechanics and Physics of Solids, Vol. 16, 1968, p. 1.

16. F. A. McClintock, "Plasticity Aspects of Fracture", in Fracture, H. Liebowitz Ed., Vol. 3, Academic Press, New York, 1971, p. 47.

17. N. E. Dowling, unpublished research, Westinghouse R&D Center, 1977.

18. R. W. Landgraf, "The Resistance of Metals to Cyclic Deformation", Achievement of High Fatigue Resistance in Metals and Alloys, ASTM STP 467, 1970, p. 3.

19. J. Morrow, "Cyclic Plastic Strain Energy and Fatigue of Metals", Internal Friction, Damping and Cyclic Plasticity, ASTM STP 378, 1965, p. 45.

20. J. Dubuc, J. R. Vanasse, A. Biron and A. Bazergin, "Effect of Mean Stress and Mean Strain in Low-Cycle Fatigue of A517 and A201 Steels", Trans. of ASME, Journal of Engineering for Industry, Paper 69-PVP-1, 1969.

21. M. A. Miner, "Cumulative Damage in Fatigue", Journal of Applied Mechanics, Trans. ASME, Vol. 12, 1945, p. A-159.

22. J. Morrow, "Fatigue Properties of Metals", Section 3.2 of Fatigue Design Handbook, SAE 1968.

23. C. Calabrese and C. Laird, "High Strain Fatigue Fracture Mechanisms in Two Phase Alloys", Met. Trans., Vol. 5, August 1974, p. 1785

24. C. E. Feltner and C. Laird, "Cyclic Stress-Strain Response of FCC Metals and Alloy — I, Phenomenological Experiments", Acta Met., Vol. 15, October 1967, pp. 1621-1632 and Part II, pp. 1633-1653.

TABLE I - CHEMICAL COMPOSITION OF TEST MATERIALS (WT %)

Material	C	Si	Mn	Mg	S	P	Cr	Zn	Ti	Co	Cu	Ni	Mo	Al	Fe
10Ni-steel	0.12	0.07	0.28	--	0.006	0.008	2.03	--	--	8.07	--	10.29	1.03	--	Bal.
2219-T851 Al	--	0.088	0.25	0.003	--	--	<.0001	0.025	0.051	--	6.28	--	--	Bal.	0.25

TABLE II - ROOM TEMPERATURE MECHANICAL PROPERTIES OF TEST MATERIALS*

Material	Orientation	0.2% σ_{YS} ksi	0.2% σ_{YS} MPa	σ_{ULT} ksi	σ_{ULT} MPa	% Elong. (2 in g.L)	% Reduction in Area
10Ni-steel	long.	190.0	1309.1	197.0	1357.3	6.9	17.0
	trans.	190.0	1309.1	196.0	1350.4	6.9	17.0
2219-T851 Al	long.	52.0	358.3	66.0	454.7	8.5	19.0
	trans.	51.0	351.4	66.0	454.7	8.2	19.0

*Steel results: average of 8 tests from 4 locations.

Aluminum results: average of 6 tests from 2 locations.

TABLE III - FITTING CONSTANTS DEFINING THE CYCLIC STRESS-STRAIN AND STRAIN-LIFE PROPERTIES OF THE TEST MATERIALS

Material	A		n'	σ_f'		b	ε_f'	C	σ_{YS}^{c} *	
	ksi	MPa		ksi	MPa				ksi	MPa
10Ni-steel	316	2177.2	0.109	293.0	2018.8	-0.08	0.54	-0.647	160.5	1105.8
2219-T851 Al	103	709.7	0.121	89.0	613.2	-0.0756	0.35	-0.55	48.5	334.1

*σ_{YS}^{c} = cyclic yield strength.

TABLE IV - CRACK GROWTH RATES AND R VALUES USED FOR TESTS SIMULATING CRACK-TIP STRAIN HISTORIES

Material	R	da/dN		ΔK (ksi$\sqrt{in.}$)*
		in./cycle	m/cycle	
2219-T851 Al	0	10^{-5}	2.5×10^{-7}	10.5
2219-T851 Al	0	10^{-7}	2.5×10^{-9}	3.5
2219-T851 Al	0.8	10^{-5}	2.5×10^{-7}	6.05
2219-T851 Al	0.8	10^{-7}	2.5×10^{-9}	2.05
10Ni-steel	0	10^{-5}	2.5×10^{-7}	32.0
10Ni-steel	0	10^{-7}	2.5×10^{-9}	8.0
10Ni-steel	0.8	10^{-5}	2.5×10^{-7}	31.0
10Ni-steel	0.8	10^{-7}	2.5×10^{-9}	4.2

*1 ksi$\sqrt{in.}$ = 1.1 MPa$\sqrt{m}$

TABLE V - COMPARISON OF THE TARGETED GROWTH RATES (da/dN) WITH THOSE ESTIMATED FROM THE CYCLIC LIFE OF THE SIMULATION TESTS ($2r_Y/N_f$)

Material	R	da/dN in./cycle	$2r_Y$* in.	N_f**	$\frac{2r_Y}{N_f}$ in./cycle
10Ni-steel	0	10^{-5}	.011	1006	1.09×10^{-5}
10Ni-steel	0	10^{-7}	.000564	4576	1.2×10^{-7}
10Ni-steel	0.8	10^{-5}	.212	20,138	1.05×10^{-5}
10Ni-steel	0.8	10^{-7}	.004	37,380	1.07×10^{-7}
2219-T851 Al	0	10^{-5}	.013	1165	1.1×10^{-7}
2219-T851 Al	0	10^{-7}	.0018	12,476	1.4×10^{-7}
2219-T851 Al	0.8	10^{-5}	.110	10,383	1.06×10^{-5}
2219-T851 Al	0.8	10^{-7}	.0126	110,951	1.1×10^{-7}

*$2r_Y = \frac{1}{\pi} \left(\frac{K_{max}}{\sigma_{YS}}\right)^2$

**N_f = number of cycles to failure

1 in./cycle = 2.54×10^{-2} m/cycle

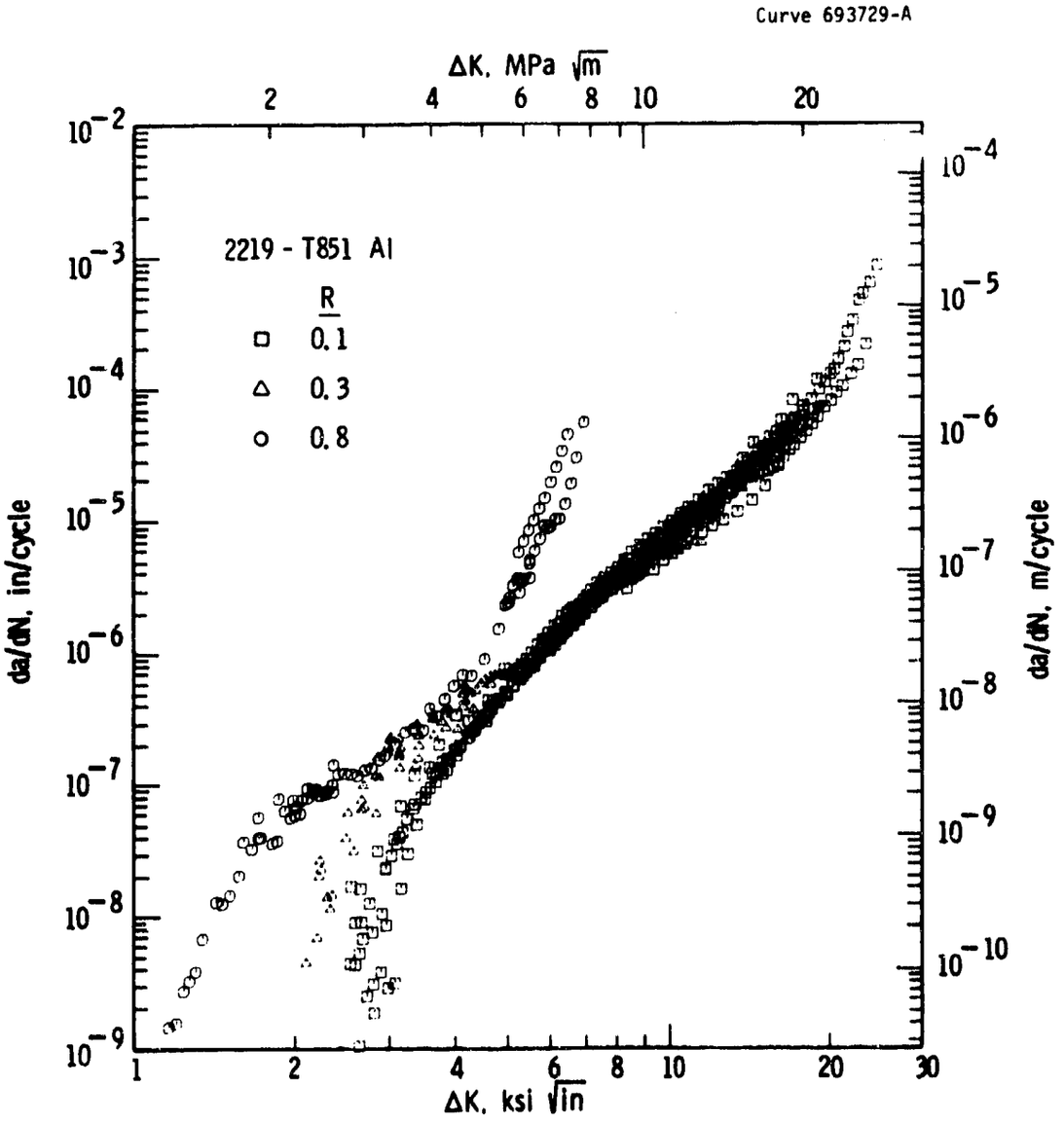

Fig. 1 — Wide range fatigue crack growth rate behavior of 2219-T851 aluminum alloy at various load ratios (Ref. 3)

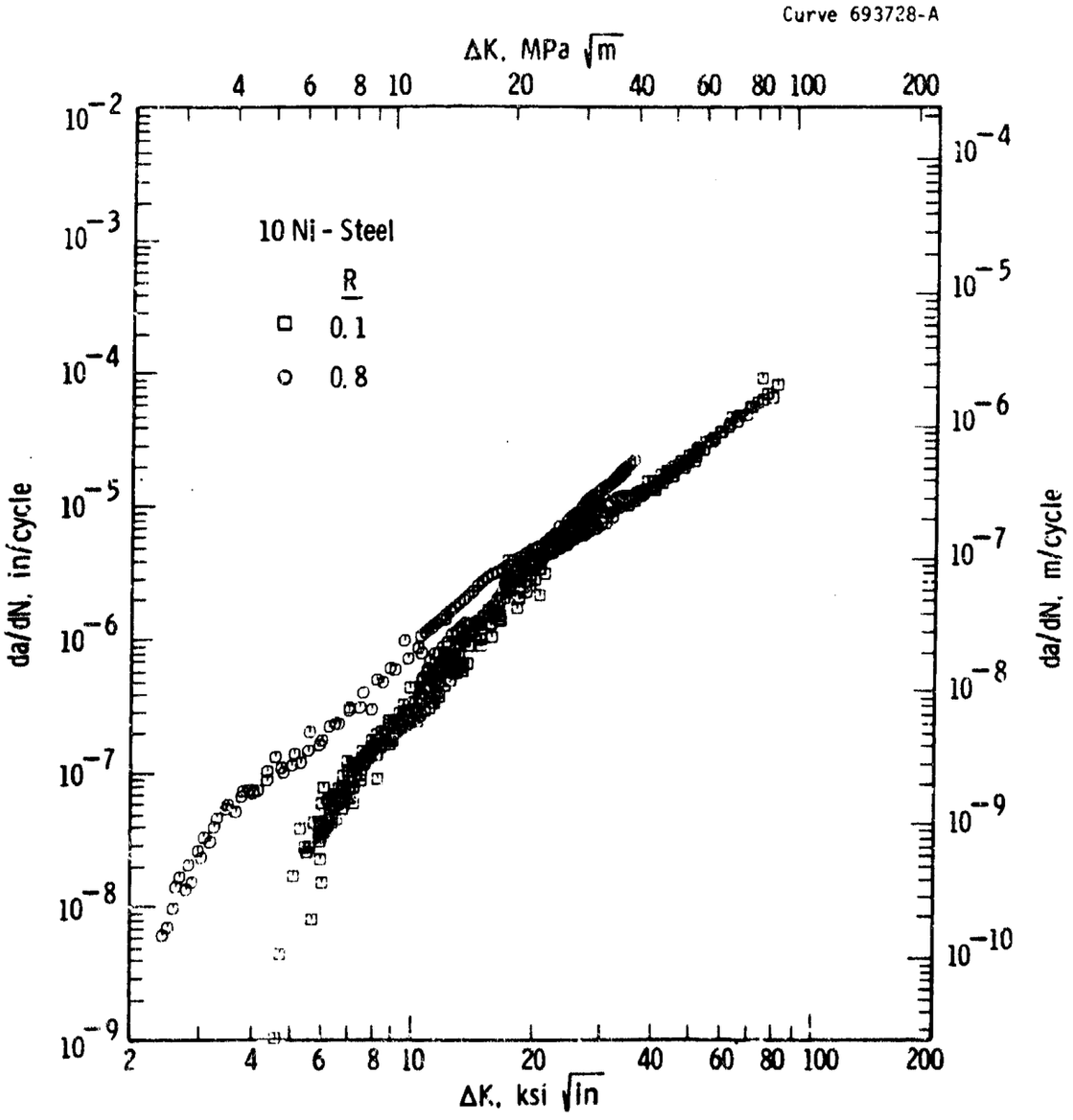

Fig. 2 — Wide range fatigue crack growth rate behavior of 10 Ni-steel at various load ratios (Ref. 3)

Dwg. 6425A49

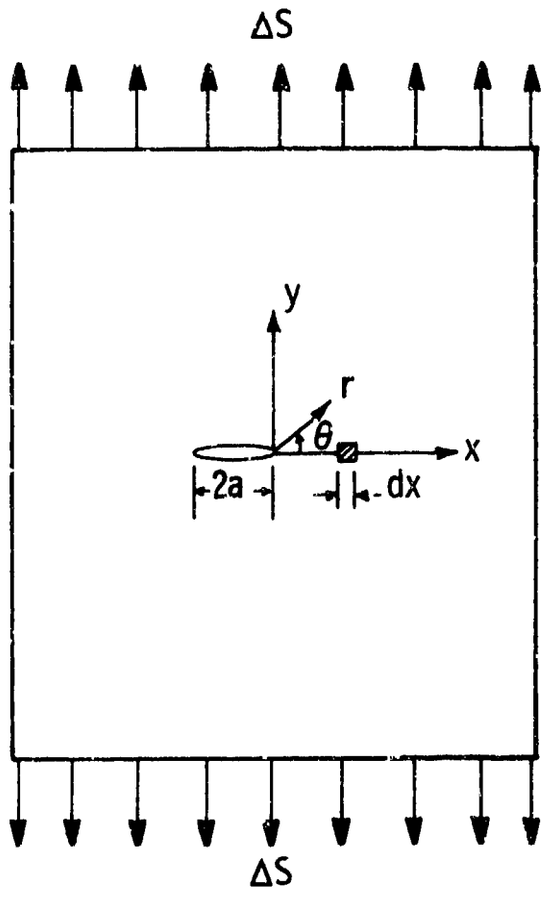

Fig. 3 — Semi-infinite cracked body loaded with a remote fatigue stress, ΔS

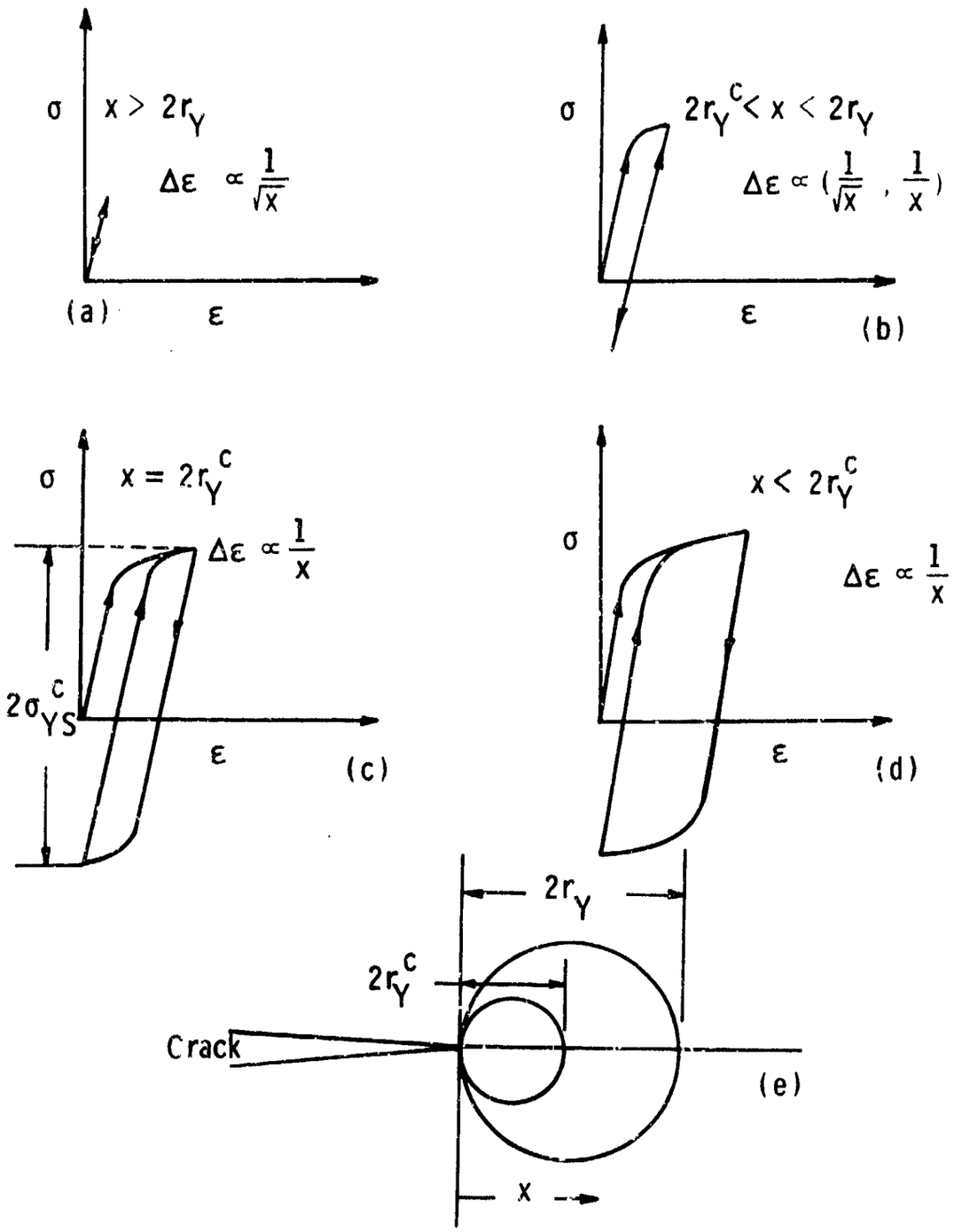

Fig. 4 — Stress-strain history of an element approaching the tip of a propagating fatigue crack

Dwg. 6425A48

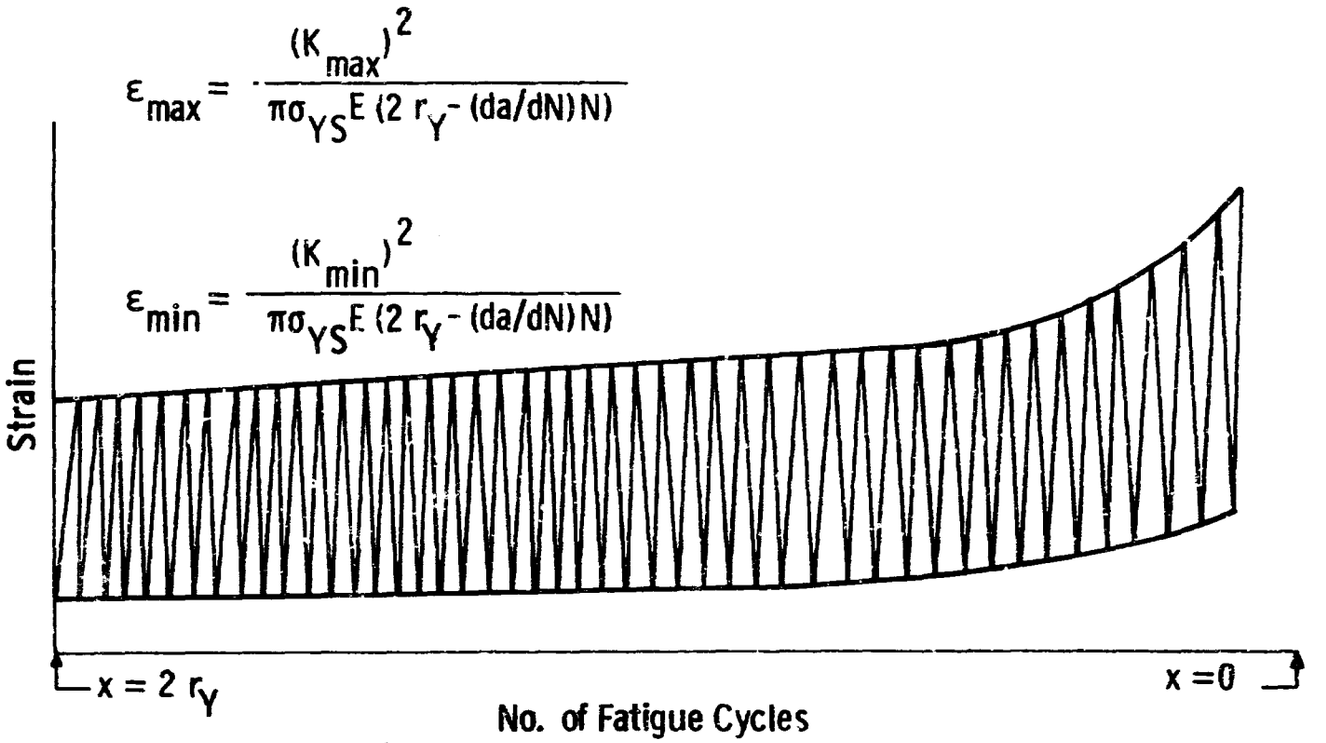

Fig. 5 — Schematic of the strain history of an infinitesimal material element being approached by the tip of a crack propagating at a constant rate, da/dN

Curve 592929-A

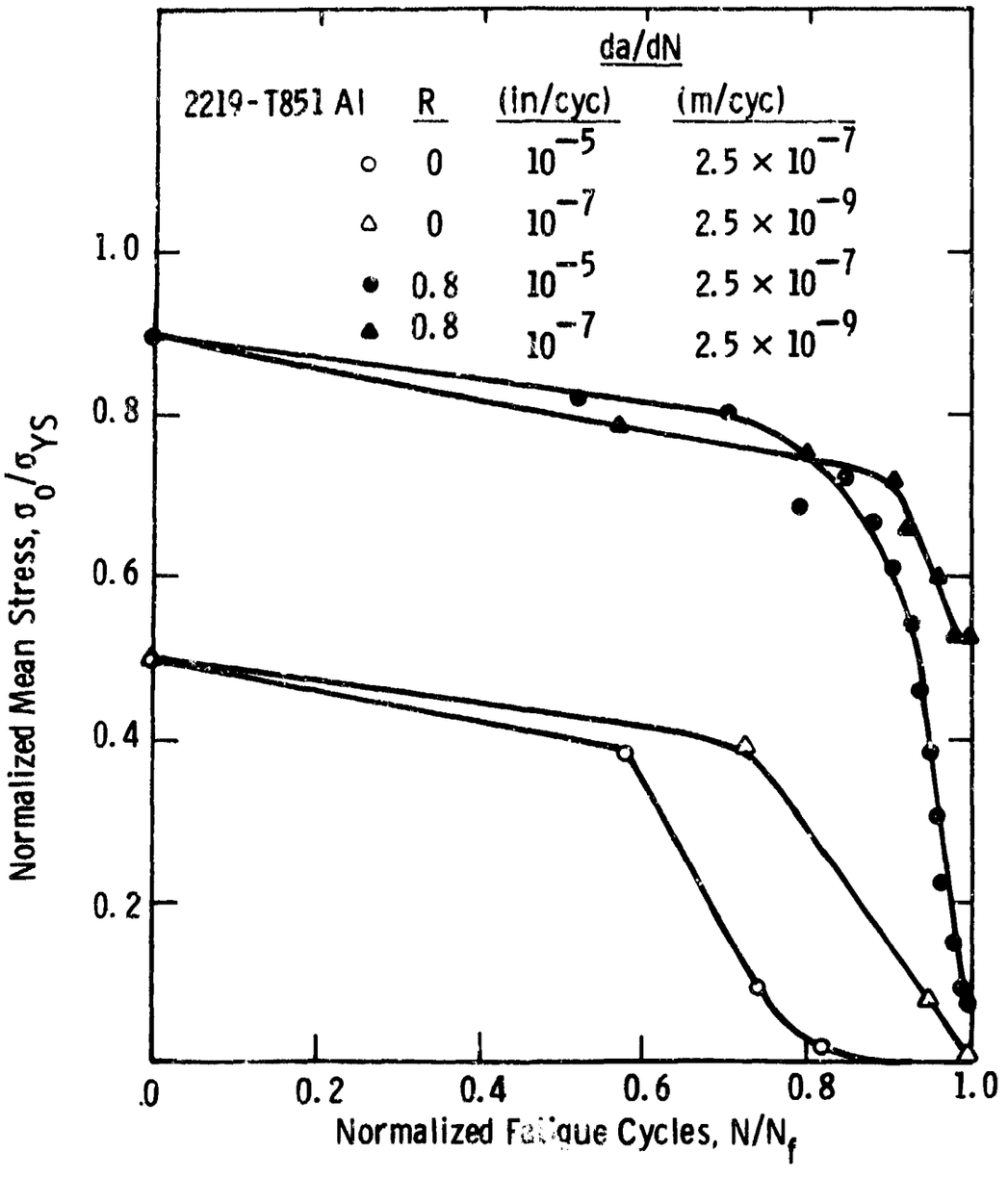

Fig. 6 — Normalized mean stress as a function of applied fatigue cycles in 2219-T851Al tests which simulate crack-tip strain histories at various growth rates and load ratios

Curve 692928-A

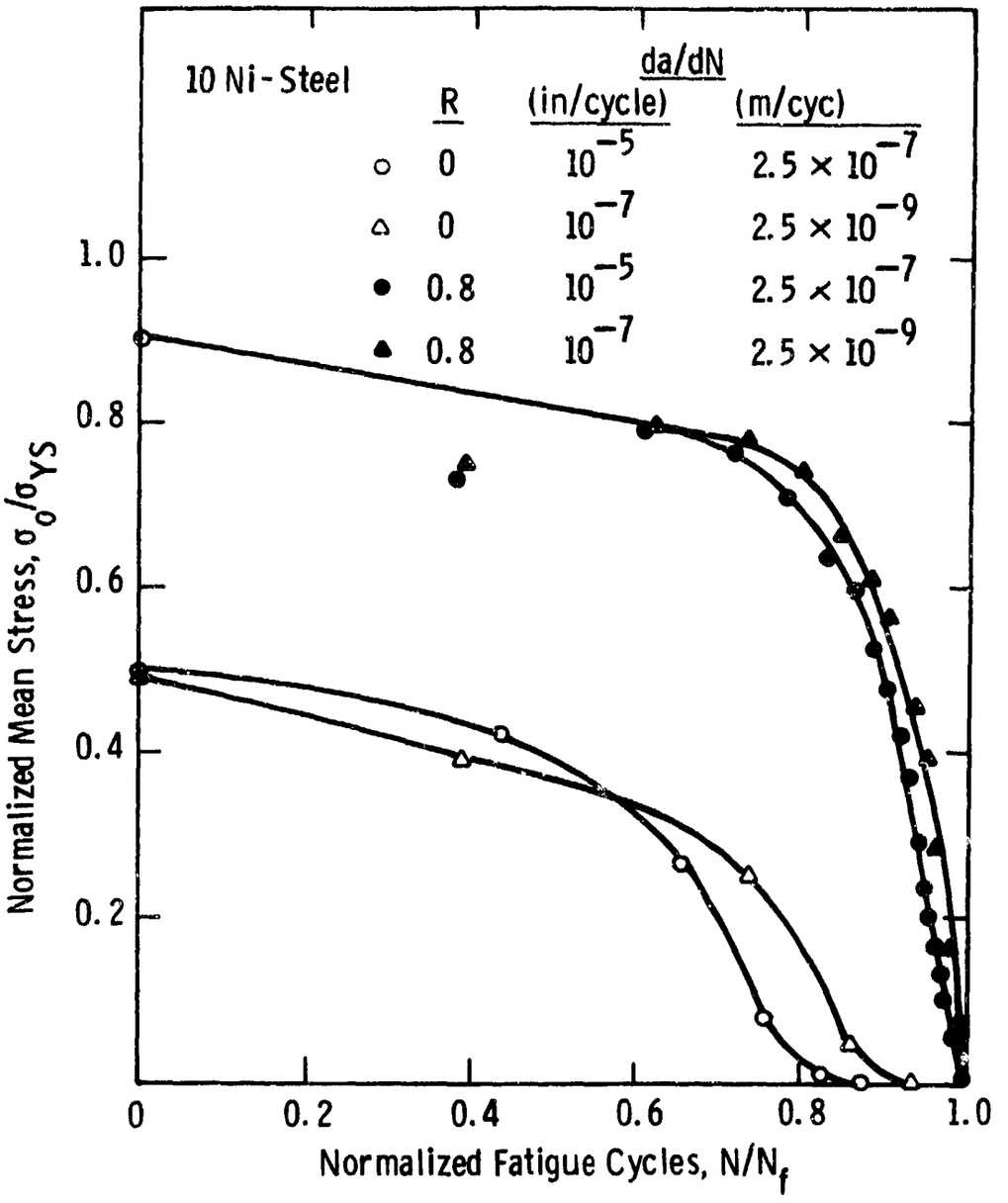

Fig. 7 — Normalized mean stress as a function of applied fatigue cycles in 10 Ni-steel tests which simulate the crack-tip strain history at various growth rates and load ratios

Curve 692932-A

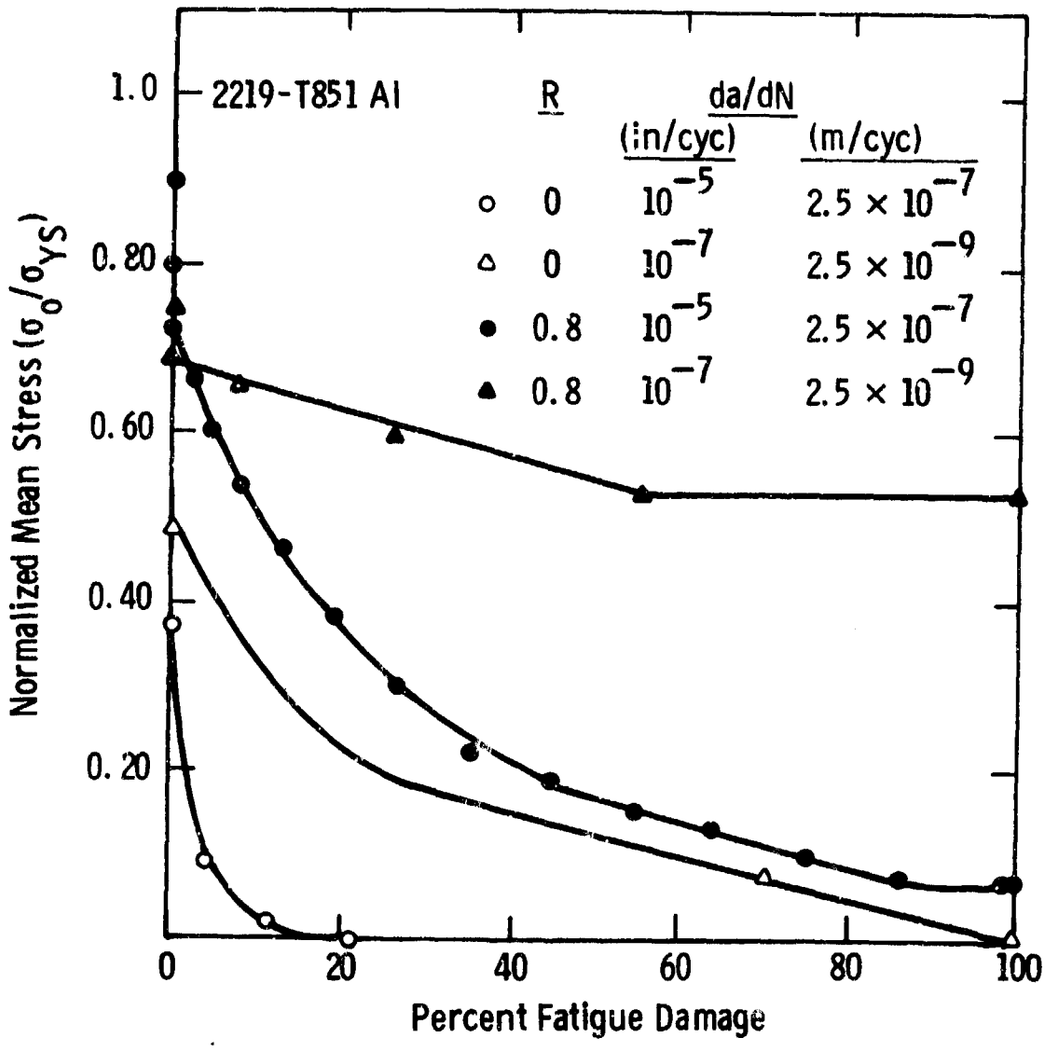

Fig. 8 — Normalized mean stress as a function of percent fatigue damage in 2219-T851 Al tests which simulate crack-tip strain histories at various growth rates and load ratios

Curve 692931-A

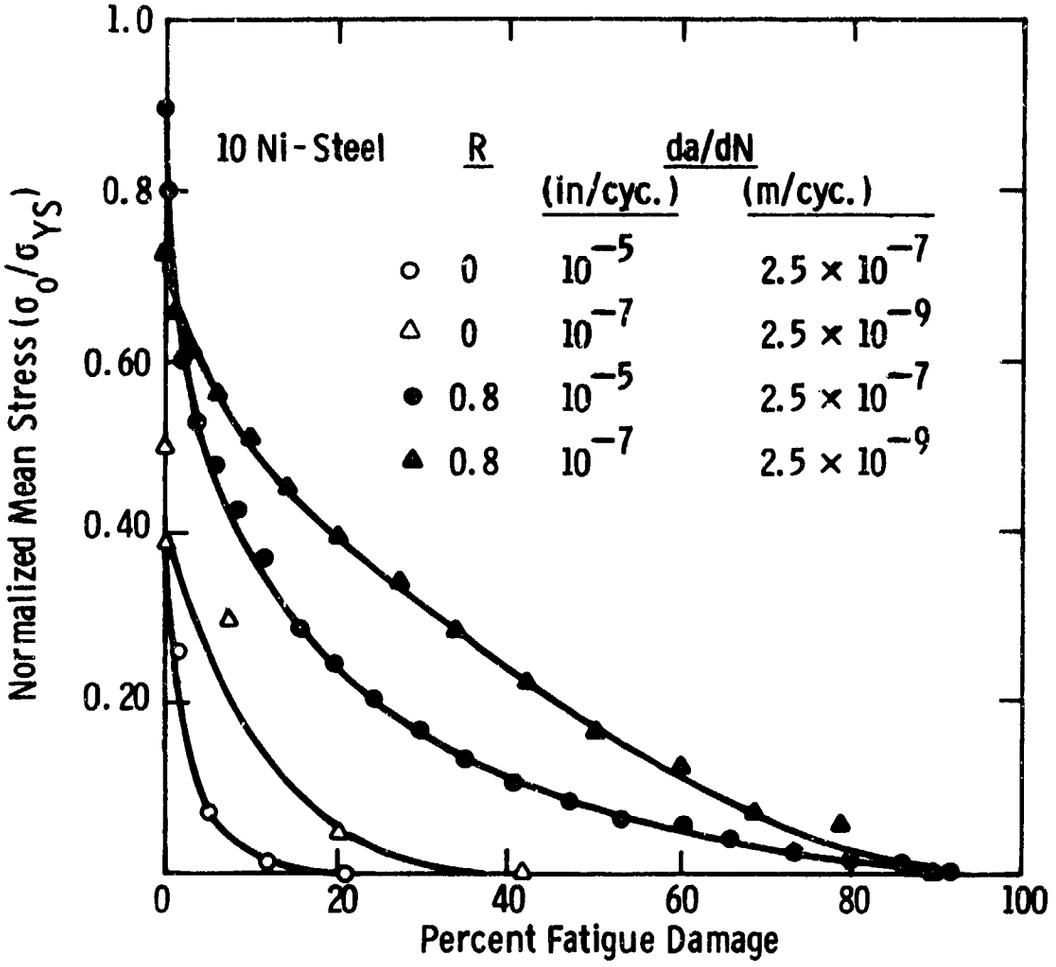

Fig. 9 — Normalized mean stress as a function of percentage fatigue damage in 10 Ni-steel tests which simulate crack-tip strain histories at various growth rates and load ratios

Curve 692927-A

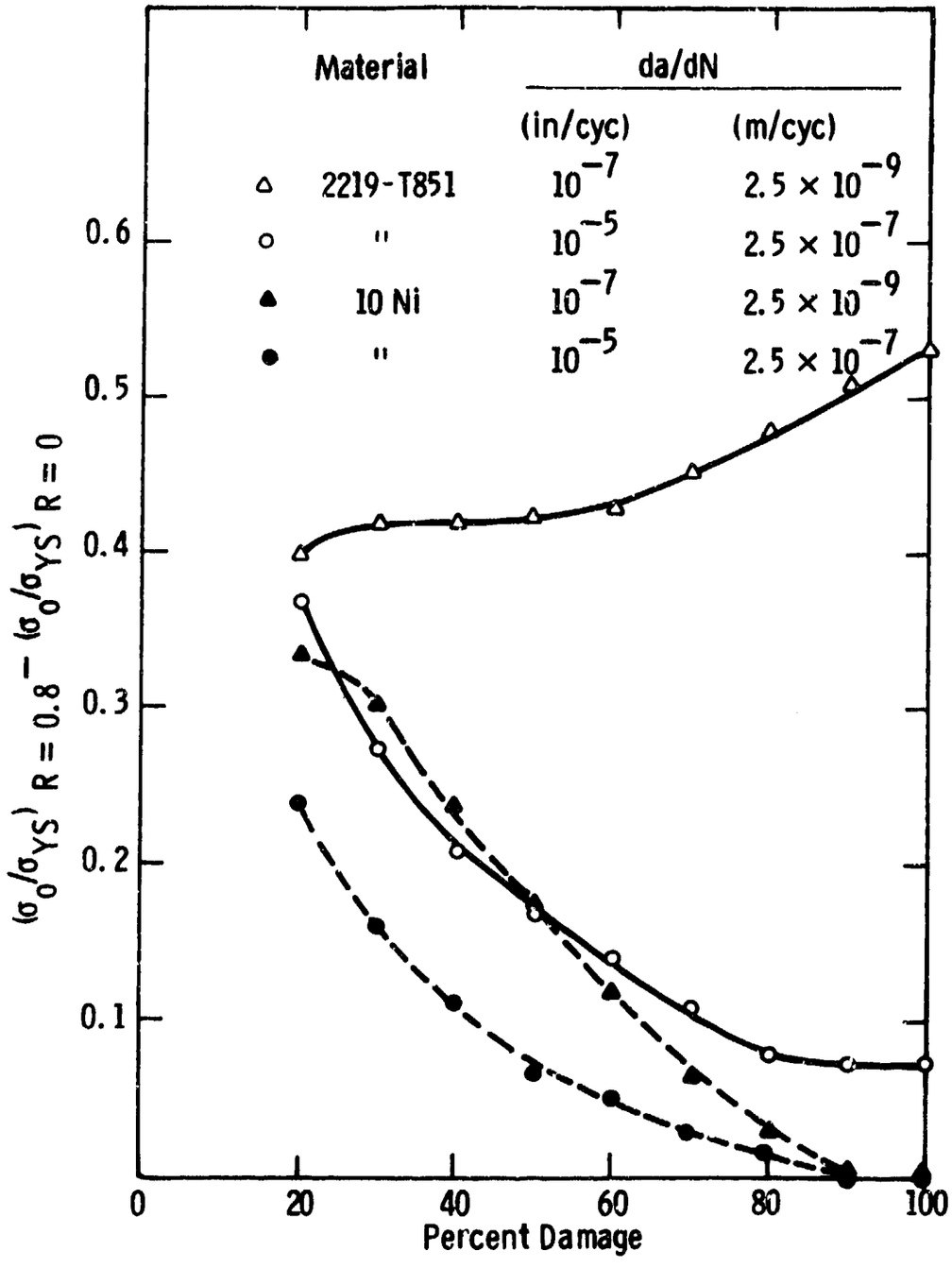

Fig. 10 — Comparison between the stress relaxation behavior at R = 0 versus R = 0.8 in 2219-T851 Al and in 10 Ni steel at various growth rates

☆U.S.Government Printing Office: 1978 — 757-080/20